# Nonlinear observers handling observability singularities

Javeria Ahmed

# UNIVERSITÉ D'ORLÉANS

***ÉCOLE DOCTORALE MIPTIS (Mathématiques, Informatique, Physique Théorique et Ingénierie des Systèmes)***

**LABORATOIRE PRISME**

# THÈSE présentée par:

**Javeria AHMED**

soutenue le : 3 avril **2023**

pour obtenir le grade de: **Docteur de l'Université d'Orléans**

Discipline/ Spécialité: Sciences et Technologies Industrielles

# NONLINEAR OBSERVERS HANDLING OBSERVABILITY SINGULARITIES

**THÈSE dirigée par :**

| | |
|---|---|
| **TOURÉ Youssoufi** | Professeur, Université d'Orléans |

**RAPPORTEURS :**

| | |
|---|---|
| **BESANÇON Gildas** | Professeur, INP Grenoble |
| **ZEMOUCHE Ali** | Maître de conférences HdR, Université de Lorraine |

---

**JURY :**

| | |
|---|---|
| **MORIN PASCAL** | Professeur, Sorbonne université |
| **BESANÇON Gildas** | Professeur, INP Grenoble |
| **ZEMOUCHE Ali** | Maître de conférences HdR, Université de Lorraine |
| **COURTIAL Estelle** | Maître de conférences , Université d'Orléans, co-encadrante |
| **FRUCHARD Matthieu** | Maître de conférences , Université d'Orléans, co-encadrant |

# Acknowledgements

First and foremost, I would like to express my sincere gratitude to my PhD supervisors Matthieu Fruchard and Estelle Courtial who are the best supervisors I could have ever asked for. Thank you Matthieu and Estelle for giving me the opportunity to work at the best research facility. Thank you for offering insightful scientific guidance and elegant advice, providing relentless support whenever I needed it, and most importantly thank you for understanding my family situation and giving me your full support through thick and thin. I also appreciated that you always found the time to help me, and is mostly you that I need to thank for concluding this work and therefore having had very joyful PhD years.

I also would like to acknowledge my PhD director, Youssoufi Toure for providing me with technical guidance and for the joyful conversations throughout my PhD journey. You always proved to be the trustworthy advisor and taught me a lot of what I know about the subject.

I extend my gratitude to Mr Pascal Morin for having accepted the presidency of my thesis jury. I especially thank Mr. Gildas Besancon and Mr. Ali Zemouche for having done me the honor of reporting my thesis work. This thesis would not have been possible without the work of all its members.

A special word of gratitude is owed to my friends Rahul and Yixin for their kind support in a lot of matters and with whom I share many grateful moments.

Finally, I would like to thank my loving family, mother Kausar, father Ahmad, my brother Abdur Rafay, and sister Ammara for always encouraging me and making me believe that nothing is impossible. My most sincere gratitude goes to my loving husband, Najam Ul Haq, for your unending support and encouragement throughout the years. You always believed in me and inspired me.

It was an amazing journey, and would not have been possible without the backing of the above-mentioned people. You are all remarkable, and I hope to work with you again in the future, on one project or another.

# Table of Contents

# List of figures

# List of tables

# General Introduction

## 1 Context & Objectives of the thesis

In many applications, the knowledge of internal information of a system is required for a variety of reasons that includes modeling (identification), monitoring (fault detection), or driving (control) the system. All those purposes are actually jointly required when aiming at keeping a system under control. In general, it is obvious that one cannot use as many sensors as signals of interest characterizing the system behavior due to cost, economical or technological constraints, and so on. Especially since such signals can be numerous and of various types: they typically include time-varying signals characterizing the system (state variables), constant signals (parameters), and unmeasured external signals (disturbances). Therefore, when one wants some *internal* knowledge from *external* (directly available) measurements, the challenge of observer design naturally emerges in a system approach. An observer is a dynamical system whose role is to process the incomplete and imperfect information provided by the sensors to accurately reconstruct the whole system or provide reliable estimate of all the system state variables. This makes the reconstruction—or observer—problem the heart of a general control problem. In short, an observer relies on a model, based on available measurements, and aiming at information reconstruction, i.e. it can be characterized as a *model-based*, *measurement-based*, *closed-loop*, $information\ reconstructor$. The model is a state-space representation, and usually all pieces of information to be reconstructed are driven by state variables. Based on the model, one can try to design an explicit dynamical system whose state should give an estimate of the actual state of the considered model. The considered model can be either continuous-time or discrete-time, deterministic or stochastic, finite-dimensional or infinite-dimensional. However, in this thesis, we will consider only finite-dimensional, deterministic continuous-time state space descriptions.

The role of an observer is to estimate in real-time the plant state based on the measurement from the sensor. This means that this measured signal somehow contains enough information

to determine uniquely the whole state of the system; namely the system is *observable*. Before dealing with the observer design for the dynamical systems, we need firstly to analyze whether the states of the studied dynamical system are observable or not. This property is named as *observability* in the literature.

In general, observability, defining the possibility to estimate internal states of the studied system via the available measurement and its derivatives Besançon [2007], has already been widely studied for different types of dynamical systems. Using the elementary algebraic method to analyze observability can be dated back to 1960s in the work of Kalman for linear dynamical systems Kalman [1960]. However, the generalization of the similar theory to nonlinear dynamical systems is not so trivial. Furthermore, the observability property is no longer a global property for nonlinear systems since at some local points or sets the observability can be lost. Therefore, we start with the classification of observation problems i.e. to study the different approaches to analyze the observability of the systems and to study the dynamical systems that suffers from observability defects. Observability defects can be defined as a point or set of points for which a system loses its observability or becomes unobservable rendering the whole system unobservable at those points. Since those observability defects hinder the application of designing an observer for such systems therefore, a main concern is to provide some techniques that can avoid (e.g. through state constraints which requires limiting convexity assumptions) or remove (by modifying the system around singularity) those defects.

**Note: The text is largely inspired by the works of Besançon [2007]; Khalil [2017] and Bernard [2019].**

The main subject of the thesis is to synthesize the observers for a class of nonlinear systems i.e. nonlinear oscillators and the nonlinear systems perturbed by such oscillators that suffer from observability defects. Nonlinear oscillators have attracted a remarkable research attention in the past and current literature. The reason of this interest rely on several engineering applications where an effective and robust solution to this problem is crucial. The problem of frequency estimation of a harmonic oscillator has gained notable scholarly interest since 1900s Marino and Tomei [2002]; Ziarani and Karimi-Ghartemani [2005]. For example the problems of harmonic disturbance compensation in automatic control, design of phase-looked loop circuits in telecommunication, adaptive filtering in signal processing, etc. Another class of nonlinear oscillators refered to as Hopf oscillators is also considered in this thesis. Examples of Hopf oscillators can be found in applications as diverse as biological rhythms modeling Medvedev and Cisternas [2004], epidemiology Hethcote et al. [1999], ecosystems Fussmann et al. [2000], chemical kinetics Moehlis [2002], robotics Seo et al. [2010] and fluid mechanics Shen [1991]; Noack et al. [2003]. Nonlinear dynamical systems are often affected by periodic disturbances whose knowledge and especially their frequency are of interest to control the system. In such a case, it is relevant to

rebuild this information that can not be directly accessed. Many various systems can be considered: medical diagnosis Sadelli et al. [2015, 2016], medical microrobots Gangloff et al. [2006]; Fruchard et al. [2013], frequency hopping communications or phase locking loop systems Bodson [2005] etc. However, these nonlinear oscillators suffer from observability defects such that the systems becomes unobservable at certain points. Therefore, a study of nonlinear oscillators with observability defects is presented that constitutes a main contribution of the thesis. Different approaches have been studied before to avoid these defects, a few of those will be presented in this work with their application to different systems for example biomedical microrobots and fluid mechanics, that suffers from those observability defects. Providing a way to tackle those observability defects will further lead to the second objective of the thesis i.e. propose an observer for the nonlinear oscillators in the presence of those observability defects.

Observer theory for linear systems is well-understood and many observers have been designed for both single and multi-output cases, most prominent being Luenberger observer Luenberger [1971] and Kalman filter Kalman and Bucy [1961]. Observers for nonlinear systems however are much more challenging to design and still suffer from a significant lack of generality. Nonlinear observer research has received considerable attention since early 1980s Krener and Isidori [1983]. In general for the nonlinear systems, many approaches can be found in the existing literature, among which some are mentioned in here as follow: Filtering approach based on extending the Kalman filter to deterministic nonlinear systems (Extended Kalman Filter: EKF), its convergence is guaranteed under some hypotheses for example, Baras et al. [1988] for local asymptotic convergence in the case of control affine nonlinear systems, and Deza et al. [1992]; Boizot et al. [2010] for the global stability limited to a particular class of nonlinear systems. Actually observer design may be more or less straightforward depending on the coordinates we choose to express the system dynamics. For instance, dynamics which seems nonlinear at first sight could turn out to be linear in other coordinates. Hence the importance of the choice of the coordinates for observer design. In this approach, the most widespread method is the error linearization method Krener and Isidori [1983]; Krener and Respondek [1985]; Xia and Gao [1989]; Phelps [1991]; Glumineau et al. [1996]; Respondek et al. [2004]; Zheng et al. [2007], which consists of characterizing nonlinear systems that can be transformed via change of coordinates and output variables into a linear system plus a nonlinear term depending only on the inputs and outputs measurement. These systems can be observed using Luenberger observer. Another approach for the error linearization problem has been proposed in Kazantzis and Kravaris [1998]; Kravaris et al. [2007]; Andrieu [2014]. Under some local observability hypothesis, the authors propose a change of variables resulting from the resolution of a linear first order PDE. From observability point of view, all the above mentioned classes of systems are similar to the class of linear systems in the sense that the observability is not affected by inputs. An extension to these

works is to characterize nonlinear systems which are observable independently on the inputs. For single output systems Gauthier et al. [1992]; Gauthier and Kupka [1994], this characterization is completely determined by a normal form of observability (in the local generic sense), and a high gain observer can be designed. Some extensions to multi-output systems have been proposed in literature Bornard and Hammouri [1991]; Ciccarella et al. [1993]; Gauthier and Kupka [1996]; Schaffner and Zeitz [1999]; Hammouri et al. [2002]; Shim et al. [2001]; Hammouri and Farza [2003]; Hammouri et al. [2010]; Farza et al. [2011]; Oueder et al. [2012]. All the observers proposed for nonlinear oscillators are generally based on a normal form of observability and the design of such an observer requires an inverse transformation.

The first idea of normal form is due to Bestle and Zeitz [1983] for non-autonomous nonlinear dynamical systems and Krener and Isidori [1983] for autonomous nonlinear dynamical systems where the authors introduced the so-called observer canonical form with output injection with all nonlinear terms being only function of the output. Then Krener and Respondek [1985] gave the associated canonical form with output injection for multi-output nonlinear dynamical systems without inputs, and the result for multi-output systems with inputs was studied in Xia and Gao [1989]. Based on the above works many algorithms have been developed to generalize the existing results, e.g. Phelps [1991]-algebrain approaches, Lynch and Bortoff [2001] geometric approaches. It can be noted that the diffeomorphism required to obtain normal forms are generally local and consequently less applicable for state estimation (only the trajectories that are in the domain of the transformation can be estimated). This problem has been extensively addressed in the control context in Gauthier and Kupka [1996]; Jouan and Gauthier [1996], and the details are available in Gauthier and Kupka [2001].

Since the nonlinear observer synthesis for the nonlinear oscillators and nonlinear dynamical systems disturbed by period oscillations requires a transformation of the original coordinates into observability normal forms, it follows that the dynamics of the system and of the observer are expressed in different coordinates and may even evolve in spaces of different dimensions. It is therefore necessary to invert the transformation to deduce the estimate in the original system coordinates. However, although the transformation for such nonlinear oscillators is generally well-known, its inversion can be difficult in practice. When an explicit expression of a global inverse is not available (that is the case for most of nonlinear systems), numerical inversion usually relies on the resolution of a minimization problem with a heavy computational cost. To avoid such inversion involving high computational time and cost, a lot of research has been done in this direction. For example, in the case where the transformation is a diffeomorphism, one may hope to avoid this minimization by expressing the observer dynamics in the system original coordinates via jacobian inversion instead of inversion of the mapping for each state (e.g. Deza et al. [1992]; Maggiore and Passino [2003]; Astolfi and Praly [2013]; Menini et al. [2017]; Astolfi and Possieri

[2019]).

Contrary to normal forms based on diffeomorphism transformations, the construction of an observer based on immersion techniques is a difficult task. The reasons are many and varied: the nonlinear elements of the dynamics of normal forms are generally unknown, the observer requires an inversion procedure necessitating an optimization algorithm, thereby increasing calculation times. Different solutions have been proposed regarding the solution of such issues e.g. a solution proposed consists in modifying the observer dynamics to force its state to remain in diffeomorphism image by either adding a term in the dynamics Astolfi and Praly [2013] or using carefully designed complex saturations Maggiore and Passino [2003]. However this must be done with care since it can easily destroy the observer performances (in particular convergence): extra convexity assumption are typically required on the diffeomorphism image to implement such methods. In more general case where the transformation is not a diffeomorphism, but an injective immersion, namely, the target space has a larger dimension that the system domain, some ideas have been proposed such as using Newton-like or gradient algorithms to inverse the transformation in Astolfi and Possieri [2019] and Menini et al. [2017], or continuation algorithms which "follow" the "optimal" inverse image in Hammouri et al. [2018]. However, in those cases, the convergence is only local and Hammouri et al. [2018] needs to verify a convexity assumption. A widely used method for the harmonic oscillators was suggested by Andrieu et al. [2014]; Bernard et al. [2015, 2018] for the cases when observer dynamics are of greater dimension compared to the system coordinates, where it allows to deduce the observer in system original coordinates by extending the image of diffeomorphism. The final objective of this is therefore to provide a methodology for the nonlinear oscillators for synthesizing the observer in original coordinates that are capable of handling the observability defects.

The objectives of this thesis can be summarized as:

1. For a certain class of systems i.e. nonlinear oscillators and nonlinear systems disturbed by harmonic oscillations, provide a detailed observability analysis and point out the observability defects.

2. Propose a methodology that can help to tackle those observability defects for the nonlinear systems without changing the internal dynamics of these systems.

3. Synthesize different observers for the nonlinear oscillators that are capable of handling the observability defects.

4. To get the observer back in system original coordinates, based on jacobian completion, extend the mapping image to a global diffeomorphism and to get the inverse transformation from target coordinates back to original system coordinates.

5. Provide a nonlinear dynamical model for the microrobot system including the blood velocity and pulse rate, study the observability of the system and based on the observability analysis, propose an observer that can handle the observability defects of the microrobot system.

6. Present several wake flow dynamical models and analyze the observability of each model. Then build observers for each model that can provide a way around observability singularities existing in the system and provide a comparison for different designed observers by simulating the system in several cases, e.g. observability defects avoidance and noise measurement to check the robustness of the proposed observers.

## 2) Outline of the manuscript & contributions

The outline of the thesis is given as:

**Chapter 1** By offering some insights on the ideas of observability, the first chapter gives a broad overview of the observer and observation theory. The transformation methods are briefly reviewed after that, with an emphasis on some well-known transformations that exist and are widely used for designing nonlinear observers. Since the thesis only covers the observers with global and tunable convergence, a recall on existing literature on the observers is presented. By the end of the first chapter, a brief discussion of the techniques for inverting the transformation to bring the observer back to system original coordinates from target coordinates is provided.

**Chapter 2** The second chapter highlights our main contributions of the dissertion i.e. the observer synthesis of the nonlinear oscillators and nonlinear dynamical systems affected by harmonic oscillations that suffer from observability defects. Such observability defects need to be addressed since they make the system unobservable and thus the observer synthesis is no longer possible for such systems. The chapter therefore recalls the methodology to avoid the observability defects. The observability defects avoidance is presented and is further applied to the nonlinear oscillators and nonlinear systems affected by harmonic oscillations. Another main concern of study is the inversion of transformation in order to get the observer in the original system's coordinates. Based on previous analysis, singularities and immersion techniques, this is not always an easy task. Also, the observability defects avoidance makes it harder to get the observer in original coordinates since it increases the target coordinates dimension compared to the system original coordinates. Therefore, we mainly address and provide a way of achieving a global diffeomorphism for the particular cases by extending the image of diffeomorphism through coordinate augmentation and jacobian completion. The provided methodology is then applied to the three systems for which the target coordinate dimension is greater than the

system, and the effectiveness of the proposed technique is then studied. The chapter ends with the general proposition for the observer in original coordinates irrespective of the system and observer dimensions.

**Chapter 3** There has been growing interest in the development of therapeutic microrobots since such systems have the potential to revolutionize many aspects of medicine. Therefore, in the third chapter, a nonlinear observer is developed for the application of microrobots. Based on the position of microrobot inside the human body using the imager/sensor, the observer will estimate the robot velocity as well as the blood velocity and the pulse rate. Another issue in such systems is that they suffer from observability defects, therefore based on the methodology studied in the previous chapter, an observer is proposed that is capable of providing a way around the singularity. At the end of this chapter, simulations illustrate the performance and effectiveness of the proposed observer in the presence of observability defects.

**Chapter 4** The last chapter begins with the introduction of the wake flow dynamics, its impact on the energy consideration, and the motivation behind estimating and further reducing the drag force in order to minimize the energy consumption. In this work, we study four models for the wake flow dynamics, where for each model, three observers are synthesized. Since each model also suffers from observability defects, the designed observers are capable of avoiding those observability defects in an effective manner. By the end of each section, simulations are carried out for different cases, particularly to provide a comparison between the three observers in the presence of observability defects and the measurement noise at high frequencies. The chapter ends with the conclusion of already-done approaches and with some perspectives regarding the experimental analysis of the wake flow dynamics.

**Publications**

**International Conferences**

**J. Ahmed**, E. Courtial, P. -Y. Passaggia, M. Fruchard and N. Mazellier, "Nonlinear Observer for the turbulent wake of a square cylinder," 2020 59th IEEE Conference on Decision and Control (CDC), 2020, pp. 5421-5427, doi: 10.1109/CDC42340.2020.9304341.

**J. Ahmed**, M. Fruchard, E. Courtial and Y. Touré, "Low-power High Gain Observers for Wake Flow Rebuild," 2020 59th IEEE Conference on Decision and Control (CDC), 2020, pp. 5428-5434, doi: 10.1109/CDC42340.2020.9304507.

**Article**

**J. Ahmed**, M. Fruchard and E. Courtial "Singularity-free limited high gain observer for Andronov-Hopf oscillators", Automatica (has been submitted in 2023).

Chapter 1

# Observability and Observer Design

## Chapter Content

## 1.1 Introduction

This chapter begins with a presentation of the state-space models and notations, then states the observation issue before providing an overview of different existing observer design tools. Before dealing with the observer design for dynamical systems, we need firstly to analyze whether the states of the dynamical system are observable or not. This property is refered to as observability in the literature. Therefore, this chapter aims at recalling the existing results on observability analysis approaches and on observer synthesis techniques for dynamical systems. We start with the classification of observation problems, the different approaches to analyze the observability and the categories of observers. Thence, we recall several important definitions for the observability of nonlinear dynamical systems. For some nonlinear systems, there exist some points for which the system remains no longer observable. The existence of such singular points makes the system unobservable, leading to observability defects detailed in this chapter. Another major concern for the nonlinear systems is that it is not always possible to design an observer in original coordinates. We present some observer normal forms for which global observers already exist. Some well-known observers are then summarized, including Luenberger observer, high gain observer and so on. By the end of this chapter, some techniques to get the observer from normal forms back to the original coordinates are briefly discussed.

*Notation.* To avoid repetitions, we present some notations that will be carried throughout the thesis. We denote with $\mathbb{R}$ the set of real numbers, with $\mathbb{Z}$ the set of integers and $\mathbb{Z}_{>0} = \{1, 2, \ldots\}$. $I_i$, or simply $I$, is an identity matrix of dimension $i \in \mathbb{Z}_{>0}$ and $0_{i,j}$ is a zero matrix of dimension $i \times j$, with $i, j \in \mathbb{Z}_{>0}$. We denote a triplet in *prime form* $(A_i, B_i, C_i)$ of dimension $i \in \mathbb{Z}_{>0}$, the set of matrices of the form:

$$A_i = \begin{pmatrix} 0_{i-1,1} & I_{i-1} \\ 0 & 0_{1,i-1} \end{pmatrix}, B_i = \begin{pmatrix} 0_{i-1,1} \\ 1 \end{pmatrix}, C_i^T = \begin{pmatrix} 1 \\ 0_{i-1,1} \end{pmatrix}.$$

$L_f$ denotes the Lie derivative of any function along the vector field $f$ so the Lie derivative of a function $h$ along $f$ is denoted as $L_f h(x) = \frac{\partial h}{\partial x} f(x, u)$.

## 1.2 Observation Statement and Observability

### 1.2.1 Model Under Consideration

We consider a general real system/process described by a finite-dimensional continuous-time nonlinear dynamic model of the form:

$$\Sigma_x : \begin{cases} \dot{x} = f(x, u) \\ y = h(x), \end{cases} \tag{1.1}$$

where $x \in \mathcal{X} \subset \mathbb{R}^{n_x}$ is a state vector, $u \in \mathcal{U} \subset \mathbb{R}^{n_u}$ is an input vector and $y \in \mathbb{R}^{n_y}$ is an output vector of dimensions $n_x$, $n_u$ and $n_y$ respectively. The state vector $x_0 \in \mathcal{X} \subset \mathbb{R}^{n_x}$ and the input vector $u_0 \in \mathcal{U} \subset \mathbb{R}^{n_u}$ are confined into the sets $\mathcal{X}$,$\mathcal{U}$ respectively, such that any solution of (1.1) initialized at $x_0, u_0$ are defined on $[0, +\infty)$ and remains in $\mathcal{X}$ and $\mathcal{U}$ at all positive times. The functions $f$ and $h$ are assumed to be smooth, i.e., $f \in \mathcal{C}^\infty$ and $h \in \mathcal{C}^\infty$ with respect to their arguments. The system (1.1) is said to be a single-output system if the integer $n_y$ is equal to 1, and a multi-output system if $n_y \geq 2$.

Among the nonlinear systems, some specific forms of state space representations can be distinguished:

- The autonomous systems: $\dot{x} = f(x), \quad y = h(x)$.
- The control-affine systems: $\dot{x} = f(x) + g(x)u, \quad y = h(x)$.

### 1.2.2 Observation statement

Given a system (1.1), there is a general need to know $x(t)$ in order to act on or to monitor the system. However in reality one has only access to the input $u$ and the output $y$ (through sensors) of the system. Consequently, the observation issue can be formulated as follows:

*Observation problem*: For a given system described by a representation (1.1), find an estimate $\hat{x}(t)$ of $x(t)$ from the knowledge of $u(t'), y(t')$ for $0 \leq t' \leq t$.

In order to deal with the observation problem, a first naive approach is to look for a solution in terms of optimization i.e. find the best estimate $\hat{x}(0)$ of $x(0)$ that can explain the evolution of $y(t')$ over $[0, t]$ and by integrating (1.1) from $\hat{x}(0)$ and under $u(t')$, get an estimate $\hat{x}(t)$.

$$\hat{x}(t) = argmin_{\hat{x}_f} \int_0^t |Y(t', \hat{x}_f, u) - y(t')|^2 dt', \tag{1.2}$$

where $Y(t', \hat{x}_f, u) - y(t')$ denotes the output at time $t'$ of the solution to (1.1) going through $\hat{x}_f$ at time $t$.

In order to cope with disturbances, one should rather optimize the estimate of some initial states over a moving horizon Zimmer [1994], i.e., to solve online at each iteration or rather with a finite memory window:

$$\hat{x}(t) = argmin_{\hat{x}_f} \int_{t-\bar{t}}^t |Y(t', \hat{x}_f, u) - y(t')|^2 dt'. \tag{1.3}$$

Some methods have been developed to solve this optimization problem online, in spite of its non-convexity and the presence of local minima (e.g. Alamir [1999]; Michalska and Mayne [1995];

Zimmer [1994] or see Alamir [2007] for a survey of existing algorithms). Such algorithms are often denoted as *finite horizon observers* or *moving horizon estimators* and the theory is usually developed in the discrete time context. It takes advantages of its systematic formulation, but suffers from the usual drawbacks of nonlinear optimization (computational burden, local minima ...).

An alternative approach is based on the idea that if one knows the initial value $x(0)$ through the current value of the output $y(t)$, one can get an estimate from $x(t)$ by simply integrating (1.1) from $x(0)$. The feedback-based idea is that if $x(0)$ is unknown, one can try to correct online the integration $\hat{x}(t)$ of (1.1) from some erroneous $\hat{x}(t)$, according to the measurable error $h(\hat{x}(t)) - y(t)$, namely to look for an estimate $\hat{x}(t)$ of $x(t)$ as the solution of a system:

$$\dot{\hat{x}}(t) = f(\hat{x}(t), u(t)) + k(h(\hat{x}(t)) - y(t)). \tag{1.4}$$

Such a dynamical system is refered to as an *observer*, and the above equation is the most common form of an observer for a system (1.1) (In the case of linear systems, the reader can refer to Kalman and Bucy [1961]; Luenberger [1966]).

More generally, an observer can be defined as follows:

**Definition 1 (Observer Besançon [2007])** *Considering a system described by the model (1.1), an observer is given by a dynamical equation:*

$$\dot{\hat{x}}(t) = \mathcal{F}(\hat{x}(t), u(t), y(t)) \tag{1.5}$$

*such that:*

*(i)* $\hat{x}(0) = x(0) \Rightarrow \hat{x}(t) = x(t), \quad \forall t \geq 0;$

*(ii)* $||\hat{x}(t) - x(t)|| \to 0$ *as* $t \to \infty;$

- *If (ii) holds for any* $x(0), \hat{x}(0)$*, the observer is* ***global****.*
- *If (ii) holds with exponential convergence, the observer is* ***exponential****.*
- *If (ii) holds with a convergence rate which can be tuned, the observer is* ***tunable****.*

The difference $||\hat{x} - x||$ will be refered to as *estimation error* or *observation error*.

Therefore the observation problem becomes a problem of observer design. Typically, when addressing the state observation problem for a dynamical system, we need to take into account the following two important issues:

- Is it possible to reconstruct the internal information (state $x$) over a time interval with the available information i.e. the output $y$, the input $u$ and their successive derivatives?

- How to design an observer that enables us to reconstruct the whole state $x$ with the available information?

The first issue is related to the concept of *observability* and is addressed in the following section.

### 1.2.3 Nonlinear Observability

An observer is a dynamical system relying on the measurable variables (inputs and outputs) to estimate the unmeasurable states of a dynamical system. This requires that the measurable signals $u(t)$ and $y(t)$ in some way contain sufficient information to reconstruct the overall state of the system $x(t)$, in other words, the system has to be observable. Observability is an intrinsic property of the system and a prerequisite towards the design of an observer. The purpose of this section is to discuss some conditions required on the system for possible solutions to the observer problem. Such conditions are usually called *observability* conditions. In short, they must express that there indeed is a possibility that the purpose of the observer can be achieved, namely that it might be possible to recover $x(t)$ from the only knowledge of $u$ and $y$ up to time $t$. At a first glance, this will be possible only if $y(t)$ bears the information on the full state vector when considered over some time interval. We define $X(t, x_0, u)$ as the solution of the dynamical system (1.1) at time $t$ with initial condition $x_0$ and input $u$ and $Y(t, x_0, u) = h(X(t, x_0, u))$ as the associated (1.1) output.

We first briefly recall some notions of observability i.e. the necessary or sufficient conditions that the model of the system must verify in order for an observer to exist.
In order to design an observer, a detectability property must be satisfied.

**Definition 2 (Detectability)** *System (1.1) is detectable for any $u$ in $\mathcal{U}$ and for any $(x_0', x_0'')$ in $\mathcal{X} \times \mathcal{X}$ such that*

$$Y(t, x_0', u) = Y(t, x_0'', u) \quad t \geq 0,$$

*if we have*

$$\lim_{t \to \infty} ||X(t, x_0', u) - X(t, x_0'', u)|| = 0.$$

In order to design a tunable observer, one must be able to reconstruct the state via the output measured from the initial time, and more particularly to recover the corresponding initial value of the state. Accordingly, the observability is characterized by the fact that, one must be able to distinguish between various initial states from an output measurement, or equivalently, one cannot admit *indistinguishable* states (following Hermann and Krener [1977]).

**Definition 3 (Indistinguishability)** *A pair* $(x_0', x_0'') \in \mathcal{X} \times \mathcal{X}$ *is indistinguishable for a system* (1.1) *if:*

$$\forall u \in \mathcal{U}, \quad \forall t \geq 0, \quad Y(t, x_0', u) = Y(t, x_0'', u). \tag{1.6}$$

Based on the definition, we can deduce that if two solutions are not distinguishable from the output, they necessarily converge to each other asymptotically. This ensures that, regardless of the initial conditions, one still obtains an asymptotic estimate.

Using Taylor series expansion to express $Y(t, x_0, u)$ in terms of its derivatives at time 0, one can see that distinguishability is linked to the upcoming differential definitions of observability. So following Definition 3, we can now introduce different differential geometry based observability definitions for the nonlinear dynamical system (1.1).

**Definition 4 (Global Observability)** *A system* (1.1) *is globally observable if it does not admit any indistinguishable pair in* $\mathcal{X} \subset \mathbb{R}^{n_x}$.

This definition is quite general (global), and even too general for practical use, since one might be mainly interested in distinguishing states from their neighbors. This brings us to consider a weaker notion of observability.

**Definition 5 (Weak Observability)** *A system* (1.1) *is weakly observable at* $x$ *if there exists a neighborhood* $\Omega$ *of any* $x$ *containing no indistinguishable state from* $x$.

**Definition 6 (Local Weak Observability)** *A system* (1.1) *is locally weakly observable if there exists a neighborhood* $\Omega$ *of any* $x$ *such that for any neighborhood* $V$ *of* $x$ *contained in* $\Omega$*, there is no indistinguishable state from* $x$ *in* $V$ *when considering time intervals for which trajectories remain in* $V$.

This notion of local weak observability requires that each state can be distinguished from its neighbors without going too far i.e. in its neighborhood $V \subset \mathcal{X}$. This notion is of great interest in practice, and also presents the advantage of admitting some *rank condition* characterization i.e. differential geometry characterization.
Such a condition relies on the notion of *observation space* which corresponds to the space of all observable states:

**Definition 7 (Observation Space)** *The observation space for a system* (1.1) *is defined as the smallest real vector space (denoted by* $\mathcal{O}$*) of* $\mathcal{C}^\infty$ *functions containing the components of* $h$ *and closed under Lie derivative along* $f_u := f(., u)$ *for any constant* $u \in \mathcal{U} \subset \mathbb{R}^{n_u}$ *and for any vector field* $T \in \mathcal{O}$, $L_{f_u} T \in \mathcal{O}$.

**Definition 8 (Observability Rank Condition)** *A system (1.1) is said to satisfy the observability rank condition if:*

$$\forall x_0 \in \mathcal{X}, \quad dim\, \mathrm{d}\mathcal{O}(x_0) = n_x \tag{1.7}$$

*where* $\mathrm{d}\mathcal{O}|_x$ *is the observability codistribution i.e.,* $\mathrm{d}\mathcal{O}(x) = span(\mathrm{d}T(x) : T \in \mathcal{O})$.

The involutive codistribution $d\mathcal{O}$ can be built iteratively:

- $\mathrm{d}\mathcal{O}_0$=span $\mathrm{d}h$
- $\mathrm{d}\mathcal{O}_i = \mathrm{d}\mathcal{O}_{i-1} + L_f \mathrm{d}\mathcal{O}_{i-1}, \;\; i \geq 1$
- if $\exists\; n^* : \mathrm{d}\mathcal{O}_{n^*+r} = \mathrm{d}\mathcal{O}_{n^*} \;\; \forall r > 0$, then $\mathrm{d}\mathcal{O} = \mathrm{d}\mathcal{O}_{n^*}$.

**Remark 1** *Condition (1.7) is equivalent to the Kalman rank condition for linear time invariant (LTI) dynamical systems.*

Using the observability rank condition, we can then have the following theorem Hermann and Krener [1977].

**Theorem 1** *Hermann and Krener [1977] A system (1.1) satisfying the observability rank condition at* $x_0$ *is locally weakly observable at* $x_0$.

The aforementioned theorem offers a constructive way of checking the observability of the nonlinear dynamical system (1.1).

In practice, we usually consider the nonlinear dynamical system (1.1) without inputs i.e. the autonomous system (1.8). Indeed the feedback control $u$ in (1.1) is often a smooth function of the state $x$. This leads to investigate the observability of the autonomous system:

$$\begin{cases} \dot{x} = f(x) \\ y = h(x), \end{cases} \tag{1.8}$$

where $f$ and $h$ are assumed to be smooth. We can define a mapping between the output and the state by calculating higher order derivatives of $y$, which gives

$$\begin{bmatrix} y(t) \\ \dot{y}(t) \\ \vdots \\ y^{(k)}(t) \end{bmatrix} = \begin{bmatrix} L_f^0 h(x) \\ L_f^1 h(x) \\ \vdots \\ L_f^k h(x) \end{bmatrix} = \mathcal{O}_k(x), \tag{1.9}$$

where $L_f^k h$ are the so called $k$-$th$ Lie derivatives of $h$ in the direction of the vector field $f$ which will be detailed in the subsequent section, $y^{(k)}$ represents the $k$-$th$ time derivative

of $y$ and $\mathcal{O}_k$ is the observability map at order $k$. For a certain integer $k \geq n-1$, if $\mathcal{O}_k(x)$ is a local diffeomorphism, then we can reconstruct the state $x$ from the output and its derivatives.

Based on the observability rank condition 8 and Theorem 1, we briefly recall the definitions of *immersion* and *injective immersion*.

**Definition 9 (Immersion Gauthier and Kupka [2001])** *An immersion $T$ on an open set $\mathcal{X}$ is a map such that $\frac{\partial T}{\partial x}(x)$ is full-rank for all $x$ in $\mathcal{X}$.*

**Definition 10 (Injective immersion Gauthier and Kupka [2001])** *An injective immersion $T$ on an open set $\mathcal{X}$ is a map such that $T$ is injective and $\frac{\partial T}{\partial x}(x)$ is full-rank for all $x$ in $\mathcal{X}$.*

The following definition of differential observability is based on the analysis of the output $y$ and its successive time-derivatives $\dot{y}, \ddot{y}, \ldots, y^{(k)}, k \geq n-1$.

**Definition 11 (Differential observability Gauthier and Kupka [2001])** *Consider an autonomous system (1.8), there exists an integer $n_z \geq n_x$ such that the mapping $T : \mathcal{X} \subset \mathbb{R}^{n_x} \to \mathcal{Z} \subset \mathbb{R}^{n_z}$ is defined by:*

$$T(x) = \begin{pmatrix} L_f^0 h(x) \\ L_f^1 h(x) \\ \vdots \\ L_f^{n_z-1} h(x) \end{pmatrix}. \tag{1.10}$$

- *The system (1.8) is said to be weakly differentially observable if $T(x)$ is injective on $\mathcal{X}$ for all $x \in \mathcal{X}$.*
- *The system (1.8) is said to be strongly differentially observable if $T(x)$ is an injective immersion on $\mathcal{X}$ for all $x \in \mathcal{X}$.*

However, in general, the observability rank condition is not enough for a possible observer design owing to the fact that for the design of an asymptotic state observer for the nonlinear dynamical system (1.1), the observability condition also depends on the inputs, namely it does not prevent the existence of inputs for which the observability vanishes. This means that the purpose of observer design requires a look at the inputs. Notions of *universal inputs* and *uniform observability* and the corresponding propositions for systems (1.1) are introduced here (as in G. Bornard and Gilles [1995] for instance):

**Definition 12 (Universal Inputs)** *An input $u$ is universal for a system (1.1) if $\forall x_0 \neq x_0'$, $\exists t' \geq 0$ such that $y(t', x_0, u)) \neq y(t', x_0', u))$.*

*An input $u$ is a singular input if it is not universal.*

**Proposition 1** *An input $u$ is a universal input on $[0,t]$ for system (1.1) if and only if $\int_0^t ||y(t',x_0,u)) - y(t',x_0',u))||^2 dt' > 0$ for all $x_0 \neq x_0'$.*

In general, characterizing such singular inputs is not easy.

**Definition 13 (Uniformly Observable Systems (resp. locally))** *Gauthier and Bornard [1980] A system is uniformly observable (UO) if every input is universal.*

This property actually means that the observability is independent of the inputs and thus can allow an observer design to be also independent of the inputs. For systems which are not uniformly observable, observers will depend on the inputs, and not all inputs will be admissible. In this work we will assume that all inputs are universal and the system is uniformly observable and therefore maintain our focus on observers design for uniformly observable systems.

### 1.2.4 Observability Defects

We assume that the system under consideration is uniformly observable, and the inputs are universal. However it is sometimes the case that some state variables are structurally unobservable and therefore it is impossible to observe such state variables that are structurally unobservable. In such cases, if a proper observability analysis has to be carried out, the so-called *observability singularity set* can be determined. The observability singularity set can be defined as a set or a combination of points in the state space whereby the observability matrix is not full rank meaning that we loose access to information about certain state variables.

Suppose that $\forall x \in \mathcal{X}$, rank $d\mathcal{O}_k(x) \leq n_x$, so there may exist some subset $\mathcal{S} \subset \mathcal{X}$:

$$\mathcal{S} = \{x \in \mathcal{X} \subset \mathbb{R}^{n_x} : s(x) = 0\} : dim\ \mathrm{d}\mathcal{O}(x) < n_x. \tag{1.11}$$

where $s : \mathcal{X} \mapsto \mathbb{R}^{n_x}$.

The system (1.1) is observable $\forall x \in \mathcal{X} \backslash \mathcal{S}$, but some states are no longer observable on $\mathcal{S}$.

The following examples illustrate the procedure involved.

**Example 1** *Let us consider the following simple system:*

$$\begin{aligned} \dot{x}_1 &= x_2 + x_2^2 \\ \dot{x}_2 &= -x_2^3 + 1 \\ y &= x_1 \end{aligned} \tag{1.12}$$

*By computing the Lie derivatives of the corresponding output of the system, we get the following observability matrix*

$$d\mathcal{O}_1(x) = \begin{pmatrix} 1 & 0 \\ 0 & 1 + 2x_2 \end{pmatrix}, \tag{1.13}$$

*and the observability singularity set is consequently*

$$\mathcal{S}_1 = \{x \in \mathcal{X} \subset \mathbb{R}^2 : x_2 = -0.5\}. \tag{1.14}$$

*Even though we have a singularity at $x_2 = -0.5$, the system is observable because if we calculate further Lie derivatives of the output, we get:*

$$\mathrm{d}\mathcal{O}(x) = d\mathcal{O}_2(x) = \begin{pmatrix} 1 & 0 \\ 0 & 1 + 2x_2 \\ 0 & -8x_2^3 - 3x_2^2 + 2 \end{pmatrix} \tag{1.15}$$

*and there exists no longer any observability singularity for any $x \in \mathbb{R}^2$ so $\mathcal{S} = \emptyset$.*

Now we consider another system to understand why and how observability defects affect the system.

**Example 2** *Consider the system given by the following set of equations:*

$$\begin{aligned} \dot{x}_1 &= x_1 x_2 - x_1^3 \\ \dot{x}_2 &= 0 \\ y &= x_1. \end{aligned} \tag{1.16}$$

*Calculating the Lie derivatives of the output, we get the following observability matrix*

$$d\mathcal{O}_1(x) = \begin{pmatrix} 1 & 0 \\ x_2 - 3x_1^2 & x_1 \end{pmatrix}. \tag{1.17}$$

*It is straightforward that the system is singular for $x_1 = 0$, and the observability singularity set is:*

$$\mathcal{S}_1 = \{x \in \mathcal{X} \subset \mathbb{R}^{n_x} : x_1 = 0\}. \tag{1.18}$$

*The system (1.16) has an observability singularity for $x_s = (0 \ x_2)$, meaning that one cannot access to any information about the state variable $x_2$ when $x_1$ is null. Now if we compute the further derivatives of the system, we still get the observability matrix where the singularity at $x_1 = 0$ remains so $\mathcal{S} = \mathcal{S}_1$. Hence the system is only observable for $x \in \mathbb{R}^2 \backslash \{x_1 = 0\}$.*

It is clear that all the above systems seems to contain a singularity if considering only $\mathcal{O}_k$ involving the $(n-1)$ first Lie derivatives of $h$ along $f$. The system given by Example 1 is globally observable considering $\mathcal{O} = \mathcal{O}_2$, i.e., at the price of an observability map $\mathcal{O} : \mathcal{X} \subset \mathbb{R}^2 \to T_x\mathcal{X} \subset \mathbb{R}^3$. The situation is definitely different in Example 2 since $\mathrm{d}\mathcal{O}$ is singular on $\mathcal{S}$ whatever the differentiation order.

Based on the order of differentiating of the function $f$ along vector $h$, we can define the observability defects as:

- $\mathcal{S} : dim\ \mathrm{d}\mathcal{O}(x) < n_x, \quad \forall x \in \mathcal{S}$: Observability defect
- $\mathcal{S}_k : dim\ \mathrm{d}\mathcal{O}_k(x) < n_x, \quad \forall x \in \mathcal{S}_k$: Observability defect considering only $y^{(i)}, i \leq k$.

The handling of observability defects and the method to tackle such defects is one of the main contribution of this thesis and will be studied in detail in the next chapters.

## 1.3 Observer Normal Forms

From the design methodology point of view, there exist two different methods. The first method tries to directly design an observer. The second method usually relies on the transformation of the studied system into a simpler form (called as observer normal form) which enables us to apply existing observers.

Indirect methods for designing nonlinear observers are based on coordinates transformation techniques. For instance, dynamics which seem nonlinear at first sight could turn out to be linear in other coordinates (e.g. see Bestle and Zeitz [1983]; Guay [2002]; Hou and Pugh [1999]; Krener and Isidori [1983]; Krener and Respondek [1985]) so that the nonlinearities are dependent only on the measurable inputs and outputs of the system (Gauthier et al. [1992]; Bornard and Hammouri [1991]). Depending on the coordinates we use to describe the system dynamics, the design of an observer for nonlinear systems might be less or more complicated. The basic idea of the transformation techniques is to transform the original system into a canonical form, via a change of coordinates (a diffeomorphism) for which observer designs have already been proposed in the literature. By inverting the deduced diffeomorphism, we can obtain the state estimation of the original system.

However, due to the lack of a generic design method for nonlinear systems, different methodologies (e.g. Zeitz [1984]; Kazantzis and Kravaris [1998]; Gauthier and Kupka [2001]; Yi et al. [2018]) have been developed to transform the original system $\Sigma_x$ to a canonical or normal system, further denoted as $\Sigma_z$. Each method corresponds to an observer design method for a specific class of nonlinear systems. The application of some of these observation methods for a nonlinear system requires putting the nonlinear dynamics in a linear (Luenberger [1967]) or nonlinear (Besançon [2007]; Boutat et al. [2010]) canonical form of observability. To apply this technique, three important issues need to be taken into account:

- ***First issue***: The choice of the targeted normal form for which an observer can be easily designed via existing results;
- ***Second issue***: The deduction of the diffeomorphism which can transform the studied system into the target normal form.

- ***Third issue***: The inversion to express the state estimation in the original system.

In this section, we will focus on the first issue and recall some normal forms of observability for nonlinear systems. In the sequel, $\Sigma_x$ is refered to as the system in original coordinates and $\Sigma_z$ is refered to as the the system in target coordinates for which we obtain the observer normal form and on the basis of which the observer will be designed in the later sections.

### 1.3.1 Linearization By Output Injection

The problem of linearizing an autonomous nonlinear system was originally studied in Krener and Isidori [1983], that was later extended to multi-input multi-output systems by Krener and Respondek [1985]. In those papers, the authors looked for necessary and sufficient conditions on the functions $f$ and $h$ for the existence of a local change of coordinates which brings the system into a linear form, known as observer normal form. Among the literature Fliess and Kupka [1983], the problem of immersion into a bilinear system is studied and in the particular case of control affine systems, Bossane et al. [1989] gave conditions for the existence of a local (and global) immersion.

In Jouan [2003] and Besancon and Ticlea [2006], the general problem of finding an immersion (rather than a diffeomorphism) which transforms a nonlinear system into an observer normal form is addressed. If such a transformation exists, the system is linearizable by output injection.

**Theorem 2** *Jouan [2003] A nonlinear system given by (1.1) is linearizable by output injection if and only if there exists a transformation $T : \mathbb{R}^{n_x} \to \mathbb{R}^{n_z}$, transforming the system into the particular observer normal form*

$$\begin{aligned}
\dot{z}_1 &= z_2 + \varphi_1(u, z_1) \\
&\vdots \\
\dot{z}_i &= z_{i+1} + \varphi_i(u, z_1) \\
&\vdots \\
\dot{z}_{n_z} &= \varphi_{n_z}(u, z_1) \\
y &= C_{n_z} z,
\end{aligned} \tag{1.19}$$

*where $\varphi : \mathbb{R}^{n_u} \times \mathbb{R}^{n_y} \to \mathbb{R}^{n_z}$ is a continuous function containing the system (1.19) nonlinearities.*

Thus, the linearization problem reduces to the existence of a transformation, for some integer $n_z$, a continuous function $T : \mathbb{R}^{n_x} \to \mathbb{R}^{n_z}$ verifying

$$\frac{\partial T(x)}{\partial x} f(x, u) = A_{n_z} T(x) + \varphi(u, h(x)), \quad \forall x \in \mathcal{X}, u \in \mathcal{U}, \tag{1.20}$$

where the matrice $A_{n_z}$ is in prime form and $\varphi : \mathbb{R}^{n_u} \times \mathbb{R}^{n_y} \to \mathbb{R}^{n_z}$ is a continuous function. The existence of the transformation is difficult to check and involves quite tedious symbolic calculations which do not always provide the transformation itself, and even when they do, its validity is often only local and its injectivity on $\mathcal{X}$ is not guaranteed.. However if this transformation is injective, then the system is necessarily uniformly observable.

### 1.3.2 Hurwitz Form

In Andrieu and Praly [2006], a research methodology has been presented for transforming an autonomous nonlinear system into a Hurwitz autonomous form.

**Theorem 3** *An autonomous nonlinear system given by (1.8) can be transformed into the following Hurwitz form:*

$$\dot{z} = Az + \varphi(y) \tag{1.21}$$

*if and only if there exists a continuous function $T : \mathbb{R}^{n_x} \to \mathbb{R}^{n_z}$ that is uniformly injective for all $x \in \mathcal{X}$. $A$ is a Hurwitz matrix of dimension $n_z$ and $\varphi(y) : \mathbb{R}^{n_y} \to \mathbb{R}^{n_z}$, a continuous function.*

This raises the question of finding, for some integer $n_z$, a continuous function $T : \mathbb{R}^{n_x} \to \mathbb{R}^{n_z}$ verifying

$$L_f T(x) = AT(x) + \varphi(h(x)), \quad \forall x \in \mathcal{X} \tag{1.22}$$

with $A$ some Hurwitz matrix of dimension $n_z$ and $\varphi : \mathbb{R}^{n_y} \to \mathbb{R}^{n_z}$ some continuous function. It is required that $T$ be uniformly injective on $\mathcal{X}$ to deduce an estimate of $x$ from the estimate $\hat{z}$ of $T(x)$ . In Andrieu and Praly [2006], the authors proved that the injectivity of $T$ is achieved for almost any $2 \times 2$ block diagonal Hurwitz matrix $A$ of dimension $n_z = 2(n_x + 1)n_y$ with $z \in \mathbb{R}^{n_z}$ and for any $\varphi$ verifying some growth condition under the following assumption of backward distinguishability.

**Assumption 1 (Backward distinguishability)** *Assume there exists an open bounded set $\mathcal{X}_0$, such that system (1.8) is backward $\mathcal{X}_0$ distinguishable on $\mathcal{X}$, namely there exists $t' > 0$ such that for any trajectories $x'$ and $x''$ of (1.8) and any $t' \geq t$ such that $(x'(t), x''(t)) \in \mathcal{X} \times \mathcal{X}$ and $x'(t) \neq x''(t)$, there exists $\bar{t} \in [t - t', t]$ such that*

$$h(x'(\bar{t})) \neq h(x''(\bar{t})) \tag{1.23}$$

*and $(x'(\bar{t}), x''(\bar{t})) \in \mathcal{X}_0 \times \mathcal{X}_0$ for all $\bar{t} \in [t - t', t]$.*

In other words, their respective outputs become different in backward finite time and before leaving $\mathcal{X}_0$ or two different states in $\mathcal{X}$ can be distinguished in $\mathcal{X}_o$ from the past values of the output.

The difficulty lies in the computation of the function $T$, let alone its inverse.

### 1.3.3 Triangular Form

Triangular forms became of interest when Gauthier and Bornard [1980] related their structure to uniformly observable systems, and when Zeitz [1984] introduced the phase variable form for differentially observable systems.

**Definition 14** *A triangular form for the system given by (1.1) is the following:*

$$\begin{aligned}
\dot{z}_1 &= z_2 + \varphi_1(u, z_1) \\
&\vdots \\
\dot{z}_i &= z_{i+1} + \varphi_i(u, z_1, \ldots, z_i) \\
&\vdots \\
\dot{z}_{n_z} &= \varphi_{n_z}(u, z_1, \ldots, z_{n_z}) \\
y &= z_1,
\end{aligned} \tag{1.24}$$

*where $z \in \mathcal{Z} \subset \mathbb{R}^{n_z}$ and $\varphi_i$, $i = 1, ..., n_z$ are continuous functions.*

- The system 1.24 is said to be in Lipschitz triangular form if the functions $\varphi_i(u, .)$ are globally Lipschitz on $\mathbb{R}^{n_z}$ uniformly in $u$, i.e., there exists a constant $L$ in $\mathbb{R}$ such that for all $u$ in $\mathcal{U}$, all $(z, z')$ in $(\mathbb{R}^{n_z})^2$ and for all $i$ in $\{1, \ldots, n_z\}$

$$|\varphi_i(u, z_1, \ldots, z_i) - \varphi_i(u, z'_1, \ldots, z'_i)| \leq L \sum_{j=1}^{i} |z_j - z'_j|. \tag{1.25}$$

- The system (1.24) is said to be in phase variable form if $\varphi_i = 0 \ \forall i < n_z$ and only $\varphi_{n_z}$ is non-zero Zeitz [1984].

**Theorem 4** *Based on Definition 11, if an autonomous system (1.8) is weakly (strongly) differential observable and $n_z = n_x$ then, the function $T$ defined by the output and its $(n_z - 1)$ first derivatives such that*

$$T(x) = (h(x), L_f h(x), \ldots, L_f^{n_z - 1} h(x))^T, \tag{1.26}$$

*for a certain $n_z$, transforms the autonomous system into*

$$\begin{aligned}
\dot{z}_1 &= z_2 \\
&\vdots \\
\dot{z}_i &= z_{i+1} \\
&\vdots \\
\dot{z}_{n_z} &= L_f^{n_z} h(x) \\
y &= z_1
\end{aligned} \quad . \tag{1.27}$$

*This is a Lipschitz phase-variable form if and only if there exists a function $\varphi_k$ Lipschitz on $\mathbb{R}^{n_z}$ such that*

$$\forall L \in \mathcal{X}, \quad L_f^{n_z} h(x) = \varphi_{n_z}(T(x)). \tag{1.28}$$

The $n_z th$-derivative of the output can be expressed in a Lipschitz way in terms of its $(n_z - 1)$ first derivatives. This is possible for example if $\mathcal{X}$ is bounded and $T$ is an injective immersion.

### 1.3.4 Lipschitz Triangular Form For Multi-Output Systems

In the multi-output case $y \in \mathbb{R}^{n_y}$ with $n_y > 1$ such that the system is given by the following equations

$$\Sigma_x : \begin{array}{l} \dot{x} = f(x) \\ y = h(x) \end{array} \tag{1.29}$$

with $h(x) = (h^1(x), \ldots, h^{n_y}(x))^T$, the approach can be generalized with a target system $\Sigma'_z$ in phase variable form (see Hammouri et al. [2010] for a non phase variable form extension)

**Theorem 5** *The Lipschitz triangular form for the multioutput system (1.29) in phase variable form is given by*

$$\Sigma'_z : \begin{cases} \dot{z}' = A' z' + \varphi'(u, z') \\ y = C' z' \end{cases} \tag{1.30}$$

*with $z' \in \mathcal{Z} \subset \mathbb{R}^{n_z}$:*

$$z^i = T^i(x) = \begin{pmatrix} h^i(x) \\ L_f h^i(x) \\ \vdots \\ L_f^{n_{zi}-1} h^i(x) \end{pmatrix} \qquad \forall i = 1, 2, \ldots, n_y, \quad \sum_{i=1}^{n_y} n_{zi} = n_z. \tag{1.31}$$

$\varphi' = \begin{pmatrix} \varphi_{n_{z1}} & \ldots & \varphi_{n_{zp}} \end{pmatrix}^T$ *is a Lipschitz function.* $A'_{n_{zi}}$ *and* $C'_{n_{zi}}$ *are block diagonal matrices:*

$$A' = \begin{pmatrix} A_{n_{z1}} & & \\ & \ddots & \\ & & A_{n_{zp}} \end{pmatrix}, \quad C' = \begin{pmatrix} C_{n_{z1}} & & \\ & \ddots & \\ & & C_{n_{zp}} \end{pmatrix}. \tag{1.32}$$

*The mapping from original to target coordinates defined by*

$$T(x) = \begin{pmatrix} T^1(x) \\ T^2(x) \\ \vdots \\ T^{n_z}(x) \end{pmatrix} \tag{1.33}$$

*is an injective immersion from $\mathcal{X} \subset \mathbb{R}^{n_x}$ to $\mathcal{Z} \subset \mathbb{R}^{n_z}$.*

### 1.3.5 Gauthier-Kupka Canonical Form

**Theorem 6** *Gauthier and Kupka [2001] The system (1.1) admits a canonical Gauthier-Kupka form if there exists a diffeomorphism $T : x \mapsto z = T(x)$ such that the system (1.1) can be put in the following feedforward form:*

$$\begin{aligned} \dot{z}_1 &= \bar{f}_1(z_1, z_2, u) \\ &\vdots \\ \dot{z}_{n_z-1} &= \bar{f}_{n_z-1}(z_1, \ldots, z_{n_z}, u) \\ \dot{z}_{n_z} &= \bar{f}_{n_z}(z_1, \ldots, z_{n_z}, u) \\ y &= \bar{h}(z_1) \end{aligned} \tag{1.34}$$

*with the maps $\bar{h}(z_1)$ and $\bar{f}_i(z_1, \ldots, z_{i+1}, u)$ verifying:*

$$\frac{\partial \bar{h}}{\partial z_1} \neq 0, \quad \text{and} \quad \frac{\partial \bar{f}_i}{\partial z_{i+1}} \neq 0 \quad \forall i = 1, \ldots, n_z - 1. \tag{1.35}$$

*The condition $\frac{\partial \bar{f}_i}{\partial z_{i+1}} \neq 0$ is necessary for the system (1.34) to satisfy at any point the observability rank condition.*

We have presented some common observer normal forms for single and multi-output systems. After having chosen the targeted normal form for the nonlinear dynamical system (1.1), the key work is to seek for sufficient (and necessary if they exist) conditions such that there exists a diffeomorphism which can transform the system (1.1) into the chosen targeted normal form.

## 1.4 Recall on Nonlinear Observers

Consider the nonlinear dynamical system (1.1):

$$\Sigma_x : \begin{cases} \dot{x} = f(x, u) \\ y = h(x) \end{cases}$$

where $x \in \mathcal{X} \subset \mathbb{R}^{n_x}$, $u \in \mathcal{U} \subset \mathbb{R}^{n_u}$, $y \in \mathbb{R}^{n_y}$ and the functions $f$ and $h$ are smooth, i.e., $f \in \mathcal{C}^\infty$ and $h \in \mathcal{C}^\infty$. It is assumed that system (1.1) is locally uniformly observable in the sense that the observability rank condition (1.7) is satisfied for all $x \in \mathcal{X}$ and $u \in \mathcal{U}$. The objective is to reconstruct the state $x(t)$ from the measured output $y$.

In this thesis, we are only interested in global and tunable observers with guaranteed convergence. This excludes the Extended Kalman Filters (EKF), obtained by linearizing the dynamics and the observation along the trajectory of the estimate Gelb et al. [1974]. Indeed, the convergence is only local in the sense that the estimate converges to the true state if the initial error is not too large and the linearization does not present any singularity Bonnabel and Slotine [2014] and references therein.

### 1.4.1 Luenberger Observer

In a seminal paper Luenberger [1964], the original Luenberger observer design is presented for linear systems. It is shown that an observable system can be mapped to a stable linear mapping of the output by taking the output measurement as an input. The implementation of this observer from any initial condition enables to recover the state estimation by inverting this mapping. A nice contribution to the extension of the Luenberger observer for nonlinear systems by a linearization technique has been given by Zeitz [1987]. The algorithm proposed by Zeitz [1987] which also uses time derivatives of the input, is easy to implement but it does not in general guarantee the convergence of the observer. In Shoshitaishvili [1992]; Kazantzis and Kravaris [1998], the same idea of Luenberger [1966] i.e., mapping the plant dynamics to a linear mapping of its output is progressively extended to more and more general classes of nonlinear systems. In Andrieu and Praly [2006], the authors investigated the possibility of transforming an autonomous system into a Hurwitz autonomous form and designed an observer refered to as Kazantzis Kravaris Luenberger (KKL) observer or nonlinear Luenberger observer, a similar observer proposed by Kreisselmeier and Engel [2003].

Consider the non-autonomous system of the form (1.1) transformed into the Hurwitz form:

$$\dot{z} = A_{n_z} z + \varphi(u, y), \quad y = C_{n_z} z, \tag{1.36}$$

where $\varphi : \mathbb{R}^{n_u} \times \mathbb{R}^{n_y} \to \mathbb{R}^{n_z}$ is a continuous function. The following result presented in Bernard [2019] is inspired from Luenberger [1964] observer.

**Theorem 7 (Kazantzis-Kravaris Luenberger Observer)** *A nonlinear Luenberger observer, also refered to as Kazantzis-Kravaris Luenberger Observer, for the system (1.36) is given by*

$$\dot{\hat{z}} = A_{n_z} \hat{z} + \varphi(u, y) + K(y - C_{n_z} \hat{z}), \qquad \hat{x} = T\mathcal{T}(\hat{z}), \tag{1.37}$$

*where $\mathcal{T}$ is a continuous left-inverse of $T$ and $T$ is solution of the following partial differential equation:*

$$\frac{\partial T(x)}{\partial x} f(x, u) = A_{n_z} T(x) + \varphi(u, h(x)). \tag{1.38}$$

*and $K = [k_1, \ldots, k_{n_z}]^T$ represents the observer gain matrix that can be chosen such that $(A_{n_z} - K C_{n_z})$ is Hurwitz.*

For nonlinear systems, the solution $T(x)$ of equation (1.38) always exists for $n_z$ big enough and injectivity property being relaxed by the assumption 1 of backward distinguishability. Some sufficient conditions should be imposed for (1.1) (see Krener and Xiao [2002]). Moreover, it is required that $T$ be uniformly injective on $\mathcal{X}$ to deduce from the estimate of $\hat{z}$ of $T(x)$ an estimate of $x$. Hence if $T(x)$ is uniformly injective on $\mathcal{X}$, then we can conclude that $\hat{x}$ tends to $x$ asymptotically.

### 1.4.2 High Gain Observer (HGO)

The literature places a special emphasis on high gain observers (HGO). In the late 1980s, these observers became prevalent in the literature, since then, their simplicity in the structure and the high performance in noise-free environments have attracted a large attention.

Two key papers, published in 1992, represent the beginning of research on high gain observers. The work by Gauthier et al. [1992] started a line of work that is exemplified by Besançon [2003]; Busawon et al. [1998]; Deza et al. [1992]; Gauthier and Kupka [2001, 1994]; Hammouri et al. [2002]; Viel et al. [1995]. This line of research covered a wide class of nonlinear systems and obtained global results under global growth conditions. Teel and Praly [1994, 1995] built on the ideas of Esfandiari and Khalil [1992] and the earlier work by Tornambè [1992] to prove the first nonlinear separation principle and develop a set of tools for the semiglobal stabilization of nonlinear systems. Their work drew attention to Esfandiari and Khalil [1992], and soon afterward many nonlinear control researchers started using high gain observers e.g. Alvarez-Ramirez and Femat [1999]; Andrieu et al. [2009]; Byrnes et al. [2005]; Gonzalez-Trejo et al. [1999]; Isidori [1997, 2000]; Jiang et al. [1998]; Lin and Saberi [1997]; Maggiore and Passino [2005]; Praly [2003]; Praly and Jiang [2004]; Shim et al. [2001]; Shim and Teel [2003]; Ye [2000]. These papers have studied a wide range of nonlinear control problems including stabilization, regulation, and tracking. Many research publications have also addressed the high gain observer with adaptive parameter (for example see Praly [2003]; Oueder et al. [2012]; Ullah et al. [2019]; Andrieu et al. [2009]; Prieur et al. [2012]; Zemouche et al. [2018] and references therein).

The high gain observer is developed for systems in triangular forms or systems that can be mapped to such normal forms in which the error trajectories have an exponential decay rate. In Gauthier et al. [1992], this triangular observable canonical form has been employed to design a high gain observer for a single output uniformly observable control affine systems. The error trajectory decay rate can be set arbitrarily fast by a design parameter in the observer structure, usually called the *high gain parameter*, denoted by $\theta$ in the sequel Gauthier and Kupka [1994]; Farhangfar and Shor [2020].

#### 1.4.2.1 HGO: Single Output System

Consider the nonlinear model (1.1) with a single output ($n_y = 1$), we can obtain the Lipschitz triangular form given by:

$$\begin{aligned}
\dot{z}_1 &= z_2 + \varphi_1(u, z_1) \\
&\vdots \\
\dot{z}_i &= z_{i+1} + \varphi_i(u, z_1, \ldots, z_i) \\
&\vdots \\
\dot{z}_{n_z} &= \varphi_{n_z}(u, z_1, \ldots, z_{n_z}) \\
y &= z_1,
\end{aligned} \tag{1.39}$$

where $z \in \mathcal{Z} \subset \mathbb{R}^{n_z}$ and $\varphi_i(u, z)$ are Lipschitz functions, globally in $z$ and uniformly in $u$.

$$|\varphi_i(u, z_1, \ldots, z_i) - \varphi_i(u, z'_1, \ldots, z'_i)| \leq L \sum_{j=1}^{i} |z_j - z'_j|. \tag{1.40}$$

**Theorem 8 (Gauthier et al. [1992])** *A high gain observer for the system (1.39) is given by:*

$$\begin{aligned}
\dot{\hat{z}}_1 &= \hat{z}_2 + \varphi_1(u, \hat{z}_1) + \theta k_1(y - \hat{z}_1) \\
&\vdots \\
\dot{\hat{z}}_i &= \hat{z}_{i+1} + \varphi_i(u, \hat{z}_1, \ldots, \hat{z}_i) + \theta^i k_i(y - \hat{z}_1) \\
&\vdots \\
\dot{\hat{z}}_{n_z} &= \varphi_{n_z}(u, \hat{z}_1, \ldots, \hat{z}_{n_z}) + \theta^{n_z} k_{n_z}(y - \hat{z}_1)
\end{aligned} \tag{1.41}$$

*where the high gain parameter $\theta$ is taken sufficiently large (i.e. $\theta \geq \theta^* > 1$ with $\theta^*$; related to the Lipschitz constant $L$) and $k_i$ represents the observer gains where $k_i$'s should be chosen provided that the matrix $(A_{n_z} - KC_{n_z})$ is Hurwitz i.e. all eigenvalues are on the left half complex plane. Typically, the power of the high gain parameter increases up to $n_z$ ( i.e. $\theta^{n_z}$), where $n_z$ represents the dimension of the observer state.*

It has been proven that, for a large $\theta$, the system (1.41) is an exponential observer for the system (1.1). Since the gain is proportional to $\theta^{n_z}$, a large $\theta$ will yield a high gain, and this is the reason why this kind of observer is named as high gain observer (HGO). Another great property of HGO is the ability to tune their rate of convergence arbitrarily, which is the alternative for output feedback stabilization.

**Remark 2 (Peaking phenomenon)** *The advantage of the HGO methodology is that it always guarantees the existence of an exponentially convergent observer, thanks to the tuning of a unique*

*parameter, the high gain parameter $\theta$. However when $\theta$ is chosen large or when the state dimension $n_z$ is high, difficulties arise during the numerical implementation. Most importantly, the HGO exhibits the so-called peaking phenomenon during the transient phase, i.e. the estimated state variables exhibit large peaks whose magnitude is proportional to $\theta^{n_x-1}$. The peaking phenomenon was first pointed out by Esfandiari and Khalil [1992] as an important feature of high gain observers. While this phenomenon was observed earlier in the literature Mita [1977]; Polotskii [1978], the work of Esfandiari and Khalil [1992] showed that the interaction of peaking with nonlinearities could induce finite escape time.*

**Remark 3 (Measurement noise)** *Another serious challenge for the implementation of a high gain observer is the measurement noise. The effect of measurement noise is more prominent for high dimensional systems. The reason behind this issue is the dependence of the observer states on the derivatives of the output since the HGO is developed for systems transformed into observer normal forms. Therefore, if the output is corrupted by measurement noise, it is expected that the noise will impact the accuracy of the estimates as well. Bounds on the observation error for the HGO in the presence of measurement noise for the standard HGO have been studied, for instance, in Vasiljevic and Khalil [2006]; Ahrens and Khalil [2009]; Ball and Khalil [2009], and different techniques have been developed in order to improve noise rejection, mainly based on a gain adaptation or using a low pass filter (see, among others Boizot et al. [2010]; Sanfelice and Praly [2011]; Khalil and Priess [2016]).*

#### 1.4.2.2 HGO: Multi-Output Systems

The high gain observer design was further extended to multi-output systems by Hammouri and Farza [2003]; Hammouri et al. [2010].

Consider an autonomous nonlinear system with multi-outputs which are equivalent by diffeomorphism to systems of the form (1.30):

$$\begin{aligned} \dot{z}' &= A'_{n_z} z' + B'_{n_z} \varphi'(z) \\ y &= C'_{n_z} z' \end{aligned}$$

where $z' \in \mathcal{Z} \subset \mathbb{R}^{n_z}$ and $y \in \mathbb{R}^{n_y}$ with $n_y > 1$. The continuous function $\varphi'(z)$ and the matrices $A'_{n_z}, B'_{n_z}, C'_{n_z}$ are already defined in subsection 1.3.4.

**Theorem 9** *An observer for the multi-output autonomous nonlinear system (1.30) is given as:*

$$\dot{\hat{z}}' = A'_{n_z} \hat{z}' + B'_{n_z} \varphi'_s(\hat{z}) + \Delta' K' (y' - C'_{n_z} \hat{z}') \tag{1.42}$$

*where $\Delta' = (\Delta_1, \ldots, \Delta_{n_y})$ with $\Delta_i = (\theta, \ldots, \theta^{n_z})$ is the high gain matrix and the observer gain matrix $K = (K_1, \ldots, K_{n_y})$ with $K_i = (k_1, \ldots, k_{n_z})^T$ is chosen such that $(A'_{n_z} - K' C'_{n_z})$ is Hurwitz. $\varphi'_s$ is the saturated version and Lipschitz extension of $\varphi'$ such that $\varphi'_s = \begin{pmatrix} \varphi_{1s} & \ldots & \varphi_{n_y s} \end{pmatrix}$.*

We have presented the high gain observer for the multi-output systems that are uniformly observable. However, since the observer dynamics for each $z^i$ is the same as for standard HGO for the single output system, therefore it also suffers from the issues stated in Remark 2 and 3.

#### 1.4.2.3 Adaptive High Gain Observer

For the special triangular form (1.24), high gain observers can use a time-varying gain. In Praly [2003], an adaptive law has been proposed for triangular form (1.24) where the nonlinear function $\varphi(x_1, \ldots, x_i)$ could be non-Lipschitz, but was assumed to satisfy the following similar inequality:

$$|\varphi_i(u, z_1, z_2, \ldots, z_i) - \varphi(u, z_1, z_2', \ldots, z_i')| \leq \gamma(y)(|z_2 - z_2'| + \ldots + |z_i - z_i'|). \tag{1.43}$$

Based on this assumption, the following adaptive observer has been proposed in Praly [2003].

**Theorem 10 (Adaptive HGO Praly [2003])** *An adaptive high gain observer for the nonlinear system in triangular form (1.24) is given by:*

$$\begin{aligned}
\dot{\hat{z}}_1 &= \hat{z}_2 + \varphi_1(u, \hat{z}_1) + \theta k_1(y - \hat{z}_1) \\
&\vdots \\
\dot{\hat{z}}_i &= \hat{z}_{i+1} + \varphi_i(u, \hat{z}_1, \ldots, \hat{z}_i) + \theta^i k_i(y - \hat{z}_1) \\
&\vdots \\
\dot{\hat{z}}_{n_z} &= \varphi_{n_z}(u, \hat{z}_1, \ldots, \hat{z}_{n_z}) + \theta^{n_z} k_{n_z}(y - \hat{z}_1) \\
\dot{\theta} &= l(\theta, y) \\
y &= z_1.
\end{aligned} \tag{1.44}$$

*The high gain parameter $\theta$ is an extra state to be updated, $l$ is an $(n_z + 1)$ times continuously differentiable function that satisfies:*

$$l(\theta, y) = -\frac{1}{b}\theta\left(\frac{a}{3}(\theta - 1) - \frac{2(s-1)}{\sqrt{q}}\gamma(y)\right) \tag{1.45}$$

*such that*

$$\begin{aligned}
b > 0, \quad bQ \geq QD + DQ \geq -bQ \\
D = diag(0, \ldots, n-1).
\end{aligned} \tag{1.46}$$

*The parameters $k_i$ are chosen such that there exists strictly positive real numbers $q$ and $a$, and a symmetric matrix $Q$ satisfying:*

$$\begin{aligned}
QP + P^T Q \leq -aQ \\
qI \leq Q \leq I,
\end{aligned} \tag{1.47}$$

*where*

$$P = \begin{pmatrix} 0 & 0 & \dots & 0 & -k_1 \\ 1 & 0 & \dots & 0 & -k_2 \\ \vdots & \vdots & \ddots & \vdots & \vdots \\ 0 & 0 & \dots & 0 & -k_{n_z-1} \\ 0 & 0 & \dots & 1 & -k_{n_z} \end{pmatrix}. \tag{1.48}$$

By properly choosing the function $l$, it has been proven in Praly [2003] that the observer state asymptotically converge to system's one (1.24) even if its nonlinearity does not satisfy the Lipschitz condition.

#### 1.4.2.4 Limited High Gain Observer (LHGO)

The main drawback of the standard HGO is related to the increasing power (up to the order $n_z$) of the high gain parameter $\theta$, which makes the practical numerical implementation a hard task when $n_z$ or $\theta$ are very large. Motivated by these considerations, Astolfi and Marconi [2015] proposed a new observer for the autonomous single output system (1.8) transformed into Lipschitz triangular form given by (1.27). It preserves the same high gain feature of standard HGO but substantially overtakes the implementation problems due to the high gain by employing some relevant strategies i.e. reducing the power of the high gain parameter to the power of 2 instead of target system dimension $n_z$. The idea of the limited power of high gain parameter is refered to as Limited high gain observer (LHGO) and was seminally proposed in Astolfi and Marconi [2015] with a cascade of observers of dimension $2n_z - 2$.

The LHGO was proposed for the autonomous single output nonlinear system that can be transformed into the Lipschitz phase variable triangular form:

$$\dot{z} = A_{n_z} z + B_{n_z} \varphi(z), \qquad y = C_{n_z} z \tag{1.49}$$

where $z \in \mathcal{Z} \subset \mathbb{R}^{n_z}$ and the matrices $A_{n_z}$,$B_{n_z}$ and $C_{n_z}$ are all in their prime form.

**Theorem 11 (Limited high gain observer Astolfi and Marconi [2015])** *Let*

$$\begin{aligned} \dot{\zeta}_i &= A_2 \zeta_i + N\zeta_{i+1} + \Delta_2 K_i e_i, \; i \geq 1 \\ &\vdots \\ \dot{\zeta}_{n_z-1} &= A_2 \zeta_{n_z-1} + B_2 \varphi_s(\zeta) + \Delta_2 K_{n_z-1} e_{n_z-1} \end{aligned} \tag{1.50}$$

*with* $\zeta_i \in \mathbb{R}^2$, $\zeta_{0,2} = y$ *given by convention,* $e_i = \zeta_{i-1,2} - \zeta_{i,1}$, $\Delta_2 = \begin{pmatrix} \theta & 0 \\ 0 & \theta^2 \end{pmatrix}$, $K_i = \begin{pmatrix} k_{i1} & k_{i2} \end{pmatrix}^T$ *and* $N = \begin{pmatrix} 0_{2,1} & B_2 \end{pmatrix}$, $E_i = \begin{pmatrix} -K_i & C_2^T \end{pmatrix}$, $Q_i = \begin{pmatrix} 0_{2,1} & K_i \end{pmatrix}$.

*Choosing the high gain $\theta > \theta^* \geq 1$ as in Theorem 8 and gains $K_i$ such that the matrix $M$*

$$M = \begin{pmatrix} E_1 & N & 0 & \dots & & \dots & 0 \\ Q_2 & E_2 & N & \ddots & & & \vdots \\ 0 & \ddots & \ddots & \ddots & \ddots & & \vdots \\ \vdots & \ddots & Q_i & E_i & N & \ddots & \vdots \\ \vdots & & \ddots & \ddots & \ddots & \ddots & 0 \\ \vdots & & & \ddots & Q_{m-2} & E_{m-2} & N \\ 0 & \dots & & \dots & 0 & Q_{m-1} & E_{m-1} \end{pmatrix} \tag{1.51}$$

*is Hurwitz then*

$$\dot{\zeta} = \mathcal{F}_\zeta(\zeta, y) \tag{1.52}$$

*with $\mathcal{F}_\zeta$ given by (1.50) provides a low-power high gain observer for the system (1.49).*

**Remark 4** *Despite this dimension increase, the low-power ($\Delta_2 = \begin{pmatrix} \theta & 0 \\ 0 & \theta^2 \end{pmatrix}$ depends only on $\theta, \theta^2$) high gain observer advantage is twofold: the innovation term predominance is limited and the sensitivity to output noise is consequently reduced, especially at high frequencies which is of particular interest.*

**Remark 5** *We can use either $\hat{z} = P\zeta$ or $\hat{z}' = P'\zeta$ with the block diagonal projectors $P$ given by $I_2$ and $(n_z - 1)$ matrices $B_2^T$, and $P'$ given by $(n_z - 1)$ matrices $C_2$ and $I_2$.*

In Wang et al. [2017], the LHGO was shown to be effective for a much wider class of nonlinear systems, such as systems possessing a non-strict feedback form. The new LHGO is effective in all those frameworks where the standard HGO is typically used, such as output feedback stabilization by nonlinear separation principle and output regulation Astolfi et al. [2017]. In another paper by Morfin et al. [2020], an adaptive version of the LHGO was proposed for the nonlinear system in lower triangular form (1.24) with input dependent Lipschitz constant i.e., the Lipschitz constant of $\varphi$ depends on the value of the input $u$ living in a bounded but unknown compact set $\mathcal{U}$ for all $t \geq 0$.

#### 1.4.2.5 Low Peaking Limited High Gain Observer

Although the limited high gain observer structure solves the problem of numerical implementation, the peaking phenomenon is still present. In Astolfi et al. [2016, 2018], the authors previous work was refined by increasing the state dimension to $2n_z - 1$ and minimizing the peaking effect through the addition of saturation functions in the cascade structure.

**Theorem 12 (Low peaking LHGO Astolfi et al. [2016])** *Let $sat_{\kappa_i} : \mathbb{R} \to \mathbb{R}$ denote any strictly increasing $\mathcal{C}^1$ function that satisfies:*

$$sat_{\kappa_i}(s) := s, \quad |s| \leq \kappa_i, \quad |sat_{\kappa_i}(s)| \leq \kappa_i + \Delta_{\kappa_i}, \quad s \in \mathbb{R}, \tag{1.53}$$

*with*

$$\kappa_i := \max_{z \in \mathcal{Z}} |z_i| \quad i = 1, ..., n_z.$$

*Let the gain parameters $\alpha \in \mathbb{R}^{n_z}$, $\beta \in \mathbb{R}^{n_z - 1}$ be chosen so that $\Lambda_i(s)$ is Hurwitz and $\alpha_{n_z} > 0$ for any $s \in [0, 1]$. The matrices $\Lambda_i(s) \in \mathbb{R}^{2i \times 2i}$ are recursively defined as:*

$$\begin{aligned}
\Lambda_1 &:= E_1, \\
\Lambda_i(s) &:= \begin{pmatrix} \Lambda_{i-1}(1) & sB_{2(i-1)}B_2^T \\ K_i B_{2(i-1)}^T & E_i \end{pmatrix}, \quad i = 2, ..., n_z - 1, \\
\Lambda_{n_z} &:= \begin{pmatrix} \Lambda_{n_z - 1} & 0 \\ \alpha_{n_z} B_{2(n_z-1)}^T & -\alpha_{n_z} \end{pmatrix}
\end{aligned}$$

*with $K_i := \begin{pmatrix} \alpha_i \\ \beta_i \end{pmatrix}$ and $E_i := A_2 - K_i C_2$ for $i = 1, ..., n_z - 1$.*

*Then, there exists a high gain parameter $\theta$ such that $\theta \geq \theta_0 > 1$ so that the system described by the following equations*

$$\begin{cases} \dot{\hat{z}} = & \mathcal{F}_z(\hat{z}, \eta, y) \\ \dot{\eta} = & \mathcal{F}_\eta(\hat{z}, \eta, y) \end{cases} \tag{1.54}$$

*is a limited high gain observer for the system (1.8) with $\mathcal{F}_z, \mathcal{F}_\eta$ given as:*

$$\mathcal{F}_z : \begin{cases} \dot{\hat{z}}_i = \eta_i + \alpha_i \theta e_i, & i < n_z \\ \dot{\hat{z}}_{n_z} = \varphi_s(\hat{z}) + \alpha_{n_z} \theta e_{n_z} \end{cases} \qquad \mathcal{F}_\eta : \begin{cases} \dot{\eta}_i = sat_{\kappa_{i+2}}(\eta_{i+1}) + \beta_i \theta^2 e_i, & i < n_z - 1 \\ \dot{\eta}_{n_z - 1} = \varphi_s(\hat{z}) + \beta_{n_z - 1} \theta^2 e_{n_z - 1} \end{cases} \tag{1.55}$$

*with*

$$\begin{aligned}
e_1 &:= y - \hat{z}_1, \\
e_i &:= sat_{\kappa_i}(\eta_{i-1}) - \hat{z}_i, \quad i = 2, ..., n_z.
\end{aligned} \tag{1.56}$$

*$\hat{z} \in \mathbb{R}^{n_z}$, $\eta \in \mathbb{R}^{n_z - 1}$ are the observer states with $(\hat{z}_i, \eta_i)$ being the estimates of $(z_i, z_{i+1})$.*

The redesigned observer has a $2n_z - 1$ dimension co-distributed into $n_z$ blocks, which implements gains proportional to $\theta$ and $\theta^2$. Since the $i$th and $(i+2)$th derivatives of y, i.e. $z_i$ and $z_{i+2}$ are unknown, they are substituted in the redesigned observer by $\eta_{i-1}$ and $\hat{z}_{i+1}$ respectively, which are the second and first components of the $(i-1)$th and $(i+1)$th blocks. The so-called Low peaking LHGO is then designed by interconnecting the auxiliary variables $\eta_i$ and estimated

states $\hat{z}_i$. Since the relative degree between the output $y$ and the estimate $z_i$ is $r = i$ in the proposed observer, hence the sensitivity with respect to measurement noise is reduced. In addition, when the state $z$ of a plant evolves in a known compact set $\mathcal{K}$, the peaking phenomenon can be reduced by interconnecting each block through appropriate saturation functions. Consequently, the $n_z$ estimates $\hat{z}_i$ provided by the proposed observer are peaking-free whereas additional $n_z - 1$ auxiliary variables $\eta_i$ may attain values proportional to $\theta$ (rather than $\theta^{n_z-1}$ as in the standard HGO) during the transient phase.

**Remark 6** *The low peaking LHGO solves the aforementioned problems of the standard HGO (Remarks 2 and 3), however, the increased dimension of the observer is sometimes problematic and it may increase the size of the tuning parameter. Alongside, it involves a different and somewhat lengthy computational procedure selecting the gains which still remain difficult to find like for the standard HGO.*

#### 1.4.2.6 High Gain Observer With Lower Tuning Parameter

To overcome the issues related to the high gain observer, another idea was proposed in Zemouche et al. [2018] and further refined in Bouhadjra et al. [2020]. The standard HGO methodology with the same state observer structure of dimension $n_z$ is considered. In Zemouche et al. [2018], the authors proposed to decrease the tuning parameter $\theta^*$ which in turn decreases the gain power $\theta$. A compromise index labeled as $j_0$ was introduced, with $0 \leq j_0 \leq n_z$. Thence the power of the proposed high gain is limited to $j_0$ but at an expense of solving $2^{j_0}$ LMIs instead of one with the standard HGO. The designed observer is refered to as "HG/LMI Observer".

However, the scheme behind the observer design proposed in Bouhadjra et al. [2020] is also to reduce the value of tuning parameter and the observer gain compared to the standard HGO but without solving a set of LMIs. The idea is based on state augmentation that transforms the original system of dimension $n_x$ into a new system whose dimension is $n_x + j_s$, where the new nonlinear function does not depend on $j_s$ last components of the new state.

**Theorem 13 (Bouhadjra et al. [2020])** *For the considered system given by (1.1), assume there exists a transformation given as:*

$$\begin{aligned} T &: \mathbb{R}^{n_x} \to \mathbb{R}^{n_x+j_s} \\ x &\to z = T(x) \end{aligned} \tag{1.57}$$

*that transforms the system into:*

$$\begin{aligned} \dot{z} &= A_{n_z} z + B_{n_z} f_z(z) \\ y &= C_{n_z} z \end{aligned} \tag{1.58}$$

*where the matrices* $A_{n_z}, B_{n_z}$ *and* $C_{n_z}$ *are in prime form with dimension* $n_z = n_x + j_s$ *and*

$$f_z(z) = f_z(z_1, \ldots, z_{n_x}) \longleftrightarrow \frac{\partial f_z}{\partial z_j}(z) = 0, \quad \forall j > n_x. \tag{1.59}$$

*Then an observer is given as:*

$$\dot{\hat{z}} = A_{n_z}\hat{z} + B_{n_z} f_z(\hat{z}) + L_{n_z}(y - C_{n_z}\hat{z}), \quad \hat{x} = \mathcal{T}(\hat{z}) \tag{1.60}$$

*where* $L_{n_z} = \Delta(\theta) K_{n_z}$*, with* $\Delta(\theta) = diag(\theta, \ldots, \theta^{n_x+j_s})$ *and* $\mathcal{T}$ *is the left-inverse of the mapping* $T$*. If there exists* $P > 0, \lambda > 0, Y$*, and* $\theta \geq 1$ *such that:*

$$\begin{aligned} A_{n_z}P + PA_{n_z} - C_{n_z}^T Y - Y^T C_{n_z} + \lambda I < 0, \\ K_{n_z} = P^{-1}Y^T \\ \theta > \theta_0 = \left(\frac{2k_{f_z}\lambda_{max}(P)}{\lambda}\right)^{\frac{1}{1+j_s}}, \end{aligned} \tag{1.61}$$

*then the estimation error* $\tilde{x} = x - \hat{x}$ *converges exponentially towards zero.*

By employing the relevant strategy, the issues related to the high gain observer i.e., the peaking phenomenon and the measurement noise can be successfully handled since the maximum value for $\theta$ power in $\Delta$ is now $\theta_0^{\left(\frac{n_x+j_s}{1+j_s}\right)}$ i.e., the power of $\theta$ is decreased by a factor of $\left(\frac{1+\frac{j_s}{n_x}}{1+j_s}\right)$.

## 1.5 Transformation From Observer Coordinates To Original Coordinates

In the above section, it is shown that, under certain conditions, it is possible to build an observer for a nonlinear system by transforming its dynamics into a favorable form for which a global observer is known. It follows that the dynamics of the system and that of the observer are not expressed in the same coordinates and we build the observer in $\Sigma_z$ the target coordinates. The dimension of the target coordinates $\Sigma_z$ in which the observer is build is different and often greater than the original coordinates $\Sigma_x$, $n_z > n_x$. In order to obtain the estimate for the system state or even sometimes write the observer dynamics, it is necessary to invert the transformation i.e. to find the left inverse $\mathcal{T}$ of the mapping $T$. This step can be difficult in practice, mostly when an explicit expression for the inverse is not available. Indeed, in this case, However such an optimization problem involves costly computations and might raise numerical issues. Data driven alternatives have been adhered e.g. in Ramos et al. [2020].

An alternative way is to write the observer dynamics directly in the original coordinates as suggested in Deza et al. [1992]; Farhangfar and Shor [2020] for the case when $n_z = n_x$.

**Proposition 2** *Let $\dot{\hat{z}} = \mathcal{F}_z(T(\hat{x}), u, y), y = C_{n_z} z$ be an asymptotic observer for $\Sigma_z$. If $n_z = n_x$ and $T$ defines a diffeomorphism from an open set $\mathcal{X}_o \subset \mathcal{X}$ to $\mathcal{Z}$, then an observer for the system $\Sigma_x$ is given by:*

$$\dot{\hat{x}} = \left(\frac{dT}{dx}(\hat{x})\right)^{-1} \mathcal{F}_z(T(\hat{x}), u, y). \tag{1.62}$$

**Remark 7** *Even in the simple case where $n_z = n_x$, the presence of any observability defects in the system may cause Jacobian singularities outside $\mathcal{X}_o$, thereby making it not possible to get the uniqueness of the estimate $\hat{x}$ since (1.62) would no longer be well defined. Even if $x$ remains in a subset $\mathcal{X}_o$ of $\mathcal{X}$ such that $T$ is a diffeomorphism, there is no guarantee that the estimate $\hat{x}$ will remain in $\mathcal{X}_o$, especially during the transient behaviors where peaking might occur,* i.e. *the solutions $t \to \hat{z}(t)$ may leave the image set $T(\mathcal{X}_o)$.*

**Remark 8** *Generically $n_z > n_x$ so $T$ is not a diffeomorphism but only an injective immersion, and has to be augmented into a diffeomorphism for Proposition 2 to be applied, with care about the previous remark.*

## 1.6 Conclusion

The goal of this chapter was to provide a general overview of the observer design strategies for nonlinear systems. A particular attention was devoted to the notion of observability and the tricky issue regarding the observability defect was pointed out.

The design of an observer usually requires a transformation of the original nonlinear dynamics into an observability normal form, for which the design of observer with guaranteed convergence is simplified. The pros and cons of the well-known high gain observer were discussed and some recent enhanced high gain observers were presented.

In the next chapter, we will deal with the observer design for a special class of nonlinear systems, the nonlinear oscillators. This class comprises as well as Hopf oscillators and the nonlinear systems affected by harmonic disturbances of unknown frequency. The challenge of the observer design will be to take into consideration the observability defects, disturbances and measurement noises, and to develop a method that allows the observer obtained in normal form to get back to the original coordinates for implementation purposes.

Chapter 2

# Observer design for Nonlinear Oscillators

## Chapter Content

## 2.1 Introduction

In the first chapter, we recalled some notions of observability, the existing transformation of nonlinear systems into observability normal forms and some global tunable observer design strategies with guaranteed convergence. The second chapter mainly addresses the observer synthesis for nonlinear oscillators that includes the harmonic oscillator and the Hopf oscillator and nonlinear systems affected by periodic disturbances. The chapter begins with a brief introduction of nonlinear oscillators and further continues with the modeling and observability analysis for the three classes of nonlinear oscillator systems. Since the three systems suffer from observability defects, a methodology to avoid such observability defects is addressed in detail and further applied to the these systems. For each system, inversion is required to obtain the observer in original coordinates back from the target coordinates for some observer dimension bigger than that of the original system's. Therefore an inversion method based on the Jacobian completion through coordinate augmentation is recalled that extends the image of the mapping to a global diffeomorphism. The suggested technique is then applied on the three systems with complete proof given alongside. The chapter ends with the proposition for the observer in original coordinates with observability defects avoidance using a global diffeomorphic mapping.

## 2.2 Nonlinear Oscillators

Nonlinear oscillators are very important modeling tools in biological and physical sciences, and these models have received particular attention in many engineering fields over the last few decades. In our work, we will design the observers for different nonlinear oscillators i.e., harmonic oscillators, hopf-type oscillators and for a certain class nonlinear systems that are usually affected by the harmonic oscillations of unknown frequencies.

Observability is a necessary condition and a prerequisite towards an observer design and therefore all theoretical and applied contributions require the system to be observable. We have presented in the previous chapter some notions of observability and a way to get observable normal forms for nonlinear dynamical systems. For studying the observability of the nonlinear oscillators, we will focus on the observability rank condition and differential observability given by Definitions 8 and 11 respectively.

An issue regarding designing the observers for nonlinear oscillators is the presence of observability defects. These observability singularities may prohibit the straight forward use of some of the standard tools, like feedback linearization Krener and Isidori [1983]; Krener and Respondek [1985], Luenberger observers Andrieu and Praly [2006], high gain observers Gauthier et al. [1992], etc. A way to bypass such limitations relies on immersion based observers synthe-

sis. Immersion based observers are based on projection of the system onto a target system which is expected to satisfy some desired properties. Sometimes, it is necessary to target a system whose dimension is higher than the initial system dimension in order to get a target system that is linear Levine and Marino [1986], linear and stable Andrieu and Praly [2004]; Praly et al. [2006]; Marconi et al. [2007], or to obtain a nonlinear target system under normal form Andrieu and Praly [2006]; Back and Seo [2006]. Observer synthesis in the target coordinates is thus easier, but there are issues when trying to get back to the initial coordinates of the system because of the difficulty to get the inverse expression and because of the dimension gap as well.

### 2.2.1 Harmonic Oscillators

Harmonic oscillators with unknown frequency are considered in this section. The problem of frequency estimation of a harmonic oscillator has attracted a remarkable research attention in the past and current literature (see Marino and Tomei [2002]; Ziarani and Karimi-Ghartemani [2005]). The reasons of this interest rely on several engineering applications where an effective and robust solution to the problem considered is crucial. For example, the problems of harmonic disturbance compensation in automatic control, design of phase-looked loop circuits in telecommunications, adaptive filtering in signal processing, etc. In Hsu et al. [1999], the authors propose an adaptive notch filter for global estimation of the frequency of a sinusoidal signal. The problem can also be addressed by means of classical adaptive control techniques as e.g. in Obregon-Pulido et al. [2002]; Marino and Tomei [2002]; Xia [2002]; Narendra and Annaswamy [2012]. This is motivated by the fact that a signal consisting of a finite sum of sinusoids with unknown frequencies can be thought as generated by the output of a linear system with uncertain parameters. In this framework, the problem of estimation of frequencies can be set as a problem of parameter estimation and, as expected, the theory of adaptive observers can be successfully proposed as a tool. In Hou [2005], a global dynamic estimator of frequency and amplitude of a single sinusoidal signal has been presented. As shown by the author, the proposed solution can be cast in terms of adaptive observers. However, it is potentially very sensitive to measurement noise and cannot be cast as a subsystem disturbance model affecting a more generic system.

Since every single periodic signal can be modeled by a Fourier series, hence a truncated Fourier series of order 1 is given by:

$$x_1 = Asin(\omega t + \phi), \tag{2.1}$$

where the amplitude $A \neq 0$, $\omega$ is the frequency and $\phi$ represents the phase of the periodic signal.

Differentiating $x_1$ we get:

$$\begin{aligned}\dot{x}_1 &= \omega A cos(\omega t + \phi)\\ \ddot{x}_1 &= -\omega^2 A sin(\omega t + \phi).\end{aligned} \tag{2.2}$$

Since the frequency of the harmonically disturbed signal is assumed to be constant but unknown, therefore we can consider it as a state variable $x_3 = \omega^2$ and estimate it:

$$\Sigma_x : \begin{cases}\dot{x}_1 = x_2\\ \dot{x}_2 = -x_1 x_3\\ \dot{x}_3 = 0\end{cases} \tag{2.3}$$

where $x \in \mathcal{X} \subset \mathbb{R}^3$ and $y = x_1$ is the output.

**Proposition 3 (Observability of Harmonic oscillators)** *The system given by (2.3) is (differentially) observable on $x \in \mathcal{X}\backslash\mathcal{S}_\epsilon$ with $\mathcal{S}_\epsilon = \{x \in \mathcal{X} \subset \mathbb{R}^3 : x_1^2 + x_2^2 \leq \epsilon\}$ for any $\epsilon > 0$.*

**Proof 1** *The proof consists in two steps: first the system is shown to be weakly observable,* i. e. *$T$ defines an immersion, and then $T$ is proven to be injective on $\mathcal{X}\backslash\mathcal{S}_\epsilon$. The observation set $\mathcal{O}$ is the smallest vector space that includes $h_i$ and is closed under the Lie derivative $\mathcal{L}_f$. The observability co-distribution at point $x$ is $\{\mathrm{d}\mathcal{O}(x) = \mathrm{d}T(x), T \in \mathcal{O}\}$, where $\mathrm{d}$ denotes the differential.*

*Computing the successive Lie derivatives using (2.3) yields*

$$\begin{aligned}\mathrm{d}\mathcal{L}_f^0 h(x)^T &= \begin{pmatrix}1\\0\\0\end{pmatrix}, \qquad \mathrm{d}\mathcal{L}_f^1 h(x)^T = \begin{pmatrix}0\\1\\0\end{pmatrix}\\ \mathrm{d}\mathcal{L}_f^2 h(x)^T &= \begin{pmatrix}-x_3\\0\\-x_1\end{pmatrix}, \quad \mathrm{d}\mathcal{L}_f^3 h(x)^T = \begin{pmatrix}0\\-x_3\\-x_2\end{pmatrix}.\end{aligned} \tag{2.4}$$

*Higher order differentiation will still lead to expressions where $x_1, x_2$ are a factor. Hence $\mathrm{d}\mathcal{O}(x)$ is full column rank if and only if:*

$$x_1^2 + x_2^2 \neq 0. \tag{2.5}$$

*So it is straightforward that*

$$dim\ \mathrm{d}\mathcal{O}_3(x) = 3, \quad x \in \mathcal{X} \subset \mathbb{R}^3\backslash\mathcal{S}_\epsilon. \tag{2.6}$$

*Hence there is an observability singularity for $x_s = \begin{pmatrix}0 & 0 & x_3\end{pmatrix}^T$ since dim $\mathrm{d}\mathcal{O}(x_s) = 2$, namely state $x_3$ is unobservable.*

*To prove the injectivity, we have*

$$z = T(x) = \begin{pmatrix} T_1 \\ T_2 \\ T_3 \\ T_4 \end{pmatrix} = \begin{pmatrix} x_1 \\ x_2 \\ -x_1 x_3 \\ -x_2 x_3 \end{pmatrix}. \tag{2.7}$$

*For all* $x_a, x_b \in \mathcal{X} \backslash \mathcal{S}_\epsilon$*:*

$$T_a(x_a) = T_b(x_b) \Longrightarrow x_{ai} = x_{bi}, \quad \textit{for any } i \leq 2. \tag{2.8}$$

*Then it is straightforward that* $-x_1 T_3 - x_2 T_4 \Rightarrow (x_1^2 + x_2^2)(x_{3a} - x_{3b}) = 0$ *and therefore* $x_{3a} = x_{3b}$*. Hence* $T$ *is injective on* $\mathcal{X} \backslash \mathcal{S}_\epsilon$*. Since its Jacobian is full column rank from* (2.4)*, then system* (2.3) *is strongly differentially observable on* $\mathcal{X} \backslash \mathcal{S}_\epsilon$*.*

### 2.2.2 Hopf-type oscillator

The study of nonlinear oscillators has aroused a great interest for many applications involving limit cycles bifurcations. In this section, we address a certain class of nonlinear systems refered as Hopf oscillators exhibiting bifurcations between the existence and disappearance of periodic orbits. Examples of Hopf oscillators can be found in applications as diverse as biological rhythms modeling Medvedev and Cisternas [2004], epidemiology Hethcote et al. [1999], ecosystems Fussmann et al. [2000], chemical kinetics Moehlis [2002], robotics Seo et al. [2010] and fluid mechanics Shen [1991]; Noack et al. [2003].

Amongst them, most works pertain to biological rhythm instabilities modeling and fluid mechanics. For example, Hopf oscillators are used to model the spike and relaxation modeling of neurons FitzHugh [1961] and coupled Andronov-Hopf systems are used to study the neuronal network synchronization dynamics Panteley et al. [2015]. They are also involved in electrical heart arrhythmogenesis Karagueuzian et al. [2013], or through coupling in hormonal secretion concurrent electrical and chemical mechanisms Clément and Françoise [2007].

In the context of wake control for ground or aerial vehicles, Hopf oscillators are also well-adapted to capture the periodic dynamical behavior of the fluid flow behind stationary or dynamic obstacle and subject to turbulences Noack et al. [2003]; Ahmed et al. [2020]. In Chapter 4, a detailed analysis and different observers design for the wake flow model based on Hopf oscillators will be presented.

Here we consider a general multi-output Andronov-Hopf oscillator described by the nonlinear system written as:

$$\begin{pmatrix} \dot{x}_1 \\ \dot{x}_2 \end{pmatrix} = \begin{pmatrix} \sigma & -\zeta \\ \zeta & \sigma \end{pmatrix} \begin{pmatrix} x_1 \\ x_2 \end{pmatrix} - \frac{\gamma\chi}{\lambda} g(x_1^2 + x_2^2) \begin{pmatrix} x_1 \\ x_2 \end{pmatrix}, \qquad y = \begin{pmatrix} x_1 \\ x_2 \end{pmatrix}, \tag{2.9}$$

where $g$ is a continuous function and $(\zeta, \gamma, \chi, \lambda)$ are parameters. $\sigma$ is the oscillator growth rate parameter and oscillator bifurcation parameter, whose measurement or a priori knowledge is hardly accessible. In order to estimate this parameter, we add a state variable i.e., $x_4 = \sigma$ whose derivative is null because $\sigma$ is assumed to be unknown but constant. The internal dynamics is contained in variable $x_3$. Therefore the system (2.9) can be rewritten as:

$$\begin{pmatrix} \dot{x}_1 \\ \dot{x}_2 \\ \dot{x}_3 \\ \dot{x}_4 \end{pmatrix} = \begin{pmatrix} 0 & -\zeta & 0 & 0 \\ \zeta & 0 & 0 & 0 \\ 0 & 0 & -\lambda & 0 \\ 0 & 0 & 0 & 0 \end{pmatrix} x + \begin{pmatrix} x_1(x_4 - \gamma x_3) \\ x_2(x_4 - \gamma x_3) \\ \chi g(x_1^2 + x_2^2) \\ 0 \end{pmatrix}, \tag{2.10}$$

where $x \in \mathcal{X} \subset \mathbb{R}^4$ and $y \in \mathbb{R}^2$.

**Proposition 4 (Observability of Hopf oscillators)** *System (2.10) is (differentially) observable on $x \in \mathcal{X} \backslash \mathcal{S}_\epsilon$ with $\mathcal{S}_\epsilon = \{x \in \mathbb{R}^4 : x_1^2 + x_2^2 \leq \epsilon^2\}$ for any $\epsilon > 0$.*

**Proof 2** *Following the same procedure and notations as proof of Proposition 3, the system is shown to be weakly observable,* i. e. *$T$ defines an immersion, and then $T$ is proven to be injective on $\mathcal{X} \backslash \mathcal{S}_\epsilon$.*

*We begin by computing the successive Lie derivatives using (2.10):*

$$\begin{aligned}
\mathrm{d}\mathcal{L}_f^0 h^1(x)^T &= \begin{pmatrix} 1 \\ 0 \\ 0 \\ 0 \end{pmatrix}, \mathrm{d}\mathcal{L}_f^1 h^1(x)^T = \begin{pmatrix} \Delta \\ -\zeta \\ -\gamma x_1 \\ x_1 \end{pmatrix}, \\
\mathrm{d}\mathcal{L}_f^2 h^1(x)^T &= \begin{pmatrix} -\zeta^2 + \lambda\gamma x_3 + \Delta^2 - \gamma\chi g(x_1^2 + x_2^2) - 2\gamma\chi x_1^2 g'(x_1^2 + x_2^2) \\ -2\zeta\Delta - 2\gamma\chi x_1 x_2 g'(x_1^2 + x_2^2) \\ \lambda\gamma x_1 + 2\zeta\gamma x_2 - 2\gamma x_1 \Delta \\ -2\zeta x_2 + 2x_1\Delta \end{pmatrix}, \\
\mathrm{d}\mathcal{L}_f^0 h^2(x)^T &= \begin{pmatrix} 0 \\ 1 \\ 0 \\ 0 \end{pmatrix}, \mathrm{d}\mathcal{L}_f^1 h^2(x)^T = \begin{pmatrix} \zeta \\ \Delta \\ -\gamma x_2 \\ x_2 \end{pmatrix}, \\
\mathrm{d}\mathcal{L}_f^2 h^2(x)^T &= \begin{pmatrix} -2\zeta\Delta - 2\gamma\chi x_1 x_2 g'(x_1^2 + x_2^2) \\ -\zeta^2 + \lambda\gamma x_3 + \Delta^2 - \gamma\chi g(x_1^2 + x_2^2) - 2\gamma\chi x_2^2 g'(x_1^2 + x_2^2) \\ \lambda\gamma x_2 - 2\zeta\gamma x_1 - 2\gamma x_2 \Delta \\ 2\zeta x_1 + 2x_2\Delta \end{pmatrix},
\end{aligned} \tag{2.11}$$

*where* $\Delta = (x_4 - \gamma x_3)$ *and* $g'(s)$ *is the derivative of* $g(s)$*. Higher order differentiation will still lead to expressions where* $x_1, x_2$ *can factorize the two last components of* $\mathrm{d}L_f^i h^i$ *Due to the block triangular structure of* $\mathrm{d}\mathcal{O}(x)$*,* $\mathrm{d}\mathcal{O}(x)$ *is full column rank if and only if:*

$$\lambda^2\gamma^2(4\zeta^2+1)(x_1^2+x_2^2)^2 \neq 0. \tag{2.12}$$

*So it is straightforward that*

$$\dim \mathrm{d}\mathcal{O}(x) = 4, \quad \forall x \in \mathcal{X} \subset \mathbb{R}^4 \backslash \mathcal{S}_\epsilon. \tag{2.13}$$

*However there is an observability singularity for* $x_s = (0\ 0\ x_3\ x_4)^T$ *since* $\dim\ \mathrm{d}\mathcal{O}(x_s) = 2$ *i.e., it is impossible to recover* $x_3$ *nor* $x_4$ *from the output and its derivatives at any order.*
*For convenience, let define* $T$ *upto some permutation* $P$ *to get:*

$$T : x \mapsto z = P \begin{pmatrix} T^1 \\ T^2 \end{pmatrix}, \tag{2.14}$$

*where* $P = (e_1, e_3, e_5, e_2, e_4, e_6)$ *with* $e_i$ *being the* $i$*th canonical vector of* $\mathbb{R}^6$*, so:*

$$z = \begin{pmatrix} z_1^1 \\ z_1^2 \\ z_2^1 \\ z_2^2 \\ z_3^1 \\ z_3^2 \end{pmatrix} = \begin{pmatrix} T_1^1 \\ T_1^2 \\ T_2^1 \\ T_2^2 \\ T_3^1 \\ T_3^2 \end{pmatrix} (x) = \begin{pmatrix} x_1 \\ x_2 \\ -\zeta x_2 + x_1\Delta \\ \zeta x_1 + x_2\Delta \\ -\zeta^2 x_1 + x_1\Delta^2 - 2\zeta x_2\Delta + \gamma\lambda x_1 x_3 - \gamma\chi x_1 g(x_1^2+x_2^2) \\ -\zeta^2 x_2 + x_2\Delta^2 + 2\zeta x_1\Delta + \gamma\lambda x_2 x_3 - \gamma\chi x_2 g(x_1^2+x_2^2) \end{pmatrix} \tag{2.15}$$

*For all* $x_a, x_b \in \mathcal{X}\backslash\mathcal{S}_\epsilon$*:*

$$T_a(x_a) = T_b(x_b) \Longrightarrow x_{ai} = x_{bi}, \quad \text{for any} \quad i \leq 2 \tag{2.16}$$

*Then, from* (2.15) *third and fourth equations, computing* $x_1T_2^1 + x_2T_2^2$ *using the fact that* $x_1^2 + x_2^2 \neq 0$ *on* $\mathcal{X}\backslash\mathcal{S}_\epsilon$*, it follows that:*

$$(x_1^2+x_2^2)(\Delta_a - \Delta_b) = 0 \quad \text{so} \quad \Delta_a = \Delta_b \quad \text{on} \quad \mathcal{X}\backslash\mathcal{S}_\epsilon.$$

*Finally using* $\Delta_a = \Delta_b$ *in* (2.15) *two last equations to get* $(x_1T_3^1 + x_2T_3^2)$ *thus results in* $x_{ai} = x_{bi}$ *for* $i = 3, 4$ i. e. *in* $T$ *injectivity on* $\mathcal{X}\backslash\mathcal{S}_\epsilon$*. Since its Jacobian is full column rank from* (2.13)*, then system* (2.10) *is strongly differentially observable on* $\mathcal{X}\backslash\mathcal{S}_\epsilon$*.*

### 2.2.3 Nonlinear system affected by harmonic oscillations

Nonlinear dynamical systems are often affected by periodic disturbances whose knowledge and especially their frequency are of interest to control the system. In such a case, it is relevant to rebuild this information that can not be directly accessed. Many various systems can be considered: medical diagnosis Sadelli et al. [2015, 2016], medical microrobots Gangloff et al. [2006]; Fruchard et al. [2013], frequency hopping communications or phase locking loop systems Bodson [2005] etc. It also occurs in some applications where there is an interest in compensating the disturbance using the control inputs of the system, e.g. to avoid induced vibrations in satellites, planes or helicopters Bittanti and Moiraghi [1994], or to lower the energy consumption of a vehicle.

Let consider a nonlinear dynamical model disturbed by an harmonic signal whose frequency is unknown. To access to all the information, we can synthesize an observer for the *extended system* composed of two subsystems: the nonlinear dynamical model denoted by $\Sigma_1$, and the periodic disturbance auxiliary model, denoted by $\Sigma_2$.

First we consider the class of nonlinear systems under phase variable form given by a set of differential equation as $\Sigma_1$:

$$\Sigma_1 : \dot{x}' = \begin{pmatrix} x'_2 \\ \vdots \\ x'_n \\ f(x', d_1) \end{pmatrix}, \quad y = x'_1 \tag{2.17}$$

where $x' \in \mathcal{X}_a \subset \mathbb{R}^n$, $y \in \mathbb{R}$ and $f(x', d_1)$ is the nonlinear function that is perturbed due to some periodic oscillations $d_1$.

Since every single periodic disturbance can be modeled by Fourier series as given in (2.3) at order 1, this signal is the solution of an auxiliary system $\Sigma_2$ modeling the disturbance dynamics with $d \in \mathcal{X}_b \subset \mathbb{R}^3$:

$$\Sigma_2 : \dot{d} = \begin{pmatrix} d_2 \\ -d_1 d_3 \\ 0 \end{pmatrix}. \tag{2.18}$$

The extended system $\Sigma_e$ is composed of two subsystems combined together as one system:

$$\Sigma_e \mapsto \begin{pmatrix} \Sigma_1 \\ \Sigma_2 \end{pmatrix} : \dot{x} = \begin{pmatrix} x_2 \\ \vdots \\ x_n \\ f(x_1, \ldots, x_{n+1}) \\ x_{n+2} \\ -x_{n+1}x_{n+3} \\ 0 \end{pmatrix} \tag{2.19}$$

where state vector $x = \begin{pmatrix} x' \\ d \end{pmatrix} \in \mathcal{X}$ is of dimension $\mathbb{R}^{n+3}$ and $y \in \mathbb{R}$ is the output of the nonlinear dynamical model. Using the sole output $y = x_1$, the aim is to synthesize an observer for the extended system.

The first step is to study the observability of the extended system (2.19).

**Proposition 5 (Observability of the extended system)** *The extended system given by (2.19) is (differentially) observable on $x \in \mathcal{X} \backslash \mathcal{S}_\epsilon$ with $\mathcal{S}_\epsilon = \{x \in \mathcal{X} \subset \mathbb{R}^{n+3} : x_{n+1}^2 + x_{n+2}^2 \leq \epsilon\}$ for any $\epsilon > 0$, provided that $\frac{\partial f_n}{\partial x_{n+1}}(x) \neq 0$, $\forall x \in \mathcal{X}$.*

**Proof 3** *The proof is similar to the proof of Proposition 3 and 4.*

*Let $\bar{x}_i = (x_1, \ldots, x_i)^T$ and the successive Lie derivatives of the output $y = x_1$:*

$$\begin{aligned}
L_f^0 h &= x_1 \\
L_f^1 h &= x_2 \\
&\vdots \\
L_f^i h &= x_{i+1} \\
&\vdots \\
L_f^{n-1} h &= x_n \\
L_f^n h &= f(\overline{x_{n+1}}) \\
L_f^{n+1} h &= g(\overline{x_{n+1}}) + f_{n+1} x_{n+2} \\
L_f^{n+2} h &= H(\overline{x_{n+2}}) - f_{n+1} x_{n+1} x_{n+3} \\
L_f^{n+3} h &= \sum_{i=1}^{n-1} (H_i - f_{n+1,i} x_{n+1} x_{n+3}) x_{i+1} + (H_n - f_{n+1,n} x_{n+1} x_{n+3}) f + \\
&= (H_{n+1} - f_{n+1,n-1} x_{n+1} x_{n+3} - f_{n+1} x_{n+3}) x_{n+2} - \\
&= (H^1 + 2H^2 x_{n+2}) x_{n+1} x_{n+3}
\end{aligned} \tag{2.20}$$

*where* $f_i = \frac{\partial f}{\partial x_i}$ *and* $f_{i,j} = \frac{\partial^2 f}{\partial x_j \partial x_i}$

$$g(\overline{x_{n+1}}) = \sum_{i=1}^{n-1} f_i x_{i+1} + f_n f,$$
$$H(\overline{x_{n+2}}) = H^0(\overline{x_{n+1}}) + H^1(\overline{x_{n+1}})x_{n+2} + H^2(\overline{x_{n+1}})x_{n+2}^2$$

*with* $H^0(\overline{x_{n+1}}) = \sum_{i=1}^{n-1} g_i x_{i+1} + g_n f$, $H^1(\overline{x_{n+1}}) = \sum_{i=1}^{n-1} f_{n+1,i} x_{i+1} + f_{n+1,n} f + g_{n+1}$ *and* $H^2(\overline{x_{n+1}}) = f_{n+1,n+1}$.

*By computing the* $(n-1)$ *first Lie derivatives, it is obvious that*

$$\mathrm{d}\begin{pmatrix} L_f^0 h \\ L_f^1 h \\ \vdots \\ L_f^{n-1} h \end{pmatrix} = I_n \tag{2.21}$$

*such that it is full rank and the differentials of higher order derivatives (i.e. from* $\mathrm{d}L_f^n$ *to* $\mathrm{d}L_f^{n+3}$*) can be written as:*

$$\begin{aligned}
\mathrm{d}L_f^n h &= \begin{bmatrix} * & f_{n-1} & f_n f_{n+1} & 0 & 0 \end{bmatrix} \\
\mathrm{d}L_f^{n+1} h &= \begin{bmatrix} * & * & g_n + f_{n+1,n} x_{n+2} g_{n+1} + f_{n+1,n+1} x_{n+2} & f_{n+1} & 0 \end{bmatrix} \\
\mathrm{d}L_f^{n+2} h &= \begin{bmatrix} * & * & * & H^1 + 2H^2 x_{n+2} & -f_{n+1} x_{n+1} \end{bmatrix} \\
\mathrm{d}L_f^{n+3} h &= \begin{bmatrix} * & * & * & * & -x_{n+1}(\sum_{i=1}^{n-1} f_{n+1,i} x_{n+1} x_{i+1} - f_{n+1,n} f + f_{n+1,n+1} x_{n+2} + H^1 + 2H^2 x_{n+2}) - f_{n+1} x_{n+2} \end{bmatrix}
\end{aligned} \tag{2.22}$$

*Computing further derivatives will still lead to expressions where either* $x_{n+1}$ *or* $x_{n+2}$ *can factorize the last column. Therefore, from the above expressions, it can be concluded that*

$$dim\ \mathrm{d}\mathcal{O}(x) = n+3, \quad \forall x \in \mathcal{X} \subset \mathbb{R}^{n+3} \backslash \mathcal{S}_\epsilon, \tag{2.23}$$

*i.e. the observability matrix is full rank provided that* $x_{n+1}^2 + x_{n+2}^2 \neq 0$*. However there is an observability singularity for* $x_s = \begin{pmatrix} x_1 & \dots & x_n & 0 & 0 & x_{n+3} \end{pmatrix}^T$ *since dim* $\mathrm{d}\mathcal{O}(x_s) = n+2$.

*The second part of the proof shows that the system is injective on* $\mathcal{X} \backslash \mathcal{S}_\epsilon$*. To do so, we can use the transformation (2.20), however since taking* $z_i = L_f^i h(x)$ *can give quite complicated expression, we use a simpler transformation* $z = T(x)$ *such that:*

$$z = T(x) : \begin{cases} z_i = x_i, & \forall i \leq n+2 \\ z_{n+3} = -x_{n+1} x_{n+3} \\ z_{n+4} = -x_{n+2} x_{n+3} \end{cases} = \begin{pmatrix} T_i \\ T_{n+3} \\ T_{n+4} \end{pmatrix} \tag{2.24}$$

*For all* $x_a, x_b \in \mathcal{X}\backslash\mathcal{S}_\epsilon$*:*

$$T_a(x_a) = T_b(x_b) \Longrightarrow x_{ia} = x_{ib}, \quad \textit{for any } i \leq n+2 \tag{2.25}$$

*Then it is straightforward that* $-x_{n+1}T_{n+3} - x_{n+2}T_{n+4} \Rightarrow (x_{n+1}^2 + x_{n+2}^2)(x_{n+3a} - x_{n+3b}) = 0$. *Hence* $T$ *is injective on* $\mathcal{X}\backslash\mathcal{S}_\epsilon$. *Since its Jacobian is full column rank from* (2.22)*, then system* (2.19) *is strongly differentially observable on* $\mathcal{X}\backslash\mathcal{S}_\epsilon$.

## 2.3 Observability Defects Avoidance

Owing to the fact that designing nonlinear high gain observer consists in transforming the original system into some observable normal form, even if the observer design is done using these approaches, the problem introduced by the observability defects stays persistent and is not overcomed. Observability defects (also refered to as observability singularities) cause a loss of information that is required to fully reconstruct the system state, hindering the ability to access to some unmeasured states $x_i$, $i \in \mathcal{I}_{no} \subset \{1, \ldots, n_x\}$. We have also pointed out the observability defects in section 1.2.4 i.e., there exists some point(s) or set of state variables $s(x) = 0 \in \mathbb{R}^{n_s}$, where the system tends to loose its observability property.

The observability singularity set based on the rank condition is defined as:

$$\mathcal{S} = \{x \in \mathcal{X} \subset \mathbb{R}^{n_x} : s(x) = 0_{\mathbb{R}^{n_s}}\} : dim\ \mathrm{d}\mathcal{O}(x) < n_x.$$

Since the rank condition is one of the sufficient condition for system (1.8) local weak observability Hermann and Krener [1977] and transformation into $\varphi$ variable normal form Zeitz [1984], different methods have been proposed in order to fulfill such condition and to remove the observability singularities from the system. Two examples have been provided where each system suffers from observability singularity when considering only $(n_x - 1)$ first output derivatives. For Example 1, a solution based on the immersion of the system is provided that can help in removing the singularity[1] however, such a method is not globally applicable to all the systems as can be seen in Example 2. In this section, we discuss the solution that can be used to avoid such observability defects based on the use of fictitious measurements to guarantee that $dim\ \mathrm{d}(x) = n_x$.

[1]Then using $T(x_1, x_2) \mapsto z = \begin{pmatrix} x_1 \\ x_1 + x_2^2 \\ -x_2 - 2x_2^2 \end{pmatrix}$, we have $z$ in Lipschitz phase variable form with $n_z = 3 > n_x = 2$ and an observer synthesis is given by $\dot{\hat{z}} = A_{n_z}\hat{z} + \begin{pmatrix} 0 \\ 0 \\ \varphi_3 \end{pmatrix} + K\Delta(y - \hat{z}_1)$ with $\varphi_3 : z \mapsto z_2 - 3z_3 = x_2 + 4x_2^2$. We can get observer in natural coordinates using $\hat{x} = \mathcal{T}(\hat{z})$, where the left-inverse is given as $\mathcal{T} : z \mapsto \begin{pmatrix} z_1 \\ 2z_2 + z_3 \end{pmatrix}$.

### 2.3.1 Observability defects avoidance through fictitious outputs

A method to tackle observability defects for a system with single or multiple singularities has been proposed by Andrieu et al. [2014]; Bernard et al. [2015, 2018], where the essence of the method was conceptualized as the creation of "fictitious measurements" denoted in our work as $y_f \in \mathbb{R}^{n_f}$. These fictitious outputs can be extracted by a proper selection of a function:

$$\rho : x \to max(0, \epsilon^2 - s^T s)^2, \tag{2.26}$$

for some $\epsilon > 0$. Let $s : \frac{\partial s}{\partial x_i} = 0, \forall i \in \mathcal{I}_{no}$, then $y_{fi} = \rho x_i$ provides fictitious access to the information for the unmeasured state variables only when the system is singular. Thus it allows the modified system to remain observable i.e., fulfill the rank condition (1.7) and the observer to be well-defined for all $x \in \mathcal{X} \subset \mathbb{R}^{n_x}$.

The use of fictitious outputs to remove the singularity from the observer was applied on harmonic oscillators in Bernard et al. [2018] and is given by the following proposition.

**Proposition 6 (Observability defects avoidance for Harmonic oscillators)** *To circumvent the singularities of the extended system given by (2.3) defined in Proposition 3, introduce a $\mathcal{C}^2$ mapping $\rho$ for some $\epsilon > 0$ as:*

$$\rho : x \to max(0, \epsilon^2 - (x_1^2 + x_2^2))^2. \tag{2.27}$$

*and define the fictitious outputs $y_f \in \mathbb{R}$ as:*

$$y_{f_1} = \rho x_3. \tag{2.28}$$

*The addition of the fictitious outputs results into an extension of the mapping $T$ into $T_e$ such that:*

$$\begin{array}{rcl} \mathbb{R}^3 & \to & \mathbb{R}^{n_z} \times \mathbb{R} \\ T_e : x & \mapsto & \begin{pmatrix} T(x) \\ y_f(x) \end{pmatrix} \end{array} \tag{2.29}$$

*where $T_e$ is an immersion of system from $\mathbb{R}^4 \to \mathbb{R}^{n_z} \times \mathbb{R}$.*

**Proof 4** *The Jacobian of the mapping $T_e$ defined by (2.29) is given by:*

$$\frac{\partial T_e}{\partial x}(x) = \begin{pmatrix} \frac{\partial T}{\partial x} \\ \frac{\partial y_f}{\partial x} \end{pmatrix} = \begin{pmatrix} 1 & 0 & 0 \\ 0 & 1 & 0 \\ 0_{3,1} & J_1 & J_2 \end{pmatrix} \tag{2.30}$$

*with the matrices $J_1$, $J_2$ given as:*

$$J_1 = \begin{pmatrix} -x_3 & 0 \\ 0 & -x_3 \\ \rho_1 x_3 & \rho_2 x_3 \end{pmatrix}, \quad J_2 = \begin{pmatrix} -x_1 \\ -x_2 \\ \rho \end{pmatrix}. \tag{2.31}$$

*$\rho_i$ is the partial derivatives of $\rho$ w.r.t $x_1$ and $x_2$ i.e. $\rho_i = \frac{\partial \rho}{\partial x_i}(x)$. Due to the structure of Jacobian (2.30), the $T_e$ Jacobian matrix is full rank provided that $J_2$ is also full rank. Since by construction, $\rho$ and $x_1^2 + x_2^2$ cannot be null simultaneously, it follows that $J_2$ and in turn the jacobian of $T_e$ are full rank matrices for any $x \in \mathbb{R}^{n_x}$.*

**Remark 9**

- *The number of fictitious outputs $y_f \in \mathbb{R}^{n_f}$ depends on the particular system or the states affected by the singularity.*
- *It is worth mentioning that the dynamics associated with the fictitious outputs are null for the system living on $x \in \mathbb{R}^{n_x} \backslash \mathcal{S}_\epsilon$. The fictitious outputs will be activated only when the system enters $\mathcal{S}_\epsilon$ i.e. gets close to the observability singularity $x_s \in \mathcal{S}_\epsilon$.*
- *Addition of the fictitious outputs increase the cardinality of the observer state greater than that of the system i.e. $n_z + n_f > n_x$.*

The method suggested in Andrieu et al. [2014]; Bernard et al. [2018] allows to bypass the observability defects for harmonic oscillators. In the same spirit, we apply the methodology on Hopf oscillator (2.10) and on the extended system (2.19) since they suffer from an observability defect too.

### 2.3.2 Observability defects avoidance for Hopf oscillators

In the case of Hopf oscillators, the system suffers from observability defects such that when $x_1^2 + x_2^2 = 0$, the other two state variables $x_3$ and $x_4$ become unobservable. Therefore in this case, we will introduce two fictitious outputs, each corresponding to its particular state variable.

**Proposition 7** *To circumvent the singularities of the system (2.10) defined in Proposition 4, we introduce a $\mathcal{C}^2$ mapping $\rho$ as:*

$$\rho : x \to max(0, \epsilon^2 - (x_1^2 + x_2^2))^2, \tag{2.32}$$

*so as to define fictitious outputs $y_f \in \mathbb{R}^2$ as:*

$$y_f = \begin{pmatrix} y_{f_1} \\ y_{f_2} \end{pmatrix} = \rho \begin{pmatrix} \gamma x_3 \\ x_4 \end{pmatrix} \quad \forall \gamma > 0. \tag{2.33}$$

*The mapping $T$ defined by (2.14)-(2.15) is then extended as:*

$$\begin{array}{rcl} \mathbb{R}^4 & \to & \mathbb{R}^{n_z} \times \mathbb{R}^{n_f} \\ T_e : x & \mapsto & \begin{pmatrix} T(x) \\ y_f(x) \end{pmatrix} \end{array} \tag{2.34}$$

*which defines an injective immersion.*

**Proof 5** *The Jacobian of the mapping $T_e$ defined by (2.34) is given by:*

$$\frac{\partial T_e}{\partial x}(x) = \begin{pmatrix} \frac{\partial T}{\partial x} \\ \frac{\partial y_f}{\partial x} \end{pmatrix} = \begin{pmatrix} I_2 & 0_2 \\ J_1 & J_2 \end{pmatrix} \tag{2.35}$$

*with the matrices $J_1, J_2$:*

$$J_1 = \begin{pmatrix} \Delta & -\zeta \\ \zeta & \Delta \\ a_1 & b_1 \\ a_2 & b_2 \\ \gamma\rho_1 x_3 & \gamma\rho_2 x_3 \\ \rho_1 x_4 & \rho_2 x_4 \end{pmatrix}, \quad J_2 = \begin{pmatrix} -\gamma x_1 & x_1 \\ -\gamma x_2 & x_2 \\ c_1 & d_1 \\ c_2 & d_2 \\ \gamma\rho & 0 \\ 0 & \rho \end{pmatrix} \tag{2.36}$$

*with $\Delta = x_4 - \gamma x_3$ and*

$$\begin{aligned}
a_1 =& -\zeta^2 + \lambda\gamma x_3 + \Delta^2 - \gamma\chi g(x_1^2 + x_2^2) - 2\gamma\chi x_1^2 g'(x_1^2 + x_2^2) \\
a_2 =& -2\zeta\Delta - 2\gamma\chi x_1 x_2 g'(x_1^2 + x_2^2) \\
b_1 =& -2\zeta\Delta - 2\gamma\chi x_1 x_2 g'(x_1^2 + x_2^2) \\
b_2 =& -\zeta^2 + \lambda\gamma x_3 + \Delta^2 - \gamma\chi g(x_1^2 + x_2^2) - 2\gamma\chi x_2^2 g'(x_1^2 + x_2^2) \\
c_1 =& \lambda\gamma x_1 + 2\zeta\gamma x_2 - 2\gamma x_1\Delta \\
c_2 =& \lambda\gamma x_2 - 2\zeta\gamma x_1 - 2\gamma x_2\Delta \\
d_1 =& -2\zeta x_2 + 2x_1\Delta \\
d_2 =& 2\zeta x_1 + 2x_2\Delta
\end{aligned}$$

*where $\rho_1, \rho_2$ denote the partial derivatives of $\rho$ w.r.t $x_1$ and $x_2$ respectively,* i. e. *$\rho_i = \frac{\partial\rho}{\partial x_i}(x)$ and $\Delta = (x_4 - \gamma x_3)$.*

*Due to the block triangular structure of the Jacobian (2.35), the $T_e$ Jacobian matrix is full rank provided that $J_2$ is also full rank. One has:*

$$\begin{vmatrix} c_1 & d_1 \\ c_2 & d_2 \end{vmatrix} = 2\gamma\zeta\lambda(x_1^2 + x_2^2), \quad \text{and} \quad \begin{vmatrix} \gamma\rho & 0 \\ 0 & \rho \end{vmatrix} = \gamma\rho^2, \quad \forall(\gamma, \zeta, \lambda) > 0. \tag{2.37}$$

*Since by construction, $\rho$ and $x_1^2 + x_2^2$ cannot be null simultaneously, it follows that $J_2$ and in turn the jacobian of $T_e$ are full rank matrices for any $x \in \mathbb{R}^4$. Besides, the injectivity of $T_e$ is inherited from Proposition 4, hence $T_e$ is an injective immersion on $\mathbb{R}^4$.*

### 2.3.3 Observability defects avoidance for Extended system

The observability defect in the case of extended system is similar to harmonic oscillator such that the last state variable $x_{n+3}$ becomes unobservable when $x_{n+1}^2 + x_{n+2} = 0$. In such a case we will

introduce a single fictitious output that will provide a way to provide some fictitious knowledge about the state variable $x_{n+3}$ during singularity.

**Proposition 8** *To circumvent the singularities of the extended system given by (2.19) defined in Proposition 5, we introduce a $\mathcal{C}^2$ mapping $\rho$ for some $\epsilon > 0$ as:*

$$\rho : x \to max(0, \epsilon^2 - (x_{n+1}^2 + x_{n+2}^2))^2. \tag{2.38}$$

*and define the fictitious output $y_f \in \mathbb{R}$ as:*

$$y_{f_1} = \rho x_{n+3}. \tag{2.39}$$

*The addition of the fictitious output results into an extension of the mapping $T$ given by (2.24) into an injective immersion $T_e$:*

$$\begin{array}{rcl} \mathbb{R}^{n+3} & \to & \mathbb{R}^{n_z} \times \mathbb{R} \\ T_e : x & \mapsto & \begin{pmatrix} T(x) \\ y_f(x) \end{pmatrix}. \end{array} \tag{2.40}$$

**Proof 6** *The Jacobian of the mapping $T_e$ defined by (2.40) is given by:*

$$\frac{\partial T_e}{\partial x}(x) = \begin{pmatrix} \frac{\partial T}{\partial x} \\ \frac{\partial y_f}{\partial x} \end{pmatrix} = \begin{pmatrix} & I_{n+2} & 0_{n+2,1} \\ 0_{3,n} & & J_1 \quad J_2 \end{pmatrix} \tag{2.41}$$

*with the matrices $J_1$, and $J_2$ given as:*

$$J_1 = \begin{pmatrix} -x_{n+3} & 0 \\ 0 & -x_{n+3} \\ \rho_{n+1}x_{n+3} & \rho_{n+2}x_{n+3} \end{pmatrix}, \quad J_2 = \begin{pmatrix} -x_{n+1} \\ -x_{n+2} \\ \rho \end{pmatrix} \tag{2.42}$$

*where $\rho_i$ is the partial derivatives of $\rho$ w.r.t $x_{n+1}$ and $x_{n+2}$ i.e. $\rho_i = \frac{\partial \rho}{\partial x_i}(x)$. Due to the structure of Jacobian (2.41), the $T_e$ Jacobian matrix is full rank provided that $J_2$ is also full rank. Since by construction, $\rho$ and $x_{n+1}^2 + x_{n+2}^2$ cannot be null simultaneously, it follows that $J_2$ and in turn the jacobian of $T_e$ are full rank matrices for any $x \in \mathbb{R}^{n+3}$ and injectivity is straightforward.*

## 2.4 Transformation back to original coordinates

In order to deduce an estimate of $\hat{x}$ of $x$ from $\hat{z} = T(x)$ i.e., to write the observer dynamics in original coordinates the left inversion of $T$ (denoted by $\mathcal{T}$) is required. As stated before in the last section 1.5 of Chapter 1, the computation of $\mathcal{T}$ done through elimination technique $\hat{x} = \mathcal{T}(\hat{z})$ is quite problematic and the explicit analytical expression of $\mathcal{T}$ is rarely available. The inversion

typically relies on the resolution of a minimization problem that involves costly computations and might raise numerical issues.

Another proposed method was to get the estimate in original coordinates as recalled in Proposition 2 but it is based on a strict condition that the mapping $T$ is a diffeomorphism. Even for the case where the transformation is a diffeomorphism $T : \mathcal{X} \to \mathcal{Z}$, the observer must be treated carefully, since while the true state is known to stay in the domain of $\mathcal{X}$, there is no guarantee that its estimate will stay in $\mathcal{Z}$, in particular during the transient behavior where peaking can occur (since we are dealing with the HGO, peaking phenomenon should not be ignored). In that case, the estimate may encounter Jacobian singularities, thus leading to non-converging non-complete solutions as pointed out in Bernard et al. [2018].

Different solutions have been proposed regarding the solution of such issues e.g. a solution proposed consists in modifying the observer dynamics to force its state to remain in the diffeomorphism image by either adding a term in the dynamics Astolfi and Praly [2013], through constrained optimization Astolfi et al. [2021], where the states are set to remain in a given convex set for all times or using carefully complex saturations Maggiore and Passino [2003]. However this must be done with care since it can easily destroy the observer performances (in particular convergence): extra convexity assumption is typically required on the diffeomorphism image to implement such methods. When the transformation is not a diffeomorphism, but an injective immersion, namely, the target space $\mathcal{Z}$ has a larger dimension than the system domain $\mathcal{X}$, some ideas have been proposed such as using Newton-like or gradient algorithms to inverse the transformation in Astolfi and Possieri [2019] and Menini et al. [2017], or continuation algorithms which "follow" the "optimal" inverse image in Hammouri et al. [2018]. However, in those cases, the convergence is only local and a convexity assumption also needs to be verified.

### 2.4.1 Augmentation of the mapping into global diffeomorphism

For immersion based observers, we cannot use Proposition 2 since the target space has a greater dimension than the observer i.e. $n_z > n_x$. Even when no immersion is required i.e. $n_z = n_x$, using fictitious outputs increases the dimension of the target space greater than that of the observer i.e. $(n_z + n_f) > n_x$ and it results into an extension of the mapping $T$ into $T_e : \mathbb{R}^{n_x} \to \mathbb{R}^{n_z} \times \mathbb{R}^{n_f}$. Therefore, the use of Proposition 2 in its original form is no longer valid for such systems. Our work in this thesis relies on the ideas proposed in Andrieu et al. [2014] and Bernard et al. [2015, 2018] for the case where $n_z > n_x$. The main idea is to extend the injective immersion into a diffeomorphism through the coordinate augmentation and the jacobian completion. With the new mapping, we can implement the observer in the original coordinates using the extended version of Proposition 2. The diffeomorphism denoted by $T_a$ can be achieved, atleast locally, if we are able to find the $n_z - n_x$ columns for jacobian completion or in other words if we can find

$\Psi$ that satisfies:

$$det\left(\frac{\partial T_e}{\partial x}(x) \quad \Psi(x)\right) \neq 0, \qquad \forall x \in \mathcal{X} \subset \mathbb{R}^{n_x}. \tag{2.43}$$

The approach considered here consists in extending the image of $T_e$ to get a global diffeomorphism $T_a$ through coordinate augmentation from $x \in \mathbb{R}^{n_x}$ to $x_a \in \mathbb{R}^{n_z+n_f}$ by adding some fictitious states $\tau \in \mathbb{R}^{n_z+n_f-n_x}$, so a pre-image will always exist and will be uniquely defined to get the observer back in original coordinates.

**Proposition 9 (Global diffeomorphism)** *Let us define the two new state vectors $x_a$ and $z_a$:*

$$x_a = \begin{pmatrix} x \\ \tau \end{pmatrix} \tag{2.44}$$

$$z_a = T_a(x_a) = T_e(x_a) + \Psi(x_a)\tau \tag{2.45}$$

*where $\tau \in \mathbb{R}^{n_z+n_f-n_x}$ are the exogenous variables added to the augmented state vector with the augmented mapping $T_a : \mathbb{R}^{n_x} \mapsto \mathbb{R}^{n_z+n_f}$. The matrix $\Psi(x) \in \mathbb{R}^{(n_z+n_f)\times(n_z+n_f-n_x)}$ is chosen such that it satisfies:*

$$det\left(\frac{\partial T_e}{\partial x_a}(x_a) \quad \Psi(x_a)\right) \neq 0, \qquad \forall x_a \in \mathcal{X} \subset \mathbb{R}^{n_x}. \tag{2.46}$$

*and the $\Psi(x)$ columns only depends on the state variables that remains observable i.e., $x_i, i \notin \mathcal{I}_{no}$ for any $x \in \mathbb{R}^{n_x}$, then $T_a$ defines a global diffeomorphism.*

**Remark 10** *For the cases, when $\Psi(x)$ contains the states that are structurally unobservable and becomes observable only due to presence of fictitious measurements triggered during singularity, we can only achieve local diffeomorphism. If $\Psi$ depends only on the state variables that are structurally observable, then $T_a$ defines a global diffeomorphism.*

### 2.4.2 Jacobian completion

The diffeomorphism $T_a$ can be achieved if we are able to find the $n_z - n_x$ columns for jacobian completion or in other words if we can find $\Psi$ that satisfies (2.46). However, finding $\Psi$ columns that ensures their continuity with respect to $x$ is quite difficult and can be quite problematic. This problem is very old and related to topological question Wazewski [1935]; Eckmann [2006]. In Andrieu et al. [2014] and Bernard et al. [2018], the problem was addressed with detailed analysis.

Complementing a $n_z \times n_x$ full-rank matrix into an invertible one is equivalent to finding $n_z - n_x$ independent vectors orthogonal to that matrix. Precisely, the existence of $\Psi$ satisfying (2.46) is equivalent to the existence of a $\mathcal{C}^1$ function $\Psi$, the values of which are full-rank matrices satisfying

$$\Psi(x)^T \frac{\partial T_e}{\partial x}(x) = 0, \qquad \forall x \in \mathbb{R}^{n_x}. \tag{2.47}$$

Indeed, satisfying (2.47) is equivalent to satisfy (2.46) since the following matrices are invertible:

$$\begin{pmatrix} \frac{\partial T_e}{\partial x}(x)^T \\ \Psi(x)^T \end{pmatrix} \begin{pmatrix} \frac{\partial T_e}{\partial x}(x) & \Psi(x) \end{pmatrix} = \begin{pmatrix} \frac{\partial T_e}{\partial x}(x)^T \frac{\partial T_e}{\partial x}(x) & 0 \\ 0 & \Psi(x)^T \Psi(x) \end{pmatrix}. \tag{2.48}$$

Another universal completion method based on Schur complement was also proposed in Bernard et al. [2018] for the cases when an explicit construction of $\Psi$ is not possible. This method relies on increasing the observer state dimension to $n_z + n_x$ and introducing a new mapping $T_a$ such that $T_a : \mathcal{X} \to \mathbb{R}^{n_z} \times \mathbb{R}^{n_x}$ as:

$$T_a(x) = (T_e(x), \underbrace{0, \ldots, 0}_{n_x times}). \tag{2.49}$$

In other words, adding $n_x$ components equal to zero to $T_e$ and correspondingly adding $n_x$ exponentially converging dynamics $\tau$ in observer dynamics $\mathcal{F}_z(\hat{z}, y)$ will result in the $T_a$ being completed into a diffeomorphism. Based on the Schur complement, the jacobian of the new mapping

$$\frac{\partial T_a}{\partial x}(x) = \begin{pmatrix} \frac{\partial T_e}{\partial x}(x) \\ 0_{n_x \times n_x} \end{pmatrix} \tag{2.50}$$

can be complemented by

$$\frac{\partial \Psi}{\partial x}(x) = \begin{pmatrix} -I_{n_z \times n_x} \\ \frac{\partial T_e}{\partial x}(x)^T \end{pmatrix}. \tag{2.51}$$

Hence the injective immersion $T_e$ can always be extended into a local diffeomorphism $T_a$.

### 2.4.3 Global diffeomorphism: Harmonic oscillators

**Proposition 10** *With notations of Proposition 6, we define an augmented mapping $T_a$ as:*

$$\begin{array}{rcl} \mathbb{R}^{n_z+n_f} & \to & \mathbb{R}^{n_z+n_f} \\ T_a : x_a = \begin{pmatrix} x \\ \tau \end{pmatrix} & \mapsto & z_a = T_e(x) + \Psi(x)\tau, \end{array} \tag{2.52}$$

*where $\tau \in \mathbb{R}^2$ and $\Psi \in \mathcal{C}^1(\mathbb{R}^{n_x}, \mathbb{R}^{n_z+n_f-n_x})$ is defined by*

$$\Psi : x \mapsto \begin{pmatrix} 0_{2,2} \\ J_\Psi \end{pmatrix}, \quad J_\Psi = \begin{pmatrix} 1 & 0 \\ 0 & 1 \\ x_1 & x_2 \end{pmatrix} \tag{2.53}$$

*then $T_a$ defines a global diffeomorphism on $\mathbb{R}^5$ satisfying*

$$T_a(x, 0) = \begin{pmatrix} T(x) \\ 0_{n_f,1} \end{pmatrix}, \quad \forall x \in \mathbb{R}^3 \backslash \mathcal{S}_\epsilon. \tag{2.54}$$

**Proof 7** *The Jacobian of the new augmented mapping $T_a$ can be found as:*

$$\frac{\partial T_a}{\partial x_a}(x_a) = \begin{pmatrix} I_2 & 0_{2,1} & 0_{2,2} \\ J_1 & J_2 & J_\Psi \end{pmatrix} \tag{2.55}$$

*with the matrices $J_1$, $J_2$ and $J_\Psi$ as:*

$$J_1 = \begin{pmatrix} -x_3 & 0 \\ 0 & -x_3 \\ \rho_1 x_3 & \rho_2 x_3 \end{pmatrix}, \quad J_2 = \begin{pmatrix} -x_1 \\ -x_2 \\ \rho \end{pmatrix}, J_\Psi = \begin{pmatrix} 1 & 0 \\ 0 & 1 \\ x_1 & x_2 \end{pmatrix} \tag{2.56}$$

*such that the determinant of the Jacobian of $T_a$ can be calculated as:*

$$\left| \frac{\partial T_a}{\partial x_a} \right| = \rho + x_1^2 + x_2^2 \neq 0. \tag{2.57}$$

*Since $\Psi$ columns depends only on $(x_1, x_2) \notin \mathcal{I}_{no}$ and are observable for all $x \in \mathcal{X}$, so $T_a$ is a global immersion. We now provide the injectivity proof of $T_a$.*

$$z_a = T_a(x, \tau) = \begin{pmatrix} x_1 \\ x_2 \\ -x_1 x_3 + \tau_1 \\ -x_2 x_3 + \tau_2 \\ \rho x_3 + x_4 \tau_1 + x_5 \tau_2 \end{pmatrix} \tag{2.58}$$

*From the above equation, it is quite straightforward that:*

$$\begin{aligned} T_a(x_a, \tau_a) = T_a(x_b, \tau_b) &\Longrightarrow x_{ia} = x_{ib}, \quad \forall 1 \leq i \leq 2 \\ \rho_a(x_1, x_2) = \rho_b(x_1, x_2) &\Longrightarrow \rho' = \rho \end{aligned} \tag{2.59}$$

*and*

$$\begin{aligned} -x_1 x_{3a} + \tau_{1a} &= -x_1 x_{3b} + \tau_{1b} \\ -x_2 x_{3a} + \tau_{2a} &= -x_2 x_{3b} + \tau_{2b} \\ \rho x_{3a} + x_1 \tau_{1a} + x_2 \tau_{2a} &= \rho x_{3b} + x_1 \tau_{1b} + x_2 \tau_{2b} \end{aligned} \tag{2.60}$$

*Using $\tilde{x}_i = x_{ia} - x_{ib}$ in (2.60):*

$$\begin{aligned} \tilde{\tau}_1 &= x_1 \tilde{x}_3 \\ \tilde{\tau}_2 &= x_2 \tilde{x}_3 \\ x_1 \tilde{\tau}_1 + x_2 \tilde{\tau}_2 &= -\rho \tilde{x}_3 \end{aligned} \tag{2.61}$$

*Simplifying (2.61), we get:*

$$x_1^2 \tilde{x}_3 + x_2^2 \tilde{x}_3 + \rho \tilde{x}_3 = 0 \Longrightarrow \tilde{x}_3 (\rho + x_1^2 + x_2^2) = 0 \tag{2.62}$$

*Since by definition, $\rho$ given by (2.27) gives $(\rho + x_1^2 + x_2^2) \neq 0$, therefore $\tilde{x}_3 = 0$ i.e. $x_{3a} = x_{3b}$. Using the expression in (2.61), we can find that $\tilde{\tau}_i = 0$, so $\tau_{ia} = \tau_{ib}$ for $i = 1, 2$. Hence $T_a$ is injective. Since we have already proved that $T_a$ is a global immersion therefore $T_a$ is an injective immersion on $T_a : \mathcal{X} \subset \mathbb{R}^{n_x} \to \mathcal{Z} \subset \mathbb{R}^{n_z}$.*

### 2.4.4 Global diffeomorphism: Hopf oscillators

**Proposition 11** *With notations and definitions of Proposition 7, let $\tau \in \mathbb{R}^4$ and define an augmented mapping $T_a$ as:*

$$\begin{aligned} &\mathbb{R}^{n_z+n_f} && \to && \mathbb{R}^{n_z+n_f} \\ &T_a : x_a = \begin{pmatrix} x \\ \tau \end{pmatrix} && \mapsto && z_a = T_e(x) + \Psi(x)\tau. \end{aligned} \tag{2.63}$$

*where $\Psi \in \mathcal{C}^1(\mathbb{R}^{n_x}, \mathbb{R}^{n_z+n_f-n_x})$ is defined by*

$$\Psi : x \mapsto \begin{pmatrix} 0_2 & 0_2 \\ 0_2 & \delta I_2 \\ I_2 & 0_2 \\ J_\Psi & 0_2 \end{pmatrix}, \quad J_\Psi = \begin{pmatrix} -\frac{x_1}{\lambda} & -\frac{x_2}{\lambda} \\ \frac{x_2}{2\zeta} - \frac{x_1}{\lambda} & -\frac{x_1}{2\zeta} - \frac{x_2}{\lambda} \end{pmatrix}. \tag{2.64}$$

*So $T_a$ defines a global diffeomorphism on $\mathbb{R}^8$ satisfying*

$$T_a(x, 0) = \begin{pmatrix} T(x) \\ 0_{n_z+n_f-n_x,1} \end{pmatrix}, \quad \forall x \in \mathbb{R}^4 \backslash \mathcal{S}_\epsilon. \tag{2.65}$$

**Proof 8** *It is obvious from definition (2.32), (2.33) and (2.63) that (2.65) is fulfilled. Using (2.35), (2.36) and (2.64) results in*

$$\left| \frac{\partial T_a}{\partial x_a} \right| = \gamma\delta^2(\rho^2 + (x_1^2 + x_2^2))^2 \neq 0, \quad \forall(\gamma, \delta) > 0. \tag{2.66}$$

*So $T_a$ is a global immersion. The global injectivity proof given hereinafter completes the proof.*

*$T_a$ is defined as:*

$$T_a : \begin{pmatrix} x \\ \tau \end{pmatrix} \mapsto z_a = \begin{pmatrix} z \\ y_f \end{pmatrix} + \Psi(x_1, x_2)\tau = \begin{pmatrix} \begin{pmatrix} z_{11} \\ z_{21} \end{pmatrix} \\ \begin{pmatrix} z_{12} \\ z_{22} \end{pmatrix} \\ \begin{pmatrix} z_{13} \\ z_{23} \end{pmatrix} \\ \begin{pmatrix} \rho x_3 \\ \rho x_4 \end{pmatrix} \end{pmatrix} + \begin{pmatrix} 0_2 & & 0_2 \\ 0_2 & & I_2 \\ I_2 & & 0_2 \\ -x_1 & -x_2 & 0_{1,2} \\ x_2 - x_1 & -x_1 - x_2 & 0_{1,2} \end{pmatrix} \begin{pmatrix} \tau_1 \\ \tau_2 \\ \tau_3 \\ \tau_4 \end{pmatrix}. \tag{2.67}$$

*Let $T_a(x_a) = T_b(x_b)$ where $z_{ij}$ is given by (2.14), then denoting $\tilde{\Delta} = \Delta_a - \Delta_b, \tilde{x}_i = x_{ai} - x_{bi}$ and $\tilde{\tau} = \tau_a - \tau_b$, we get:*

$$\begin{cases} x_{1a} = x_{1b} & = x_1 \\ x_{2a} = x_{2b} & = x_2 \end{cases} \tag{2.68a}$$

$$\begin{cases} -\zeta x_2 + x_1\Delta_a + \tau_{3a} = -\zeta x_2 + x_1\Delta_b + \tau_{3b} \\ \zeta x_1 + x_2\Delta_a + \tau_{4a} = \zeta x_1 + x_2\Delta_b + \tau_{4b} \end{cases} \tag{2.68b}$$

$$\begin{cases} -2\zeta x_2\tilde{\Delta} + x_1(\Delta_a^2 - \Delta_b^2) + \gamma\lambda x_1\tilde{x}_3 = -\tilde{\tau}_1 \\ 2\zeta x_1\tilde{\Delta} + x_2(\Delta_a^2 - \Delta_b^2) + \gamma\lambda x_2\tilde{x}_3 = -\tilde{\tau}_2 \end{cases} \tag{2.68c}$$

$$\begin{cases} \rho\gamma\tilde{x}_3 = -\dfrac{x_1}{\lambda}\tilde{\tau}_1 - \dfrac{x_2}{\lambda}\tilde{\tau}_2 \\ \rho\tilde{x}_4 = \left(\dfrac{x_1}{\lambda} - \dfrac{x_2}{2\zeta}\right)\tilde{\tau}_1 - \left(\dfrac{x_1}{2\zeta} + \dfrac{x_2}{\lambda}\right)\tilde{\tau}_2 \end{cases} \tag{2.68d}$$

*From (2.68b) and (2.68d), it is straightforward that:*

$$\begin{aligned} x_1\tilde{\Delta} &= -\tilde{\tau}_3 \\ x_2\tilde{\Delta} &= -\tilde{\tau}_4 \\ \rho\tilde{\Delta} &= -\frac{x_2}{2\zeta}\tilde{\tau}_1 + \frac{x_1}{2\zeta}\tilde{\tau}_2 \end{aligned} \tag{2.69}$$

*Further multiplying (2.69) by $x_1, x_2$ and $\rho$ respectively, one obtains:*

$$(\rho^2 + x_1^2 + x_2^2)\tilde{\Delta} = -x_1\tilde{\tau}_3 - x_2\tilde{\tau}_4 - \frac{\rho x_2}{2\zeta}\tilde{\tau}_1 + \frac{\rho x_1}{2\zeta}\tilde{\tau}_2 \tag{2.70}$$

*Multiplying the equations of (2.68c) by $x_2$ and $x_1$ respectively and subtracting the equations, we get:*

$$2\zeta(x_1^2 + x_2^2)\tilde{\Delta} = -x_1\tilde{\tau}_2 + x_2\tilde{\tau}_1 \tag{2.71}$$

*Adding $2\zeta$ times the last equation of (2.69) to (2.71) and simplifying yields:*

$$2\zeta((x_1^2 + x_2^2) + \rho)\tilde{\Delta} = -x_1\tilde{\tau}_2 + x_2\tilde{\tau}_1 + x_1\tilde{\tau}_2 - x_2\tilde{\tau}_1 = 0, \tag{2.72}$$

*Since from Proposition 7, we know that $(x_1^2 + x_2^2) + \rho \neq 0, \forall x \in \mathbb{R}^4$, therefore $\tilde{\Delta} = 0$, so $\Delta_a^2 - \Delta_b^2 = 0$. One can then simplify (2.69) and obtain:*

$$\tilde{\tau}_3 = \tilde{\tau}_4 = 0. \tag{2.73}$$

*Using (2.73), equations (2.68c) and (2.68d) can be reduced to:*

$$\gamma\lambda x_1\tilde{x}_3 = \tilde{\tau}_1 \tag{2.74a}$$

$$\gamma\lambda x_2\tilde{x}_3 = \tilde{\tau}_2 \tag{2.74b}$$

$$\rho\gamma\tilde{x}_3 = -\frac{x_1}{\lambda}\tilde{\tau}_1 - \frac{x_2}{\lambda}\tilde{\tau}_2 \tag{2.74c}$$

$$\rho\tilde{x}_4 = \left(\frac{x_1}{\lambda} - \frac{x_2}{2\zeta}\right)\tilde{\tau}_1 - \left(\frac{x_1}{2\zeta} + \frac{x_2}{\lambda}\right)\tilde{\tau}_2 \tag{2.74d}$$

*Further multiplying the Equations (2.74a), (2.74b) by $x_1$ and $x_2$ respectively and adding the resulting equations to (2.74c), we can get a single equation such that:*

$$\lambda\gamma(\rho + x_1^2 + x_2^2)\tilde{x}_3 = x_1\tilde{\tau}_1 + x_2\tilde{\tau}_2 - x_1\tilde{\tau}_1 - x_2\tilde{\tau}_2 = 0 \Longrightarrow \tilde{x}_3 = 0. \tag{2.75}$$

*It follows that $\tilde{\tau}_1 = \tilde{\tau}_2 = 0$ and therefore $\tilde{x}_4 = 0$. This proves that $T_a$ is globally injective and since $\Psi$ columns depends only on $(x_1, x_2) \notin \mathcal{I}_{no}$ and are observable for all $x \in \mathcal{X}$, thus $T_a$ defines a global diffeomorphism.*

### 2.4.5 Global diffeomorphism: Extended system

**Proposition 12** *With notations of Proposition 8, we define an augmented mapping $T_a$ as:*

$$\begin{array}{lll} \mathbb{R}^{n_z+n_f} & \to & \mathbb{R}^{n_z+n_f} \\ T_a : x_a = \begin{pmatrix} x \\ \tau \end{pmatrix} & \mapsto & z_a = T_e(x) + \Psi(x)\tau. \end{array} \tag{2.76}$$

*where $\Psi \in \mathcal{C}^1(\mathbb{R}^{n_x}, \mathbb{R}^{n_z - n_x})$ is defined by*

$$\Psi : x \mapsto \begin{pmatrix} 0_{n+2,2} \\ J_\Psi \end{pmatrix}, \quad J_\Psi = \begin{pmatrix} 1 & 0 \\ 0 & 1 \\ x_{n+1} & x_{n+2} \end{pmatrix}. \tag{2.77}$$

*Hence $T_a$ defines a global diffeomorphism on $\mathbb{R}^{n_z+n_f}$ satisfying*

$$T_a(x, 0) = \begin{pmatrix} T(x) \\ 0_{n_f,1} \end{pmatrix}, \quad \forall x \in \mathbb{R}^{n+3} \backslash \mathcal{S}_\epsilon. \tag{2.78}$$

**Proof 9** *The Jacobian of the new augmented mapping $T_a$ is:*

$$\frac{\partial T_a}{\partial x_a}(x_a) = \begin{pmatrix} & I_{n+2} & & 0_{n+2,1} & 0_{n+2,2} \\ 0_{3,n} & & J_1 & J_2 & J_\Psi \end{pmatrix} \tag{2.79}$$

*with the matrices $J_1$, $J_2$ and $J_\Psi$:*

$$J_1 = \begin{pmatrix} -x_{n+3} & 0 \\ 0 & -x_{n+3} \\ \rho_{n+1}x_{n+3} & \rho_{n+2}x_{n+3} \end{pmatrix}, \quad J_2 = \begin{pmatrix} -x_{n+1} \\ -x_{n+2} \\ \rho \end{pmatrix}, J_\Psi = \begin{pmatrix} 1 & 0 \\ 0 & 1 \\ x_{n+1} & x_{n+2} \end{pmatrix} \tag{2.80}$$

*so the determinant of the Jacobian of $T_a$ is:*

$$\left| \frac{\partial T_a}{\partial x_a} \right| = \rho + x_{n+1}^2 + x_{n+2}^2 \neq 0. \tag{2.81}$$

*So $T_a$ is a global immersion. We now provide the $T_a$ injectivity proof.*

$$z_a = T_a(x,\tau) = \begin{pmatrix} x_1 \\ \vdots \\ x_{n+2} \\ -x_{n+1}x_{n+3} + \tau_1 \\ -x_{n+2}x_{n+3} + \tau_2 \\ \rho x_{n+3} + x_{n+1}\tau_1 + x_{n+2}\tau_2 \end{pmatrix} \tag{2.82}$$

*From the above equation, it is quite straightforward that:*

$$\begin{aligned} T_a(x_a,\tau_a) = T_a(x_b,\tau_b) &\Longrightarrow x_{ia} = x_{ib}, \quad \forall 1 \le i \le n+2 \\ \rho_a(x_{n+1},x_{n+2}) = \rho_b(x_{n+1},x_{n+2}) &\Longrightarrow \rho' = \rho \end{aligned} \tag{2.83}$$

*and*

$$\begin{aligned} -x_{n+1}x_{n+3a} + \tau_{1a} &= -x_{n+1}x_{n+3b} + \tau_{1b} \\ -x_{n+2}x_{n+3a} + \tau_{2a} &= -x_{n+2}x_{n+3b} + \tau_{2b} \\ \rho x_{n+3a} + x_{n+1}\tau_{1a} + x_{n+2}\tau_{2a} &= \rho x_{n+3b} + x_{n+1}\tau_{1b} + x_{n+2}\tau_{2b} \end{aligned} \tag{2.84}$$

*Using $\tilde{x}_i = x_{ia} - x_{ib}$ in (2.84):*

$$\begin{aligned} \tilde{\tau}_1 &= x_{n+1}\tilde{x}_{n+3} \\ \tilde{\tau}_2 &= x_{n+2}\tilde{x}_{n+3} \\ x_{n+1}\tilde{\tau}_1 + x_{n+2}\tilde{\tau}_2 &= -\rho\tilde{x}_{n+3} \end{aligned} \tag{2.85}$$

*Simplifying (2.85), we get:*

$$x_{n+1}^2\tilde{x}_{n+3} + x_{n+2}^2\tilde{x}_{n+3} + \rho\tilde{x}_{n+3} = 0 \Longrightarrow \tilde{x}_{n+3}(\rho + x_{n+1}^2 + x_{n+2}^2) = 0 \tag{2.86}$$

*Since $(\rho + x_{n+1}^2 + x_{n+2}^2) \neq 0$, it follows that $\tilde{x}_{n+3} = 0$ and hence $x_{n+3a} = x_{n+3b}$. Using then (2.85), one gets $\tilde{\tau}_i = 0$ so $\tau_{ia} = \tau_{ib}$ for $i = 1, 2$. Hence $T_a$ is a global diffeomorphism.*

## 2.5 Observer in original coordinates

**Proposition 13** *The dynamic system*

$$\dot{\hat{x}}_a = \left(\frac{\partial T_a}{\partial x_a}(\hat{x}_a)\right)^{-1} \begin{pmatrix} \mathcal{F}_z(T_a(\hat{x}_a),\eta,y) \\ -K_{n_f}T_{n_f}(\hat{x}_a) \end{pmatrix} \tag{2.87}$$

*is an arbitrarily fast converging observer for systems (2.3),(2.10) and (2.19) in their natural coordinates on any bounded subset of $\mathbb{R}^{n_z+n_f}$, where $\mathcal{F}_z$, is defined e.g. in Propositions 8-12 and $T_a$ by Propositions 6-12. $K_{n_f}$ is a positive definite diagonal matrix of dimension $n_f$. The notation $T_{n_f}$ stands for the last $n_f$ components of $T_a$ representing the dynamics associated with the fictitious outputs.*

**Proof 10** *By continuity $T_a^{-1}$ is $\mathcal{C}^1$, hence it is L-Lipschitz on any compact of $\mathbb{R}^{n_z+n_f}$. It follows that, using $z_a^* = T_a(x,0) = T_e(x)$:*

$$\begin{aligned} \|x(t)-\hat{x}(t)\| + \|\tau(t)\| &\leq \sqrt{2}\left\| \begin{matrix} x-\hat{x} \\ \tau \end{matrix} \right\| \\ &\leq \sqrt{2}\left\| \begin{pmatrix} x \\ 0 \end{pmatrix} - \begin{pmatrix} \hat{x} \\ \tau \end{pmatrix} \right\| \\ &\leq \sqrt{2}\|T_a^{-1}(z_a^*) - T_a^{-1}(\hat{z}_a)\| \\ &\leq L\sqrt{2}\|z_a^* - \hat{z}_a| \\ &\leq L\sqrt{2}\|T_e(x) - T_a(\hat{x},\tau)\|. \end{aligned} \tag{2.88}$$

*Since $T_e$ is injective and $\mathcal{F}_z, \mathcal{F}_\eta$ defines a converging observer from Propositions 8-12, it follows that*

$$\lim_{t\to\infty} \|x(t)-\hat{x}(t)\| + \|\tau(t)\| = 0. \tag{2.89}$$

The augmentation and the extension can be done without modifying the observer dynamics, while maintaining the convergence.

## 2.6 Conclusion

In this chapter, we have studied the two nonlinear oscillators: the harmonic oscillator and the Hopf oscillator. We also studied the class of phase variable nonlinear systems affected by harmonic oscillations of unknown frequency. For each system, a model has been presented and a detailed observability analysis has been done. From the observability analysis, it has been concluded that each system suffers from some observability defects, and therefore a method suggested by Andrieu et al. [2014]; Bernard et al. [2018] has been recalled and applied to the three systems in order to avoid the observability defects. Inversion of the mapping was not possible using the Proposition 2 given in the previous chapter due to the dimension gap between the target coordinates and the system original coordinates, as well as the addition of fictitious outputs to remove the observability defects. Therefore, a method previously suggested by Andrieu et al. [2014] has been applied to extend the image of the mapping to a global diffeomorphism through coordinate augmentation and jacobian completion. The method has been applied to the three models, where the augmentation and the extension have been done without modifying the observer dynamics while maintaining the convergence. Detailed proofs for the global diffeomorphism of each model have also been provided. The chapter ends with a proposition for obtaining the observer in original coordinates with no observability singularities.

The next two chapters are devoted to the applications of the results provided in this chapter. Each chapter will provide an application of the observer design based on the nonlinear oscillators,

where it will utilize the strategies proposed in this chapter to avoid the observability defects and to extend the image into a global diffeomorphism. The effectiveness of the proposed techniques will be evaluated with the help of simulations and experimental results.

Chapter 3

# Application to Medical Microrobots

## Chapter Content

This chapter addresses the observer synthesis for the application of medical microrobots. We begin with a brief literature review on the microrobots. It is then followed by the modeling of the forces acting on the microrobot system where the microrobot system is affected by the unknown blood velocity. Hence a nonlinear dynamical system that combines the microrobot model as well as the blood velocity dynamics is given afterwards. An observability analysis is then provided, which takes into account the observability defects present in the nonlinear extended model of the microrobots, similar to Proposition 5. To avoid such observability defects, we propose to modify the system as in Proposition 8. Since the resulting mapping to a normal form is an immersion and also due to the addition of fictitious outputs, the observer dimension becomes greater compared to the system's original dimension, therefore an extension of this mapping to a global diffeomorphism is suggested for the extended model. Finally, the low peaking limited high gain observer is proposed for the microrobot system in the original coordinates. Simulations then illustrate the proposed approach proving the efficiency of the designed observer, followed by a brief conclusion.

## 3.1 Context and Motivation

There has been a growing interest in the development of therapeutic microrobots and nanorobots for some years Nelson et al. [2010]. Such systems have the potential to revolutionize many aspects of medicine i.e., to perform complex surgical procedures or diagnosis, reach remote places with lessened medical side effects, and shorten the patient convalescence Kristo et al. [2003]; Kosa et al. [2007]; Handbook et al. [2007]; Zhang et al. [2009]; Ergeneman et al. [2008]. Miniaturize systems magnetically propelled by remote actuation can achieve swimming through the blood vessels network in order to provide targeted therapy, even for hard-to-reach human organs such as the pancreas or brain. In comparison to existing tethered medical devices, such as flexible endoscopes and catheters, these mobile microrobots could access complex and small regions of the human body such as gastrointestinal Than et al. [2012], brain Purdy et al. [2005], spinal cord Roy et al. [2006], blood capillaries Miloro et al. [2012] and inside the eye Ullrich et al. [2013] without damaging the blood or lymphatic vessels. Furthermore, many internal locations of the body are either inaccessible or hard to reach in a tethered way. Although designing functional medical microrobots is challenging from an engineering perspective, the potential rewards are vast.

The first studies in untethered robots are by using principles that would later become microrobot actuation principles, such as a magnetic stereotaxis system Meeker et al. [1996] to guide a tiny permanent magnet inside the human body and a magnetically driven screw which moved through tissues Ishiyama et al. [2001]. Micro-Electro-Mechanical systems were developed in the

1990s as a result of scientific and technical advancements, allowing microrobots size to be reduced by several orders of magnitude. The feasibility of the actuation of these microrobots was studied by Quate et al. [1991] in superparamagnetic particles and by Gillies et al. [1994] on magnetic particles. As medical carriers, these micro or nanorobotic systems provide deep access to the human body or sensitive areas for diagnosis or therapeutic purposes.

Until the 2000s, the majority of research focused on the viability of such carriers. Even though the research in this field is very active, the field still suffers from a lack of modeling, control and observation tools that are adapted to this context. The blood system is particularly complex with its branches and bifurcations: without control, a microrobot would be quickly dragged by the flow from its target. It is, therefore, necessary not only to have a faithful image of this network thanks to the medical imagers but also to know the physical laws that dominate the robot dynamics in this environment.

Among the numerous prototypes that have been developed, those possessing a deported actuation are the most promising. Indeed these robots do not embed any energy source thus inducing smaller sizes. The kind of deported actuators required to control such robots depends on the propulsion strategy. A variable magnetic field is necessary for robots with elastic flagellum Lagomarsino et al. [2003]; Evans and Lauga [2010] or helical flagella Dreyfus et al. [2005]. The control of bead-pulled robots or swarm of robots Abbott et al. [2009]; Mathieu et al. [2006]; Martel and Mohammadi [2010] is provided by the magnetic field gradients of either magnetic resonance imaging (MRI) devices or magnetic setups and is thus better suited for present medical applications.

Whatever the proposed design, these systems are subject to different forces whose modeling is necessary in order to estimate and control their dynamic behaviors in a fluidic environment Arcese et al. [2011]; Vartholomeos and Mavroidis [2012]. Fluid flow in the microrobot environment presents a significant design challenge. We consider a microrobot designed to work in the circulatory system. In addition to dealing with varying blood vessels diameter, the microrobot must compete against the pulsating flow of blood, which is significant to a small, untethered device and even is prominent with respect to other involved forces. In the literature, the blood velocity is assumed to be known or set to a constant mean value, while it is a key nonlinear parameter of the drag force that prevails at a small scale. Since these untethered robots are actuated by the magnetic fields or magnetic gradients and their localization is ensured by a medical imager, the measurement of the blood velocity is a difficult task that is often assigned to other sensors e.g. ultrasonic sensors, at least in vessels close to the sensor. For example we can use a sensor which is based on the Doppler effect Ponzini et al. [2010]; Holloway Jr and Watkins [1977], or an MRI (magnetic resonance imaging) Gatehouse et al. [2005], however the major drawback of these two methods is that the temporal and spatial resolutions are not precise enough for estimating

the drag force or other robot forces. Hence the measurement is not usable when controlling the navigation of microrobots in blood vessels. Another solution relies on a priori knowledge of the blood velocity. Works related to the numerical resolution of the velocity profiles using Computational Fluid Dynamics software had been reported in the literature Kim et al. [2006]; Yong et al. [2008]. However, these studies cannot be used for real-time purposes because they are based on Navier Stokes equations whose resolution is computationally time consuming. In Arcese et al. [2011], the authors proposed analytical expressions of the blood velocity profiles. These expressions are valid in the neighborhood of a bifurcation but require an excellent knowledge of the vessel geometry. The blood velocity could also be considered as a disturbance and be rejected in the control low, like in Gangloff et al. [2006] for breathing compensation or considered as an unknown input. However, the knowledge of blood velocity is relevant for the navigation since the main force depends on it. Finally, online estimation of the blood velocity seems to be an interesting approach to avoid the drawbacks of the aforementioned methods, whilst also providing a diagnostic tool for the medical staff. For the online estimation of the blood velocity, a solution is to model the speed of the blood in the form of a state representation, the latter will be combined with that of the dynamics of the microrobot in order to synthesize an observer who will replace the physical sensors, using the only microrobot position measurement given by an imager.

Since an imager is already necessary to localize the robot and thus provides an output of the system, one can exploit an extended model of the system to reconstruct its unmeasured states. Observers of robot velocity have already been studied in Arcese et al. [2013]. We propose to extend this approach as done before in Fruchard et al. [2013], in order to estimate the blood velocity behavior. Another issue to be taken into consideration is the pulse rate of the blood, always considered as a constant Fruchard et al. [2013]; Sadelli et al. [2016]. However, the pulse rate varies depending on the state in which the patient is, for example at rest or stressed. To accede to it, one can either consider the pulse as a system output using a pulse sensor, or rather rebuild it using an observer.

## 3.2 Modeling

Microrobots navigating in blood vessels are subjected to various forces that affect their dynamics. Many works have been conducted on modeling these forces: electrostatic force Matsuyama and Yamamoto [1998], contact force Gilardi and Sharf [2002], van der Waals force Iimura et al. [2009], steric force Decuzzi et al. [2005], magnetic force Vartholomeos and Mavroidis [2012], see e.g. Arcese et al. [2011] for a review.

In our study, we focus only on the dominant forces. One of the most disturbing force applying

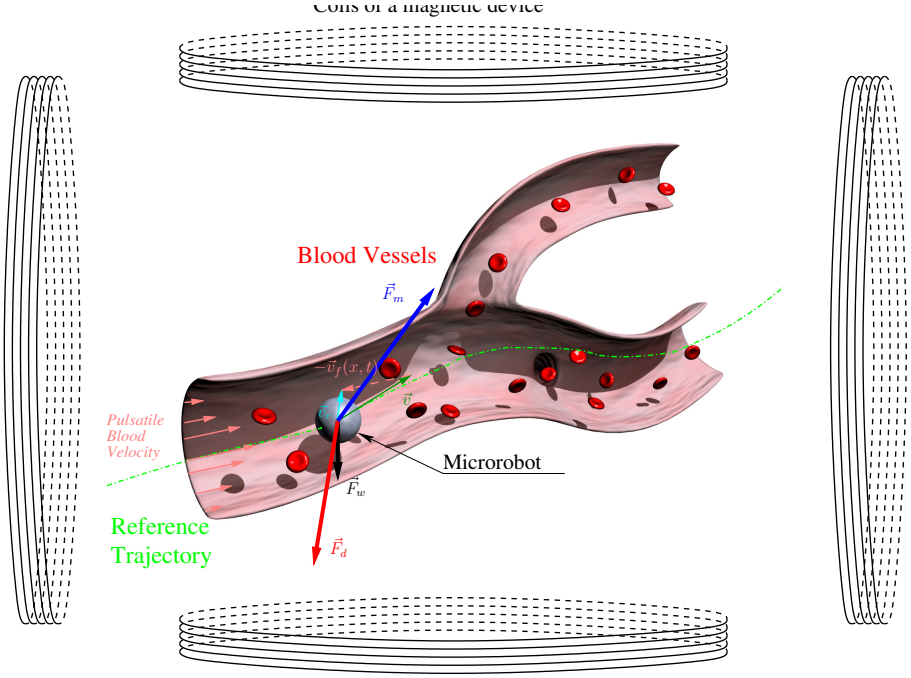


on the microrobot is the hydrodynamic force, which is exerted by the blood flow. The magnetic motive force produces a net thrust in a magnetic robot to propel it. The microrobot is also subject to its apparent weight, which is the contribution of gravity and buoyancy. Other forces such as electrostatic, van der waals, contact forces etc can be neglected as long as the microrobot navigates along the vessel centerline. We now detail the dominant forces acting on the microrobot and their analytical expressions.

### 3.2.1 Hydrodynamic drag force

The nature of the fluid flow is characterized by its Reynolds number $Re$, a dimensionless number equal to the ratio of inertial over viscous forces:

$$Re = \frac{\rho_f ||\overrightarrow{v}_r|| L}{\beta \mu}, \tag{3.1}$$

where $\rho_f, \mu$ are the density and dynamic viscosity of the fluid, respectively, $\overrightarrow{v}_r$ is the relative velocity of the microrobot ($v$) with respect to the blood ($v_f(x,t)$) such that $\overrightarrow{v}_r = \overrightarrow{v} - \overrightarrow{v}_f(x,t)$ and $L = 2r$ is the characteristic dimension, with $r$ denoting the radius of the microrobot. $\beta$ is a dimensionless ratio related to the wall effect caused by the vessel occlusion by the microrobot of radius $r$ Kehlenbeck and Felice [1999].

The drag force exerted by the fluid on the microrobot is empirically given by

$$\overrightarrow{F}_d = -\frac{1}{2} A C_d \rho_f \left( \frac{||\overrightarrow{v}_r||}{\beta} \right)^2 \frac{\overrightarrow{v}_r}{||\overrightarrow{v}_r||}, \tag{3.2}$$

where $A$ is the frontal area of the body relative to the flow. $C_d$ is the drag coefficient, a dimensionless number quantifying the resistance of a body in a moving fluid; it depends on the microrobot's geometry and surface state and is given by Nguyen and Schulze [2003]:

$$C_d = \frac{24}{Re} + \frac{6}{1+\sqrt{Re}} + 0.4. \tag{3.3}$$

The drag force thus depends -in general nonlinearly- on the fluid relative velocity in the robot's frame.

Replacing the drag coefficient $C_d$ and considering the surface area $A = \pi r^2$ in (3.2), we obtain a simplified expression for the nonlinear drag force:

$$F_d = -\left(a|v_r| + bv_r^2 + c\frac{v_r^2}{1+d\sqrt{|v_r|}}\right)\frac{\overrightarrow{v_r}}{\overrightarrow{\|v_r\|}} \tag{3.4}$$

with the parameters (a, b, c, d) defined as:

$$\begin{aligned} a &= \frac{6\pi\mu r}{\beta} \qquad b = \frac{0.2\rho_f \pi r^2}{\beta^2} \\ c &= \frac{3\rho_f \pi r^2}{\beta^2} \qquad d = \sqrt{\frac{2r\rho_f}{\beta\mu}}. \end{aligned} \tag{3.5}$$

In particular case, when the microrobots navigate in capillaries, or venules, where the blood flow is very slow and the size of the robot has to decrease as the vessels radius decreases, the Reynolds number is low such that $Re << 1$, hence the Stokes flow approximation is valid. As a result, drag force is linear such that $b = c = 0$.

### 3.2.2 Magnetic Motive Force

Magnetic coils, classically paired as Helmholtz, Maxwell or Golay coils, are used to design magnetic devices and produce magnetic fields and gradients. Magnetic fields and gradients are a source of energy for the microrobot propulsion in the cardiovascular system Dario et al. [1998]; Kosa et al. [2007]; Nelson et al. [2010]. Indeed these fields and gradients can in turn induce magnetic motive forces and torques on magnetic dipoles. Since we focus here on spheric bead pulling, torques are useless and the magnetic motive force is given by:

$$\overrightarrow{F}_m = \tau_m V(\overrightarrow{M}.\overrightarrow{\nabla})\overrightarrow{B}, \tag{3.6}$$

where $V$ is the microrobot volume, $\overrightarrow{B}$ is the magnetic field, $\overrightarrow{M}$ is the magnetization of the microrobot, and $\tau_m = \frac{V_m}{V}$ is the ferromagnetic volume.

### 3.2.3 Apparent Weight

Any body immersed in a fluid experiences a force called apparent weight, which is the contribution of the force of gravity and buoyancy:

$$\overrightarrow{F}_w = V(\rho_\mu - \rho_f)\overrightarrow{g}, \tag{3.7}$$

where $\rho_\mu, \rho_f$ are the microrobot and the fluid densities respectively. $V$ is the volume of the body and $g$ is the gravity acceleration. The density of the microrobot is composed of a magnetic material density $\rho_m$ and the non-magnetic material density $\rho_c$, and is given by:

$$\rho_\mu = \tau_m \rho_m + (1 - \tau_m)\rho_c, \tag{3.8}$$

where $\tau_m$ is the magnetic volume ratio, equal to the ratio of the total volume to the volume of magnetic material in the microrobot.

### 3.2.4 Blood Velocity Model

The blood circulating through the vascular structure of the human body is a viscous fluid and its characteristics and physical values vary depending on the type of blood vessel in which it is circulating , e.g. it behaves like a newtonian or non-newtonian fluid owing to large variations in its viscosity (from simple to fifty-folds) for the same person. As previously said, the blood velocity measurement by the means of ultrasonic sensors or its computation through discretization of the Navier-Stokes equation is not usable for real-time control purposes. A solution for such problem is then to take inspiration from the Wormersley model Womersley [1955]; the fluid speed is therefore given as $v_f(x,t) = v_s(x)\xi_1$, where $v_s(x)$ is a form factor which characterizes the pulsatile blood flow profile e.g. a parabolic profile of the blood is a newtonian fluid in the considered blood vessel and $\xi_1$ represents the temporal speed, solution of a system of autonomous differential equations.

We assume that the pulsatile blood velocity $\xi_1$ is modeled by a truncated Fourier series of order 1:

$$\xi_1 = A_0 + A_1 cos(\omega t + \varphi), \tag{3.9}$$

where $A_0$ and $A_1$ are respectively the mean value and the amplitude of the blood velocity $\xi_1$, and $\omega, \varphi$, the heartbeat and phase shift respectively. By differentiating $\xi_1$, we get

$$\xi_2 = \dot{\xi}_1 = -\omega A_1 sin(\omega t + \varphi). \tag{3.10}$$

Since the heartbeat depends on the patient condition and health and therefore can vary with time, it is here considered as an uncertain state variable. By deriving the signal (3.9) with respect

to time, $\xi \in \mathcal{K}_\xi \subset \mathbb{R}^4$ is solution of the following nonlinear system:

$$\Sigma_\xi = \begin{cases} \dot{\xi}_1 &= \xi_2 \\ \dot{\xi}_2 &= \xi_3 \\ \dot{\xi}_3 &= -\xi_2\xi_4 \\ \dot{\xi}_4 &= 0, \end{cases} \tag{3.11}$$

where $\xi_4 = \omega^2$ represents the pulse rate to be estimated.

### 3.2.5 State-Space Representation

Let $p_1$ and $p_2$ denote, respectively, the microrobot position and its velocity, $u$ as the control input, and $\xi_1$ the blood velocity, the system derived from (3.4), (3.6) and (3.7) is:

$$\Sigma_1 = \begin{cases} \dot{p}_1 = p_2 \\ \dot{p}_2 = f_d(p_2 - \xi_1) + \dfrac{\tau_m M}{\rho} u \\ y = p_1 \end{cases} \tag{3.12}$$

where the output $y$ is the position of the microrobot, measured by the imager. The expression of the function $f(p_2, \xi_1)$ is given by:

$$f_d(p_2 - \xi_1) = \left[ -\sigma(p_2 - \xi_1) \left( a|p_2 - \xi_1| + b(p_2 - \xi_1)^2 + c\frac{(p_2 - \xi_1)^2}{1 + d\sqrt{|p_2 - \xi_1|}} \right) + V(\rho_f - \rho_\mu)g \right] \frac{1}{m}, \tag{3.13}$$

where the sign function $\sigma$ is defined by

$$\sigma(s) = \begin{cases} -1, & \text{if} \quad s < 0 \\ 0, & \text{if} \quad s = 0 \\ 1, & \text{if} \quad s > 0. \end{cases} \tag{3.14}$$

Since the measurement is limited only to the position of the microrobot, i.e. $y = x_1$, and the blood velocity $\xi_1$ intervenes in the reduced system, the control of this reduced system requires either a good robustness to the uncertainty on $\xi_1$, or to compensate for this term, which requires its estimation. To this end, we present the state representation of an extended system combining the dynamics of the reduced microrobot system (3.13) and the blood flow dynamics (3.11):

$$\Sigma_2 = \begin{cases} \dot{x} = f(x) + gu \\ y = h(x) \end{cases} \tag{3.15}$$

where $g = \begin{bmatrix} 0 & \frac{\tau_m M}{\rho} & 0_{1\times 4} \end{bmatrix}^T$ and the function $f(x)$ is given as:

$$f(x) = \begin{pmatrix} x_2 \\ f_d(x_2 - x_3) \\ x_4 \\ x_5 \\ -x_4 x_6 \\ 0 \end{pmatrix}, \tag{3.16}$$

where the state vector $x = [p^T, \xi^T]^T \in \mathcal{X} \subset \mathbb{R}^6$ and output $y = x_1$. So from the state space representation of extended system, we perceive the non-linearities emanating from the microrobot dynamics as well as the blood velocity model.

## 3.3 Observability Analysis

In order to build an observer, a first prerequisite is to study the conditions guaranteeing the observability of the sytem.

**Proposition 14** *System (3.15) is observable on any connected subset of $\mathcal{X}\backslash\mathcal{S}_{\mu robots}$ where $\mathcal{S}_{\mu robots} = \{x \in \mathcal{X} \subset \mathbb{R}^6 : x_4^2 + x_5^2 \leq \epsilon\}$ for any $\epsilon > 0$.*

**Proof 11** *Let the observation set $\mathcal{O}$ denote the smallest vector space that contains $h$ and closed under the Lie derivative $\mathcal{L}_f$,* i.e. *such that $\forall \sigma \in \mathcal{O}$, $\mathcal{L}_T(\sigma) \in \mathcal{O}$. $\mathrm{d}\mathcal{O} = Span\{\mathrm{d}T, T \in \mathcal{O}\}$ is the observability co-distribution where $d$ denote the differential. A system is weakly observable if* $\dim \mathrm{d}\mathcal{O}(x) = \dim \mathcal{X}$.

*Using the output $y = x_1$ in (4.5), we compute the successive Lie derivatives*

$$\begin{aligned}
\mathcal{L}_f^0 h(x) =& x_1, \\
\mathcal{L}_f^1 h(x) =& x_2, \\
\mathcal{L}_f^2 h(x) =& f_d(x_2 - x_3), \\
\mathcal{L}_f^3 h(x) =& f_d'(f_d - x_4), \\
\mathcal{L}_f^4 h(x) =& (i - f_d'' x_4)(f_d - x_4) - f_d' x_5, \\
\mathcal{L}_f^5 h(x) =& (j + k x_4 + f_d''' x_4^2 - f_d'' x_5)(f_d - x_4) + (2 f_d'' x_4 - i - f_d f_d'')x_5 + f_d' x_4 x_6, \\
\mathcal{L}_f^6 h(x) =& l(\bar{x}_5) + f_d' x_5 x_6 + x_4 x_6(-3 f_d'' x_4 + i + 2 f_d f_d''),
\end{aligned} \tag{3.17}$$

*where* $i = f_d'' f_d + f_d'^2$, $j = i' f_d + i f_d'$ *and* $k = -f_d f_d''' - i' - f_d' f_d''$. *Therefore, we get*

$$d\mathcal{L}_f^i h = \begin{pmatrix} 1 & 0 & 0 & 0 & 0 & 0 \\ 0 & 1 & 0 & 0 & 0 & 0 \\ 0 & f_d & -f_d' & 0 & 0 & 0 \\ 0 & * & * & -f_d' & 0 & 0 \\ 0 & * & * & * & -f_d' & 0 \\ 0 & * & * & * & * & v_1 \\ 0 & * & * & * & * & v_2 \end{pmatrix}, \tag{3.18}$$

*where*

$$v = \begin{pmatrix} \frac{\partial \mathcal{L}_f^5}{\partial x_6} \\ \frac{\partial \mathcal{L}_f^6}{\partial x_6} \end{pmatrix} = \begin{pmatrix} f_d' x_4 \\ f_d' x_5 + x_4(-3 f_d'' x_4 + i + 2 f_d f_d'') \end{pmatrix}. \tag{3.19}$$

*It has been proven in Fruchard et al. [2013] that*

$$\left| \frac{\partial f_d}{\partial x_3} \right| \in [\alpha_1, \alpha_2], \quad 0 < \alpha_1 < \alpha_2 < \infty, \quad \forall x \in \mathcal{X},$$

*where* $\mathcal{X}$ *is a compact subset of* $\mathbb{R}^6$.

*Since* $f_d' \neq 0$ *from Fruchard et al. [2013], then* $v^T v = 0 \Leftrightarrow x_4^2 + x_5^2 = 0$. *We conclude that* $\dim \mathrm{d}\mathcal{O}(x) = 6$ *on any connected subset out of* $\mathcal{S}_{\mu robots} = \{x \in \mathbb{R}^6 : |x_4^2 + x_5^2| < \epsilon\}$, *for any* $\epsilon > 0$. *However there is a singularity of the system observability for* $x_s = (x_1 \ x_2 \ x_3 \ 0 \ 0 \ x_6)^T$ *since* $\dim \mathrm{d}\mathcal{O}(x_s) = 5$.

Consequently the system (3.15) is not observable on

$$\mathcal{S} = \{x \in \mathcal{X} \subset \mathbb{R}^6 : x_4^2 + x_5^2 = 0\}. \tag{3.20}$$

Physically, this singularity is related to the fact that one can not access to any information about the pulse state $x_6$ when $x_4^2 + x_5^2 = 0$. Note that this is physically impossible since, due to system (3.11), $x_4$ and $x_5$ cannot vanish simultaneously, however, one can get $x_4^2 + x_5^2 = 0$, especially during the transient phase, unless some mechanism prevent the estimation to leave $\mathcal{X} \backslash \mathcal{S}_{\mu robots}$.

## 3.4 Nonlinear observer synthesis

While dealing with the microrobots, our extended system has a higher dimension and a very high lipshcitz constant therefore using the standard HGO can be quite problematic since the power of the high gain parameter increases with the dimension increase. Therefore, in this work, we are interested particularly in the low peaking limited high gain observer design, since it is well-adapted for the estimation of the nonlinear systems and ought to provide a fast error convergence

by tuning the high gain parameter. Alongside, the power of the high gain parameter is limited to 2 irrespective of the system dimension therefore it is quite suitable for this application. However, in order to design the observer, we need to map the system in a form for which this observer can be designed. Using $z = T(x)$ defined by (1.27) for $n_z = n_x + 1$, system (3.15) can be mapped to a phase variable form, however since the microrobot system is partially in feedback therefore for the sake of simplicity we transform the system using a simplified mapping such that:

$$\begin{aligned} z_i &= x_i, \quad \forall i = 1, ..., 5 \quad \text{and} \\ z_6 &= -x_4 x_6 \\ z_7 &= -x_5 x_6. \end{aligned} \tag{3.21}$$

Using (3.21) we get the system in Gauthier Kupka form, where $z \in \mathcal{Z} \subset \mathbb{R}^7$ is the state vector in target coordinates and $y = z_1$ is the measured output.

Since it is possible to estimate the full-state vector of the extended system (3.15) using the sole output accessible to measurement, observer for the system (3.15) can be designed.

### 3.4.1 Low Peaking Limited High Gain Observer

The low peaking limited high gain observer covers the essential feature of limited high gain observer (i.e. limited power of the high gain parameter $\theta$ upto the power of 2) and provides even more reliable results related to the peaking effect compared to HGO and LHGO. Based on Theorem 12, we can design the LPLHGO for the microrobot system.

**Proposition 15 (LPLHGO for microrobots)** *The low peaking limited high gain observer for the system (3.21) is given as:*

$$\begin{aligned} \dot{\hat{z}} &= \mathcal{F}_z(\hat{z}, \eta, y) \\ \dot{\eta} &= \mathcal{F}_\eta(\hat{z}, \eta, y) \end{aligned} \tag{3.22}$$

*with $\mathcal{F}_z$ and $\mathcal{F}_\eta$ given as:*

$$\mathcal{F}_z : \begin{cases} \dot{\hat{z}}_1 = \eta_1 + \alpha_1\theta(y - \hat{z}_1) \\ \quad \vdots \\ \dot{\hat{z}}_i = \eta_i + \alpha_i\theta(sat_{\kappa_i}(\eta_{i-1}) - \hat{z}_i) \\ \quad \vdots \\ \dot{\hat{z}}_7 = \varphi_{7s}(\hat{z}) + \alpha_7\theta(sat_{\kappa_7}(\eta_6) - \hat{z}_7) \end{cases} \qquad \mathcal{F}_\eta : \begin{cases} \dot{\eta}_1 = sat_{\kappa_3}(\eta_2) + \beta_1\theta^2(y - \hat{z}_1) \\ \quad \vdots \\ \dot{\eta}_i = sat_{\kappa_{i+2}}(\eta_{i+1}) + \beta_i\theta^2(sat_{\kappa_i}(\eta_{i-1}) - \hat{z}_i) \\ \quad \vdots \\ \dot{\eta}_6 = \varphi_{7s}(\hat{z}) + \beta_6\theta^2(sat_{\kappa_6}(\eta_5) - \hat{z}_6) \end{cases} \tag{3.23}$$

*such that $\hat{z} \in \mathbb{R}^7$, $\eta \in \mathbb{R}^6$ are the observer states and with*

$$\kappa_i := \max_{z \in \mathcal{Z}} |z_i| \quad i = 1, ..., n_z.$$

We can get the observer in original coordinates using the inversion of $T : \hat{x} = \mathcal{T}(\hat{z})$:

$$\mathcal{T}(\hat{z}) = \begin{pmatrix} z_1 \\ \vdots \\ z_5 \\ -\left(\frac{z_4 z_6 + z_5 z_7}{z_4^2 + z_5^2}\right) \end{pmatrix} \tag{3.24}$$

From the left-inverse, it is clear that the system is singular when $z_4^2 + z_5^2 = 0$ and the inversion is no longer possible in such a case.

Another method to get the observer in natural coordinates is by using Proposition (2) provided that the mapping $T$ is a diffeomorphism:

$$\dot{\hat{x}} = \left(\frac{\partial T}{\partial x}(\hat{x})\right)^{-1} \dot{\hat{z}}. \tag{3.25}$$

The Jacobian of the mapping $T$ is given as

$$\begin{aligned} \frac{\partial T}{\partial x}(x) &= \begin{pmatrix} I_5 & 0_{5,1} \\ J_1(x) & J_2(x) \end{pmatrix} \quad \text{with} \\ J_1(x) &= \begin{pmatrix} 0_{2,3} & -x_6 I_2 \end{pmatrix}, \quad J_2(x) = \begin{pmatrix} -x_4 \\ -x_5 \end{pmatrix} \end{aligned} \tag{3.26}$$

where the matrix $J_2$ depends on $x_4$ and $x_5$, meaning that in such a case when $x_4 = x_5 = 0$, the jacobian will loose its rank and there will be singularity in the system and therefore it will not be possible to get any information about the variable $x_6$. The presence of the structural singularity in $J_2$ thereby causes an obstruction during the invertibility of the jacobian matrix.

Therefore, a need to achieve diffeomorphism and to remove this observability singularity is necessary to get the observer in original coordinates.

### 3.4.2 Main Results

#### 3.4.2.1 Observability defects avoidance

Observability defects in the system 3.15 cause a loss of information for the state variable $x_6$ that is required to fully reconstruct the system state. Technically this observability singularity undermine the immersion and injectivity property of $T$, so the observer in Proposition 15 is no more well defined and encounter singularity. To solve this issue, we use the technique introduced before in section 2.3.1 of Chapter 2 by adding a fictitious output to the current state vector. The presence of this output provides fictitious access to the information for the state variable $x_6$, when the system is singular, allowing the modified system to remain observable and the observer to be well-defined.

**Proposition 16 (Observability defects avoidance)** *To circumvent the singularity of the system 3.15 defined in Proposition 14, we introduce a $\mathcal{C}^2$ mapping $\rho$ as:*

$$\rho : x \to max(0, \epsilon^2 - (x_4^2 + x_5^2))^2, \tag{3.27}$$

*so as to define a fictitious output $y_f \in \mathbb{R}^{n_f}$ as:*

$$y_f = \rho x_6. \tag{3.28}$$

*Extending the mapping $T$ defined by (3.21) as:*

$$T_e : \begin{array}{ccc} \mathbb{R}^6 & \to & \mathbb{R}^{n_z} \times \mathbb{R}^{n_f} \\ x & \mapsto & \begin{pmatrix} T(x) \\ y_f(x) \end{pmatrix} \end{array} \tag{3.29}$$

*then defines an injective immersion from $\mathbb{R}^6$ to $\mathbb{R}^8$.*

**Proof 12** *The Jacobian of the mapping $T_e$ defined by (3.29) is given by:*

$$\frac{\partial T_e}{\partial x}(x) = \begin{pmatrix} \frac{\partial T}{\partial x} \\ \frac{\partial y_f}{\partial x} \end{pmatrix} = \begin{pmatrix} I_5 & 0_{5,1} \\ \bar{J}_1 & \bar{J}_2 \end{pmatrix} \tag{3.30}$$

*with matrices $\bar{J}_1, \bar{J}_2$:*

$$\bar{J}_1 = \begin{pmatrix} 0_{1,3} & -x_6 & 0 \\ 0_{1,3} & 0 & -x_6 \\ 0_{1,3} & \rho_4 x_6 & \rho_5 x_6 \end{pmatrix}, \quad \bar{J}_2 = \begin{pmatrix} -x_4 \\ -x_5 \\ \rho \end{pmatrix}, \tag{3.31}$$

*where $\rho_4, \rho_5$ denote the partial derivatives of $\rho$ w.r.t $x_4$ and $x_5$ respectively,* i. e. *$\rho_i = \frac{\partial \rho}{\partial x_i}(x)$.*

*Due to the block triangular structure of the Jacobian (3.30), the $T_e$ Jacobian matrix is full rank provided that $\bar{J}_2$ is also full rank.*

*Since by construction, $\rho$ and $x_4^2 + x_5^2$ cannot be null simultaneously, it follows that $\bar{J}_2$ and in turn the jacobian of $T_e$ are full rank matrices for any $x \in \mathbb{R}^{n_x}$. Besides, injectivity of $T_e$ is inherited from Proposition 14, hence $T_e$ is an injective immersion on $\mathbb{R}^6$.*

**Remark 11** *The number of fictitious outputs $n_f$ depends on the particular system or the states affected by the singularity. Since in our case, only one states $x_6$ become unobservable in a neighbourhood $\mathcal{S}_{\mu robots}$ of $x_s$, it is sufficient to set the number of fictitious output to one.*

**Remark 12** *It is worth mentioning that the dynamics associated with the fictitious output is null for the system living on $x \in \mathcal{X} \subset \mathbb{R}^6 \backslash \mathcal{S}_{\mu robots}$. The fictitious outputs will be activated only when the system enters $\mathcal{S}_{\mu robots}$ i.e. gets close to the observability singularity $x_s \in \mathcal{S}_{\mu robots}$.*

#### 3.4.2.2 Augmentation of $T_e$ into a global diffeomorphism

Recalling the approach defined in Chapter 2, we extend the image of $T_e$ to get a global diffeomorphism $T_a$ through coordinate augmentation from $x \in \mathbb{R}^6$ to $x_a \in \mathbb{R}^8$ by adding two fictitious states $\tau \in \mathbb{R}^2$, so a pre-image will always exist and will be uniquely defined.

**Proposition 17** *With notations of Proposition 16, let $\tau \in \mathbb{R}^2$ and define an augmented mapping $T_a$ as:*

$$T_a : \begin{array}{ccc} \mathbb{R}^8 & \to & \mathbb{R}^8 \\ x_a = \begin{pmatrix} x \\ \tau \end{pmatrix} & \mapsto & z_a = T_e(x) + \Psi(x)\tau, \end{array} \tag{3.32}$$

*where $\Psi(x)$ is a $(8 \times 2)$ matrix chosen as*

$$\Psi(x_a) = \begin{pmatrix} 0_{5,2} \\ I_2 \\ x_4 \quad x_5 \end{pmatrix}. \tag{3.33}$$

*Then, $T_a$ defines a global diffeomorphism on $\mathbb{R}^8$ satisfying*

$$T_a(x, 0) = \begin{pmatrix} T(x) \\ 0 \end{pmatrix}, \quad \forall x \in \mathcal{X} \subset \mathbb{R}^6 \backslash \mathcal{S}_{\mu robots}. \tag{3.34}$$

**Proof 13** *The jacobian matrix of $T_a$ given by (3.32) is:*

$$\frac{\partial T_a}{\partial x_a}(x_a) = \begin{pmatrix} I_5 & 0_{5,1} & 0_{5,2} \\ \bar{\bar{J}}_1(x_a) & \bar{J}_2(x_a) & J_\Psi(x_a) \end{pmatrix} \tag{3.35}$$

*where the matrices $\bar{\bar{J}}_1(x_a) = \bar{J}_1(x_a) + \frac{\partial \Psi}{\partial x}\tau$ and $\bar{J}_2(x_a)$ is given by (3.31) and the jacobian is completed by the $\Psi$ columns (see (3.33)) given by:*

$$J_\Psi(x_a) = \begin{pmatrix} 1 & 0 \\ 0 & 1 \\ x_4 & x_5 \end{pmatrix} \tag{3.36}$$

*It is straightforward that*

$$\left| \frac{\partial T_a}{x_a} \right| = (\rho + x_4^2 + x_5^2)^2 > 0, \quad \forall x \in \mathcal{X}. \tag{3.37}$$

*$\frac{\partial T_a}{\partial x_a}$ is invertible on any bounded subset of $\mathbb{R}^6$, and the observer (15) is thus well defined on any bounded subset of $\mathbb{R}^8$.*

*To check the injectivity of $T_a$ we provide the following proof:*

$$z_a = T_a(x,\tau) = \begin{pmatrix} x_1 \\ x_2 \\ x_3 \\ x_4 \\ x_5 \\ -x_4x_6 + \tau_1 \\ -x_5x_6 + \tau_2 \\ \rho(x_4,x_5)x_6 + x_4\tau_1 + x_5\tau_2 \end{pmatrix} \tag{3.38}$$

$$T_a(x',\tau') = T_a(x,\tau) \Longrightarrow x'_i = x_i, \quad \forall i \leq 5 \quad so \;\; \rho' = \rho \tag{3.39}$$

*and*

$$\begin{aligned} -x_4x'_6 + \tau'_1 &= -x_4x_6 + \tau_1 \\ -x_5x'_6 + \tau'_2 &= -x_5x_6 + \tau_2 \\ \rho x'_6 + x_4\tau'_1 + x_5\tau'_2 &= \rho x_6 + x_4\tau_1 + x_5\tau_2 \end{aligned} \tag{3.40}$$

*Using $\tilde{x}_i = x'_i - x_i$ in (3.40):*

$$\begin{aligned} \tilde{\tau}_1 &= x_4\tilde{x}_6 \\ \tilde{\tau}_2 &= x_5\tilde{x}_6 \\ x_4\tilde{\tau}_1 + x_5\tilde{\tau}_2 &= -\rho\tilde{x}_6 \end{aligned} \tag{3.41}$$

*Combining (3.41), we get:*

$$x_4^2\tilde{x}_6 + x_5^2\tilde{x}_6 + \rho\tilde{x}_6 = 0 \Longrightarrow \tilde{x}_6(\rho + x_4^2 + x_5^2) = 0 \tag{3.42}$$

*Since by definition $(\rho + x_4^2 + x_5^2) \neq 0$, therefore $\tilde{x}_6 = 0$ so $x'_6 = x_6$. Using the expression in (3.41), we then find that $\tilde{\tau}_i = 0$ so $\tau'_i = \tau$. Hence $T_a$ is a global diffeomorphism.*

**Proposition 18 (Singularity-free LPLHGO for microrobots)** *The dynamic system*

$$\begin{cases} \dot{\hat{x}}_a = \left(\dfrac{\partial T_a}{\partial x_a}(\hat{x}_a)\right)^{-1} \begin{pmatrix} \mathcal{F}_z(T_a(\hat{x}_a),\eta,y) \\ -K_{n_f}T_{n_f}(\hat{x}_a) \end{pmatrix} \\ \dot{\eta} = \mathcal{F}_\eta(T_a(\hat{x}_a),\eta,y) \end{cases} \tag{3.43}$$

*is an arbitrarily fast converging observer for system (3.15) in its original coordinates on any bounded subset of $\mathbb{R}^{n_z+n_f}$. $\mathcal{F}_z, \mathcal{F}_\eta$ are defined in Proposition 15. $T_a$ is defined by Proposition 17, $K_{n_f} > 0$ is the gain related to the fictitious output and the notation $T_{n_f}$ stands for the last components of $T_a$ representing the dynamics associated with the fictitious output. By continuity $T_a^{-1}$*

*is $\mathcal{C}^1$, hence it is L-Lipschitz on any compact of $\mathbb{R}^8$. It follows that, using $z_a^* = T_a(x,0) = T_e(x)$:*

$$\begin{aligned}
\|x(t)-\hat{x}(t)\| + \|\tau(t)\| &\leq \sqrt{2}\left\|\begin{matrix} x-\hat{x} \\ \tau \end{matrix}\right\| \\
&\leq \sqrt{2}\left\|\begin{pmatrix} x \\ 0 \end{pmatrix} - \begin{pmatrix} \hat{x} \\ \tau \end{pmatrix}\right\| \\
&\leq \sqrt{2}\|T_a^{-1}(z_a^*) - T_a^{-1}(\hat{z}_a)\| \\
&\leq L\sqrt{2}\|z_a^* - \hat{z}_a| \\
&\leq L\sqrt{2}\|T_e(x) - T_a(\hat{x},\tau)\|.
\end{aligned} \tag{3.44}$$

*Since $T_e$ is injective immersion and defines a converging observer from Proposition 15-17, it follows that*

$$\lim_{t\to\infty} \|x(t)-\hat{x}(t)\| + \|\tau(t)\| = 0. \tag{3.45}$$

| | |
|---|---|
| $A_0$ | 0.1 |
| $A_1$ | 0.033 |
| $\omega$ | $2\pi$ |
| $\varphi$ | $\frac{74\pi}{180}$ |
| $M$ | $1.23 \times 10^6$ |
| $\tau_m$ | 0.75 |
| $\rho$ | 2000 |
| $x_0$ | $\begin{pmatrix} 0 & 0 & A_0 + A_1 cos(\omega t + \varphi) & -\omega A_1(\omega t + \varphi) & -\omega^2 A_1 cos(\omega t + \varphi) & \omega^2 \end{pmatrix}$ |
| $\begin{pmatrix} \alpha_1 & \alpha_2 & \alpha_3 & \alpha_4 & \alpha_5 & \alpha_6 & \alpha_7 \end{pmatrix}$ | $\begin{pmatrix} 110 & 110 & 110 & 110 & 110 & 110 & 101 \end{pmatrix}$ |
| $\begin{pmatrix} \beta_1 & \beta_2 & \beta_3 & \beta_4 & \beta_5 & \beta_6 \end{pmatrix}$ | $\begin{pmatrix} 13363.6 & 118.3 & 2842.3 & 1036.7 & 802.2 & 320.8 \end{pmatrix}$ |
| $k_1$ | 2 |
| $k_2$ | 4 |
| $k_8$ | 1 |
| $\theta$ | 8.5 |
| $\epsilon$ | 0.005 |

Table 3.1: Initial conditions and gains for the system and observers

### 3.4.3 Simulation Results

Simulations have been led for the proposed low peaking limited high gain observer for the micro-robot system in the original coordinates for two scenarios: the nominal case and the singularity avoidance case. The initial conditions, physical, controller and observer parameters are given in

Table 3.1, where the observer gains are chosen quite high for the fast convergence. For the sake of simplicity, i.e. to avoid computing an optimal reference trajectory to be stabilized along, the controller is here designed to keep the microrobot at a fixed point using backstepping control law and the gains $k_i$ Arcese et al. [2013].

#### 3.4.3.1 Nominal case

The first case is the nominal one where $\hat{x}_4$ and $\hat{x}_5$ are initialized close to the initial conditions of $x_4$ and $x_5$, so it is unlikely that the system experience any singularity. Figures 3.1 illustrate the estimation error between the simulated and estimated microrobot position and velocity as well as the error for the blood velocity and the pulse rate $\omega$. The effect of saturation functions in reducing the peaking effect can be seen in the simulations since the estimated states quickly converges to the system states within the first 0.05 second with a very little peaking, as can be seen in Figures 3.1(a) and 3.1(b). Similarly for the blood velocity, the peaking effect is negligible and the estimated states converge to the real states in less than 0.1 second. However, in figure 3.1(e), the peaking is quite obvious while estimating the pulse rate, and it takes around 3-4 seconds for the estimated pulse rate to converge to its nominal value (Figure 3.1(f)) The fictitious output in this case remains inactivated throughout the simulation since there is no singularity in the system, hence it is not illustrated here.

#### 3.4.3.2 Singularity Avoidance

In the second case, to check the effectiveness of the observer during observability defects, we initialized the observer with the states $\hat{x}_4$ and $\hat{x}_5$ being null. The effect of singularity is visible on the pulse rate estimation in Figures 3.2(c) and 3.2(d), where during the initial time period, the peaking is increased due to activated fictitious output. The last two figures 3.2(e) and 3.2(f) represents the $\tau$ states and $y_f$ where the fictitious output is activated briefly before returning to zero while the $\tau$ states require some time to converge to zero. The activated fictitious output has no impact on the estimation of microrobot position and velocity which are the same as Figures 3.1(a) and 3.1(b).

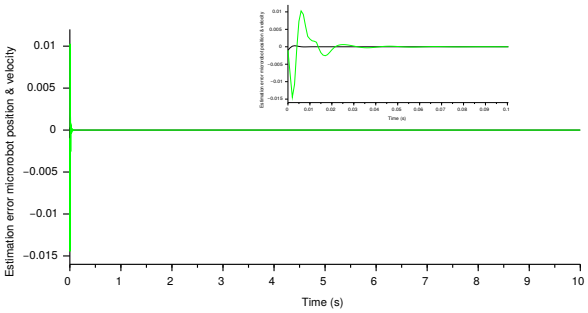


(a) Microrobot position and velocity estimation error

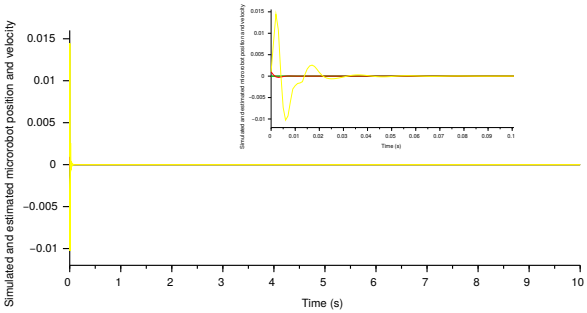


(b) Simulated & estimated microrobot position and velocity

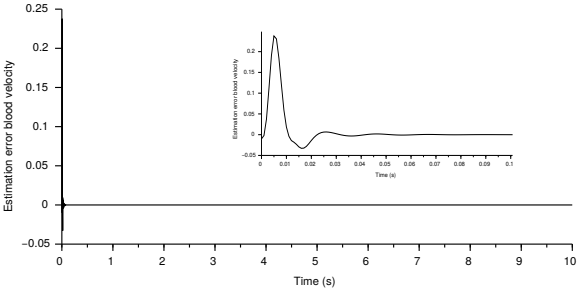


(c) Blood velocity estimation error

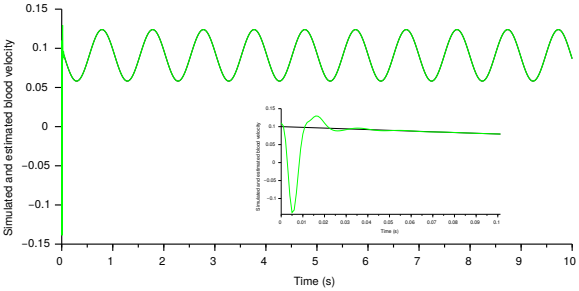


(d) Simulated and estimated blood velocity

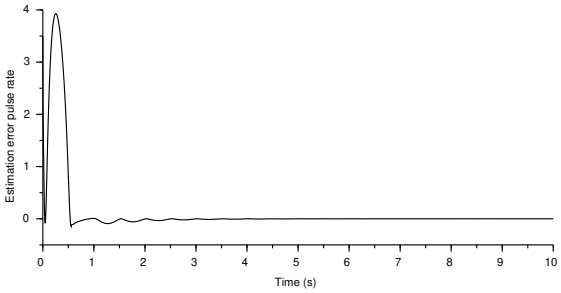


(e) Pulse rate estimation error

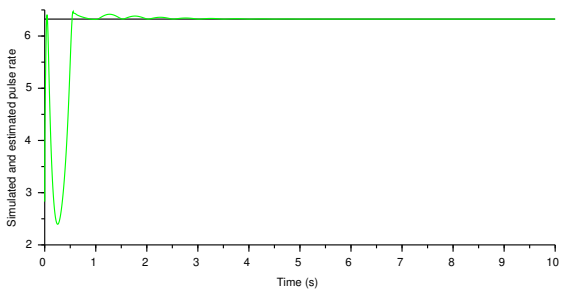


(f) Simulated and estimated pulse rate

Figure 3.1: Case A from (a) to (f): simulation for nominal case. Figure (a) represents the estimation error of microrobot position and velocity in black and green lines respectively, Figure (c) represents blood velocity error and Figure (e) represents the pulse rate estimation error. Figures (b) represents the states and estimated microrobot position and velocity states, such that simulated states are in black and green lines while the estimated states $\hat{x}$ are in red and yellow lines respectively, Figures (d) and (f) represents the simulated states in black lines and estimated states in green lines for blood velocity and pulse rate respectively.

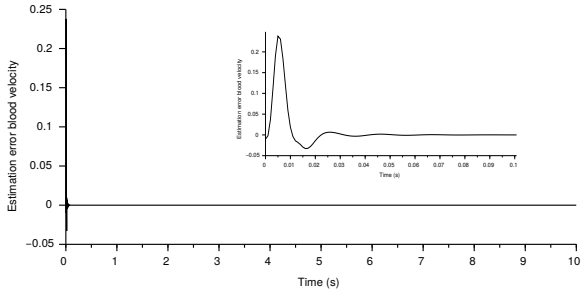


(a) Blood velocity estimation error

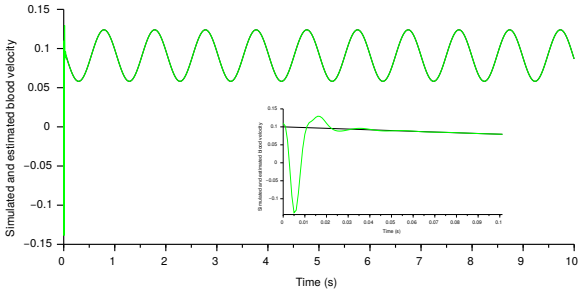


(b) Simulated and estimated blood velocity

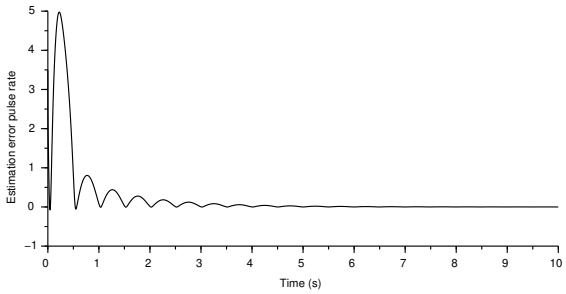


(c) Pulse rate estimation error

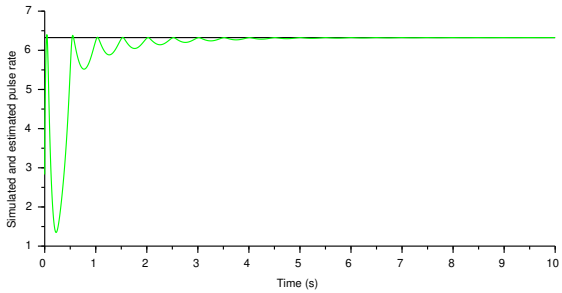


(d) Simulated and estimated pulse rate

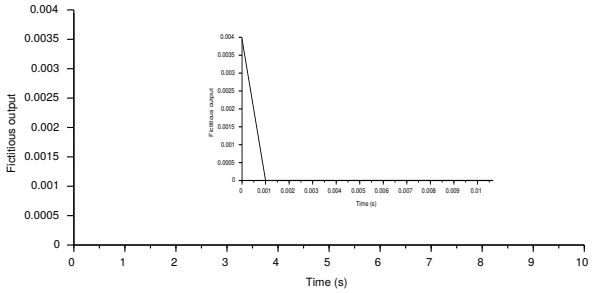


(e) fictitious output

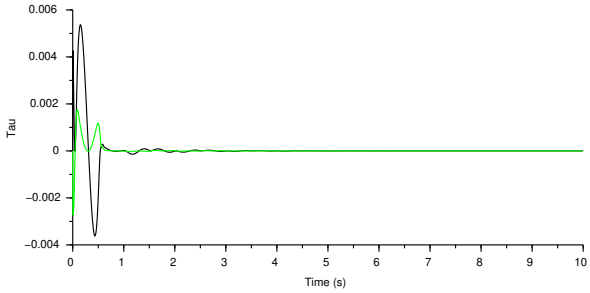


(f) Tau states

Figure 3.2: Case A from (a) to (f): simulation for singularity avoidance case. Figure (a) represents blood velocity error and Figure (c) represents the pulse rate estimation error. Figures (b) and (d) represents the states and estimated states, such that states are in black lines while the estimated states $\hat{x}$ are in green lines respectively for blood velocity and pulse rate. The last two figures (e) and (f) shows the activated fictitious output in black and tau states in black and green lines.

## 3.5 Conclusion

The core idea of this chapter was to estimate the microrobot position and velocity as well as the velocity of the blood in which a microrobot is immersed using the sole measurement of the microrobot position, given by an imager. An additional factor that needed to be taken into account was the blood pulse rate which in this case was also estimated as a state variable using an observer. We first provided a global overview of the forces acting on microrobot navigating in the blood vessels, and then we have presented a dynamic system based on the dominant forces acting on these microrobot. Since our goal was to also estimate the blood velocity and its pulse rate, we gave a state space representation for the blood speed and then we presented an extended dynamical system, which combined the dynamical model of the microrobot with the blood speed model.

The proposed extended model observability was then studied, revealing the presence of some observability defects. Therefore, we applied the methodology introduced in Chapter 2 to bypass the observability singularity. Due to addition of the fictitious outputs in the target state space and also because of the dimension gap between the target coordinates and the original coordinates, an extension of the mapping to a global diffeomorphism has been done.

Finally an observer capable of handling the observability defects was proposed in order to estimate the full-state vector required to implement the control law. The state observer was combined with a control law based on backstepping technique and the efficiency of the proposed approach has been illustrated by simulation results.

Chapter 4

# Application to Wake Flow Dynamics

## Chapter Content

The first section of this chapter comprises the introduction and a brief literature review on wake flow dynamics. The second section introduces the modeling of the wake flow dynamics based on different schemes, and we will introduce four different models of increasing complexity: Minimal model, SPOD model, Multi-output model and Hybrid model. For each model, a brief introduction followed by the observability analysis is provided. Based on the observability analysis, then for each system we will design the three observers namely: the classical high gain observer, the limited high gain observer and the low peaking limited high gain observer. For each observer, two designs will be presented: first the standard form of these observers for each model, and afterwards a second design addressing the observability defects avoidance. By the end of each section, we will present the simulation and experimental results for each model in order to check the effectiveness of each observer under different scenarios. The simulation results are then followed by a brief discussion for each scenario to compare the performances of these observers under different conditions.

## 4.1 Context and Motivation

The analysis of wake flow and its impact on the energy consumption in the transportation sector becomes an increasingly important issue for these structures dynamics are responsible for an increased drag, and in turn of undue energy. Vehicles, especially road vehicles or boats which are not streamlined are considered as bluff bodies where the flow is massively separated in the near wake. This separated area, called the wake is described by very small velocity magnitudes and flow moving in the upstream direction. Ground transportation in a globalizing world accounts for $15-20\%$ of the total greenhouse gas emissions, where the wake dynamics is generally admitted to contribute one-third of the total vehicle drag Hucho et al. [1998] and reducing them therefore appears as a remarkable action Palmer [2007]; Dekker et al. [2012]; Baude et al. [2017]. The turbulent wakes downstream the bluff body can be very complex, exhibiting coherent structures with different scales. Predicting the flow inside the wake is a challenging issue and has a profound impact on our capability in controlling such flows. For instance, in the case of vehicles at cruising speeds, a decrease of 2% in the drag coefficient can result in 1% energy consumption for road vehicles. This ratio becomes even closer to unity for naval and aircraft applications.

The strongly intermittent behavior of the flow depends on the Reynolds number: an essential non-dimensional parameter in fluid dynamics as the ratio of inertial forces to viscous forces (see Equation (3.1) of section 3.2.1). At high Reynolds numbers, vortex shedding occurs in the wake, leading to a significant pressure drop on the rear surface of the body. This phenomenon gives rise to structural vibrations, acoustic noise and also increases the unstationary drag force. The control of vortex shedding is then of major interest for engineering applications. Active control

in fluid mechanics is a promising and challenging research area. Promising because lower energy consumption and better performances are expected by decreasing the drag force. Challenging because observation and control require both real-time tractable and robust models with respect to dynamic changes in the wake flow Ma et al. [2000]; Östh et al. [2014]. However, the estimation of the drag force on a vehicle remains a challenge Sovran [2012]. Thus far, methods to determine the drag of a bluff body relies on dense measurements of pressure to ensure minimum errors for the calculation of the resulting forces exerted by the pressure and skin friction. In the case of bluff body flows, the latter often plays a minor role and methods that can be used in real time for the observation of the drag coefficient from sparse pressure measurements and eventually the feedback control of such flows are of major scientific and industrial interest Cooper [1993].

The main challenge in mathematical and physical modeling and the prediction of wake dynamics resides in the number of states, or modes, necessary to describe the physics and how these modes contribute to drag force. Some of these modes seem to be necessary to accurately capture the broad range of unstable frequencies in a turbulent flow Ma et al. [2000]; Volpe et al. [2015]; Thacker et al. [2013]; Östh et al. [2014]. These modes can be organized in a spectrum that counts several types of strongly amplified, self-excited, or intermittent modes which need to either be represented or filtered to capture and model the wake dynamics. Unless the number of modes or states used to represent the dynamics is kept small, a dynamical system cannot be used in real time in a data-assimilation-type scheme where the sensors output can be used to predict in real time. In addition, the unstable character of the wake prevents the use of linear models which grow unbounded in time and therefore do not capture the finite amplitude dynamics Sipp et al. [2010]; Rowley and Dawson [2017].
Since linear models are unable to recover instabilities characterizing the wake flows, hence forth a need to construct nonlinear model is required. Recent methods have allowed for constructing nonlinear reduced order models solely based on sparse time-resolved measurements Brunton et al. [2016]; Loiseau and Brunton [2018]. In this framework, the wake flow behind a cylinder is a well documented flow where the primary instability is a Hopf-type bifurcation which, in the laminar regime, is known to reach a finite amplitude and saturate to a limit cycle. The saturation process was highlighted in Ma et al. [2000]; Stuart [1958]; Deane et al. [1991]; Noack et al. [2003] by the interaction between the vortex shedding mode and the steady state, which induces a shift to the flow, also known as shift mode Mantič-Lugo et al. [2014]; Passaggia and Ehrenstein [2018]. While the vortex shedding modes are characterized by a growth rate and a frequency mode, the shift mode only possesses a decay rate which varies with the growth rate and both are strongly coupled. In the case of a cylinder, the shift mode is associated with a shortening recirculation region and is directly related to the magnitude of the vortex shedding , the latter being dependent on the Reynolds number. While this process is now well understood in the case of the laminar

flow, this model scenario yet has to be tested for turbulent flow conditions at high Reynolds number. In particular, we are interested in the capacity of this empirical Galerkin model to capture the wake dynamics and the instantaneous evolution of the drag coefficient. In order to eventually implement a control law, it is of major importance to design an observer that can separate the turbulent dynamics from the vortex shedding mode and evaluate the pertinence of a simplistic dynamical model for representing the drag on a bluff body.

## 4.2 Modeling

The evolution of fluid flow is governed by the well-known Navier-Stokes (NS) equations, a set of an incompressibility condition and a nonlinear partial differential equation. The NS equations are characterized by strong nonlinearities, high dimensionality and time-delays making fluid flow control a challenging area, especially if real applications are targeted. In the past fifteen years, reduced-order model (ROM) approaches have been extensively developed in the literature to cope with the aforementioned difficulties. The objective is to obtain a low-order ODE model from the NS equation. The most popular ways of obtaining ROMs are the Proper Orthogonal Decomposition (POD) Berkooz et al. [1993], more recently the Dynamic Mode Decomposition Rowley et al. [2009]; Schmid [2010] and the Optimal Mode Decomposition Wynn et al. [2013]. Among ROMs, low-dimensional Galerkin models showed promising results for feedback control design Sipp and Schmid [2016].

Most of the energy present in the wake dynamics of the flow along time can be modeled by the mean flow and coherent structures (modes), neglecting the incoherent structures in a first approximation. Therefore, in this study, a Galerkin model (GM) based on a Karhunen-Loève expansion around the unstable steady NS solution $u_{mean}$ is used. The flow $u(s,t)$ is then described by the orthonormal Galerkin approximation $u^{[N]}$, where the velocity $u(s,t)$ is expressed as a function of space and time i.e.

$$u(s,t) \approx u^{[N]} = u_{mean} + \sum_{i=1}^{N} a_{mi}(t) u_i(s), \tag{4.1}$$

with N, the order of truncation. The velocity in the flow field is decomposed into mean flow $u_{mean}$ and various velocity terms where $u_i(s)$ denote the orthonormal spatial modes and $a_{mi}(t)$ are the temporal mode amplitudes. For time periodic flows, structures are described by pairs of modes, acting as modal oscillators. One mode plays a crucial role to robustify the low order Galerkin model with respect to Reynolds range and transient dynamics Noack et al. [2003]; Lehmann et al. [2007]: it's the *shift mode*, denoted by $a_\Delta$. The shift mode represents the energy exchange between the mean flow and vortex shedding. Considering that the fundamental mode captures more than 80% of the energy exchange, the expression of velocity can be limited

to first three modes and higher harmonics can be neglected at first. The Galerkin approximation of order three is then written as follows

$$u(s,t) \approx u_{mean} + a_{m1}(t)u_1(s) + a_{m2}(t)u_2(s) + a_{\Delta}(t)u_{\Delta}(s). \tag{4.2}$$

It is refered to as Minimal Galerkin representation Noack et al. [2003] using the dominant von karman modes $a_{m1}, a_{m2}$ and the shift mode $a_{\Delta}$. In the later section, a more refined Galerkin representation is presented that includes higher modes and is refered to as Hybrid model in our studies, following Luchtenburg et al. [2009] to represent energy exchanges between concurrent structures dynamics.

## 4.3 Minimal Model

The Galerkin projection of (4.2) onto the NS equation leads to a low-order dimensional nonlinear model where the amplitudes $a_{mi}$ vary as a function of time similarly to a nonlinear oscillator system. Finally the dynamical equations of the temporal coefficients Noack et al. [2003] are given by:

$$\begin{pmatrix} \dot{a}_{m1} \\ a_{m2} \\ a_{\Delta} \end{pmatrix} = \begin{pmatrix} \mu & -1 & -a_{m1} \\ 1 & \mu & -a_{m2} \\ a_{m1} & a_{m2} & -1 \end{pmatrix} \begin{pmatrix} a_{m1} \\ a_{m2} \\ a_{\Delta} \end{pmatrix} \tag{4.3}$$

where $\mu > 0$ is a growth rate parameter. Considering the oscillating amplitude $A_{mp} = \sqrt{a_{m1}^2 + a_{m2}^2}$, the above model (4.3) can be re-written as:

$$\begin{pmatrix} \dot{A}_{mp} \\ \dot{a_{\Delta}} \end{pmatrix} = \begin{pmatrix} (\mu - a_{\Delta})A_{mp} \\ A_{mp}^2 - a_{\Delta} \end{pmatrix}. \tag{4.4}$$

Since the growth rate $\mu$ is a key parameter but usually difficult to identify, therefore, we consider it as a constant and estimate it as a state variable $x_3$. In the sequel, we denote the state vector $x = \begin{pmatrix} A_{mp} & a_{\Delta} & \mu \end{pmatrix} \in \mathcal{X} \subset \mathbb{R}^3$ and consider the dynamical nonlinear minimal model:

$$\begin{aligned} \dot{x} = f(x) &= \begin{pmatrix} x_1(x_3 - x_2) \\ x_1^2 - x_2 \\ 0 \end{pmatrix} \\ y = h(x) &= x_1, \end{aligned} \tag{4.5}$$

where $y$ is the measured output.

### 4.3.1 System Equilibria

**Theorem 14** *$\forall \mu \in \mathbb{R}_+^*$, system (4.5) equilibria are given by:*

- $x^* = (0\ 0\ \mu)^T$ *is an unstable equilibrium ;*
- $x^{**} = (\sqrt{\mu}\ \mu\ \mu)^T$ *is a locally stable equilibrium;*
- $x^{***} = (-\sqrt{\mu}\ \mu\ \mu)^T$ *is a locally stable equilibrium.*

**Proof 14** *A first order analysis is sufficient to state on the stability of the equilibria. It is straightforward that* $f(x) = 0$ *if and only if* $x \in \{x^*, x^{**}, x^{***}\}$ *and we have*

$$\frac{\partial f}{\partial x}(x) = \begin{pmatrix} x_3 - x_2 & -x_1 & x_1 \\ 2x_1 & -1 & 0 \\ 0 & 0 & 0 \end{pmatrix}. \tag{4.6}$$

*The eigenvalues of* $\frac{\partial f}{\partial x}$ *lie in the set*

$$\{0, \frac{(x_3 - x_2 - 1) \pm \sqrt{(x_3 - x_2)^2 + 2(x_3 - x_2) + 1 - 8x_1^2}}{2}\}. \tag{4.7}$$

*The null eigenvalue is linked to the marginal stability of* $x_3$*, inherited from the last line of* $\frac{\partial f}{\partial x}$ *and simply expresses that* $x_3$ *is a constant.*

- *The eigenvalues of* $\frac{\partial f}{\partial x}(x^*)$ *lie in* $\{0, -1, \mu\}$ *so* $x^*$ *is a saddle point for* $\mu > 0$ *and is an unstable equilibrium.*
- *The eigenvalues of* $\frac{\partial f}{\partial x}(x^{**})$ *lie in* $\{0, \frac{-1 \pm \sqrt{1-8\mu}}{2}\}$ *so* $x^{**}$ *is a stable equilibrium whose basin of attraction is* $\{x \in \mathbb{R}_+^* \times \mathbb{R}^2\}$.
- *The eigenvalues of* $\frac{\partial f}{\partial x}(x^{***})$ *lie in* $\{0, \frac{-1 \pm \sqrt{1-8\mu}}{2}\}$ *so* $x^{***}$ *is a stable equilibrium whose basin of attraction is* $\{x \in \mathbb{R}_-^* \times \mathbb{R}^2\}$.

*These local results can be checked using* $V = (x - x_e)^T \frac{\partial f}{\partial x}(x_e)(x - x_e)$ *as a Lyapunov candidate function for* $x_e \in \{x^*, x^{**}, x^{***}\}$*. In practice, this bistability* $\{x^{**}, x^{***}\}$ *means that the system jumps from one equilibrium to another (up and bottom or left and right), where the control objective would be to keep it centered (i.e., unstable equilibrium* $x^*$*), what turbulence induced disturbances prevent from occuring in real life.*

### 4.3.2 Observability Analysis

Rebuilding the unmeasured states is mandatory to *i)* understand the macro-physics at work in the wake, i.e. the dominant structure dynamics, and *ii)* synthesize control laws aiming at stabilizing the wake around some desired trajectory. A first prerequisite is to study the conditions guaranteeing the observability of the sytem.

**Theorem 15** *System (4.5) is observable on any bounded connected subset of $\mathcal{X}\backslash\mathcal{S}_\epsilon$ where $\mathcal{S}_\epsilon = \{x \in \mathcal{X} \subset \mathbb{R}^3 : |x_1| \leq \epsilon\}$ for any $\epsilon > 0$.*

**Proof 15** *Using the output $y$ in (4.5) and using the notations of Chapter 2, we compute the successive Lie derivatives*

$$\begin{aligned}
\mathcal{L}_f^0 h(x) &= h(x) = x_1 \\
\mathcal{L}_f^1 h(x) &= x_1(x_3 - x_2) \\
\mathcal{L}_f^2 h(x) &= x_1[(x_3 - x_2)^2 - x_1^2 + x_2] \\
\mathcal{L}_f^3 h(x) &= x_1[(x_3 - x_2)^3 + (x_3 - x_2)(3x_2 - 5x_1^2) + x_1^2 - x_2]
\end{aligned} \tag{4.8}$$

*Differentiation at higher orders will still lead to expressions of $\mathcal{L}_f^i h(x)$ where $x_1$ is a factor. We get*

$$\begin{aligned}
\mathrm{d}\mathcal{L}_f^0 h(x)^T &= \begin{pmatrix} 1 \\ 0 \\ 0 \end{pmatrix}, \quad \mathrm{d}\mathcal{L}_f^1 h(x)^T = \begin{pmatrix} x_3 - x_2 \\ -x_1 \\ x_1 \end{pmatrix} \\
\mathrm{d}\mathcal{L}_f^2 h(x)^T &= \begin{pmatrix} (x_3 - x_2)^2 - 3x_1^2 + x_2 \\ x_1(1 - 2(x_3 - x_2)) \\ 2x_1(x_3 - x_2) \end{pmatrix}.
\end{aligned} \tag{4.9}$$

*It is obvious that $\dim \mathrm{d}\mathcal{O}(x) = 3$ on any connected subset of $\mathcal{X}\backslash\mathcal{S}_\epsilon$, for any $\epsilon > 0$. However there is a singularity of the system observability for $x_s = (0\ x_2\ x_3)^T$ since $\dim \mathrm{d}\mathcal{O}(x_s) = 1$.*

We can give the observability singularity set for the minimal model as:

$$\mathcal{S} = \{x \in \mathcal{X} \subset \mathbb{R}^3 : x_1 = 0\}. \tag{4.10}$$

Physically, this singularity is related to the fact that one can not access to any information about state $x_2$ or $x_3$ when $x_1$ is null. This event rarely occurs on an uncontrolled system; yet, since the control objective will aim at stabilizing the system around $x^*$, the study and the avoidance of the observability singularity become decisive for the flow estimation.

### 4.3.3 Nonlinear Observer Synthesis for Minimal Systems

We have a nonlinear system therefore we map the system (4.5) into a phase variable form (1.27):

$$z = T(x) = \begin{pmatrix} x_1 \\ x_1(x_3 - x_2) \\ x_1[(x_3 - x_2)^2 - x_1^2 + x_2] \end{pmatrix}, \quad y = z_1 \tag{4.11}$$

where $z \in \mathcal{Z} \subset \mathbb{R}^3$ and measured output $y \in \mathbb{R}$.

In the next sections, we will synthesize three observers for the minimal wake flow model namely: the standard HGO, Limited HGO and the Low peaking LHGO. However, since from Theorem 15, the system suffers from observability defects, hence we will also propose the standard HGO, Limited HGO and Low peaking LHGO in original coordinates that are capable of avoiding the observability defects.

#### 4.3.3.1 HGO for Minimal Model

Based on Theorem 8, we can design the high gain observer for the minimal model.

**Proposition 19 (Standard HGO for minimal model)** *The standard high gain observer for the system (4.11) is given as:*

$$\dot{\hat{z}} = A_{n_z} z + B_{n_z} \varphi_s(z) + \Delta K(y - \hat{z}_1) \tag{4.12}$$

*where $\varphi_s$ is the saturated version of $\varphi$ on $\mathcal{X}$ such that:*

$$\varphi_3(\hat{x}) = \hat{x}_1[(\hat{x}_3 - \hat{x}_2)^3 + (\hat{x}_3 - \hat{x}_2)(3\hat{x}_2 - 5\hat{x}_1^2) + \hat{x}_1^2 - \hat{x}_2]. \tag{4.13}$$

*The high gain matrix $\Delta$ is a diagonal matrix formed in ascending powers of a gain $\theta > \theta^* > 1$ whose choice is related to the Lipschitz constant of $\varphi$ and the observer gain vector $K = \begin{pmatrix} k_1 & k_2 & k_3 \end{pmatrix}^T$ is chosen to have the matrix $(A_{n_z} - KC_{n_z})$ Hurwitz.*

We can get the observer in original coordinates using the inversion of $T : \hat{x} = \mathcal{T}(\hat{z})$, but we rather use the approach stated in Proposition (2) to get the observer in original coordinates:

$$\dot{\hat{x}} = \frac{\partial T}{\partial x}(\hat{x})^{-1} \dot{\hat{z}}. \tag{4.14}$$

In our study, it is obvious that hte mapping $T$ is a diffeomorphism only on $\mathcal{O}_\epsilon^- = \{x \in \mathcal{X} : x_1 < -\epsilon\}$ or on $\mathcal{O}_\epsilon^+ = \{x \in \mathcal{X} : x_1 > \epsilon\}$ due to the observability singularity (4.10).

**Remark 13** *This standard high gain observer is not defined at the observability singularity since $T$ is by construction singular for $\hat{x}_1 = 0$.*

$$\frac{\partial T}{\partial x}(x) = \begin{pmatrix} 1 & 0 & 0 \\ x_3 - x_2 & -x_1 & x_1 \\ (x_3 - x_2)^2 - 3x_1^2 + x_2 & x_1(1 - 2(x_3 - x_2)) & 2x_1(x_3 - x_2) \end{pmatrix} \tag{4.15}$$

The observability singularity at $x_1 = 0$ stated in Theorem 15 means that there is no access to any information about states $x_2$ and $x_3$ when $x_1 = 0$. Therefore we use the method suggested previously in Proposition 2.3.1 of Chapter 2 and add some fictitious outputs $y_f \in \mathbb{R}^{n_f}$ in our

system, allowing for an access to the last two states. However, completing the $z$ state by these fictitious outputs make the cardinality of the extended target state space greater than the cardinality of the original $x$ state space i.e. $T_e : \mathbb{R}^{n_x} \to \mathbb{R}^{n_z+n_f}$. It follows that the mapping $T$ is no more surjective. We thus use the Proposition 9 to augment $T_e$ into a global diffeomorphism $T_a$ using a dynamic extension and a jacobian matrix completion.

**Proposition 20 (Singularity-free HGO for minimal model)** *Let*

$$\rho : x \mapsto max(0, \epsilon^2 - x_1^2)^2 \tag{4.16}$$

*for some $\epsilon > 0$. Consider the fictitious output $y_f \in \mathbb{R}^2$ such that:*

$$y_f(x) = \begin{pmatrix} \rho(x)x_2 \\ \rho(x)x_3 \end{pmatrix}, \tag{4.17}$$

*and under the assumptions and notations of Proposition 19, we define two new state vectors $x_a$ and $z_a$ such as*

$$x_a = \begin{pmatrix} x \\ \tau \end{pmatrix} \text{ and } z_a = T_a(x_a) = \begin{pmatrix} z \\ y_f \end{pmatrix} + \Psi(x)\tau \tag{4.18}$$

*where $\tau \in \mathbb{R}^2$ are the exogenous variables added to the original state vector and*

$$\Psi : x \mapsto \begin{pmatrix} 0 & 0 \\ \rho(x) & 0 \\ 0 & -\rho(x) \\ x_1 & x_1 \\ 0 & x_1 \end{pmatrix}. \tag{4.19}$$

*Then a high gain observer for system (4.5) on any bounded subset $\mathcal{X}_a \in \mathbb{R}^5$ avoiding the singularity is given by*

$$\dot{\hat{x}}_a = \frac{\partial T_a}{\partial x_a}(\hat{x}_a)^{-1}\mathcal{F}_z(\hat{x}_a, y) \tag{4.20}$$

*where*

$$\mathcal{F}_z : (\hat{x}_a, y) \mapsto \begin{pmatrix} A_{n_z}T_a(\hat{x}_a) + B_{n_z}\varphi_s(\hat{x}) + \Delta K(y - C_{n_z}\hat{x}_a) \\ -k_4 T_{a_4}(\hat{x}_a) \\ -k_5 T_{a_5}(\hat{x}_a) \end{pmatrix} \tag{4.21}$$

*with $T_{a_i}$ denoting the $i$-th component of $T_a$ given in (4.18) , $k_4, k_5 > 0$ and $K$, $\Delta$ given by Theorem 19.*

**Proof 16** *To circumvent the observability singularity, we modify the system outside $\mathcal{O}_\epsilon = \{x_a \in \mathcal{X} \subset \mathbb{R}^3 : |x_1| > \epsilon\}$ by adding the fictitious output $y_f$ given by (4.17). It is worth noticing that this fictitious output is null on $\mathcal{O}_\epsilon$ so the system is not affected when living on $\mathcal{O}_\epsilon$,*

*except for the time of convergence of the $\tau$ to be zero. Defining a new mapping $T_e : x \mapsto (z, y_f)$, whose jacobian matrix is*

$$\frac{\partial T_e}{\partial x}(x) = \begin{pmatrix} 1 & 0_{1,2} \\ J_1(x) & J_2(x) \end{pmatrix} \tag{4.22}$$

*with $0_{1,2}$ denoting the null matrix having $1 \times 2$ entries and matrices*

$$J_1(x) = \begin{pmatrix} x_3 - x_2 \\ (x_3 - x_2)^2 - 3x_1^2 + x_2 \\ \rho_1 x_2 \\ \rho_1 x_3 \end{pmatrix}, J_2(x) = \begin{pmatrix} -x_1 & x_1 \\ x_1 - 2x_1(x_3 - x_2) & 2x_1(x_3 - x_2) \\ \rho & 0 \\ 0 & \rho \end{pmatrix} \tag{4.23}$$

*where $\rho_1$ denote the partial derivative of $\rho$ with respect to $x_1$, i.e. $\rho_1 = \frac{\partial \rho}{\partial x_1}(x)$.*

*The jacobian matrix of $T_e$ is thus full rank provided that $J_2$ is also full rank. The determinant of the first two lines of $J_2$ is $(-x_1^2)$ whilst the determinant of its last two lines is $\rho^2$. By definition (4.16), $\rho$ and $x_1$ cannot be simultaneously null and it follows that $J_2(x)$ is full rank on $\mathbb{R}^3$. The fictitious outputs thus enable to get around the observability singularity.*

*Since the mapping $T_e$ is an injective immersion from $\mathbb{R}^3$ in $\mathbb{R}^5$, a way to get a one-to-one mapping is to extend it into a global diffeomorphism $T_a$. To do so, we propose a dynamic extension by augmenting the original state $x$ with $\tau = \begin{pmatrix} \tau_1 & \tau_2 \end{pmatrix}^T$ as given by (4.18)-(4.19). The resulting jacobian matrix of $T_a$ is*

$$\frac{\partial T_a}{\partial x_a}(x_a) = \begin{pmatrix} 1 & 0_{1,4} \\ \bar{J}_1(x_a) & \bar{J}_2(x_a) \end{pmatrix} \tag{4.24}$$

*where the matrices $\bar{J}_1(x_a)$ and $\bar{J}_2(x_a)$, completed by the $\Psi$ columns (see (4.19)), and $\bar{J}_1(x_a)$ are given by*

$$\begin{aligned} \bar{J}_1(x_a) &= J_1(x_a) + \begin{pmatrix} \rho_1 \tau_1 \\ -\rho_1 \tau_2 \\ \tau_1 + \tau_2 \\ \tau_2 \end{pmatrix}, \\ \bar{J}_2(x_a) &= \begin{pmatrix} -x_1 & x_1 & \rho & 0 \\ x_1 - 2x_1(x_3 - x_2) & 2x_1(x_3 - x_2) & 0 & -\rho \\ \rho & 0 & x_1 & x_1 \\ 0 & \rho & 0 & x_1 \end{pmatrix}. \end{aligned} \tag{4.25}$$

*It is straightforward that $\det \bar{J}_2(x_a) = -(\rho^2 + x_1^2)^2 < 0$, so $\frac{\partial T_a}{\partial x_a}$ is invertible on any bounded subset of $\mathbb{R}^3 \times \mathbb{R}^2$, and the observer (4.20) is thus well defined on any bounded subset of $\mathbb{R}^5$.*

*To ensure that we have*

$$\lim_{t \to \infty} \|x(t) - \hat{x}(t)\| + \|\hat{\tau}(t)\| = 0 \tag{4.26}$$

*along the solutions* $(x, \hat{x}, \hat{\tau})(t)$ *of* (4.5) *and* (4.20)-(4.21)*, one can notice that the inverse mapping* $T_a^{-1} : z_a \mapsto x_a$ *is given by*

$$T_a^{-1}(z_a) = \begin{pmatrix} z_1 \\ \frac{-z_1^2\alpha^2 - z_1\rho\beta(z_1^2+\rho^2)+\gamma(z_1^2+\rho^2)^2}{(z_1^2+\rho^2)^3} \\ \frac{-z_1^2\alpha^2 - z_1\rho\beta(z_1^2+\rho^2)+(\gamma+\alpha)(z_1^2+\rho^2)^2}{(z_1^2+\rho^2)^3} \\ \frac{\beta}{z_1^2+\rho^2} \\ \frac{z_1\rho\alpha(\alpha-(z_1^2+\rho^2))}{(z_1^2+\rho^2)^3} + \frac{\delta}{z_1^2+\rho^2} \end{pmatrix} \tag{4.27}$$

*with*

$$\begin{aligned} \alpha(z) &= z_1 z_2 + \rho(z_5 - z_4) \\ \beta(z) &= \rho z_2 - z_1(z_5 - z_4) \\ \gamma(z) &= z_1 z_3 + z_1^4 + \rho z_4 \\ \delta(z) &= z_1 z_5 - \rho(z_1^3 + z_3). \end{aligned} \tag{4.28}$$

*So* $T_a^{-1} \in \mathcal{C}^1(\mathbb{R}^5)$ *and it follows that it is a L-Lipschitz mapping on any bounded subset of* $\mathbb{R}^5$*. Besides, from* (4.18)-(4.19)*, we have* $T_a(x, 0) = T_e$*, so it is straightforward that for* $z_a = T_a(x, 0)$*:*

$$\begin{aligned} \|T_a^{-1}(z_a) - T_a^{-1}(\hat{z}_a)\| &\leq L\|z_a - \hat{z}_a\| \\ \left\| \begin{pmatrix} x \\ 0_{2,1} \end{pmatrix} - \begin{pmatrix} \hat{x} \\ \hat{\tau} \end{pmatrix} \right\| &\leq L\|T_e(x) - T_a(\hat{x}, \hat{\tau})\|. \end{aligned} \tag{4.29}$$

*Since we have proven in Proposition 19 that the first three lines of* (4.21) *define a converging observer of* (4.11)*, it follows from* (4.29) *that* (4.26) *holds. The dynamics of the last two states* $z_a$ *in* (4.21) *are arbitrarily set by any strictly positive gains* $k_4$ *and* $k_5$ *in order to make the fictitious outputs go back to zero.*

#### 4.3.3.2 LHGO for Minimal Model

Based on Theorem 11, we can design the limited high gain observer for the minimal model given by (4.5).

**Proposition 21 (LHGO for the minimal model)** *The Limited high gain observer for the system* (4.11) *is given as:*

$$\dot{\zeta} = \mathcal{F}_\zeta(\zeta, \hat{x}, y) = \begin{pmatrix} \zeta_{12} + \theta k_{11}(y - \zeta_{11}) \\ \zeta_{22} + \theta^2 k_{21}(y - \zeta_{11}) \\ \zeta_{22} + \theta k_{21}(\zeta_{12} - \zeta_{21}) \\ \varphi_{3s} + \theta^2 k_{22}(\zeta_{12} - \zeta_{21}) \end{pmatrix} \tag{4.30}$$

*and we can therefore get the LHGO in target coordinates using either* $\hat{z} = P\zeta$ *or* $z' = P'\zeta'$. *Based on Proposition 2, we can get the observer in original coordinates since we can use either* $\hat{x} = P\hat{x}$ *or* $\hat{x}' = P'\hat{x}'$. *This observer also faces the problem linked with the observability singularity at* $\hat{x}_1 = 0$.

Since the LHGO underlies a mapping $T$ from $x \in \mathcal{X} \subset \mathbb{R}^{n_x}$ to $\zeta \in \mathbb{R}^{n_\zeta}$ with $n_\zeta = 2n_z - 1 > n_x$, the mapping is not surjective. An additional step in such a case for the observer synthesis is to augment the mapping into a diffeomorphism by augmenting the mapping domain. Since the state of the observer of Theorem 11 is redundant in the form (using $\hat{z} = P\zeta$ and $z' = P'\zeta'$), we can define

$$\zeta = \begin{pmatrix} \zeta_1 \\ \\ \zeta_2 \\ \\ \vdots \\ \zeta_{n-2} \\ \\ \zeta_{n-1} \\ \\ \end{pmatrix} = \begin{pmatrix} \begin{pmatrix} \zeta_{1\,1} \\ \zeta_{1\,2} \end{pmatrix} \\ \begin{pmatrix} \zeta_{2\,1} \\ \zeta_{2\,2} \end{pmatrix} \\ \vdots \\ \begin{pmatrix} \zeta_{n_x-2\,1} \\ \zeta_{n_x-2\,2} \end{pmatrix} \\ \begin{pmatrix} \zeta_{n_x-1\,1} \\ \zeta_{n_x-1\,2} \end{pmatrix} \end{pmatrix} = \begin{pmatrix} \begin{pmatrix} \hat{z}_1 \\ \hat{z}_2 \end{pmatrix} \\ \begin{pmatrix} \\ \hat{z}_3 \end{pmatrix} \\ \vdots \\ \begin{pmatrix} \\ \hat{z}_{n_x-1} \end{pmatrix} \\ \begin{pmatrix} \\ \hat{z}_{n_x} \end{pmatrix} \end{pmatrix} = \begin{pmatrix} \begin{pmatrix} \hat{z}'_1 \\ \end{pmatrix} \\ \begin{pmatrix} \hat{z}'_2 \\ \end{pmatrix} \\ \vdots \\ \begin{pmatrix} \hat{z}'_{n_x-2} \\ \end{pmatrix} \\ \begin{pmatrix} \hat{z}'_{n_x-1} \\ \hat{z}'_n \end{pmatrix} \end{pmatrix}, \tag{4.31}$$

an original way of addressing a diffeomorphism augmentation is to merge the two states $\hat{z}$ and $\hat{z}'$ defining a new augmented state $\hat{\bar{z}} = \begin{pmatrix} \hat{z}_1 & \hat{z}_2 & \hat{z}'_2 & \hat{z}_3 & \dots & \hat{z}'_{n-1} & \hat{z}_n \end{pmatrix}^T$ associated with a original coordinate augmented state $\bar{x} = \begin{pmatrix} x_1 & x_2 & x'_2 & x_3 & \dots & x'_{n-1} & x_n \end{pmatrix}^T \in \mathbb{R}^{n_\zeta}$.

**Proposition 22** *For minimal model, defining the original coordinate augmented state* $\bar{x}$ *and* $\bar{T}$ *as*

$$\bar{T} : \bar{x} = \begin{pmatrix} x_1 \\ x_2 \\ x'_2 \\ x_3 \end{pmatrix} \mapsto \bar{z} = \begin{pmatrix} x_1 \\ x_1(x_3 - x_2) \\ x_1(x_3 - x'_2) \\ x_1((x_3 - x_2)^2 - x_1^2 + x_2) \end{pmatrix} \tag{4.32}$$

$\bar{T}$ *is a diffeomorphism on* $\bar{\mathcal{O}}_\epsilon = \{\bar{x} \in \mathcal{X} \subset \mathbb{R}^4 : |x_1| > \epsilon\}$.

**Proof 17** *The jacobian of the mapping* $\bar{T}$ *is given as:*

$$\frac{\partial \bar{T}}{\partial \bar{x}}(\bar{x}) = \begin{pmatrix} 1 & 0_{1,n_\zeta - 1} \\ * & J \end{pmatrix}. \tag{4.33}$$

*and differentiating* $\bar{T}$ *leads to*

$$J = \begin{pmatrix} -x_1 & 0 & x_1 \\ 0 & -x_1 & x_1 \\ x_1(1-2(x_3-x_2)) & 0 & 2x_1(x_3-x_2) \end{pmatrix} \tag{4.34}$$

*so we have*

$$\left|\frac{\partial \bar{T}}{\partial \bar{x}}(\bar{x})\right| = -x_1^3$$

*and* $\bar{T}$ *is a diffeomorphism on* $\bar{\mathcal{O}}_\epsilon$.

Invertibility of the jacobian matrix of $\bar{T}$ is now possible as long as the estimated augmented state remains away from the observability singularity. Yet there is no guarantee that the estimated state stays in this set.

To avoid loosing any access to some unmeasured states because of the observability rank loss pinpointed in Theorem 15, for instance the loss of information about $x_2$ and $x_3$ when $x_1 = 0$ for system, a way to get around the observability singularity is to follow Proposition 2.3.1 and add some fictitious outputs aiming at getting information about these states around the singularity.

**Proposition 23 (Singularity-free LHGO for minimal model)** *For system* (4.32)*, adding respectively fictitious outputs* $y_f \in \mathbb{R}^{n_f}$

$$y_f(x) = \begin{pmatrix} \rho(x)x_2 \\ \rho(x)x_2' \\ \rho(x)x_3 \end{pmatrix} \tag{4.35}$$

*where* $\rho$ *is the differentiable function given by* (4.16)*.*

*We define two new state vectors* $x_a$ *and* $z_a$ *such as:*

$$x_a = \begin{pmatrix} \bar{x} \\ \tau \end{pmatrix} \text{ and } \quad z_a = T_a(x_a) = \begin{pmatrix} \bar{z} \\ y_f \end{pmatrix} + \Psi(x)\tau \tag{4.36}$$

*where* $\tau \in \mathbb{R}^3$ *are the exogenous variables added to the augmented state vector* $\bar{x}$ *and*

$$\Psi(\bar{x}) = \begin{pmatrix} 0 & 0 & 0 \\ 1 & 0 & -1 \\ 0 & 1 & -1 \\ 0 & 0 & 1 \\ x_1 & 0 & 0 \\ 0 & x_1 & 0 \\ 0 & 0 & x_1 \end{pmatrix}. \tag{4.37}$$

*Then a limited high gain observer for system (4.5) avoiding the singularity is given by*

$$\dot{\hat{x}}_a = \frac{\partial T_a}{\partial x_a}(\hat{x}_a)^{-1}\mathcal{F}(\zeta, \hat{x}_a, y), \tag{4.38}$$

*where*

$$\mathcal{F} : (\zeta, \hat{x}_a, y) \mapsto \begin{pmatrix} \mathcal{F}_\zeta(\zeta, \hat{x}_a, y) \\ -K_3 T_{a3}(\hat{x}_a)) \end{pmatrix}, \tag{4.39}$$

*$\mathcal{F}_\zeta$ is given by Proposition 21, $K_3$ is a positive definite diagonal matrix of dimension 3. The notation $T_{a3}$ stands for the last 3 components of $T_a$ representing the dynamics associated with the fictitious outputs.*

**Proof 18** *Adding the fictitious outputs to the state $\bar{z}$ results in an extended state $z_e = \begin{pmatrix} \bar{z} \\ y_f \end{pmatrix}$. Extending the transformation $T_e$ mapping $\bar{x} \in \mathbb{R}^{n_\zeta}$ to $z_e \in \mathbb{R}^{n_\zeta + n_f}$ results in an injective immersion on the domain $\mathbb{R}^{n_\zeta}$. The Jacobian of the new mapping is given as:*

$$\frac{\partial T_e}{\partial x_a}(x_a) = \begin{pmatrix} 1 & 0_{1,n_\zeta - 1} \\ * & J \\ * & J_f \end{pmatrix} \tag{4.40}$$

*where $J$ is given by (4.34) and $J_f = \rho I_3$. Since by construction $2x_1^2 + \rho(x) > 0$, it is straightforward that $\frac{\partial T_e}{\partial x_e}(x_e)$ has a constant rank for any $\bar{x} \in \mathbb{R}^{n_\zeta}$. The observability singularity has been solved, but using Proposition 2 requires a diffeomorphism to get an observer in original coordinates.*

*The proof for this part consists in augmenting the immersion $T_e$ defined on the full domain $\mathbb{R}^{n_\zeta}$ to $\mathbb{R}^{n_\zeta + n_f}$ into a global diffeomorphism $T_a$ on $\mathbb{R}^{n_\zeta + n_f}$, which requires an augmentation of the original coordinates $\bar{x} \in \mathbb{R}^{n_\zeta}$ to $x_a = \begin{pmatrix} \bar{x} \\ \tau \end{pmatrix} \in \mathbb{R}^{n_\zeta + n_f}$. Since $\Psi$ depends only on $x_1$, differentiating $T_a$ using (4.40) leads to the resulting jacobian matrix of $T_a$ as*

$$\frac{\partial T_a}{\partial x_a}(x_a) = \begin{pmatrix} 1 & 0_{1,q-1} & \\ * & J & \Psi(x_1) \\ * & J_f & \end{pmatrix} \tag{4.41}$$

*Due to expressions (4.37), it follows that*

$$\left| \frac{\partial T_a}{\partial x_a}(x_a) \right| = -(\rho + x_1^2)^3. \tag{4.42}$$

*By construction of function $\rho$, the Jacobian determinant is strictly negative for all $x_a \in \mathbb{R}^{n_\zeta}$, thus $T_a$ defines a global diffeomorphism.*

*It can be checked that* $T_a^{-1} \in \mathcal{C}^1$*, hence it is L-Lipschitz on any compact of* $\mathbb{R}^{n_\zeta+n_f}$*. It follows that, using* $z_a^* = T_a(\bar{x}, 0) = T_e(\bar{x})$*:*

$$\begin{aligned} \|\bar{x}(t) - \hat{\bar{x}}(t)\| + \|\tau(t)\| &\leq \sqrt{2}\left\|\begin{matrix}\bar{x} - \hat{\bar{x}} \\ \tau\end{matrix}\right\| \\ &\leq \sqrt{2}\left\|\begin{pmatrix}\bar{x} \\ 0\end{pmatrix} - \begin{pmatrix}\hat{\bar{x}} \\ \tau\end{pmatrix}\right\| \\ &\leq \sqrt{2}\|T_a^{-1}(z_a^*) - T_a^{-1}(\hat{z}_a)\| \\ &\leq L\sqrt{2}\|z_a^* - \hat{z}_a\| \\ &\leq L\sqrt{2}\|T_e(\bar{x}) - T_a(\hat{\bar{x}}, \tau)\|. \end{aligned} \tag{4.43}$$

*Since* $T_e$ *is injective and* (4.38) *defines a converging observer from Proposition 23, it follows that*

$$\lim_{t\to\infty} \|\bar{x}(t) - \hat{\bar{x}}(t)\| + \|\hat{\tau}(t)\| = 0. \tag{4.44}$$

#### 4.3.3.3 LPLHGO for Minimal Model

Based on Theorem 12, we can design the low peaking LHGO for the minimal model.

**Proposition 24 (LPLHGO for minimal models)** *The low peaking limited high gain observer for the system* (4.11) *is given as:*

$$\begin{aligned} \dot{\hat{z}} &= \mathcal{F}_z(\hat{z}, \eta, y) \\ \dot{\eta} &= \mathcal{F}_\eta(\hat{z}, \eta, y) \end{aligned} \tag{4.45}$$

*with* $\mathcal{F}_z$ *and* $\mathcal{F}_\eta$ *given as:*

$$\mathcal{F}_z : \begin{cases} \dot{\hat{z}}_1 = \eta_1 + \alpha_1\theta(y - \hat{z}_1) \\ \dot{\hat{z}}_2 = \eta_2 + \alpha_2\theta(sat_{\kappa_2}(\eta_1) - \hat{z}_2) \\ \dot{\hat{z}}_3 = \varphi_{3s}(\hat{z}) + \alpha_3\theta(sat_{\kappa_3}(\eta_2) - \hat{z}_3) \end{cases} \qquad \mathcal{F}_\eta : \begin{cases} \dot{\eta}_1 = sat_{\kappa_3}(\eta_2) + \beta_1\theta^2(y - \hat{z}_1) \\ \dot{\eta}_2 = \varphi_{3s}(\hat{z}) + \beta_2\theta^2(sat_{\kappa_2}(\eta_1) - \hat{z}_2) \end{cases} \tag{4.46}$$

*such that* $\hat{z} \in \mathbb{R}^3$*,* $\eta \in \mathbb{R}^2$ *are the observer states, and with the saturation function and gains* $\alpha_i, \beta_i$ *satisfying the strong stability requirements in Theorem 12.*

Since $n_z = n_x$, therefore we can obtain the observer in original coordinates by using Proposition 2 such that:

$$\begin{cases} \dot{\hat{x}} = \left(\dfrac{\partial T}{\partial x}(\hat{x})\right)^{-1} \mathcal{F}_z(T(\hat{x}), \eta, y) \\ \dot{\eta} = \mathcal{F}_\eta(T(\hat{x}), \eta, y) \end{cases} \tag{4.47}$$

Moreover note that, based on the observability analysis done for the minimal models in Theorem 15, $T$ is diffeomorphism only on $\mathcal{O}_\epsilon^-$ or on $\mathcal{O}_\epsilon^+$ due to the observability singularity. The Jacobian of $T$ is given as:

$$\frac{\partial T}{\partial x}(x) = \begin{pmatrix} 1 & 0 & 0 \\ x_3 - x_2 & -x_1 & x_1 \\ (x_3 - x_2)^2 - 3x_1^2 + x_2 & x_1(1 - 2(x_3 - x_2)) & 2x_1(x_3 - x_2) \end{pmatrix}, \tag{4.48}$$

and its determinant can be found as:

$$\left|\frac{\partial T}{\partial x}\right| = x_1^2. \tag{4.49}$$

It concludes that the LPLHGO is not defined at the observability singularity.

In order to get rid of this singularity, we add some fictitious outputs to the state vector $z$. By following the same procedure as done before in the case of HGO and LHGO before in Propositions 20 and 23, we can get the new LPLHGO that is capable of avoiding the singularity with the new mapping $T_a$ that is globally diffeomorphic. Since the computations and proof for the LPLHGO are clearly related to what has been done for HGO so in order to avoid repetition, we can directly write the LPLHGO in original coordinates in the next Proposition, where the expressions for the new mapping $T_a$ and its determinant are the same as given in Proposition 20.

**Proposition 25 (Singularity-free LPLHGO for minimal models)** *The dynamic system*

$$\begin{cases} \dot{\hat{x}}_a = \left(\dfrac{\partial T_a}{\partial x_a}(\hat{x}_a)\right)^{-1} \begin{pmatrix} \mathcal{F}_z(T_a(\hat{x}_a), \eta, y) \\ -K_2 T_{a2}(\hat{x}_a) \end{pmatrix} \\ \dot{\eta} = \mathcal{F}_\eta(T_a(\hat{x}_a), \eta, y) \end{cases} \tag{4.50}$$

*is an arbitrarily fast converging observer for system (4.5) in its original coordinates on any bounded subset of $\mathbb{R}^{n_z+n_f}$. $\mathcal{F}_z, \mathcal{F}_\eta$ are defined in Proposition 24 and, $T_a$ is defined by Proposition 20, $K_2$ is a positive definite diagonal matrix of dimension 2. The notation $T_{a2}$ stands for the last 2 components of $T_a$ representing the dynamics associated with the fictitious outputs.*

### 4.3.4 Simulation Results

Simulations are performed for the high gain observer, the limited high gain observer and the low peaking limited high gain observer in original coordinates as proposed in Propositions 20, 23 and 25 respectively for different scenarios. The initial conditions and parameter values are given in Table 4.1. The results are obtained for different high gains to obtain a similar convergence rate for all the observers for a fair comparison. The performance comparison is led through three cases: case A is the nominal one, where no observability defects nor any disturbance is considered; case B illustrates the observability defects avoidance; robustness to output noise is then addressed in the last case C.

| | |
|---|---|
| $x_0$ | $\begin{pmatrix} 0.4 & 0.4 & 0.02 \end{pmatrix}$ |
| $\hat{x}_0$ | $\begin{pmatrix} 0 & 0.2 & 0.01 \end{pmatrix}$ |
| $K_{HGO}$ | $\begin{pmatrix} 1.8 & 1.07 & 0.51 \end{pmatrix}^T$ |
| $K_{LHGO}$ | $\left( \begin{pmatrix} k_{11} \\ k_{12} \end{pmatrix} \quad \begin{pmatrix} k_{21} \\ k_{22} \end{pmatrix} \right)^T = \left( \begin{pmatrix} 1.8 \\ 0.1 \end{pmatrix} \quad \begin{pmatrix} 1.8 \\ 0.02 \end{pmatrix} \right)^T$ |
| $K_{LPLHGO}$ | $\left( \begin{pmatrix} \alpha_1 & \alpha_2 & \alpha_3 \end{pmatrix} \atop \begin{pmatrix} \beta_1 & \beta_2 \end{pmatrix} \right)^T = \left( \begin{pmatrix} 1.8 & 1.8 & 1.8 \end{pmatrix} \atop \begin{pmatrix} 0.1 & 0.02 \end{pmatrix} \right)^T$ |
| $K_{n_f}$ | $I_2$ |
| $\theta_{HGO}$ | 5 |
| $\theta_{LHGO}$ | 5 |
| $\theta_{LPLHGO}$ | 8 |
| $\epsilon$ | 0.01 |

Table 4.1: Initial conditions and gains for the system and observers

#### 4.3.4.1 Case A: Nominal Case

In order to avoid any observability singularity yet with no guarantee, the initial conditions for the observers are chosen fairly near to the system's initial condition i.e., $\hat{x}_0 = \begin{pmatrix} 0.2 & 0.2 & 0.01 \end{pmatrix}$ so as to illustrate the difference between the three observers given by Propositions 19,21 and 24 without concern about the singularity avoidance. Figure 4.1(a) illustrates that the high gain observer exhibits a significant peaking during the transient phase despite an observer initialization quite close to the system state, for the limited HGO the peaking is reduced (Figure 4.1(c)) in comparison to standard HGO due to the fact that observer high gain is limited to the power of 2 instead of system dimension, however, it still accounts for an observer with high peaking and finally, the low peaking limited HGO is successful in reducing the peaking phenomenon by far, as can be noticed on Figure 4.1(e), thus proving the usefulness of using the saturations in the observer synthesis.

#### 4.3.4.2 Case B: Observability Defects Avoidance

To investigate the influence of singularity avoidance on the observer dynamics, the observers are initialized at $\hat{x}_{10} = 0$ in the second set of simulations as can be seen in Figures 4.2,4.3 and 4.4. The singularity-free observer's efficiency in avoiding the singularity is demonstrated by the fact that the fictitious outputs were triggered during the initial time periods, as depicted in Figures 4.2(c),4.3(c) and 4.4(c). The effect of these outputs vanishes when $|x_1| > \epsilon$; then it follows that

the last $\hat{z}_a$ state of the target system converges to zero, thus inducing the extra coordinates $\tau$ to be stabilized at the origin (see Fig. 4.2(d),4.3(d) and 4.4(d)). Thence the standard HGO, LHGO and LPLHGO observers estimation errors converge asymptotically to zero as illustrated by Figures 4.2(a),4.3(a) and 4.4(a). However, the increase in the peaking is quite evident in the case of HGO and limited HGO particularly during the fictitious output activation time, whilst the presence of the saturations shows the effectiveness of LPLHGO in handling the peaking effect quite nicely in this case as well.

#### 4.3.4.3 Case C: Output Noise

In fluid mechanics, measurements are always affected by high frequency noises due to turbulence imparted by the incoherent structures. So special attention has to be paid to robustness to such noises when observing the system. Therefore, a measurement noise on the output in included in the last case C, illustrated in Figures 4.5, 4.6 and 4.7, i.e. a white gaussian noise of variance 1 followed by a high pass filter with a cutoff frequency set to 1000 Hz. In such a case, only practical stability is guaranteed in a ball of radius proportional to the noise amplitude.

The simulations show that the addition of output noise has quite an impact in the case of HGO. In comparison, it is clear that LHGO and LPLHGO outperforms the high gain observer in this regard since the noise-induced errors are significantly smaller as can be seen from Figures 4.5(a), 4.6(a) and 4.7(a).

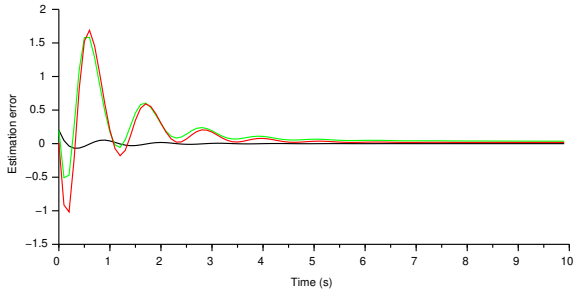


(a) HGO estimation error

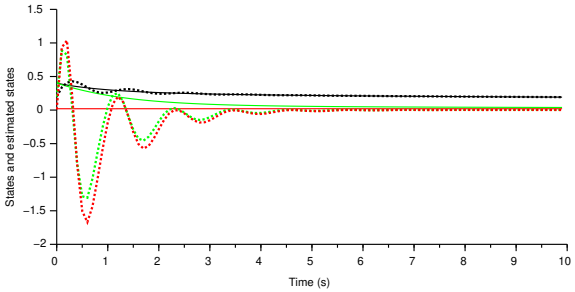


(b) HGO states and estimated states

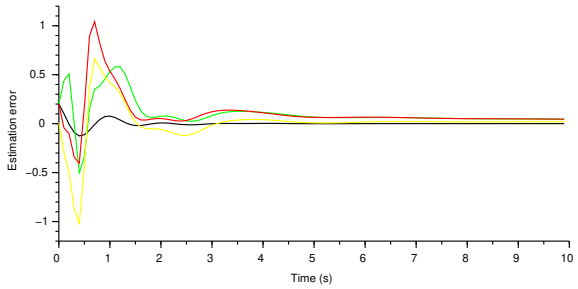


(c) LHGO estimation error

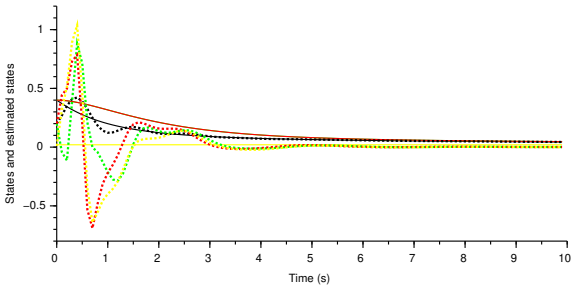


(d) LHGO states and estimated states

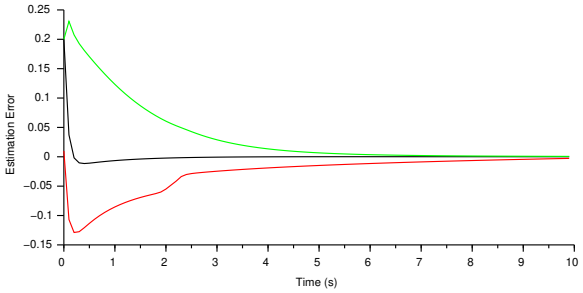


(e) LPLHGO estimation error

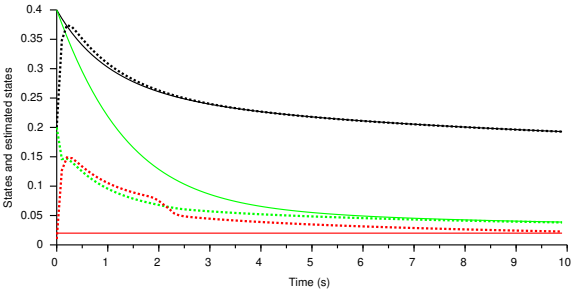


(f) LPLHGO states and estimated states

Figure 4.1: Minimal model: Case A from (a) to (f): simulation for nominal case. Figures (a) and (e) depicts the estimation error $\tilde{x}_1, \tilde{x}_2, \tilde{x}_3$ by black, green and red lines for HGO and LPLHGO respectively, while Figure (c) represents the estimation error $\tilde{x}_1, \tilde{x}_2, \tilde{x}_3$ and $\tilde{x}_4$ by black, green, red and yellow lines respectively for LHGO. Figures (b) and (e) represents the states and estimated states, such that states $x$ are in solid while the estimated states $\hat{x}$ are in dotted black, green and red lines respectively for HGO and LPLHGO and Figure (d) depicts the states and estimated states, such that states are in solid while the estimated states $\hat{x}$ are in dotted black, green, red and yellow lines respectively for LHGO.

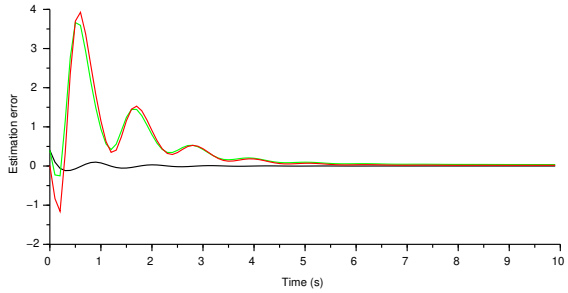


(a) HGO estimation error

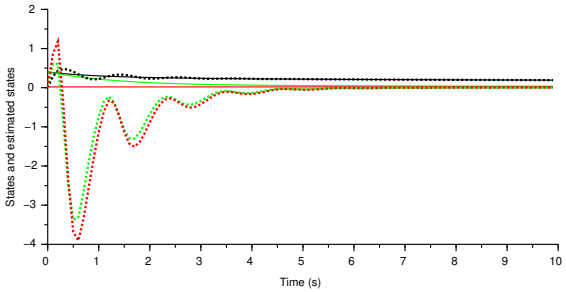


(b) HGO states and estimated states

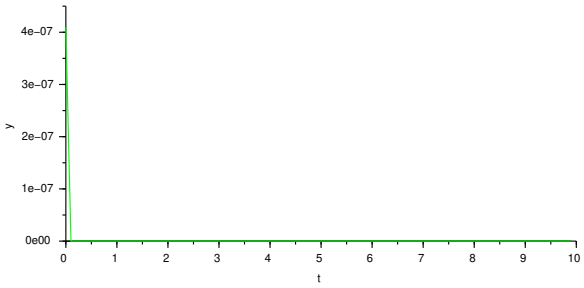


(c) HGO fictitious outputs $y_f$

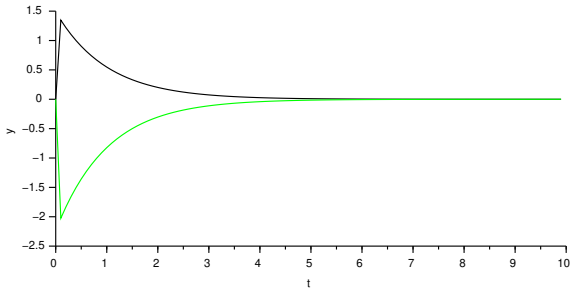


(d) HGO $\tau$ states

Figure 4.2: Minimal model: Case B: HGO with observability defects avoidance. Figure (a) depicts the estimation error $\tilde{x} = x - \hat{x}$ in black, green and red respectively, figure (b) represents the states $x$ in solid while the estimated states in dotted black, green and red lines respectively. Figures (c) and (d) shows the activated fictitious outputs $y_f$ and $\tau$ in black and green lines respectively.

### 4.3.5 Experimental Setup and Results

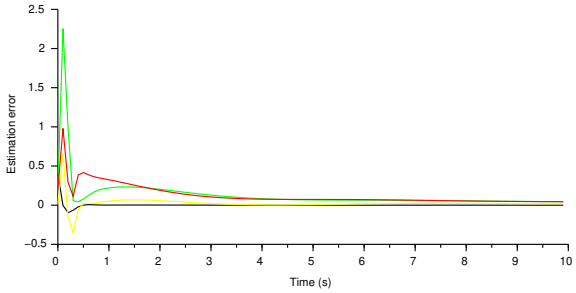


(a) LHGO estimation error

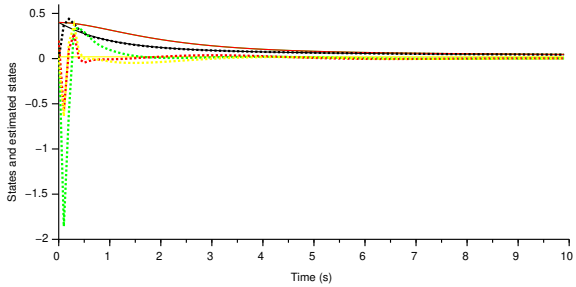


(b) LHGO states and estimated states

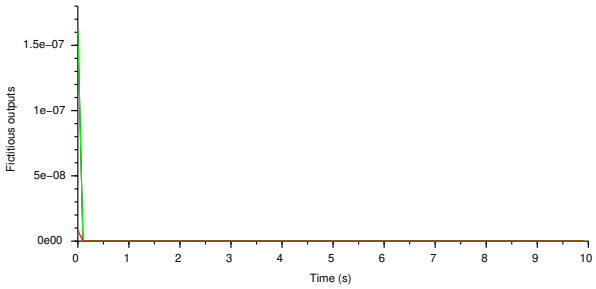


(c) LHGO fictitious outputs $y_f$

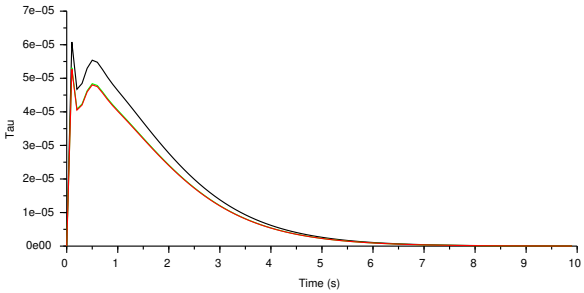


(d) LHGO $\tau$ states

Figure 4.3: Minimal model: Case B: LHGO with observability defects avoidance. Figure (a) depicts the estimation error $\tilde{x} = x - \hat{x}$ in black, green, red and yellow respectively, figure (b) represents the states $x$ in solid while the estimated states $\hat{x}$ in dotted black, green, red and yellow respectively. Figures (c) and (d) shows the activated fictitious outputs $y_f$ and $\tau$ in black, green and red lines respectively.

#### 4.3.5.1 Experimental Setup

Experiments were led in the $40 \times 40$ cm$^2$ test section of an open wind tunnel. The speed of the incoming flow $U_\infty$, ranging between 5 and 10 m/s, is used to generate the flow around a cubic obstacle of height $H = 0.1m$. The cylinder is equipped with 9 pressure taps located on the sides and on the back of the object as shown in Fig. 4.8. While the confinement is not an issue, it should be noted that the blockage ratio is 1/4 in the test section which has an influence on the characteristics of the vortex shedding compared to the unconfined flow. The Reynolds number $Re = U_\infty H/\nu$, where $\nu = 1.8\ 10^{-5}$ m$^2$/s is the kinematic viscosity of the air, was in the range of $[2.7; 5.5] \times 10^4$. A second non-dimensional number of importance is the frequency of the vortex shedding $f = StU_\infty/H$, where the Strouhal number $St = 0.14$ in the case of the square cylinder.

The side pressure sensors were used to measure the amplitude of vortex shedding while seven pressure sensors positioned on the back of the cylinder were used to measure the pressure

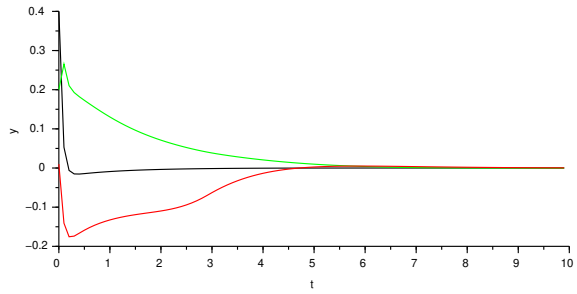


(a) LPLHGO estimation error

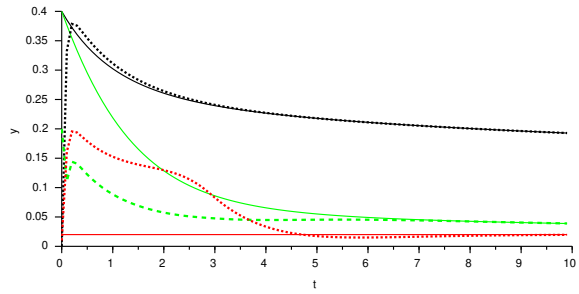


(b) LPLHGO states and estimated states

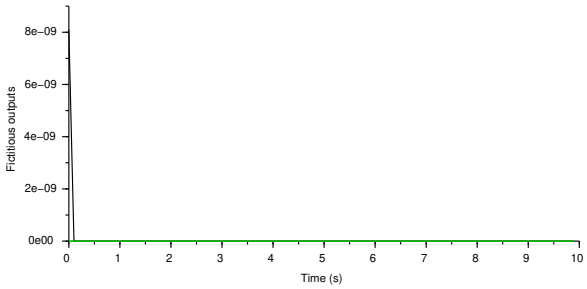


(c) LPLHGO fictitious outputs $y_f$

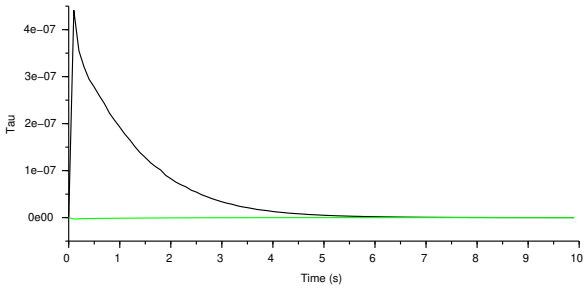


(d) LPLHGO $\tau$ states

Figure 4.4: Minimal model: Case B: LPLHGO with observability defects avoidance. Figure (a) depicts the estimation error $\tilde{x} = x - \hat{x}$ in black, green and red respectively, figure (b) represents the states $x$ in solid while the estimated states in dotted black, green and red lines respectively. Figures (c) and (d) shows the activated fictitious outputs $y_f$ and $\tau$ in black and green lines respectively.

component of the drag force onto the bluff body. The variables are nondimensionalized as follows:

$$\bar{\mathbf{x}} = \bar{\mathbf{x}}^*/H, \ \mathbf{u} = \mathbf{u}^*/U_\infty, \quad \text{and} \quad p = 2p^*/(\rho U_\infty^2), \tag{4.51}$$

where the starred quantities are the dimensional quantities. Pressures were considered as the pressure coefficient $C_p = 2(p - p_\infty)/(\rho U_\infty^2)$ measured at each position on the cylinder. The side faces contribute only to the lift coefficient $C_L$ whereas the drag coefficient $C_D$ corresponds to the projection of the pressure coefficient onto the front and back surfaces. Total drag is defined as the sum of pressure and friction drags: $C_D = C_p + C_f$. Numerical simulations and experimental measurements report mean values of $C_D \approx 2.2$ Iaccarino et al. [2003]; Meliga et al. [2016] from Reynolds Averaged Navier-Stokes (RANS) simulations and $C_D \approx 2.19$ Trias et al. [2015] from Direct Numerical Simulations (DNS) and mean $C_L = 0$ for very similar Reynolds numbers. In the present experiment, these mean values are found to be $[C_{D,exp}, C_{L,exp}] \approx [1.97, 0.05]$ which is in good agreement. In addition, Iaccarino et al. [2003] and Meliga et al. [2016] found using RANS

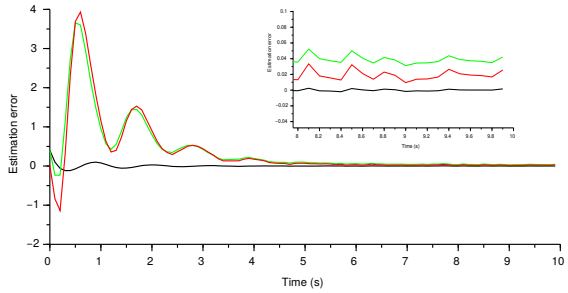


(a) HGO estimation error

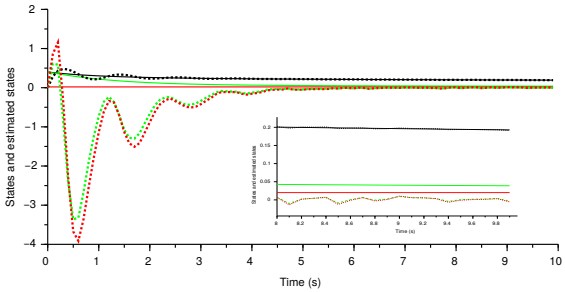


(b) HGO states and estimated states

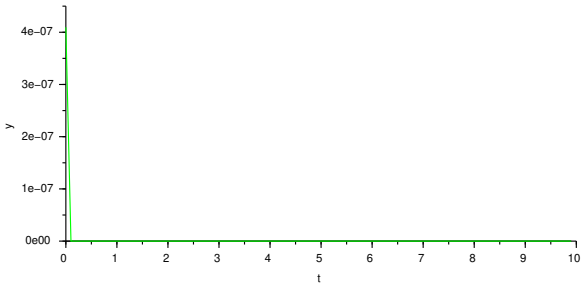


(c) HGO fictitious outputs $y_f$

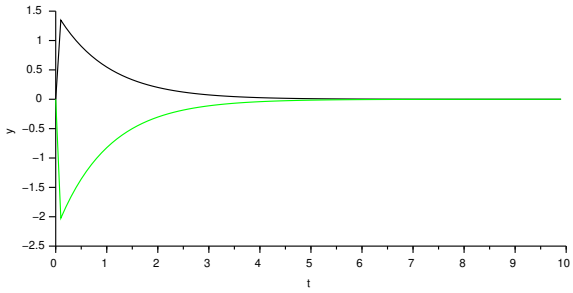


(d) HGO $\tau$ states

Figure 4.5: Minimal model: Case C: HGO with observability defects avoidance and additional output noise. Figure (a) depicts the estimation error $\tilde{x} = x - \hat{x}$ in black, green and red respectively, figure (b) represents the states $x$ in solid while the estimated states in dotted black, green and red lines respectively. Figures (c) and (d) shows the activated fictitious outputs $y_f$ and $\tau$ in black and green lines respectively.

simulations that the drag coefficient of the steady state is $C_{D,steady} \approx 1.71$ for a similar Reynolds number, which is directly related to the shift mode $x_2$, that is $\Delta C_{D,exp}(t) = C_{D,exp}(t) - C_{D,steady}$.

Fluctuations can also be used to compare DNS results Trias et al. [2015] with the present experiments. In particular, the fluctuations of the lift coefficient provide another mean to compare the amplitude of the oscillations from the pressure taps located on the sides of the square cylinder where Trias et al. [2015] report $rms(C_L(t)) \approx 1.71$. This coefficient can only be inferred from two pressure taps (see Fig. 4.8) and provide an estimation $rms(C_{L,exp}(t)) \approx 0.54$ which is well below the value found in the literature. This difference may be attributed to the sparse measurements on these faces of the square cylinder.

In the case of a bluff body, drag is more conveniently controlled by modifying the size of the recirculation region, which in turn, is slaved to the amplitude of the vortex shedding, at least in the laminar case. It is however less clear that the dominant vortex shedding mode alone is

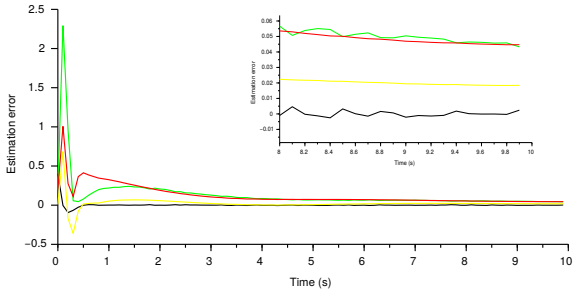


(a) LHGO estimation error

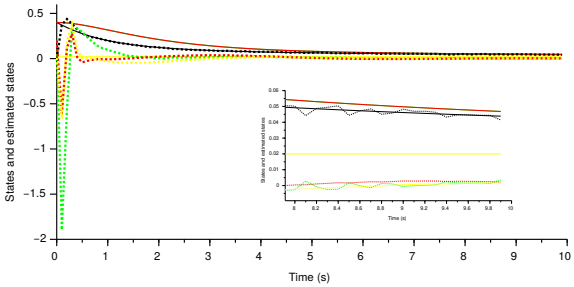


(b) LHGO states and estimated states

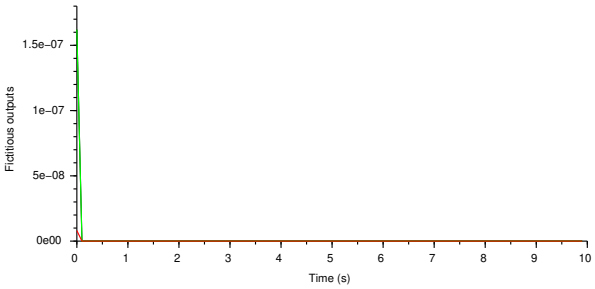


(c) LHGO fictitious outputs $y_f$

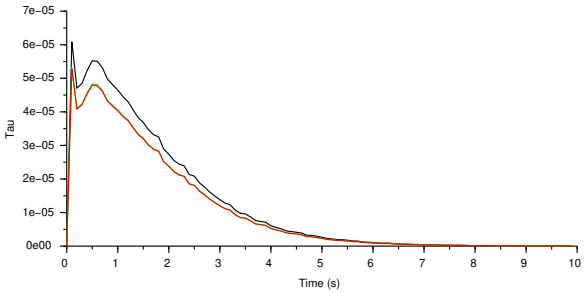


(d) LHGO $\tau$ states

Figure 4.6: Minimal model: Case C: LHGO with observability defects avoidance and additional output noise. Figure (a) depicts the estimation error $\tilde{x} = x - \hat{x}$ in black, green, red and yellow respectively, figure (b) represents the states $x$ in solid while the estimated states $\hat{x}$ in dotted black, green, red and yellow respectively. Figures (c) and (d) shows the activated fictitious outputs $y_f$ and $\tau$ in black, green and red lines respectively.

enough to predict the modification of the shift mode in the turbulent case and the prediction of the pressure at the base from a minimum number of sensors remains an open question. The interest of the present experiment is also to relate the amplitude of the shift mode through the amplitude of the vortex shedding which can be evaluated using sensors located on both sides of the bluff body. As shown in Stuart [1958]; Deane et al. [1991], the velocity on opposite sides of the bluff body is shifted by a phase of $\pi/2$. However, using pressure measurements $(p_1, p_2)$, the signal obtained from similar locations are shifted with a phase of $\pi$ Kurtulus et al. [2007]. To overcome this problem, we define $\bar{p}_1 = (p_1 - p_2)/2$ and $\bar{p}_2$ the temporal derivative of the former.

The amplitude of the vortex shedding can be written as:

$$A_{mp}(t) = \sqrt{\bar{p}_1^2(t) + \bar{p}_2^2(t)}, \tag{4.52}$$

illustrated in Fig. 4.9(a). Fig. 4.9(c) shows that the mean pressure at the base and thus

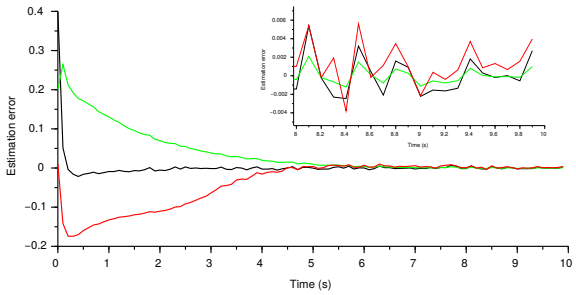


(a) LPLHGO estimation error

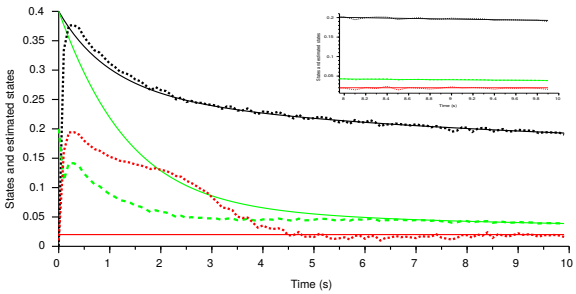


(b) LPLHGO states and estimated states

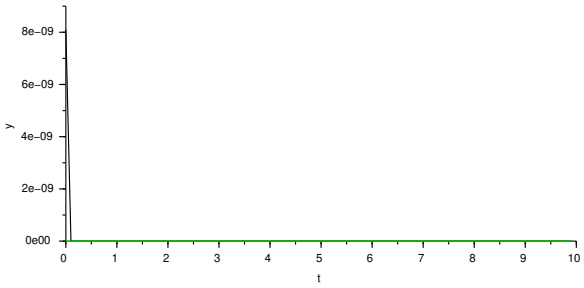


(c) LPLHGO fictitious outputs $y_f$

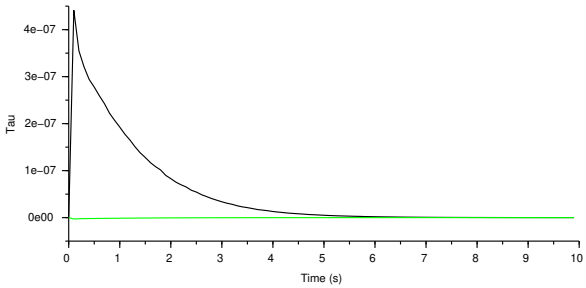


(d) LPLHGO $\tau$ states

Figure 4.7: Minimal model: Case C: LPLHGO with observability defects avoidance and additional output noise. Figure (a) depicts the estimation error $\tilde{x} = x - \hat{x}$ in black, green and red respectively, figure (b) represents the states $x$ in solid while the estimated states in dotted black, green and red lines respectively. Figures (c) and (d) shows the activated fictitious outputs $y_f$ and $\tau$ in black and green lines respectively.

the drag coefficient deviation from the steady state $\Delta C_{D,exp}(t)$ is essentially insensitive to the intermittency of the vortex shedding amplitude. The small oscillation of $\Delta C_{D,exp}(t)$ are magnified in 4.9(b) together with a low-pass filter computed over 20 periods of vortex shedding where the slow dynamics appear to be well correlated with the variations of the amplitude $A_{mp}$. As proposed by Sharma et al. [2011] a brief time-scale analysis shows that the shear-time scale $t_s \sim H/StU_\infty \sim \mathcal{O}(10^{-1})$ akin to vortex shedding is much shorter than the turbulent time scale $t_{nl} \sim H/Stu' \sim \mathcal{O}(10^0)$ where $u'$ is the amplitude of the turbulent fluctuations, typically of the order $\mathcal{O}(U_\infty/10)$. This nonlinear time scale is visible for instance in Fig. 4.9 and Fig. 4.10 and modulates the amplitude of the vortex shedding in time, resulting in the intermittent amplitude $A_{mp}(t)$.

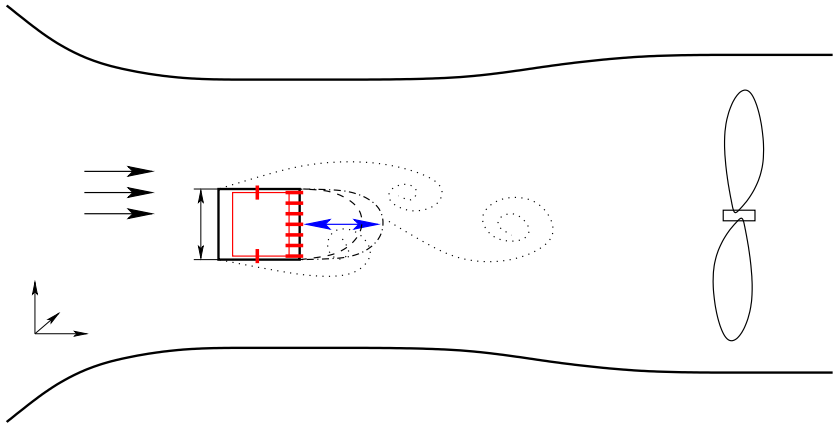

Figure 4.8: Sketch of the open wind tunnel and the square cylinder experiment. The thick red lines show the pressure taps while the pressure transducer is located inside the bluff body. The double arrow in blue shows the recirculation area while the vortex shedding is shown with dotted line.

#### 4.3.5.2 Experimental Results

We apply the high gain observer proposed in Proposition 20 to the experimental data. Since we have no access to the shift mode nor to the growth rate, we provide theoretical values based on the experimental equilibrium $x^{***}$: $(0.3974,\ 0.1210,\ 0.1210)^T$. The observer is initialized with $\hat{x}(0) = \begin{pmatrix} 1 & 1 & 1 \end{pmatrix}^T$ and $\tau(0) = 0_{2,1}$. Gains are chosen as $K = \begin{pmatrix} 0.31 & 0.07 & 0.05 \end{pmatrix}^T$ and the high gain as $\theta = 1.1$ to filter the signal high frequencies. After a $6s$ long transient phase, the observer converges both to the measured amplitude and to the theoretical values of the shift mode and growth rate (Fig. 4.10). The filtering effect of the observer drastically reduces the noise impact on the estimated states. Statistical analysis is given in Table 4.2. Despite a very simple model, it seems that the proposed approach is able to catch the dynamics of the mode. However, since many modes are implied for this large Reynolds number, it will be of great interest to compare the theoretical and estimated values to their true values, and to estimate the contribution of the other modes dynamics.

| Variable | Mean value | Standard deviation |
|---|---|---|
| $y = x_1$ | 0.3479 | 0.1486 |
| $\hat{x}_1$ | 0.3430 | 0.0377 |
| $\hat{x}_2$ | 0.1191 | 0.0255 |
| $\hat{x}_3$ | 0.1138 | 0.0498 |

Table 4.2: Statistical values for experiments

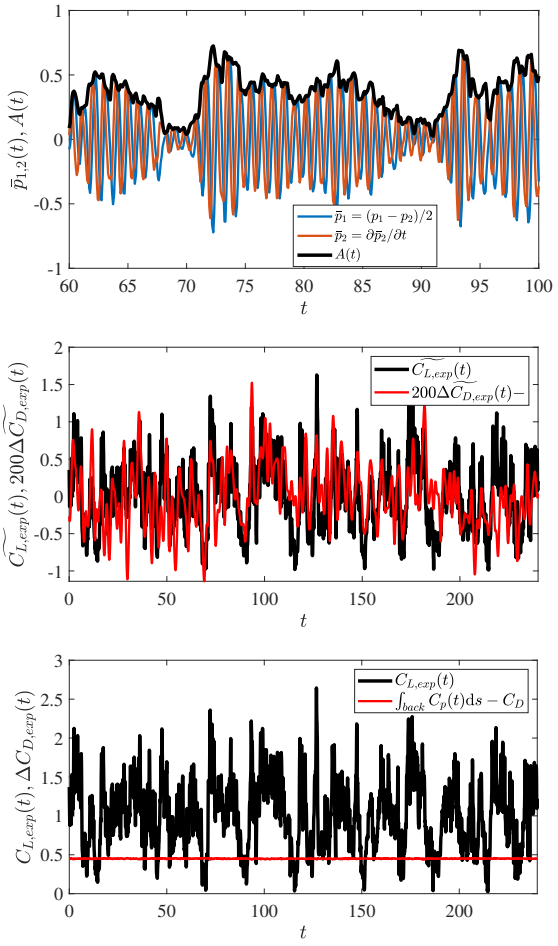


Figure 4.9: (a) Temporal evolution of the mean pressure $\bar{p} = (p_1 - p_2)$ (blue) where $p_1$ and $p_2$ are the pressures measured on the sides of the square cylinder respectively, parallel to the flow and the temporal derivative (red). (b) Estimated lift coefficient $\widetilde{C}_{L,exp}(t)$ (black) compared with fluctuations of the pressure on the back $\Delta\widetilde{C}_{D,exp}(t)$ magnified by a factor 200. The ($\widetilde{\ }$) denotes that the mean was subtracted. (c) Temporal evolution of the lift coefficient $C_{L,exp}$ and the shift of the drag coefficient $\Delta C_{D,exp}(t)$ with respect to the steady state.

## 4.4 SPOD Model

The estimation of coherent structures from experimental or numerical data is an important step in the identification of a nonlinear reduced-order model (ROM). This mainly includes the construction of coherent structures (modes) that inherit most of the energy present in the flow along the time. There are different methods of estimating coherent structures, like DMD, POD, etc. Spectral proper orthogonal decomposition (SPOD) has been used to estimate the coherent structures that are physically meaningful as it evolves with a clear separation of phenomena

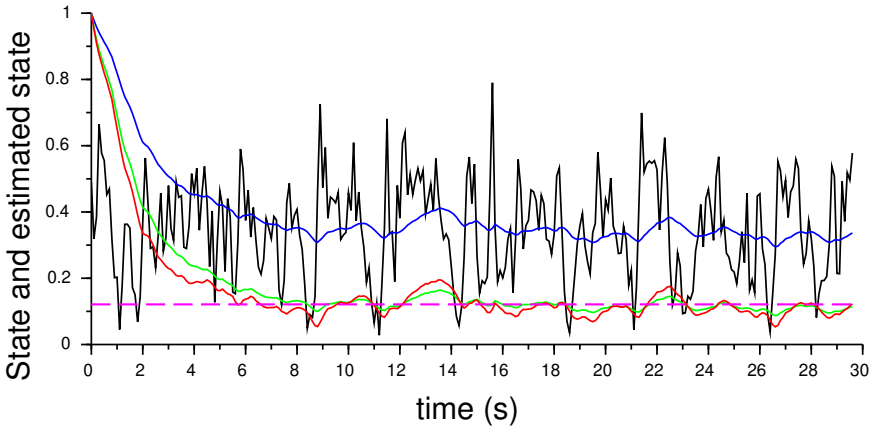


Figure 4.10: Minimal model: Experimental estimated states. The black solid line represents the measured output $y = x_1$ on the system, the purple dotted line is the theoretical shift mode and growth ratio at the equilibrium, computed as $\langle y \rangle^2$. Estimated states $\hat{x}_1$, $\hat{x}_2$ and $\hat{x}_3$ are depicted by blue, green and red solid lines respectively.

occurring at multiple frequencies and energies, and these modes oscillate in their frequency.

The coherent structures are estimated by SPOD which characterizes these modes both in time and spatial coordinates, which is an advantage over POD modes. Time-varying mode amplitudes of these coherent structures are then estimated, and filtered through a Sgolay filter. The identification of the dynamics is carried out with the Galerkin projection from the wind tunnel measurement at Reynolds number 1000, that contains only the attractor dynamics. Identification from this type of flow date requires enforcement of physical constraints in these regimes that confirm their presence.

$$\frac{d}{dt}\begin{bmatrix} a_{m1} \\ a_{m2} \\ a_\Delta + c \end{bmatrix} = \begin{bmatrix} \mu & -S_t & -\gamma a_{m1} \\ S_t & \mu & -\gamma a_{m2} \\ \chi a_{m1} & \chi a_{m2} & -\lambda \end{bmatrix} \begin{bmatrix} a_{m1} \\ a_{m2} \\ a_\Delta + c \end{bmatrix} \tag{4.53}$$

with $c > 0$, the identification of the unknown parameters is carried out by solving the optimization problem to minimize the cost function, as given in Table 4.3.

Using the oscillating amplitude $A_{mp} = \sqrt{a_{m1}^2 + a_{m2}^2}$; we derive our state space model $x \in \mathcal{X} \subset \mathbb{R}^3$ with $x_1$ being the oscillating amplitude and $x_2$ as the new shift mode $a_\Delta + c$, representing the energy exchange between the mean flow and oscillatory perturbation and finally

| Polynomial | $\frac{da_{m1}}{dt}$ | $\frac{da_{m2}}{dt}$ | $\frac{da_{\Delta}}{dt}$ |
|---|---|---|---|
| 1 | - | - | $0.7417(c)$ |
| $a_{m1}$ | $0.0164(\mu)$ | $0.221(S_t)$ | - |
| $a_{m2}$ | $0.221(S_t)$ | $0.0164(\mu)$ | - |
| $a_{m1}a_{\Delta}$ | $0.0221\ (\gamma)$ | - | - |
| $a_{m2}a_{\Delta}$ | - | $-0.0221\ (\gamma)$ | - |
| $a_{\Delta}$ | - | - | $-0.0248(\lambda)$ |
| $a_{m1}^2 + a_{m2}^2$ | - | - | $0.7343\ (\chi)$ |

Table 4.3: Identified modeling Parameters for system SPOD

$x_3$ a constant growth rate parameter $\mu$. Therefore, it can be rewritten as:

$$\dot{x} = f(x) = \begin{pmatrix} x_1(x_3 - \gamma x_2) \\ \chi x_1^2 - \lambda x_2 \\ 0 \end{pmatrix}, y = h(x) = Cx = x_1, \tag{4.54}$$

where $y$ is the measured output of the system with $C = (1 \quad 0 \quad 0)$.

**Proposition 26** *Based on Theorem 15, system (4.54) is observable on* $\mathcal{O}_\epsilon = \{x \in \mathcal{X} \subset \mathbb{R}^3 : |x_1| > \epsilon\}$ *for any* $\epsilon > 0$ *and the observability singularity set for the identified minimal SPOD model:*

$$\mathcal{S} = \{x \in \mathcal{X} \subset \mathbb{R}^3 : x_1 = 0\}. \tag{4.55}$$

The proof of Proposition 26 for observability analysis of SPOD model is quite similar to the proof of Theorem 15, hence it is avoided here for the sake of compactness and to avoid repetitions.

### 4.4.1 Nonlinear Observer synthesis for SPOD model

We have a nonlinear system therefore, we begin by transforming the minimal nonlinear system into observability normal form:

$$z = T(x) = \begin{pmatrix} x_1 \\ x_1(x_3 - \gamma x_2) \\ x_1[(x_3 - \gamma x_2)^2 - \gamma\chi x_1^2 + \gamma\lambda x_2] \end{pmatrix}, \quad y = z_1, \tag{4.56}$$

where $z \in \mathcal{Z} \subset \mathbb{R}^3$ and measured output $y \in \mathbb{R}$.

Since the SPOD model also suffers from observability defects, hence in this section we will design the nonlinear observer for SPOD model with singularity avoidance. In the sequel, we will present the design of standard HGO, LHGO and LPLHGO in original coordinates that are capable of avoiding observability defects.

#### 4.4.1.1 HGO for SPOD model

Based on Theorem 8, we can design the high gain observer for the SPOD model.

**Proposition 27 (Standard HGO for SPOD model)** *The standard high gain observer for the system (4.56) is given as:*

$$\dot{\hat{z}} = A_{n_z} z + B_{n_z} \varphi_s(z) + \Delta K(y - \hat{z}_1), \tag{4.57}$$

*where $\varphi_s$ is the Lipschitz extension of $\varphi$ given by:*

$$\varphi_3(\hat{x}) = \hat{x}_1[(\hat{x}_3 - \gamma\hat{x}_2)^3 + (\hat{x}_3 - \gamma\hat{x}_2)(3\gamma\lambda\hat{x}_2 - 5\gamma\chi\hat{x}_1^2) + \gamma\lambda\chi\hat{x}_1^2 - \gamma\lambda^2\hat{x}_2]. \tag{4.58}$$

*The high gain matrix $\Delta$ is a diagonal matrix formed in ascending powers of a gain $\theta > \theta^* > 1$ and the observer gain matrix $K = \begin{pmatrix} k_1 & k_2 & k_3 \end{pmatrix}^T$ is chosen so as to have $(A_{n_z} - KC_{n_z})$ Hurwitz.*

**Remark 14** *This standard high gain observer is not defined at the observability singularity since $T$ is by construction singular for $\hat{x}_1 = 0$.*

$$\frac{\partial T}{\partial x}(x) = \begin{pmatrix} 1 & 0 & 0 \\ x_3 - \gamma x_2 & -\gamma x_1 & x_1 \\ (x_3 - \gamma x_2)^2 - 3\gamma\chi x_1^2 + \gamma\delta x_2 & \gamma x_1(\lambda - 2(x_3 - \gamma x_2)) & 2x_1(x_3 - \gamma x_2) \end{pmatrix}. \tag{4.59}$$

The observability singularity at $x_1 = 0$ stated in Proposition 26 means that there is no access to any information about state $x_2$ nor $x_3$ when $x_1 = 0$. We use the same procedure as done before for the observability defects avoidance for the minimal model and get the observer in original coordinates.

**Proposition 28 (Singularity-free HGO for SPOD model)** *Let*

$$\rho : x \mapsto max(0, \epsilon^2 - x_1^2)^2 \tag{4.60}$$

*for some $\epsilon > 0$. Consider the fictitious output $y_f \in \mathbb{R}^2$ such that:*

$$y_f(x) = \begin{pmatrix} \gamma\rho(x)x_2 \\ \rho(x)x_3 \end{pmatrix}, \tag{4.61}$$

*and under the assumptions and notations of Proposition 19, we define two new state vectors $x_a$ and $z_a$ such as*

$$x_a = \begin{pmatrix} x \\ \tau \end{pmatrix} \text{ and } z_a = T_a(x_a) = \begin{pmatrix} z \\ y_f \end{pmatrix} + \Psi(x)\tau, \tag{4.62}$$

*where $\tau \in \mathbb{R}^2$ are the exogenous variables added to the original state vector and $\Psi$ is given as:*

$$\Psi : x \mapsto \begin{pmatrix} 0 & 0 \\ \rho(x) & 0 \\ 0 & -\lambda\rho(x) \\ x_1 & x_1 \\ 0 & x_1 \end{pmatrix}. \tag{4.63}$$

*The determinant of the new mapping $T_a$ comes out to be:*

$$\left|\frac{\partial T_a}{\partial x_a}(x_a)\right| = -\gamma\lambda(x_1^2 + \rho^2)^2, \qquad \forall(\gamma, \lambda > 0). \tag{4.64}$$

*Then a high gain observer for system (4.5) on any bounded subset $\mathcal{X} \in \mathbb{R}^3$ avoiding the singularity is given by*

$$\dot{\hat{x}}_a = \frac{\partial T_a}{\partial x_a}(\hat{x}_a)^{-1}\mathcal{F}_z(\hat{x}_a, y), \tag{4.65}$$

*where*

$$\mathcal{F}_z : (\hat{x}_a, y) \mapsto \begin{pmatrix} A_{n_z}T_a(\hat{x}_a) + B_{n_z}\varphi_s(\hat{x}) + \Delta K(y - C_{n_z}\hat{x}_a) \\ -k_4 T_{a_4}(\hat{x}_a) \\ -k_5 T_{a_5}(\hat{x}_a) \end{pmatrix} \tag{4.66}$$

*with $T_{a_i}$ denoting the $i$-th component of $T_a$ given in (4.62) , $k_4, k_5 > 0$ and $K$, $\Delta$ given by Theorem 19.*

The proof of this proposition is similar to the proof given for HGO for minimal model (i.e., Proof 16), therefore it is omitted here to avoid repetition.

#### 4.4.1.2 LHGO for SPOD model

Based on Theorem 11, we can design the limited high gain observer for the SPOD model given by (4.54).

**Proposition 29 (LHGO for SPOD model)** *The limited high gain observer for the system (4.56) is given as:*

$$\dot{\zeta} = \mathcal{F}_\zeta(\zeta, \hat{x}, y) = \begin{pmatrix} \zeta_{12} + \theta k_{11}(y - \zeta_{11}) \\ \zeta_{22} + \theta^2 k_{21}(y - \zeta_{11}) \\ \zeta_{22} + \theta k_{21}(\zeta_{12} - \zeta_{21}) \\ \varphi_{3s} + \theta^2 k_{22}(\zeta_{12} - \zeta_{21}) \end{pmatrix}, \tag{4.67}$$

*and we can therefore get the LHGO in target coordinates using either $\hat{z} = P\zeta$ or $z' = P'\zeta'$. Based on Proposition 2, we can get the observer in original coordinates since we can use either $\hat{x} = P\hat{x}$ or $\hat{x}' = P'\hat{x}'$. This observer also faces the problem linked with the observability singularity at $\hat{x}_1 = 0$.*

The mapping $T$ is an immersion from $x \in \mathcal{X} \subset \mathbb{R}^{n_x}$ to $\zeta \in \mathbb{R}^{n_\zeta}$ such that $n_\zeta = 2n_z - 1 > n_x$, therefore we augment the mapping domain into diffeomorphism using the same methology as done previously for the minimal model.

**Proposition 30** *For the SPOD model, defining the original coordinate augmented state $\bar{x}$ and $\bar{T}$ as*

$$\bar{T} : \bar{x} = \begin{pmatrix} x_1 \\ x_2 \\ x_2' \\ x_3 \end{pmatrix} \mapsto \bar{z} = \begin{pmatrix} x_1 \\ x_1(x_3 - \gamma x_2) \\ x_1(x_3 - \gamma x_2') \\ x_1((x_3 - \gamma x_2)^2 - \gamma\chi x_1 + \gamma\lambda x_2) \end{pmatrix}. \tag{4.68}$$

*$\bar{T}$ is a diffeomorphism on $\bar{\mathcal{S}}_\epsilon = \{\bar{x} \in \mathcal{X} \subset \mathbb{R}^4 : |x_1| > \epsilon\}$.*

**Proof 19** *The jacobian of the mapping $\bar{T}$ is given as:*

$$\frac{\partial \bar{T}}{\partial \bar{x}}(\bar{x}) = \begin{pmatrix} 1 & 0_{1,n_\zeta - 1} \\ * & J \end{pmatrix} \tag{4.69}$$

*with*

$$J = \begin{pmatrix} -\gamma x_1 & 0 & x_1 \\ 0 & -\gamma x_1 & x_1 \\ \gamma x_1(\lambda - 2(x_3 - \gamma x_2)) & 0 & 2x_1(x_3 - \gamma x_2) \end{pmatrix}, \tag{4.70}$$

*leads to the determinant of $\bar{T}$:*

$$\left| \frac{\partial \bar{T}}{\partial \bar{x}}(\bar{x}) \right| = -\gamma\lambda x_1^3, \qquad \forall(\gamma, \lambda > 0).$$

*This proves $\bar{T}$ is a diffeomorphism on $\bar{\mathcal{S}}_\epsilon$.*

To avoid the observability defects pinpointed in Proposition 26, we add some fictitious outputs aiming at getting information about $x_2, x_2'$ and $x_3$ around the singularity.

**Proposition 31 (Singularity-free LHGO for SPOD model)** *For system (4.68), adding respectively fictitious outputs $y_f \in \mathbb{R}^{n_f}$*

$$y_f(x) = \begin{pmatrix} \gamma\rho(x)x_2 \\ \gamma\rho(x)x_2' \\ \rho(x)x_3 \end{pmatrix}, \tag{4.71}$$

*where $\rho$ is given in (4.16). We define two new state vectos, $x_a$ and $z_a$, which are as follows:*

$$x_a = \begin{pmatrix} \bar{x} \\ \tau \end{pmatrix} \quad \text{and} \quad z_a = T_a(x_a) = \begin{pmatrix} \bar{z} \\ y_f \end{pmatrix} + \Psi(\bar{x})\tau, \tag{4.72}$$

*where* $\tau \in \mathbb{R}^3$ *are the exogenous variables added to the augmented state vector* $\bar{x}$ *and*

$$\Psi(\bar{x}) = \begin{pmatrix} 0 & 0 & 0 \\ 1 & 0 & -1 \\ 0 & 1 & -\lambda \\ 0 & 0 & \lambda \\ x_1 & 0 & 0 \\ 0 & x_1 & 0 \\ 0 & 0 & x_1 \end{pmatrix}. \tag{4.73}$$

*The determinant of* $T_a$ *comes out to be:*

$$\left| \frac{\partial T_a}{\partial x_a}(x_a) \right| = -\gamma^2 \lambda (\rho + x_1^2)^3, \qquad \forall (\gamma, \lambda > 0). \tag{4.74}$$

*Then a Limited high gain observer for system* (4.5) *avoiding the singularity is given by*

$$\dot{\hat{x}}_a = \frac{\partial T_a}{\partial x_a}(\hat{x}_a)^{-1} \mathcal{F}(\zeta, \hat{x}_a, y), \tag{4.75}$$

*where*

$$\mathcal{F} : (\zeta, \hat{x}_a, y) \mapsto \begin{pmatrix} \mathcal{F}_\zeta(\zeta, \hat{x}_a, y) \\ -K_3 T_{a3}(\hat{x}_a)) \end{pmatrix} \tag{4.76}$$

$\mathcal{F}_\zeta$ *is given by Proposition 29 and* $K_3$ *is a positive definite diagonal matrix of dimension* 3. *The notation* $T_{a3}$ *stands for the last* 3 *components of* $T_a$ *representing the dynamics associated with the fictitious outputs.*

The proof of this proposition is akin to Proof 18.

#### 4.4.1.3 LPLHGO for SPOD model

Based on Theorem 12, we can design the low peaking LHGO for the SPOD model.

**Proposition 32 (LPLHGO for SPOD model)** *The low peaking limited high gain observer for the system* (4.56) *is given as:*

$$\begin{aligned} \dot{\hat{z}} &= \mathcal{F}_z(\hat{z}, \eta, y) \\ \dot{\eta} &= \mathcal{F}_\eta(\hat{z}, \eta, y) \end{aligned} \tag{4.77}$$

*with* $\mathcal{F}_z$ *and* $\mathcal{F}_\eta$ *given in Proposition 24.*

Since $n_z = n_x$, therefore we can obtain the observer in original coordinates by using Proposition 2. However, based on the observability analysis done for the SPOD model in Proposition 26, $T$ is diffeomorphism only on $\mathcal{S}_\epsilon$ due to the observability singularity. The Jacobian of $T$ is given as:

$$\frac{\partial T}{\partial x}(x) = \begin{pmatrix} 1 & 0 & 0 \\ x_3 - \gamma x_2 & -\gamma x_1 & x_1 \\ (x_3 - \gamma x_2)^2 - 3\gamma\chi x_1^2 + \gamma\lambda x_2 & \gamma x_1(\lambda - 2(x_3 - \gamma x_2)) & 2x_1(x_3 - x_2) \end{pmatrix} \tag{4.78}$$

and its determinant can be found as:

$$\left|\frac{\partial T}{\partial x}\right| = -\gamma\lambda x_1^2 \tag{4.79}$$

so the LPLHGO is not defined at the observability singularity. By following the same procedure as done before in the case of HGO and LHGO in Propositions 20 and 23, we can get the new LPLHGO that is capable of avoiding the singularity. The observer synthesis procedure of LPLHGO for the SPOD model is same as that of minimal model, therefore we save the space and directly write the LPLHGO in original coordinates in the next Proposition.

**Proposition 33 (Singularity-free LPLHGO for SPOD model)** *The dynamic system*

$$\begin{cases} \dot{\hat{x}}_a = \left(\dfrac{\partial T_a}{\partial x_a}(\hat{x}_a)\right)^{-1} \begin{pmatrix} \mathcal{F}_z(T_a(\hat{x}_a), \eta, y) \\ -K_2 T_{a2}(\hat{x}_a) \end{pmatrix} \\ \dot{\eta} = \mathcal{F}_\eta(T_a(\hat{x}_a), \eta, y) \end{cases} \tag{4.80}$$

*is an arbitrarily fast converging observer for system (4.54) in its original coordinates on any bounded subset of* $\mathbb{R}^{n_z+n_f}$. $\mathcal{F}_z, \mathcal{F}_\eta$ *are defined in Proposition 24 and,* $T_a$ *is defined by Proposition 20,* $K_2$ *is a positive definite diagonal matrix of dimension* 2. *The notation* $T_{a2}$ *stands for the last* 2 *components of* $T_a$ *representing the dynamics associated with the fictitious outputs.*

### 4.4.2 Simulation Results for SPOD Model

| | |
|---|---|
| $x_0$ | $\begin{pmatrix} 0.2 & 0.75 & 0.0164 \end{pmatrix}$ |
| $\hat{x}_0$ | $\begin{pmatrix} 0 & 0.6 & 0.02 \end{pmatrix}$ |
| $K_{HGO}$ | $\begin{pmatrix} 0.33 & 0.036 & 0.0018 \end{pmatrix}^T$ |
| $K_{LHGO}$ | $\left(\begin{pmatrix} k_{11} \\ k_{12} \end{pmatrix} \quad \begin{pmatrix} k_{21} \\ k_{22} \end{pmatrix}\right)^T = \left(\begin{pmatrix} 0.18 \\ 0.01 \end{pmatrix} \quad \begin{pmatrix} 0.18 \\ 0.002 \end{pmatrix}\right)^T$ |
| $K_{LPLHGO}$ | $\left(\begin{pmatrix} \alpha_1 & \alpha_2 & \alpha_3 \\ \beta_1 & \beta_2 \end{pmatrix}\right)^T = \left(\begin{pmatrix} 0.18 & 0.18 & 0.18 \\ \begin{pmatrix} 0.01 & 0.002 \end{pmatrix} \end{pmatrix}\right)^T$ |
| $K_{n_f}$ | $10 I_2$ |
| $\theta_{HGO}$ | 3.5 |
| $\theta_{LHGO}$ | 3 |
| $\theta_{LPLHGO}$ | 5 |
| $\epsilon$ | 0.01 |

Table 4.4: Initial conditions and gains for the system and observers for SPOD model

The high gain observer, limited high gain observer, and low peaking limited high gain observer in original coordinates proposed in Propositions 28, 31, and 33, respectively are simulated for different scenarios. Table 4.4 provides the initial conditions and observer gains, while the parameter values for the system are given in Table 4.3. The results are provided for different high gains to obtain a similar convergence rate for all the observers. Similar to what was done before in the case of the minimal model, the performance comparison is guided through three cases: case A is the nominal one, where no observability defect or disurbance is considered; case B illustrates the observability defects avoidance; and finally in case C, the robustness to output noise is addressed.

#### 4.4.2.1 Case A: Nominal Case

The initial condition for the state variable $\hat{x}_1$ is chosen non-null i.e., $\hat{x}_1 = 0.21$ to try avoiding any observability defect and study the different observer behaviors under nominal conditions. The first figure 4.11(a) presents a high peaking due to the fact that high gain observer increases the power of the high gain parameter. In comparison to HGO, the effect of peaking is reduced in the case of LHGO due to high gain power limited to two (Figure 4.11(c)). The peaking is infact further reduced for LPLHGO owing to the saturations present between the interconnections as can be seen in 4.11(e).

#### 4.4.2.2 Case B: Observability Defects Avoidance

The three observers are initialized at zero in the second set of simulations, as can be seen in Figures 4.12,4.13 and 4.14 to examine the impact of singularity avoidance on the observer dynamics. The fact that fictitious outputs were activated during the initial few seconds can be seen in Figures 4.12(c),4.13(c) and 4.14(c), and the estimation error converges to zero as soon as $x$ goes back to $\mathcal{O}_\epsilon$, showing that the three observers were efficient enough in handling the singularity. The activation of fictitious outputs in this scenario is the reason behind the increased peaking, and each observer's response to dealing with the peaking effect is comparable to that in nominal case.

#### 4.4.2.3 Case C: Output Noise

Since the measurements are affected by high frequency noises, therefore while observing the system, particular emphasis must be paid to robustness to such noises. As a result, the final case C includes studying the system with the white gaussian measurement noise with a cutoff frequency set to 1000 Hz followed by a variance 1 on the output. Only practical stability is ensured in such a scenario as can be seen in Figures 4.15, 4.16 and 4.17. The simulations demonstrate that

in the case of HGO, the inclusion of the output noise has a significant influence. Compared to the HGO, it is evident that LHGO and LPLHGO perform better in this regard as the noise-induced errors are significantly smaller as can be seen from Figures 4.15(a), 4.16(a) and 4.17(a).

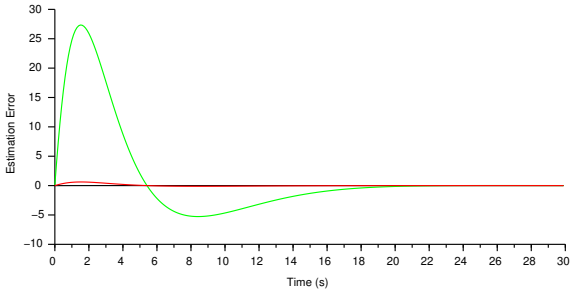


(a) HGO estimation error

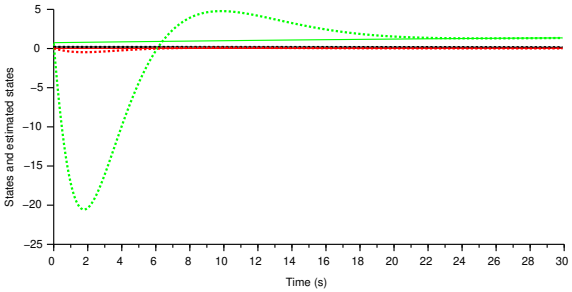


(b) HGO states and estimated states

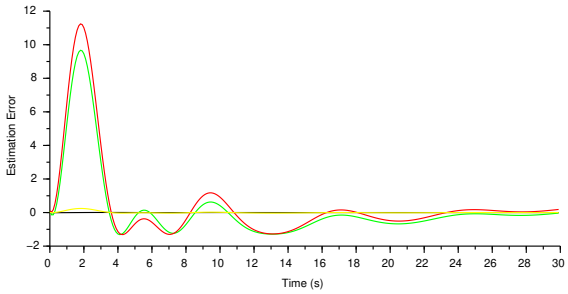


(c) LHGO estimation error

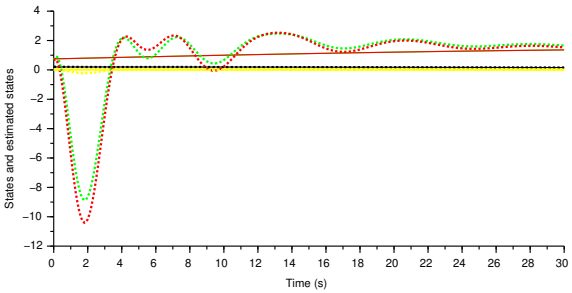


(d) LHGO states and estimated states

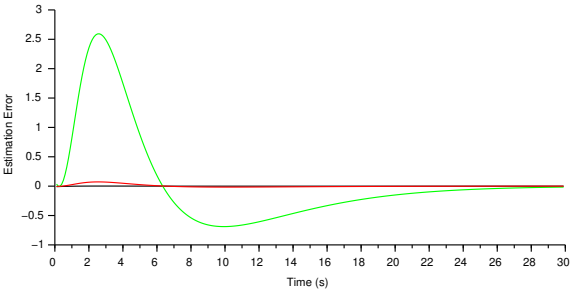


(e) LPLHGO estimation error

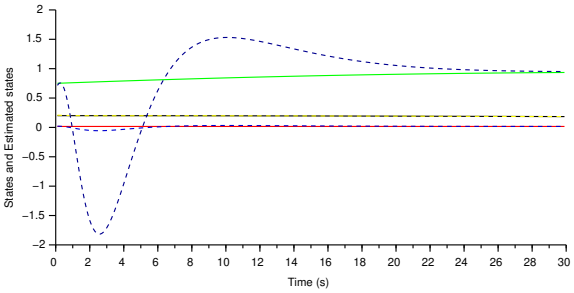


(f) LPLHGO states and estimated states

Figure 4.11: SPOD: Case A from (a) to (f): simulation for nominal case. Figures (a) and (e) depicts the estimation error $\tilde{x}_1, \tilde{x}_2, \tilde{x}_3$ by black, green and red lines for HGO and LPLHGO respectively, while Figure (c) represents the estimation error $\tilde{x}_1, \tilde{x}_2, \tilde{x}_3$ and $\tilde{x}_4$ by black, green, red and yellow lines respectively for LHGO. Figures (b) and (e) represents the states and estimated states, such that states $x$ are in solid while the estimated states $\hat{x}$ are in dotted black, green and red lines respectively for HGO and LPLHGO and Figure (d) depicts the states and estimated states, such that states are in solid while the estimated states $\hat{x}$ are in dotted black, green, red and yellow lines respectively for LHGO.

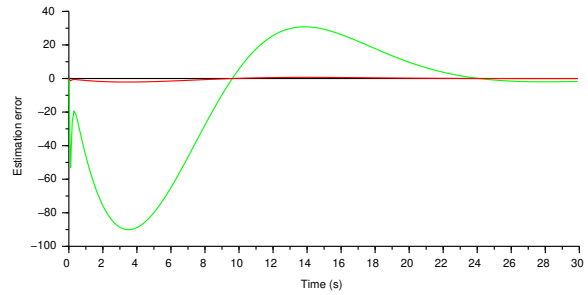


(a) HGO estimation error

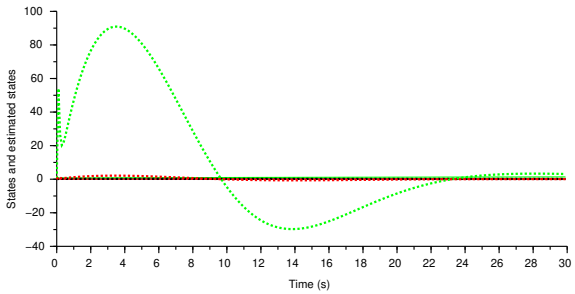


(b) HGO states and estimated states

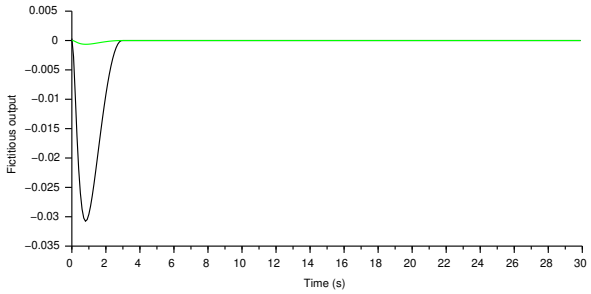


(c) HGO fictitious outputs $y_f$

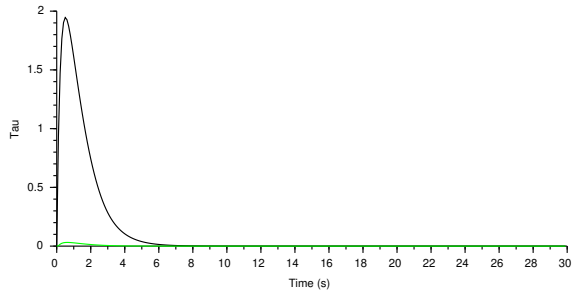


(d) HGO $\tau$ states

Figure 4.12: SPOD: Case B: HGO with observability defects avoidance. Figure (a) depicts the estimation error $\tilde{x} = x - \hat{x}$ in black, green and red respectively, figure (b) represents the states $x$ in solid while the estimated states in dotted black, green and red lines respectively. Figures (c) and (d) shows the activated fictitious outputs $y_f$ and $\tau$ in black and green lines respectively.

## 4.5 Multi-Output Wake Flow Model

The Galerkin projection of (4.2) onto the Navier-Stokes equation leads to a low-order dimensional nonlinear model where the amplitudes $a_{mi}(t)$ vary as a function of time similarly to a nonlinear oscillator system. The dynamical equations of the temporal coefficients Noack et al. [2003] are given by :

$$\begin{pmatrix} \dot{a}_{m1} \\ \dot{a}_{m2} \\ \dot{a_\Delta + c} \end{pmatrix} = \begin{pmatrix} \mu & -S_t & -\gamma a_{m1} \\ S_t & \mu & -\gamma a_{m2} \\ \chi a_{m1} & \chi a_{m2} & -\lambda \end{pmatrix} \begin{pmatrix} a_{m1} \\ a_{m2} \\ a_\Delta + c \end{pmatrix}. \tag{4.81}$$

with c>0. The parameters $(\mu, St, \gamma, \lambda, \chi)$ are specific to fluid mechanics and are identified using SPOD as discussed in the previous section.

We derive the state space model $x \in \mathcal{X} \subset \mathbb{R}^4$ with $x_1 = a_{m1}$ and $x_2 = a_{m2}$ being the oscillating amplitude that are accessible to measurement thanks to particle image velocimetry sensors attached on both the sides of the cylinder. $x_3 = a_\Delta + c$ is the shifted mode, representing

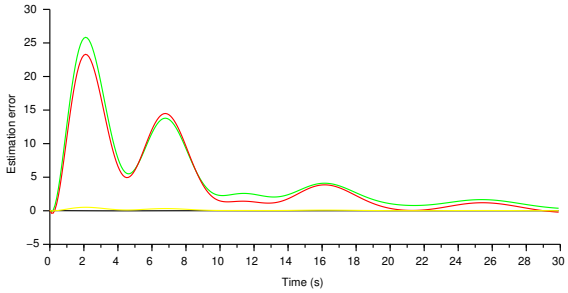


(a) LHGO estimation error

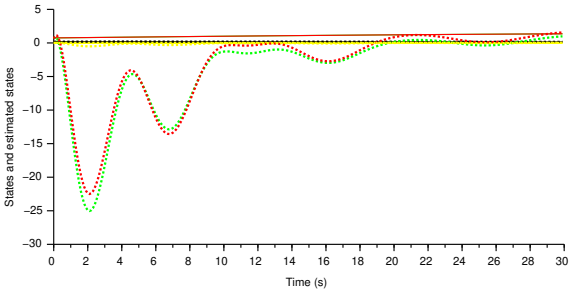


(b) LHGO states and estimated states

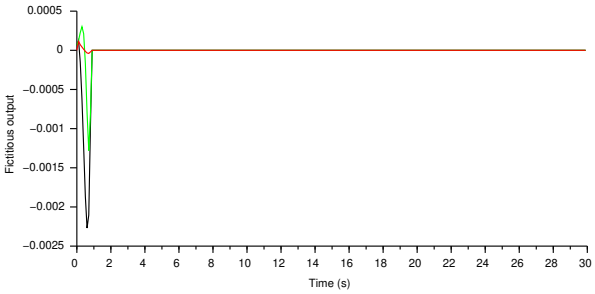


(c) LHGO fictitious outputs $y_f$

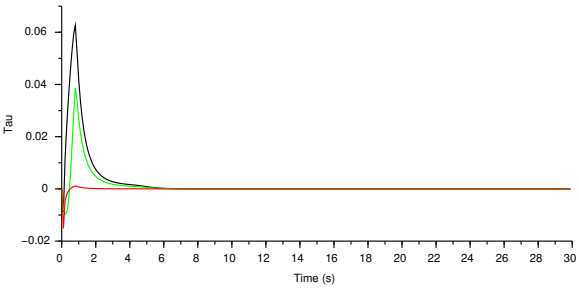


(d) LHGO $\tau$ states

Figure 4.13: SPOD: Case B: LHGO with observability defects avoidance. Figure (a) depicts the estimation error $\tilde{x} = x - \hat{x}$ in black, green, red and yellow respectively, figure (b) represents the states $x$ in solid while the estimated states $\hat{x}$ in dotted black, green, red and yellow respectively. Figures (c) and (d) shows the activated fictitious outputs $y_f$ and $\tau$ in black, green and red lines respectively.

the energy exchange between the mean flow and the oscillatory perturbation. The growth rate parameter $\mu$ is a key parameter but usually difficult to identify since it infact may depend on other modes: we consider it as a constant and estimate it as $x_4$.

Therefore, (4.81) can be rewritten as:

$$\dot{x} = \begin{pmatrix} \dot{x}_1 \\ \dot{x}_2 \\ \dot{x}_3 \\ \dot{x}_4 \end{pmatrix} = \begin{pmatrix} -S_t x_2 + x_1(x_4 - \gamma x_3) \\ S_t x_1 + x_2(x_4 - \gamma x_3) \\ -\lambda x_3 + \chi(x_1^2 + x_2^2) \\ 0 \end{pmatrix}, \qquad x = \begin{pmatrix} a_{m1} \\ a_{m2} \\ a_\Delta + c \\ \mu \end{pmatrix} \in \mathcal{X} \subset \mathbb{R}^4, \qquad y = \begin{pmatrix} x_1 \\ x_2 \end{pmatrix} \in \mathbb{R}^2, \tag{4.82}$$

where we now have access to both $x_1 = a_{m1}$ and $x_2 = a_{m2}$.

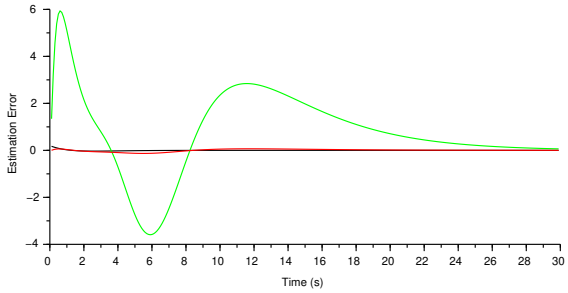


(a) LPLHGO estimation error

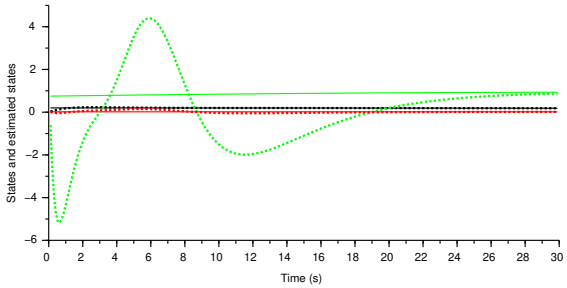


(b) LPLHGO states and estimated states

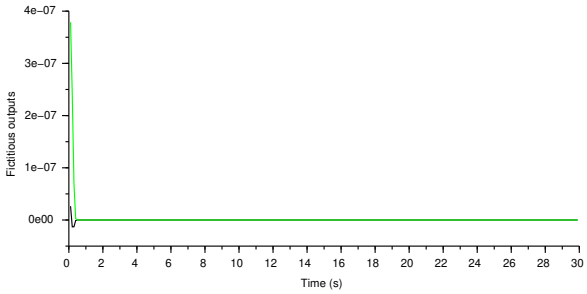


(c) LPLHGO fictitious outputs $y_f$

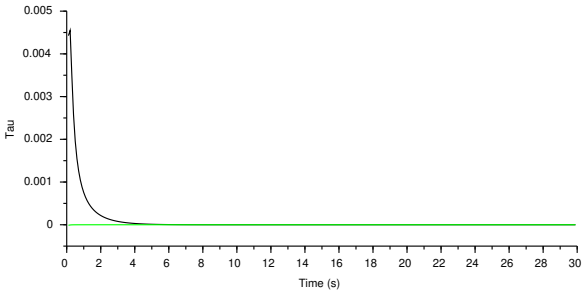


(d) LPLHGO $\tau$ states

Figure 4.14: SPOD: Case B: LPLHGO with observability defects avoidance. Figure (a) depicts the estimation error $\tilde{x} = x - \hat{x}$ in black, green and red respectively, figure (b) represents the states $x$ in solid while the estimated states in dotted black, green and red lines respectively. Figures (c) and (d) shows the activated fictitious outputs $y_f$ and $\tau$ in black and green lines respectively.

### 4.5.1 Observability Analysis for Multi-output Wake flow Model

**Proposition 34 (Observability of the system)** *Based on Theorem 15, system (4.82) is (differentially) observable on* $\mathcal{O}_\epsilon = \{x \in \mathcal{X} \subset \mathbb{R}^4 : x_1^2 + x_2^2 > \epsilon^2\}$ *for any* $\epsilon > 0$.

**Proof 20** *The observation set* $\mathcal{O}$ *is the smallest vector space that includes* $h_i$ *and is closed under the Lie derivative* $\mathcal{L}_f$, *and* $\mathrm{d}\mathcal{O}(x) = \{\mathrm{d}T(x), T \in \mathcal{O}\}$ *is the observability co-distribution at point* $x$, *where* d *denotes the differential. The system (4.82) is weakly observable if* $\dim \mathrm{d}\mathcal{O}(x) = 4$. *Computing the successive Lie derivatives using* $h^1(x) = x_1$ *and* $h^2(x) = x_2$ *yields*

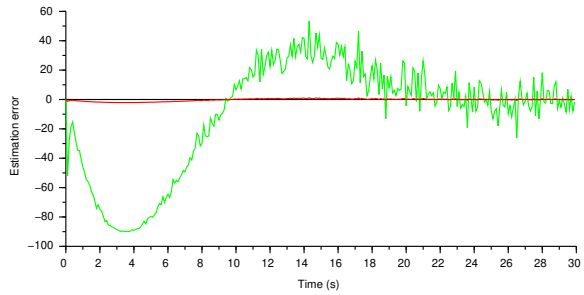


(a) HGO estimation error

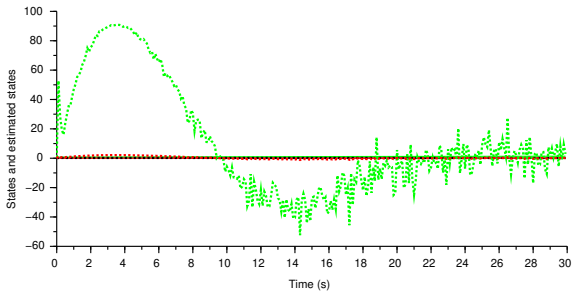


(b) HGO states and estimated states

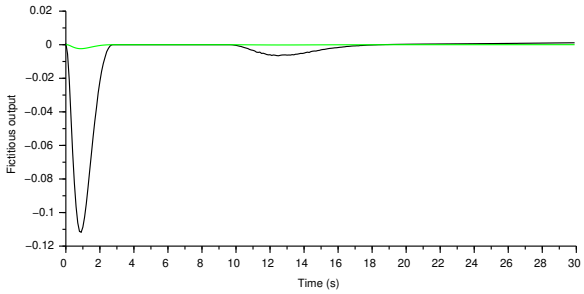


(c) HGO fictitious outputs $y_f$

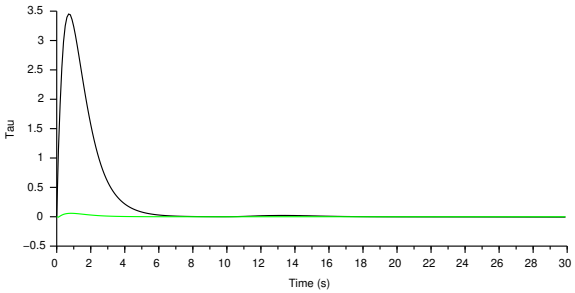


(d) HGO $\tau$ states

Figure 4.15: SPOD: Case C: HGO with observability defects avoidance and additional output noise. Figure (a) depicts the estimation error $\tilde{x} = x - \hat{x}$ in black, green and red respectively, figure (b) represents the states $x$ in solid while the estimated states in dotted black, green and red lines respectively. Figures (c) and (d) shows the activated fictitious outputs $y_f$ and $\tau$ in black and green lines respectively.

$$\begin{aligned}
\mathrm{d}\mathcal{L}_f^0 h^1(x)^T &= \begin{pmatrix} 1 \\ 0 \\ 0 \\ 0 \end{pmatrix}, \quad \mathrm{d}\mathcal{L}_f^1 h^1(x)^T = \begin{pmatrix} q_1 \\ -S_t \\ -\gamma x_1 \\ x_1 \end{pmatrix}, \quad \mathrm{d}\mathcal{L}_f^2 h^1(x)^T = \begin{pmatrix} a_{11} \\ b_{11} \\ c_{11} \\ d_{11} \end{pmatrix} \\
\mathrm{d}\mathcal{L}_f^0 h^2(x)^T &= \begin{pmatrix} 0 \\ 1 \\ 0 \\ 0 \end{pmatrix}, \quad \mathrm{d}\mathcal{L}_f^1 h^2(x)^T = \begin{pmatrix} S_t \\ q_1 \\ -\gamma x_2 \\ x_2 \end{pmatrix}, \quad \mathrm{d}\mathcal{L}_f^2 h^2(x)^T = \begin{pmatrix} a_{21} \\ b_{21} \\ c_{21} \\ d_{21} \end{pmatrix},
\end{aligned} \tag{4.83}$$

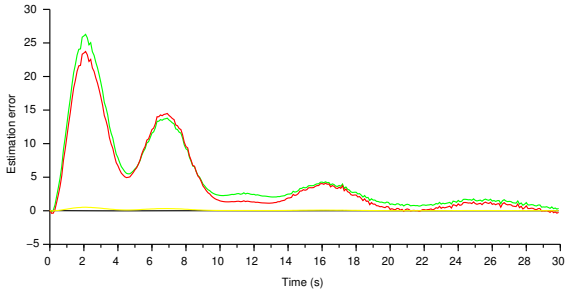


(a) LHGO estimation error

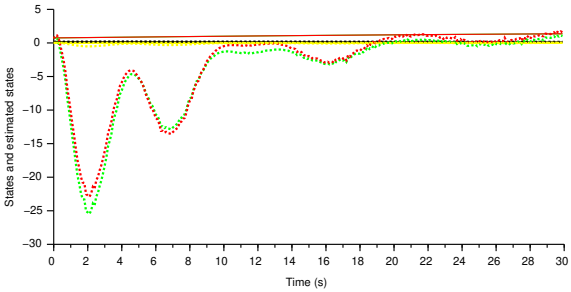


(b) LHGO states and estimated states

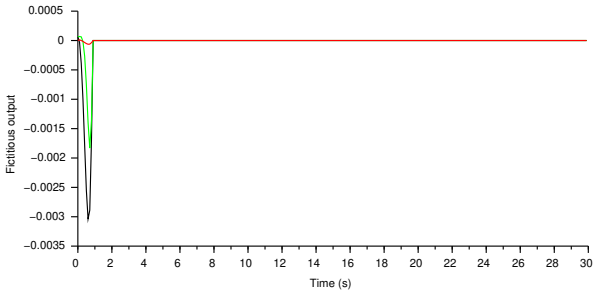


(c) LHGO fictitious outputs $y_f$

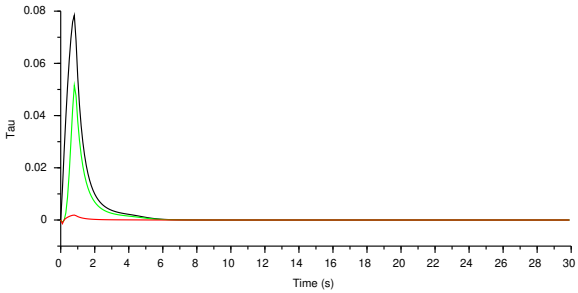


(d) LHGO $\tau$ states

Figure 4.16: SPOD: Case B: LHGO with observability defects avoidance and additional output noise. Figure (a) depicts the estimation error $\tilde{x} = x - \hat{x}$ in black, green, red and yellow respectively, figure (b) represents the states $x$ in solid while the estimated states $\hat{x}$ in dotted black, green, red and yellow respectively. Figures (c) and (d) shows the activated fictitious outputs $y_f$ and $\tau$ in black, green and red lines respectively.

*where* $q_1 = (x_4 - \gamma x_3)$ *and the expression for the* $\mathrm{d}L_f h^i(x)$ *components are given as:*

$$\begin{aligned} a_{11} &= -S_t^2 + \gamma\lambda x_3 + q_1^2 - \gamma\chi(3x_1^2 + x_2^2) & a_{21} &= 2S_t q_1 - 2\gamma\chi x_1 x_2 \\ b_{11} &= -2S_t q_1 - 2\gamma\chi x_1 x_2 & b_{21} &= -S_t^2 + \gamma\lambda x_3 + q_1^2 - \gamma\chi(x_1^2 + 3x_2^2) \\ c_{11} &= \gamma\lambda x_1 + 2S_t\gamma x_2 - 2\gamma x_1 q_1 & c_{21} &= \gamma\lambda x_2 - 2\gamma S_t x_1 - 2\gamma x_2 q_1 \\ d_{11} &= -2S_t x_2 + 2x_1 q_1 & d_{21} &= 2S_t x_1 + 2x_2 q_1. \end{aligned} \tag{4.84}$$

*Higher order differentiation will still lead to expressions where* $x_1, x_2$ *are a factor.*
*Due to the block triangular structure of* $\mathrm{d}\mathcal{O}(x)$, $\mathrm{d}\mathcal{O}(x)$ *is full column rank if and only if:*

$$\lambda^2\gamma^2(4S_t^2 + 1)(x_1^2 + x_2^2)^2 \neq 0. \tag{4.85}$$

*So it is straightforward that*

$$\dim \mathrm{d}\mathcal{O}(x) = 4, \quad \forall x \in \mathcal{O}_\epsilon. \tag{4.86}$$

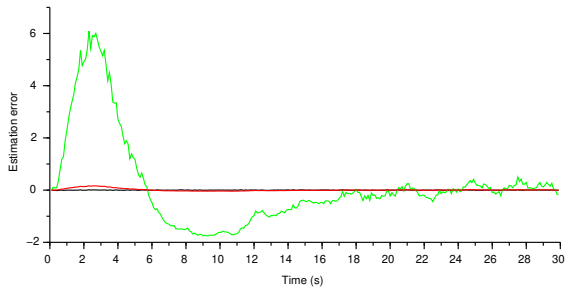


(a) LPLHGO estimation error

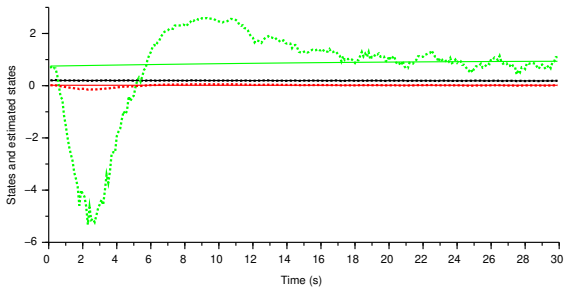


(b) LPLHGO states and estimated states

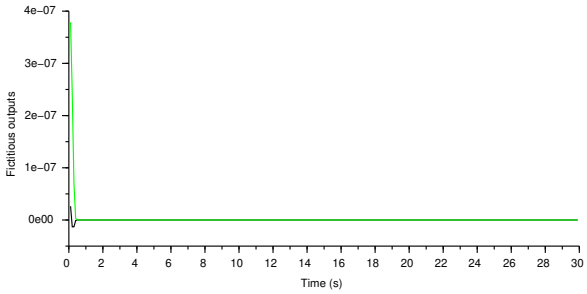


(c) LPLHGO fictitious outputs $y_f$

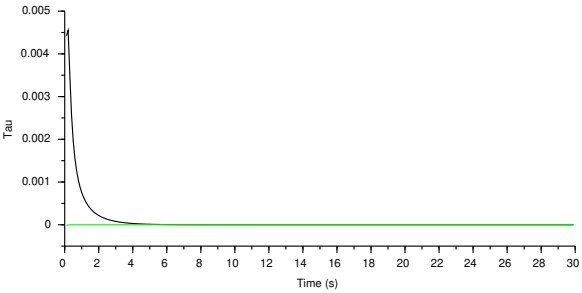


(d) LPLHGO $\tau$ states

Figure 4.17: SPOD: Case C: LPLHGO with observability defects avoidance and additional output noise. Figure (a) depicts the estimation error $\tilde{x} = x - \hat{x}$ in black, green and red respectively, figure (b) represents the states $x$ in solid while the estimated states in dotted black, green and red lines respectively. Figures (c) and (d) shows the activated fictitious outputs $y_f$ and $\tau$ in black and green lines respectively.

*However there is an observability singularity for* $x_s = (0\ 0\ x_3\ x_4)^T$ *since* $\dim\{\mathrm{d}\mathcal{O}\}(x_s) = 2$ *and* $x_3$ *nor* $x_4$ *can be recovered in this set.*

*The observability singularity set for the multi-output wake flow model is thus:*

$$\mathcal{S} = \{x \in \mathcal{X} \subset \mathbb{R}^4 : x_1^2 + x_2^2 = 0\}. \tag{4.87}$$

*For convenience, let define* $T$ *as in* (1.33) *to get the observable normal form (as previously done in Section 1.3.4) upto some permutation* $\bar{P}$ *to get:*

$$T : x \mapsto z = \bar{P} \begin{pmatrix} T^1 \\ T^2 \end{pmatrix}, \tag{4.88}$$

*where* $\bar{P} = (e_1, e_3, e_5, e_2, e_4, e_6)$ *with* $e_i$ *being the* $i$*th canonical vector of* $\mathbb{R}^6$*, so:*

$$z = \begin{pmatrix} z_1^1 \\ z_1^2 \\ z_2^1 \\ z_2^2 \\ z_3^1 \\ z_3^2 \end{pmatrix} = \begin{pmatrix} T_1^1 \\ T_1^2 \\ T_2^1 \\ T_2^2 \\ T_3^1 \\ T_3^2 \end{pmatrix}(x) = \begin{pmatrix} x_1 \\ x_2 \\ -S_t x_2 + x_1 q_1 \\ S_t x_1 + x_2 q_1 \\ -S_t^2 x_1 + x_1 q_1^2 - 2S_t x_2 q_1 + \gamma\lambda x_1 x_3 - \gamma\chi x_1(x_1^2 + x_2^2) \\ -S_t^2 x_2 + x_2 q_1^2 + 2S_t x_1 q_1 + \gamma\lambda x_2 x_3 - \gamma\chi x_2(x_1^2 + x_2^2) \end{pmatrix} \tag{4.89}$$

*For all* $x_a, x_b \in \mathcal{X}\backslash\mathcal{S}_\epsilon$ *where* $\mathcal{S}_\epsilon = \{x \in \mathcal{X} : x_1^2 + x_2^2 \leq \epsilon^2\}$*:*

$$T_a(x_a) = T_b(x_b) \Longrightarrow x_{ai} = x_{bi}, \quad \text{for any} \quad i \leq 2. \tag{4.90}$$

*Then, from* (4.89) *third and fourth equations, computing* $x_1 T_2^1 + x_2 T_2^2$ *using the fact that* $x_1^2 + x_2^2 \neq 0$ *on* $\mathcal{X}\backslash\mathcal{S}_\epsilon$*, it follows that:*

$$(x_1^2 + x_2^2)(q_{1a} - q_{1b}) = 0 \quad \text{so} \quad q_{1a} = q_{1b} \quad \text{on} \quad \mathcal{X}\backslash\mathcal{S}_\epsilon.$$

*Finally using* $q_{1a} = q_{1b}$ *in* (4.89) *two last equations to get* $(x_1 T_3^1 + x_2 T_3^2)$ *thus results in* $x_{ai} = x_{bi}$ *for* $i = 3, 4$ i. e. *in* $T$ *injectivity on* $\mathcal{X}\backslash\mathcal{S}_\epsilon$*. Since its Jacobian is full column rank from* (4.86)*, then system* (4.82) *is strongly differentially observable on* $\mathcal{X}\backslash\mathcal{S}_\epsilon$*.*

### 4.5.2 Nonlinear Observer Synthesis

Since the system suffers from observability defects at $x_1^2 + x_2^2 = 0$, HGO, LHGO and LPLHGO observers will be synthesized so as to ensure this singularity.

#### 4.5.2.1 HGO for Multi-output Wake Flow Model

Based on Theorem 9, we can design the high gain observer for the multi-output wake flow model given by (4.88).

**Proposition 35 (Standard HGO for multi-output wake flow model)** *The multi-output high gain observer for the system* (4.88) *is given as:*

$$\dot{\hat{z}}' = \mathcal{F}_z(\hat{z}', y) \tag{4.91}$$

*such that*

$$\mathcal{F}_z = A' z' + B' \varphi_s(z') + \Delta' K'(y - C' z'), \tag{4.92}$$

*where the observer state vector* $z' = \begin{pmatrix} z^1 & z^2 \end{pmatrix}^T$ *and the measured output* $y = \begin{pmatrix} y_1 & y_2 \end{pmatrix}^T$ *respectively and the matrices*

$$A' = \begin{pmatrix} A_3 & 0 \\ 0 & A_3 \end{pmatrix}, \quad B' = \begin{pmatrix} B_3 & 0 \\ 0 & B_3 \end{pmatrix}, \quad C' = \begin{pmatrix} C_3 & 0 \\ 0 & C_3 \end{pmatrix}, \tag{4.93}$$

*where* $A_i, B_i, C_i$ *are all in their prime form and* $\varphi'_s$ *is the saturated version of* $\varphi' = \begin{pmatrix} \varphi^1 \\ \varphi^2 \end{pmatrix} \in \mathbb{R}^2$ *where last components are given below:*

$$\begin{aligned}
\varphi^1 &= S_t^3 x_2 - \gamma\lambda^2 x_1 x_3 + \gamma\lambda\chi x_1(x_1^2 + x_2^2) + 2S_t\chi x_2(x_1^2 + x_2^2) + x_1 q_1^3 - 2\gamma\chi x_1 q_1(x_1^2 + x_2^2) \\
&= -3\gamma\chi x_1^3 q_1 + \gamma\chi S_t x_2^3 - 3S_t^2 x_1 q_1 - 3\gamma\lambda S_t x_2 x_3 + 3\gamma\lambda x_1 x_3 q_1 - 3S_t x_2 q_1^2 + \gamma\chi S_t x_1^2 x_2 - 3\gamma\chi x_1 x_2^2 q_1 \\
\varphi^2 &= -S_t^3 x_1 - \gamma\lambda^2 x_2 x_3 + \gamma\lambda\chi x_2(x_1^2 + x_2^2) - 2S_t\chi x_1(x_1^2 + x_2^2) + x_2 q_1^3 - 2\gamma\chi x_2 q_1(x_1^2 + x_2^2) \\
&= -3\gamma\chi x_2^3 q_1 - \gamma\chi S_t x_1^3 - 3S_t^2 x_2 q_1 + 3\gamma\lambda S_t x_1 x_3 + 3\gamma\lambda x_2 x_3 q_1 + 3S_t x_1 q_1^2 - \gamma\chi S_t x_1 x_2^2 - 3\gamma\chi x_1^2 x_2 q_1
\end{aligned} \tag{4.94}$$

$\Delta' = \begin{pmatrix} \Delta^1 & 0 \\ 0 & \Delta^2 \end{pmatrix}$ *with each* $\Delta^i$ *being a diagonal high gain matrix of dimension* 3 *and* $K' = (K^1 \;\; K^2)$ *is the observer gain matrix that is chosen to get* $(A' - K'C')$ *Hurwitz.*

Since the observer suffers from observability defects for $x_1^2 + x_2^2 = 0$, therefore we proceed towards building a singularity-free high gain observer for system (4.88).

**Proposition 36 (Singularity-free HGO for Multi-output wake flow model)** *Let*

$$\rho : x \mapsto max(0, \epsilon^2 - (x_1^2 + x_2^2))^2 \tag{4.95}$$

*for some* $\epsilon > 0$. *Consider the fictitious output* $y_f \in \mathbb{R}^2$ *such that:*

$$y_f(x) = \begin{pmatrix} \gamma\rho(x)x_3 \\ \rho(x)x_4 \end{pmatrix}. \tag{4.96}$$

*Extending the mapping* $T$ *defined by* (4.88) *as:*

$$T_e : \begin{array}{ccc} \mathbb{R}^4 & \to & \mathbb{R}^6 \times \mathbb{R}^2 \\ x & \mapsto & \begin{pmatrix} T(x) \\ y_f(x) \end{pmatrix}. \end{array} \tag{4.97}$$

*With notations and definitions of Proposition 35, let* $\tau \in \mathbb{R}^4$ *and define an augmented mapping* $T_a$ *as:*

$$T_a : \begin{array}{ccc} \mathbb{R}^8 & \to & \mathbb{R}^8 \\ x_a = \begin{pmatrix} x \\ \tau \end{pmatrix} & \mapsto & z_a = T_e(x) + \Psi(x)\tau, \end{array} \tag{4.98}$$

*where* $\Psi \in \mathcal{C}^1(\mathbb{R}^{n_x}, \mathbb{R}^{n_z - n_x})$ *is defined by*

$$\Psi : x \mapsto \begin{pmatrix} 0_2 & 0_2 \\ 0_2 & cI_2 \\ I_2 & 0_2 \\ J_\Psi & 0_2 \end{pmatrix}, \quad J_\Psi = \begin{pmatrix} -\frac{x_1}{\lambda} & -\frac{x_2}{\lambda} \\ \frac{x_2}{2S_t} - \frac{x_1}{\lambda} & -\frac{x_1}{2S_t} - \frac{x_2}{\lambda} \end{pmatrix}; \quad \lambda, c > 0. \tag{4.99}$$

*Then* $T_a$ *defines a global diffeomorphism on* $\mathbb{R}^8$.

*A singularity-free high gain observer for the multi-output wake flow model is given by:*

$$\dot{\hat{x}} = \left(\frac{\partial T_a}{\partial x_a}(x_a)\right)^{-1} \mathcal{F}(\hat{x}_a, y) \tag{4.100}$$

*with*

$$\mathcal{F}(\hat{x}_a, y) = \begin{pmatrix} \mathcal{F}_z(\hat{x}_a, y) \\ K_4 T_{a4}(\hat{x}_a) \end{pmatrix}, \tag{4.101}$$

*where* $K_4$ *and* $T_{a4}$ *represents the last four components of the observer gain and mapping* $T_a$ *respectively, associated with the fictitious outputs, and* $\mathcal{F}_z$ *given in Proposition 35.*

**Proof 21** *The Jacobian of the mapping* $T_e$ *defined by (4.97) is given by:*

$$\frac{\partial T_e}{\partial x}(x) = \begin{pmatrix} \frac{\partial T}{\partial x} \\ \frac{\partial y_f}{\partial x} \end{pmatrix} = \begin{pmatrix} I_2 & 0_2 \\ J_1 & J_2 \end{pmatrix} \tag{4.102}$$

*with matrices* $J_1, J_2$*:*

$$J_1 = \begin{pmatrix} q_1 & -S_t \\ S_t & q_1 \\ a_{11}(x) & b_{11}(x) \\ a_{21}(x) & b_{21}(x) \\ \gamma\rho_1 x_3 & \gamma\rho_2 x_3 \\ \rho_1 x_4 & \rho_2 x_4 \end{pmatrix}, \quad J_2 = \begin{pmatrix} -\gamma x_1 & x_1 \\ -\gamma x_2 & x_2 \\ c_{11}(x) & d_{11}(x) \\ c_{21}(x) & d_{21}(x) \\ \gamma\rho & 0 \\ 0 & \rho \end{pmatrix}, \tag{4.103}$$

*where the expression for the coefficients are given before in (4.84) and* $\rho_1, \rho_2$ *denote the partial derivatives of* $\rho$ *w.r.t* $x_1$ *and* $x_2$ *respectively,* i. e. $\rho_i = \frac{\partial \rho}{\partial x_i}(x)$.

*Due to the block triangular structure of the Jacobian (4.102), the* $T_e$ *Jacobian matrix is full rank provided that* $J_2$ *is also full rank. One has:*

$$\begin{vmatrix} c_{11} & d_{11} \\ c_{21} & d_{21} \end{vmatrix} = 2\gamma S_t \lambda (x_1^2 + x_2^2), \quad \text{and} \quad \begin{vmatrix} \gamma\rho & 0 \\ 0 & \rho \end{vmatrix} = \gamma\rho^2. \tag{4.104}$$

*Since by construction,* $\rho$ *and* $x_1^2 + x_2^2$ *cannot be null simultaneously, it follows that* $J_2$ *and in turn the jacobian of* $T_e$ *are full rank matrices for any* $x \in \mathbb{R}^4$. *However,* $T_e$ *is an immersion from*

$\mathbb{R}^4$ *to* $\mathbb{R}^6$*, therefore we extend it into a global diffeomorphism* $T_a$ *by augmenting the original state* $x$ *with* $\tau = \begin{pmatrix}\tau_1 & \tau_2 & \tau_3 & \tau_4\end{pmatrix}$.

*Using* (4.102), (4.103) *and* (4.99) *results in*

$$\left|\frac{\partial T_a}{\partial x_a}\right| = \gamma c^2(\rho^2 + (x_1^2 + x_2^2))^2 \neq 0, \quad \forall(\gamma, c > 0). \tag{4.105}$$

*So* $T_a$ *is a global diffeomorphism. The global injectivity proof is given as follows:*

$$T_a : \begin{pmatrix} x \\ \tau \end{pmatrix} \mapsto z_a = \begin{pmatrix} z \\ y_f \end{pmatrix} + \Psi(x_1, x_2)\tau = \begin{pmatrix} \begin{pmatrix} z_{11} \\ z_{21} \end{pmatrix} \\ \begin{pmatrix} z_{12} \\ z_{22} \end{pmatrix} \\ \begin{pmatrix} z_{13} \\ z_{23} \end{pmatrix} \\ \begin{pmatrix} \rho x_3 \\ \rho x_4 \end{pmatrix} \end{pmatrix} + \begin{pmatrix} 0_2 & 0_2 \\ 0_2 & I_2 \\ I_2 & 0_2 \\ -x_1 & -x_2 \quad 0_{1,2} \\ x_2 - x_1 & -x_1 - x_2 \quad 0_{1,2} \end{pmatrix} \begin{pmatrix} \tau_1 \\ \tau_2 \\ \tau_3 \\ \tau_4 \end{pmatrix}. \tag{4.106}$$

*Let* $T_a(x_a) = T_b(x_b)$ *where* $z_{ij}$ *is given by* (4.88)*, then denoting* $\tilde{q}_1 = q_{1a} - q_{1b}, \tilde{x}_i = x_{ai} - x_{bi}$ *and* $\tilde{\tau} = \tau_a - \tau_b$*, we get:*

$$\begin{cases} x_{1a} = x_{1b} & = x_1 \\ x_{2a} = x_{2b} & = x_2 \end{cases} \tag{4.107a}$$

$$\begin{cases} -S_t x_2 + x_1 q_{1a} + \tau_{3a} = -S_t x_2 + x_1 q_{1b} + \tau_{3b} \\ S_t x_1 + x_2 q_{1a} + \tau_{4a} = S_t x_1 + x_2 q_{1b} + \tau_{4b} \end{cases} \tag{4.107b}$$

$$\begin{cases} -2S_t x_2 \tilde{q}_1 + x_1(q_{1a}^2 - q_{1b}^2) + \gamma\lambda x_1 \tilde{x}_3 = -\tilde{\tau}_1 \\ 2S_t x_1 \tilde{q}_1 + x_2(q_{1a}^2 - q_{1b}^2) + \gamma\lambda x_2 \tilde{x}_3 = -\tilde{\tau}_2 \end{cases} \tag{4.107c}$$

$$\begin{cases} \rho\gamma\tilde{x}_3 = -\dfrac{x_1}{\lambda}\tilde{\tau}_1 - \dfrac{x_2}{\lambda}\tilde{\tau}_2 \\ \rho\tilde{x}_4 = \left(\dfrac{x_1}{\lambda} - \dfrac{x_2}{2S_t}\right)\tilde{\tau}_1 - \left(\dfrac{x_1}{2S_t} + \dfrac{x_2}{\lambda}\right)\tilde{\tau}_2 \end{cases} \tag{4.107d}$$

*From* (4.107b) *and* (4.107d)*, it is straightforward that:*

$$\begin{aligned} x_1\tilde{q}_1 &= -\tilde{\tau}_3 \\ x_2\tilde{q}_1 &= -\tilde{\tau}_4 \\ \rho\tilde{q}_1 &= -\frac{x_2}{2S_t}\tilde{\tau}_1 + \frac{x_1}{2S_t}\tilde{\tau}_2 \end{aligned} \tag{4.108}$$

*Further multiplying* (4.108) *by* $x_1, x_2$ *and* $\rho$ *respectively, one obtains:*

$$(\rho^2 + x_1^2 + x_2^2)\tilde{q}_1 = -x_1\tilde{\tau}_3 - x_2\tilde{\tau}_4 - \frac{\rho x_2}{2S_t}\tilde{\tau}_1 + \frac{\rho x_1}{2S_t}\tilde{\tau}_2 \tag{4.109}$$

*Multiplying the equations of* (4.107c) *by* $x_2$ *and* $x_1$ *respectively and subtracting the equations, we get:*

$$2S_t(x_1^2 + x_2^2)\tilde{q}_1 = -x_1\tilde{\tau}_2 + x_2\tilde{\tau}_1 \tag{4.110}$$

*Adding* $2S_t$ *times the last equation of* (4.108) *to* (4.110) *and simplifying yields:*

$$2S_t((x_1^2 + x_2^2) + \rho)\tilde{q}_1 = -x_1\tilde{\tau}_2 + x_2\tilde{\tau}_1 + x_1\tilde{\tau}_2 - x_2\tilde{\tau}_1 = 0, \tag{4.111}$$

*Since* $(x_1^2 + x_2^2) + \rho \neq 0, \forall x \in \mathbb{R}^4$, *it follows that* $\tilde{q}_1 = 0$, *so* $q_{1a}^2 - q_{1b}^2 = 0$. *One can then simplify* (4.108) *and obtain:*

$$\tilde{\tau}_3 = \tilde{\tau}_4 = 0. \tag{4.112}$$

*Using* (4.112), *equations* (4.107c) *and* (4.107d) *can be reduced to:*

$$\gamma\lambda x_1\tilde{x}_3 = \tilde{\tau}_1 \tag{4.113a}$$

$$\gamma\lambda x_2\tilde{x}_3 = \tilde{\tau}_2 \tag{4.113b}$$

$$\rho\gamma\tilde{x}_3 = -\frac{x_1}{\lambda}\tilde{\tau}_1 - \frac{x_2}{\lambda}\tilde{\tau}_2 \tag{4.113c}$$

$$\rho\tilde{x}_4 = \left(\frac{x_1}{\lambda} - \frac{x_2}{2S_t}\right)\tilde{\tau}_1 - \left(\frac{x_1}{2S_t} + \frac{x_2}{\lambda}\right)\tilde{\tau}_2 \tag{4.113d}$$

*Further multiplying the equations* (4.113a), (4.113b) *by* $x_1$ *and* $x_2$ *respectively and adding the resulting equations to* (4.113c), *we can get*

$$\lambda\gamma(\rho + x_1^2 + x_2^2)\tilde{x}_3 = x_1\tilde{\tau}_1 + x_2\tilde{\tau}_2 - x_1\tilde{\tau}_1 - x_2\tilde{\tau}_2 = 0 \Longrightarrow \tilde{x}_3 = 0. \tag{4.114}$$

*It follows that* $\tilde{\tau}_1 = \tilde{\tau}_2 = 0$ *and therefore* $\tilde{x}_4 = 0$. *Hence* $\bar{T}$ *is globally injective.*

*By continuity* $T_a^{-1}$ *is* $\mathcal{C}^1$, *hence it is L-Lipschitz on any compact of* $\mathbb{R}^8$. *It follows that, using* $z_a^* = T_a(x, 0) = T_e(x)$ *similar to the proof given before in the minimal model. Since* $T_e$ *is injective and defines a converging observer from Proposition 36, it follows that*

$$\lim_{t\to\infty} \|x(t) - \hat{x}(t)\| + \|\tau(t)\| = 0. \tag{4.115}$$

#### 4.5.2.2 LPLHGO for Multi-output Wake Flow Model

For the multi-output case, we directly synthesize the LPLHGO for it recovers the main advantages of the LHGO whilst also reducing the peaking.

**Proposition 37 (LPLHGO for multi-output wake flow model)** *The low peaking LHGO for the system* (4.88) *is given by:*

$$\begin{aligned} \dot{\hat{z}}' &= \mathcal{F}_z(\hat{z}', \eta, y) \\ \dot{\eta} &= \mathcal{F}_\eta(\hat{z}', \eta, y) \end{aligned} \tag{4.116}$$

*with*

$$\begin{aligned}
\dot{\hat{z}}_1^1 &= \eta_1^1 + \alpha_1\theta(y_1 - \hat{z}_1^1) & \dot{\hat{z}}_1^2 &= \eta_1^2 + \alpha_1\theta(y_2 - \hat{z}_1^2)\\
\dot{\hat{z}}_2^1 &= \eta_2^1 + \alpha_2\theta(sat_{r_2}(\eta_1^1) - \hat{z}_2^1) & \dot{\hat{z}}_2^2 &= \eta_2^2 + \alpha_2\theta(sat_{r_2}(\eta_1^2) - \hat{z}_2^2)\\
\dot{\hat{z}}_3^1 &= \phi_s^1(\hat{z}) + \alpha_3\theta(sat_{r_3}(\eta_2^1) - \hat{z}_3^1) & \dot{\hat{z}}_3^2 &= \phi_s^2(\hat{z}) + \alpha_3\theta(sat_{r_3}(\eta_2^2) - \hat{z}_3^2)\\
\dot{\eta}_1^1 &= sat_{r_3}(\eta_2^1) + \beta_1\theta^2(y_1 - \hat{z}_1^1) & \dot{\eta}_1^2 &= sat_{r_3}(\eta_2^2) + \beta_1\theta^2(y_2 - \hat{z}_1^2)\\
\dot{\eta}_2^1 &= \phi_s^1(\hat{z}) + \beta_2\theta^2(sat_{r_2}(\eta_1^1) - \hat{z}_2^1) & \dot{\eta}_2^2 &= \phi_s^2(\hat{z}) + \beta_2\theta^2(sat_{r_2}(\eta_1^2) - \hat{z}_2^2)
\end{aligned} \tag{4.117}$$

*where $\varphi_s'$ is the saturated version of $\varphi'$ and the expression for its last components $\varphi_s^i$ is given in (4.94) and the observer gains $\alpha_i, \beta_i$ are chosen so as to satisfy the strong stability requirements as discussed before in Theorem 12*

Since the system suffers from observability defects, therefore in the next Proposition we propose the singularity-free low peaking LHGO for the multi-output wake flow model.

**Proposition 38 (Singularity-free LPLHGO for multi-output wake flow model)** *To avoid singularity, we add the fictitious outputs $y_f$ given by (4.96) and the function $\rho$ is given by (4.95). Let $\tau \in \mathbb{R}^4$ and define an augmented mapping $T_a$ as (4.98) where $\Psi \in \mathcal{C}^1(\mathbb{R}^{n_x}, \mathbb{R}^{n_z - n_x})$ is defined by (4.99), so $T_a$ is a global diffeomorphism.*

*The dynamic system*

$$\begin{cases} \dot{\hat{x}}_a = \left(\dfrac{\partial T_a}{\partial x_a}(\hat{x}_a)\right)^{-1} \begin{pmatrix} \mathcal{F}_z(T_a(\hat{x}_a), \eta, y) \\ -K_4 T_4(\hat{x}_a) \end{pmatrix} \\ \dot{\eta} = \mathcal{F}_\eta(T_a(\hat{x}_a), \eta, y) \end{cases} \tag{4.118}$$

*is an arbitrarily fast converging observer for system (4.82) in its original coordinates on any bounded subset of $\mathbb{R}^{n_z+n_f}$. $\mathcal{F}_z, \mathcal{F}_\eta$ are defined in Proposition 37 and, $K_4$ is a positive definite diagonal matrix of dimension 4. The notation $T_{a4}$ stands for the last 4 components of $T_a$ representing the dynamics associated with the fictitious outputs.*

The proof for singularity-free LPLHGO is similar to the proof for Proposition 36 for singularity-free HGO for multi-output wake flow model and is therefore avoided here. With $c$ and $\lambda$ some positive gains, the jacobian of $T_a$ can be found out as:

$$\left|\frac{\partial T_a}{\partial x_a}\right| = \gamma c^2(\rho^2 + (x_1^2 + x_2^2))^2 \neq 0, \tag{4.119}$$

### 4.5.3 Simulation Results for Multi-output wake flow model

Based on the initial conditions and observer gains given in Table 4.5, simulations have been performed for the high gain observer and low peaking limited high gain observers in natural

| | |
|---|---|
| $x_0$ | $\begin{pmatrix} 0.1 & 0.1 & 0.1 & 0.164 \end{pmatrix}$ |
| $\hat{x}_0$ | $\begin{pmatrix} 0 & 0 & 0.2 & 0.2 \end{pmatrix}$ |
| $K_{HGO}$ | $\begin{pmatrix} 0.18 & 1.07 & 0.51 \end{pmatrix}^T$ |
| $K_{LPLHGO}$ | $\begin{pmatrix} \begin{pmatrix} \alpha_1 & \alpha_2 & \alpha_3 \end{pmatrix} \\ \begin{pmatrix} \beta_1 & \beta_2 \end{pmatrix} \end{pmatrix}^T = \begin{pmatrix} \begin{pmatrix} 1.8 & 1.8 & 1.8 \end{pmatrix} \\ \begin{pmatrix} 0.01 & 0.002 \end{pmatrix} \end{pmatrix}^T$ |
| $K_{n_f}$ | $10 I_2$ |
| $\theta_{HGO}$ | $5$ |
| $\theta_{LPLHGO}$ | $5$ |
| $\epsilon$ | $\sqrt{0.1}$ |

Table 4.5: Initial conditions and gains for the system and observers

coordinates proposed in Propositions 36 and 38 respectively. case A is the nominal one, where no observability defects nor any disturbance is considered; case B illustrates the handling of observability defects; robustness to output noise is then addressed in the last case C.

#### 4.5.3.1 Case A: Nominal Case

The initial conditions for both observers are chosen to be the same and fairly near the system's initial condition so one can expect the observer to stay away from $\mathcal{S}_\epsilon$. The behavior of both observers in terms of peaking is similar to what has been observed in the minimal and SPOD models. The high peaking effect in case of HGO accounts for the increasing high gain power as the dimension increases, whereas in the case of LPLHGO, the peaking is reduced to a significantly smaller values due to limited high gain and the presence of saturations in the cascaded structure of the observer. The convergence of the estimation errors for HGO and LPLHGO to zero for both observers is around 10–12 seconds, as can be seen in Figures 4.18(a) and 4.18(c) respectively.

#### 4.5.3.2 Case B: Observability Defects Avoidance

In the second case, both observers are initialized at zero as can be seen in Figures 4.19 and 4.20. Fictitious outputs are activated that leads to an increase in the peaking effect particularly for the HGO while for LPLHGO, the peaking is only slightly increased as depicted in Figures 4.19(c) and 4.20(c). The effect of these outputs vanishes when $|\hat{x}_1^2 + \hat{x}_2^2| > \epsilon^2$; then it follows that the last $\hat{z}_a$ state of the target system converges to zero, thus inducing the extra coordinates $\tau$ to be stabilized at the origin. Thence the standard HGO and LPLHGO observers estimation errors converge asymptotically to zero as illustrated by Figures 4.19(a) and 4.20(a).

#### 4.5.3.3 Case C: Output Noise

In the last case, a measurement noise is added to the dynamics of the observer to investigate the effect of turbulence due to high frequency noises. The noise is chosen to be white gaussian noise with variance equal to 1 and a high pass filter with cutoff frequency chosen to be 1000 Hz. The simulations results from Figures 4.21(a) and 4.22(a), illustrates that only practical stability can be achieved for HGO and LPLHGO. In the case of LPLHGO, the noise induced errors are one order of magnitude smaller, thus proving better suited for fluid mechanics applications.

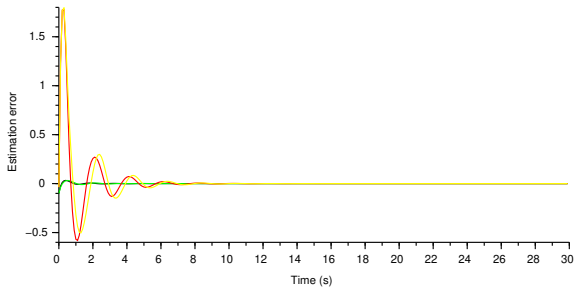


(a) HGO estimation error

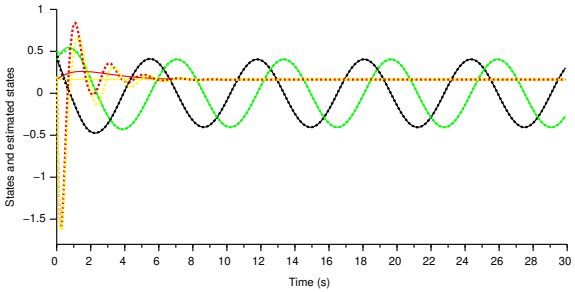


(b) HGO states and estimated states

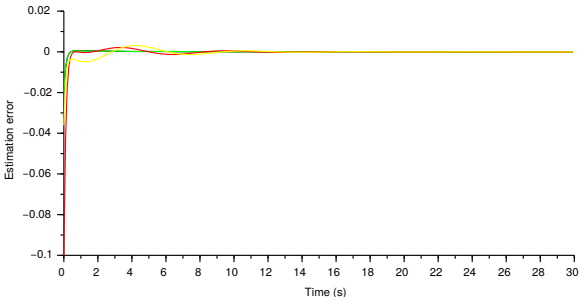


(c) LPLHGO estimation error

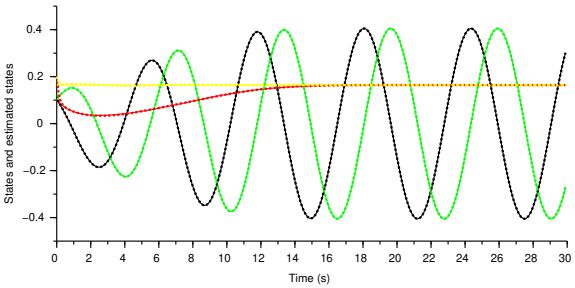


(d) LPLHGO states and estimated states

Figure 4.18: Multi-output: Case A from (a) to (d): simulation in nominal case. Figures (a) and (c) depicts the estimation error $\tilde{x}_1, \tilde{x}_2, \tilde{x}_3, \tilde{x}_4$ by black, green, red and yellow lines for HGO and LPLHGO respectively. Figures (b) and (d) represents the states and estimated states, such that states $x \in \mathbb{R}^4$ are in solid while the estimated states $\hat{x} \in \mathbb{R}^4$ are in dashed black, green, red and yellow lines respectively for HGO and LPLHGO.

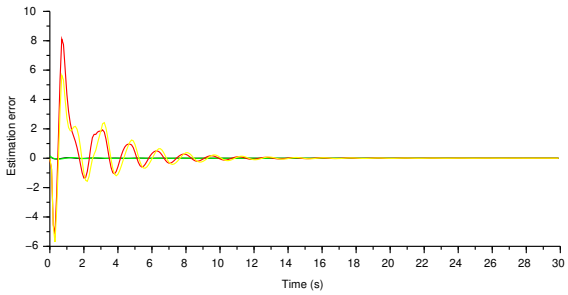


(a) HGO estimation error

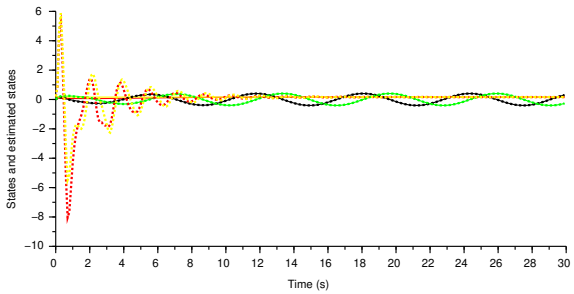


(b) HGO states and estimated states

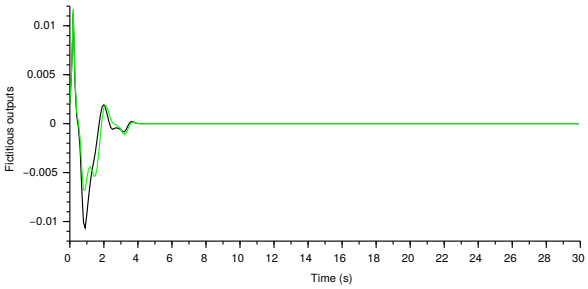


(c) HGO fictitious outputs $y_f$

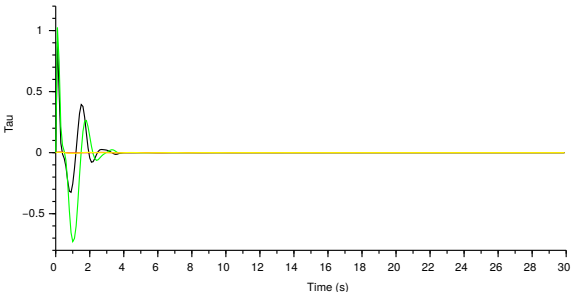


(d) HGO $\tau$ states

Figure 4.19: Multi-output: Case B: HGO with observability defects avoidance: Figure (a) depicts the estimation error $\tilde{x} = x - \hat{x}$ in black, green, red and yellow respectively, figure (b) represents the states $x$ in solid while the estimated states in dotted black, green, red and yellow lines respectively. The last two figures (c) and (d) represents the activated fictitious outputs in black, green lines and $\tau$ states in black, green, red and yellow lines respectively.

## 4.6 Hybrid Model

A more refined Galerkin representation including higher damped ($\mu' > 0$) modes $(a_{m3}, a_{m4})$ interacting with the first two ones through the shift mode is considered in this section. The model is refered to as a hybrid model Noack et al. [2003]; Luchtenburg et al. [2009] between the empirical Galerkin model (4.3) and higher dimensional invariant-manifold model. It is expected to be more precise as it captures more energy of the system, and also explain the emergence of other structures (hence the second mode $(a_{m3}, a_{m4})$) when killing the first one. The hybrid model behaves as a double oscillator, where one mode dies and the other one rises. The new

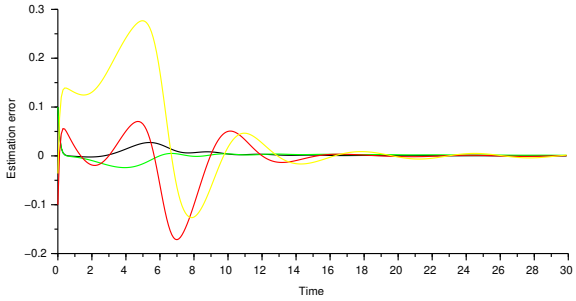


(a) LPLHGO estimation error

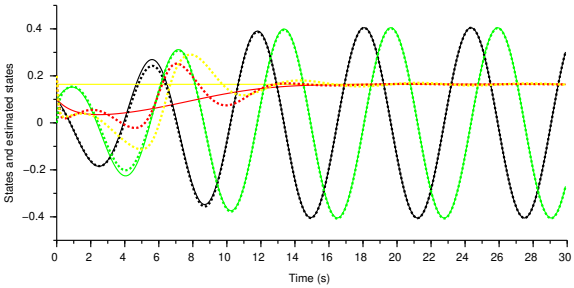


(b) LPLHGO states and estimated states

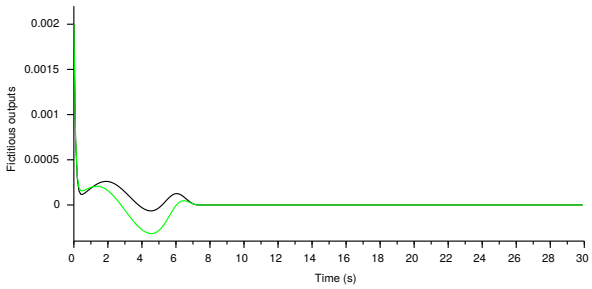


(c) LPLHGO fictitious outputs $y_f$

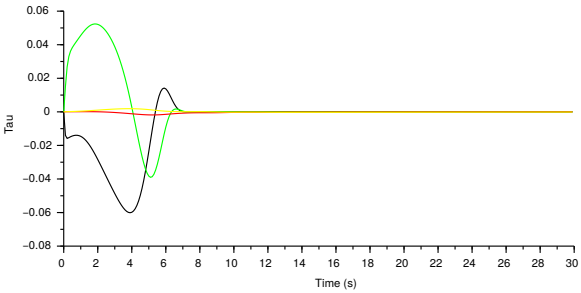


(d) LPLHGO $\tau$ states

Figure 4.20: Multi-output: Case B: LPLHGO with observability defects avoidance: Figure (a) depicts the estimation error $\tilde{x} = x - \hat{x}$ in black, green, red and yellow respectively, figure (b) represents the states $x$ in solid while the estimated states in dotted black, green, red and yellow lines respectively. The last two figures (c) and (d) represents the activated fictitious outputs in black, green lines and $\tau$ states in black, green, red and yellow lines respectively.

system can be written as:

$$\begin{pmatrix} \dot{a}_{m1} \\ a_{m2} \\ a_{m3} \\ a_{m4} \\ a_\Delta \\ \mu \end{pmatrix} = \begin{pmatrix} (\mu - a_\Delta)a_1 - a_2 \\ (\mu - a_\Delta)a_2 + a_1 \\ (-\mu' - a_\Delta)a_3 - a_4 \\ (-\mu' - a_\Delta)a_4 + a_3 \\ a_1^2 + a_2^2 + a_3^2 + a_4^2 - a_\Delta \\ 0 \end{pmatrix} \tag{4.120}$$

Considering the oscillation amplitudes $A_i = a_{2i-1}^2 + a_{2i}^2$, the above model becomes a system of order 4, thereby using the state vector $x_{hyb} = \begin{pmatrix} A_1 & A_2 & a_\Delta & \mu \end{pmatrix} \in \mathcal{X} \subset \mathbb{R}^4$, system (4.120) becomes

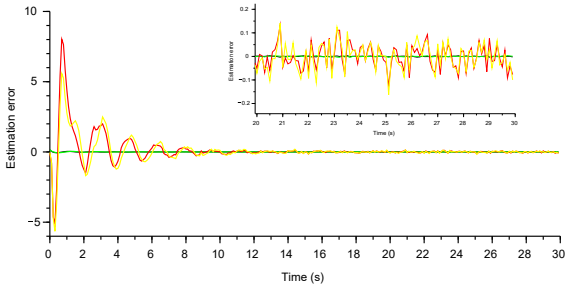


(a) HGO estimation error

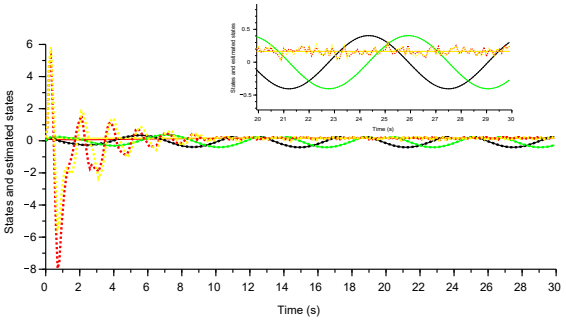


(b) HGO states and estimated states

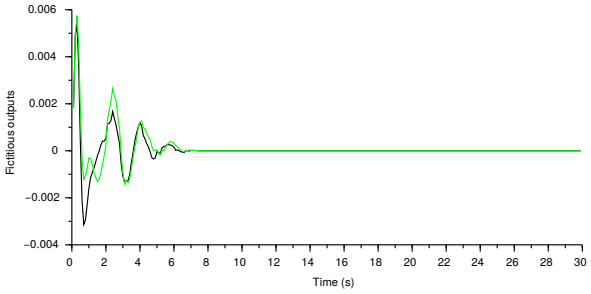


(c) HGO fictitious outputs $y_f$

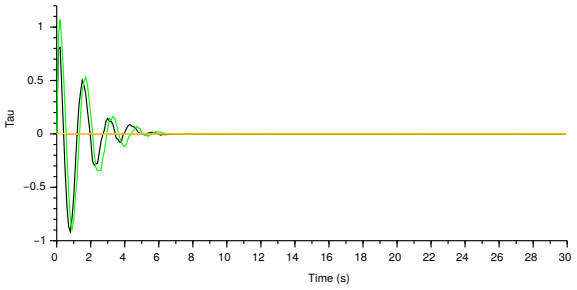


(d) HGO $\tau$ states

Figure 4.21: Multi-output: Case C: HGO with observability defects avoidance and output noise: Figure (a) depicts the estimation error $\tilde{x} = x - \hat{x}$ in black, green, red and yellow respectively, figure (b) represents the states $x$ in solid while the estimated states in dotted black, green, red and yellow lines respectively. The last two figures (c) and (d) represents the activated fictitious outputs in black, green lines and $\tau$ states in black, green, red and yellow lines respectively.

$$\dot{x}_{hyb} = f(x) = \begin{pmatrix} 2x_1(x_4 - x_3) \\ 2x_2(-\mu' - x_3) \\ x_1 + x_2 - x_3 \\ 0 \end{pmatrix}, \quad y = x_1. \tag{4.121}$$

### 4.6.1 Observability Analysis

A first prerequisite is to study the conditions guaranteeing the observability of the sytem.

**Proposition 39 (Observability of hybrid model)** *System given by (4.121) is observable on any connected subset of* $\mathcal{O}_\epsilon = \{x \in \mathcal{X} \subset \mathbb{R}^4 : |x_1| > \epsilon, |x_2 + x_3 + \mu'| > \epsilon'\}$ *for any* $\epsilon, \epsilon' > 0$, *respectively.*

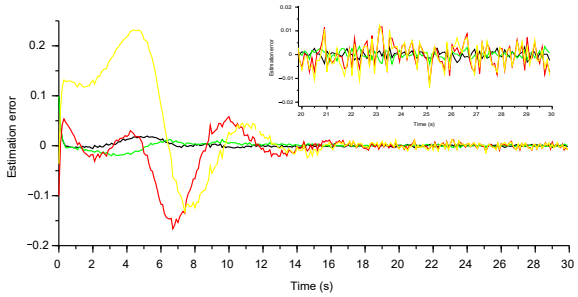


(a) LPLHGO estimation error

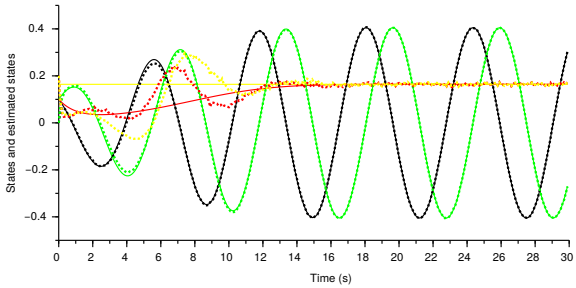


(b) LPLHGO states and estimated states

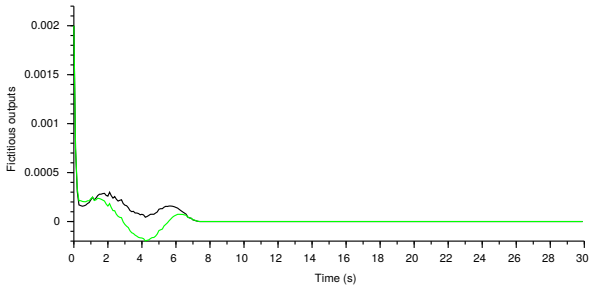


(c) LPLHGO fictitious outputs $y_f$

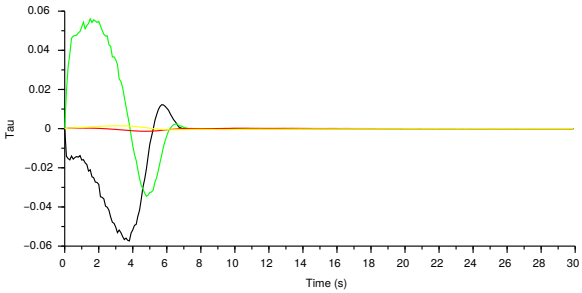


(d) LPLHGO $\tau$ states

Figure 4.22: Multi-output: Case C: LPLHGO with observability defects avoidance and output noise: Figure (a) depicts the estimation error $\tilde{x} = x - \hat{x}$ in black, green, red and yellow respectively, figure (b) represents the states $x$ in solid while the estimated states in dotted black, green, red and yellow lines respectively. The last two figures (c) and (d) represents the activated fictitious outputs in black, green lines and $\tau$ states in black, green, red and yellow lines respectively.

**Proof 22** *Let $\mathcal{O}$ denote the smallest vector space containing $h$ and closed under the Lie derivative $\mathcal{L}_f$. A system is said weakly observable if $\dim \mathrm{d}\mathcal{O}(x) = \dim \mathcal{X}$ where $\mathrm{d}\mathcal{O} = \{\mathrm{d}T, T \in \mathcal{O}\}$ is the observability co-distribution.*

*Computing the differentials of the successive Lie derivatives of the output $y = h(x)$ along the system vector field $f$ leads to the observability co-distribution $\mathrm{d}\mathcal{O}_{hyb}$ for system (4.121), whose determinant is:*

$$|\mathrm{d}\mathcal{O}_{hyb}| = -16x_1^3(x_2 + x_3 + \mu'). \tag{4.122}$$

In particular, an observability singularity appears in particular when $x_1 = 0$, whereas the control aims at forcing the oscillation amplitude to zero. The designed observer should be able to handle this singularity in order to synthesize control laws based on the estimated states.

### 4.6.2 Nonlinear Observer Synthesis

We begin by designing a high gain observer given by Theorem 8 for the hybrid system given by (4.121). But before designing we need to transform the system (4.121) into observable normal form, such that using $z = T(x)$ we obtain:

$$z = \begin{pmatrix} x_1 \\ 2x_1(x_4 - x_3) \\ 4x_1(x_4 - x_3)^2 - 2x_1(x_1 + x_2 - x_3) \\ 2x_1 \begin{pmatrix} 4(x_4 - x_3)^3 + (x_1 + x_2 - x_3) - 2x_2(-\mu' - x_3) \\ -2(x_4 - x_3)(4x_1 + 3x_2 - 3x_3) \end{pmatrix} \end{pmatrix}. \tag{4.123}$$

#### 4.6.2.1 HGO for Hybrid Model

Based on Theorem 8, we design a HGO for the system given by (4.123)

**Proposition 40 (HGO for hybrid systems)** *The standard high gain observer for the system in target coordinates (4.123) is given by:*

$$\dot{\hat{z}} = A_{n_z} z + B_{n_z} \varphi(\hat{z}) + \Delta K(y - C_{n_z} x), \tag{4.124}$$

*where $z \in \mathcal{Z} \subset \mathbb{R}^4$ and $\Delta$ is the diagonal matrix of dimension 4, and the observer gain matrix $K = \begin{pmatrix} k_1 & k_2 & k_3 & k_4 \end{pmatrix}^T$ is chosen so as to get $A_{n_z} - KC_{n_z}$ Hurwitz.*

The jacobian of the mapping $T$ is given as:

$$\frac{\partial T}{\partial x}(x) = \begin{pmatrix} 1 & 0_{1,q-1} \\ * & J \end{pmatrix} \tag{4.125}$$

with

$$J = 2x_1 \begin{pmatrix} 0 & -1 & 1 \\ -1 & 1 - 4q_1 & 4q_1 \\ q_2 & q_3 & q_4 \end{pmatrix}, \tag{4.126}$$

where

$$\begin{aligned} q_1 &= x_4 - x_3 \\ q_2 &= 1 - 6q_1 + 2(\mu' + x_3) \\ q_3 &= 12q_1^2 - 8x_1 - 6x_2 + 6x_3 \\ q_4 &= -12q_1^2 + 6q_1 + 8x_1 + 8x_2 - 6x_3 - 1 \end{aligned} \tag{4.127}$$

and the determinant is given by

$$\left| \frac{\partial T}{\partial x} \right| (x) = -16x_1^3(x_2 + x_3 + \mu'). \tag{4.128}$$

$T$ is diffeomorphism on $\mathcal{O}_\epsilon = \{x \in \mathbb{R}^4 : |x_1| > \epsilon, |x_2 + x_3 + \mu'| > \epsilon'\}$.

In order to avoid the observability defects and to achieve global diffeomorphism, we build a singularity-free high gain observer in the next Proposition.

**Proposition 41 (Singularity-free HGO for hybrid model)** *Let $\rho$ be defined as in (4.16) and $F : d + F'(d) \neq 0, \forall d$ where $d = x_2 + x_3 + \mu'$. For system (4.123), consider the fictitious outputs:*

$$y_f = \begin{pmatrix} \rho(x_1)d^2 \\ \rho(x_1)(x_3 - x_2) \\ \rho(x_1)(x_4 - x_3) \\ F(d) \end{pmatrix}. \tag{4.129}$$

*We define the two new state vectors $x_a$ and $z_a$ such as:*

$$x_a = \begin{pmatrix} x \\ \tau \end{pmatrix}, \quad \text{and} \quad z_a = T_a(x_a) = \begin{pmatrix} z \\ y_f \end{pmatrix} + \Psi(x)\tau, \tag{4.130}$$

*where $z$ is given by (4.123) and $\tau \in \mathbb{R}^4$ are the exogenous variables added to the state vector $x$ and completion by $\Psi \in \mathbb{R}^{8\times 4}$:*

$$\Psi(x) = \begin{pmatrix} 0 & 0 & 0 & 0 \\ 0 & 1 & -1 & 0 \\ 1 & 0 & -1 & 0 \\ 0 & 0 & -1 & -2x_1 \\ x_1 & 0 & 0 & -2\rho \\ -x_1 & x_1 & 0 & 0 \\ 0 & -x_1 & x_1 & 0 \\ 0 & 0 & 0 & 1 \end{pmatrix}. \tag{4.131}$$

*Then $T_a$ defines a global diffeomorphism.*

*A singularity-free high gain observer for the hybrid model is given by:*

$$\dot{\hat{x}} = \left(\frac{\partial T_a}{\partial x_a}(x_a)\right)^{-1} \mathcal{F}(\hat{x}_a, y) \tag{4.132}$$

*with $\mathcal{F}_z$ given in Proposition 40 and*

$$\mathcal{F}(\hat{x}_a, y) = \begin{pmatrix} \mathcal{F}_z(\hat{x}_a, y) \\ K_4 T_{a4}(\hat{x}_a) \end{pmatrix}, \tag{4.133}$$

*where $K_4$ and $T_{a4}$ represent the last four components of the observer gain and mapping $T_a$ respectively, associated with the fictitious outputs.*

**Proof 23** *Defining a new mapping $T_e : x \mapsto (z, y_f)$, whose jacobian matrix is*

$$\frac{\partial T_e}{\partial x}(x) = \begin{pmatrix} 1 & 0 & 0 & 0 \\ * & & J & \\ \rho' d^2 & 2d\rho & 2d\rho & 0 \\ \rho'(x_3 - x_2) & -\rho & \rho & 0 \\ \rho'(x_4 - x_3) & 0 & -\rho & \rho \\ 0 & F' & F' & 0 \end{pmatrix}, \tag{4.134}$$

*where $\rho'_i$ denote the partial derivative of $\rho$ with respect to $x_i$, i.e. $\rho'_i = \frac{\partial \rho'}{\partial x_i}(x)$.*

*Since the mapping $T_e$ is an immersion from $\mathbb{R}^4$ in $\mathbb{R}^8$, a way to get a one-to-one mapping is to extend it into a global diffeomorphism $T_a$.*

*The determinant of the new mapping $T_a$ comes out to be:*

$$\left| \frac{\partial T_a}{\partial x_a}(x_a) \right| = -4(\rho + x_1^2)(\rho + 2x_1^2)^2(d + F'), \tag{4.135}$$

*where $F : d + F' \neq 0$, so $T_a$ is a global diffeomorphism.*

*Now we present the proof of injectivity, where from proposition 41, $T_a$ is given as:*

$$T_a : \begin{pmatrix} x \\ \tau \end{pmatrix} \mapsto z_a = \begin{pmatrix} z \\ y_f \end{pmatrix} + \Psi(x_1)\tau = \begin{pmatrix} z_1 \\ z_2 \\ z_3 \\ z_4 \\ \rho(x_1)d^2 \\ \rho(x_1)(x_3 - x_2) \\ \rho(x_1)(x_4 - x_3) \\ F(d) \end{pmatrix} + \Psi(x) \begin{pmatrix} \tau_1 \\ \tau_2 \\ \tau_3 \\ \tau_4 \end{pmatrix} \tag{4.136}$$

*with $\Psi$ given by (4.131).*

*Let $T_a(x_a) = T_b(x_b)$ and denoting $\tilde{x}_i = x_{ia} - x_{ib}$, $\tilde{q}_1 = q_{1a} - q_{1b}$ and $\tilde{\tau}_i = \tau_{ia} - \tau_{ib}$, we get:*

$$x_{1a} = x_{1b} = x_1 \tag{4.137a}$$

$$2x_1\tilde{q}_1 + \tilde{\tau}_2 - \tilde{\tau}_3 = 0 \tag{4.137b}$$

$$4x_1\tilde{q}_1^2 - 2x_1(\tilde{x}_2 - \tilde{x}_3) + \tilde{\tau}_1 - \tilde{\tau}_3 = 0 \tag{4.137c}$$

$$2x_1[4\tilde{q_1}^3 + \tilde{x}_2 - \tilde{x}_3 + 2\mu'\tilde{x}_2 + 2(x_{2a}x_{3a} - x_2x_3) - 2\tilde{q}_1(4x_1) - 6q_{1a}(x_{2a} - x_{3a}) + 6q_{1b}(x_{2b} - x_{3b}) - \tilde{\tau}_4] - \tilde{\tau}_3 = 0 \tag{4.137d}$$

$$\rho(\tilde{d^2}) + x_1\tilde{\tau}_1 - 2\rho\tilde{\tau}_4 = 0 \tag{4.137e}$$

$$\rho(\tilde{x}_3 - \tilde{x}_2) - x_1\tilde{\tau}_1 + x_1\tilde{\tau}_2 = 0 \tag{4.137f}$$

$$\rho(\tilde{x}_4 - \tilde{x}_3) - x_1\tilde{\tau}_2 + x_1\tilde{\tau}_3 = 0 \tag{4.137g}$$

$$F(d_a) - F(d) + \tilde{\tau}_4 = 0 \tag{4.137h}$$

*Multiplying* (4.137b) *by* $x_1$ *and adding to* (4.137g)*:*

$$(2x_1^2 + \rho)\tilde{q}_1 = 0 \Rightarrow \tilde{x}_3 = \tilde{x}_4 \tag{4.138}$$

*Equations* (4.137b) *and* (4.137c) *are reduced to*

$$\begin{aligned} \tilde{\tau}_2 = \tilde{\tau}_3, \;\; i.e., \;\; \tilde{q}_1 = 0 \Rightarrow q_{1a} = q_{1b} \\ -2x_1(\tilde{x}_2 - \tilde{x}_3) + \tilde{\tau}_1 - \tilde{\tau}_3 = 0 \end{aligned} \tag{4.139}$$

*Now multiplying* (4.139) *by* $x_1$ *and adding to* (4.137f)*, we get:*

$$(2x_1^2 + \rho)(\tilde{x}_3 - \tilde{x}_2) = 0 \Rightarrow \tilde{x}_2 = \tilde{x}_3 = \tilde{x}_4 \;\; and \;\; \tilde{\tau}_1 = \tilde{\tau}_2 = \tilde{\tau}_3 \tag{4.140}$$

*and we are left with*

$$2x_1(2\mu'\tilde{x}_2 + 2(x_{2a}x_{3a} - x_{2b}x_{3b}) - \tilde{\tau}_4) - \tilde{\tau}_3 = 0 \tag{4.141a}$$

$$\rho(d_a^2 - d_b^2) + x_1\tilde{\tau}_1 - 2\rho\tilde{\tau}_4 = 0 \tag{4.141b}$$

*Simplifying the expressions, we can get:*

$$\begin{aligned} d_a^2 - d_b^2 = (d_a - d_b)(d_a + d_b) &= 2\tilde{x}_2(x_{2a} + x_{2b} + x_{3a} + x_{3b} + 2\mu') \\ &= 2\tilde{x}_2(2(x_2 + x_{3a} + \mu')) \\ &= 4\tilde{x}_2(x_2 + x_{3a} + \mu') \\ 2\mu'\tilde{x}_2 + 2(x_{2a}x_{3a} - x_{2b}x_{3b}) &= 2\tilde{x}_2(x_2 + x_{3a} + \mu') \end{aligned} \tag{4.142}$$

*Multiplying* (4.137d) *by* $x_1$ *and adding to* (4.137e)*:*

$$\begin{aligned} 4(x_1^2 + \rho)\tilde{x}_2(x_2 + x_{3a} + \mu') - 2(x_1^2 + \rho)\tilde{\tau}_4 = 0 \\ i.e., \;\; 2(x_1^2 + \rho)(-\tilde{\tau}_4 + 2\tilde{x}_2(x_2 + x_{3a} + \mu')) = 0 \\ further\ reduced\ to \quad 2(x_1^2 + \rho)(-\tilde{\tau}_4 + \frac{1}{2}(d_a^2 - d_b^2)) = 0 \end{aligned} \tag{4.143}$$

*Using* (4.137h) *in* (4.143)*:*

$$2(x_1^2 + \rho)(F(d_a) - F(d_b) + \frac{1}{2}(d_a^2 - d_b^2)) = 0 \tag{4.144}$$

*yet since* $F : d + \frac{\partial F}{\partial d} > 0$ *for instance, its antiderivative is strictly increasing so*

$$\left[\frac{d^2}{2} + F + k\right]_{d_a}^{d_b} = F(d_a) - F(d_b) + \frac{1}{2}d_a^2 - \frac{1}{2}d_b^2 = 0 \Rightarrow d_a = d_b \;\; i.e., \tilde{d} = 0 \tag{4.145}$$

*yet* $\tilde{d} = \tilde{x}_2 + \tilde{x}_3$*, so together with* $\tilde{x}_2 = \tilde{x}_3$*, we get* $\tilde{x}_2 = 0$*. Similarly from* (4.138) *we have* $\tilde{x}_3 = \tilde{x}_4 \Rightarrow \tilde{x}_3 = \tilde{x}_4 = 0$*. Therefore* $T_a$ *is injective.*

#### 4.6.2.2 LHGO for Hybrid Model

Based on Theorem 11, we can synthesize the limited high gain observer for the minimal system given by (4.121).

**Proposition 42 (LHGO for hybrid model)** *The Limited high gain observer for the system (4.123) is given as:*

$$\dot{\zeta} = \mathcal{F}_\zeta(\zeta, \hat{x}, y) = \begin{pmatrix} \zeta_{12} + \theta k_{11}(y - \zeta_{11}) \\ \zeta_{22} + \theta^2 k_{21}(y - \zeta_{11}) \\ \zeta_{22} + \theta k_{12}(\zeta_{12} - \zeta_{21}) \\ \zeta_{32} + \theta^2 k_{22}(\zeta_{12} - \zeta_{21}) \\ \zeta_{32} + \theta k_{31}(\zeta_{22} - \zeta_{31}) \\ \varphi_{4s} + \theta^2 k_{32}(\zeta_{22} - \zeta_{31}) \end{pmatrix} \tag{4.146}$$

*and we can therefore get the LHGO in target coordinates using either $\hat{z} = P\zeta$ or $z' = P'\zeta'$. Based on Proposition 2, we can get the observer in original coordinates since we can use either $\hat{x} = P\hat{x}$ or $\hat{x}' = P'\hat{x}'$.*

Following the augmentation given before for minimal system, we get the following Proposition:

**Proposition 43** *For the hybrid system, defining the original coordinate augmented state $\bar{x}$ and $\bar{T} : \bar{x} = \begin{pmatrix} x_1 & x_2 & x_2' & x_3 & x_3' & x_4 \end{pmatrix}^T$ as*

$$\bar{x} = \begin{pmatrix} x_1 \\ 2x_1(x_4 - x_3) \\ 2x_1(x_4 - x_3') \\ 4x_1(x_4 - x_3)^2 - 2x_1(x_1 + x_2 - x_3) \\ 4x_1(x_4 - x_3)^2 - 2x_1(x_1 + x_2' - x_3) \\ 2x_1 \begin{pmatrix} 4(x_4 - x_3)^3 + (x_1 + x_2 - x_3) - 2x_2(-\mu' - x_3) \\ -2(x_4 - x_3)(4x_1 + 3x_2 - 3x_3) \end{pmatrix} \end{pmatrix}. \tag{4.147}$$

*$\bar{T}$ is a diffeomorphism on $\bar{\mathcal{O}}_\epsilon = \{\bar{x} \in \mathbb{R}^6 : |x_1| > \epsilon, |x_2 + x_3 + \mu'| > \epsilon'\}$.*

**Proof 24** *The jacobian of the mapping $\bar{T}$ is given as:*

$$\frac{\partial \bar{T}}{\partial \bar{x}}(\bar{x}) = \begin{pmatrix} 1 & 0_{1,n_\zeta - 1} \\ * & J \end{pmatrix} \tag{4.148}$$

*with*

$$J = 2x_1 \begin{pmatrix} 0 & 0 & -1 & 0 & 1 \\ 0 & 0 & 0 & -1 & 1 \\ -1 & 0 & 1 - 4q_1 & 0 & 4q_1 \\ 0 & -1 & 1 - 4q_1 & 0 & 4q_1 \\ q_2 & 0 & q_3 & 0 & q_4 \end{pmatrix}, \tag{4.149}$$

*where* $q_1 = x_4 - x_3$, $q_2 = 1 - 6q_1 + 2(\mu' + x_3)$, $q_3 = 12q_1^2 - 8x_1 - 6x_2 + 6x_3$ *and* $q_4 = -12q_1^2 + 6q_1 + 8x_1 + 8x_2 - 6x_3 - 1$. *The determinant is given by*

$$\left|\frac{\partial \bar{T}}{\partial \bar{x}}(\bar{x})\right| = -16x_1^3(x_2 + x_3 + \mu'),$$

*so* $\bar{T}$ *is a diffeomorphism on* $\bar{\mathcal{O}}_\epsilon$.

To avoid the observability defects pinpointed in Proposition 39, we add some fictitious outputs aiming at getting information around the singularity.

**Proposition 44 (Singularity-free LHGO for hybrid model)** *For system (4.68), defining an augmented state vector* $x_a$ *and mapping* $T_a$ *as:*

$$x_a = \begin{pmatrix} \bar{x} \\ \tau \end{pmatrix} \quad \text{and} \quad z_a = T_a(x_a) = \begin{pmatrix} \bar{z} \\ y_f \end{pmatrix} + \Psi(\bar{x})\tau \tag{4.150}$$

*with the fictitious outputs given as:*

$$y_f = \begin{pmatrix} \rho(x_1)x_2 \\ \rho(x_1)x_2' \\ \vdots \\ \rho(x_1)x_4 \\ F(d) \end{pmatrix}, \tag{4.151}$$

*where* $\rho$ *and* $F$ *are given in Proposition 41.* $\tau \in \mathbb{R}^6$ *are the exogenous variables added to the augmented state vector* $\bar{x}$ *and*

$$\Psi(\bar{x}) = \begin{pmatrix} 0_{1,4} & 0 \\ H & 0_{4,1} \\ -B_5^T & -2x_1 \\ x_1 I_5 & 0_{5,1} \\ 0_{1,4} & 1 \end{pmatrix} \text{ with } H = \begin{pmatrix} 0_2 & I_2 & -1_{2,1} \\ I_2 & 0_2 & -1_{2,1} \end{pmatrix}. \tag{4.152}$$

*Then* $T_a$ *defines a diffeomorphism and the determinant of* $T_a$ *comes out to be:*

$$\left|\frac{\partial T_a}{\partial x_a}(x_a)\right| = -(\rho + 2x_1^4)^4(2x_1^2(F' + 2(x_2 + x_3 + \mu')) + \rho). \tag{4.153}$$

*A limited high gain observer for system (4.121) avoiding the singularity is given by*

$$\dot{\hat{x}}_a = \frac{\partial T_a}{\partial x_a}(\hat{x}_a)^{-1}\mathcal{F}(\zeta, \hat{x}_a, y) \tag{4.154}$$

*where* $\mathcal{F}_\zeta$ *is given by Proposition 42 and*

$$\mathcal{F} : (\zeta, \hat{x}_a, y) \mapsto \begin{pmatrix} \mathcal{F}_\zeta(\zeta, \hat{x}_a, y) \\ -K_6 T_{a6}(\hat{x}_a)) \end{pmatrix}. \tag{4.155}$$

$K_6$ *is a positive definite diagonal matrix of dimension* 6. *The notation* $T_{a6}$ *stands for the last* 6 *components of* $T_a$ *representing the dynamics associated with the fictitious outputs.*

#### 4.6.2.3 LPLHGO for Hybrid Model

Based on Theorem 12, we can synthesize a low peaking LHGO for the hybrid model.

**Proposition 45 (LPLHGO for hybrid model)** *The low peaking limited high gain observer for the system (4.123) is given as:*

$$\begin{aligned}\dot{\hat{z}} &= \mathcal{F}_z(\hat{z},\eta,y)\\ \dot{\eta} &= \mathcal{F}_\eta(\hat{z},\eta,y)\end{aligned} \tag{4.156}$$

*with $\mathcal{F}_z$ and $\mathcal{F}_\eta$ given as:*

$$\mathcal{F}_z:\begin{cases}\dot{\hat{z}}_1 = \eta_1 + \alpha_1\theta(y-\hat{z}_1)\\ \dot{\hat{z}}_2 = \eta_2 + \alpha_2\theta(sat_{\kappa_2}(\eta_1)-\hat{z}_2)\\ \dot{\hat{z}}_3 = \eta_3 + \alpha_3\theta(sat_{\kappa_3}(\eta_2)-\hat{z}_3)\\ \dot{\hat{z}}_4 = \varphi_{4s}(\hat{z}) + \alpha_4\theta(sat_{\kappa_4}(\eta_3)-\hat{z}_4)\end{cases} \qquad \mathcal{F}_\eta:\begin{cases}\dot{\eta}_1 = sat_{\kappa_3}(\eta_2) + \beta_1\theta^2(y-\hat{z}_1)\\ \dot{\eta}_2 = sat_{\kappa_4}(\eta_3) + \beta_2\theta^2(sat_{\kappa_2}(\eta_1)-\hat{z}_2)\\ \dot{\eta}_3 = \varphi_{4s}(\hat{z}) + \beta_3\theta^2(sat_{\kappa_3}(\eta_2)-\hat{3}_2)\end{cases} \tag{4.157}$$

*such that $\hat{z}\in\mathbb{R}^4$, $\eta\in\mathbb{R}^3$ are the observer states and $\alpha_i,\beta_i,\kappa_i$ given in Theorem 12.*

Since $n_z = n_x$, we can obtain the observer in original coordinates by using Proposition 2. However, based on the observability analysis done for the hybrid model in Proposition 39, $T$ is diffeomorphism only on $\mathcal{O}_\epsilon$ and LPLHGO is not defined at the observability singularity. By following the same procedure as done before in the case of HGO and LHGO before in Propositions 41 and 44, we can get the new LPLHGO that is capable of avoiding the singularity. The observer synthesis procedure of LPLHGO for the hybrid system is same as that of minimal systems, therefore we save the space and directly write the LPLHGO in original coordinates in the next Proposition.

**Proposition 46 (Singularity-free LPLHGO for hybrid model)** *The dynamic system*

$$\begin{cases}\dot{\hat{x}}_a = \left(\dfrac{\partial T_a}{\partial x_a}(\hat{x}_a)\right)^{-1}\begin{pmatrix}\mathcal{F}_z(T_a(\hat{x}_a),\eta,y)\\ -K_4T_{a4}(\hat{x}_a)\end{pmatrix}\\ \dot{\eta} = \mathcal{F}_\eta(T_a(\hat{x}_a),\eta,y)\end{cases} \tag{4.158}$$

*is an arbitrarily fast converging observer for system (4.121) in its original coordinates on any bounded subset of $\mathbb{R}^{n_z+n_f}$. $\mathcal{F}_z,\mathcal{F}_\eta$ are defined in Proposition 45 and, $T_a$ is defined by Proposition 41, $K_4$ is a positive definite diagonal matrix of dimension 4. The notation $T_{a4}$ stands for the last 4 components of $T_a$ representing the dynamics associated with the fictitious outputs.*

### 4.6.3 Simulation Results

Simulations are performed for the three observers given by propositions 41, 44 and 46 in original coordinates for three different scenarios. Initial conditions and other parametric values are given

| | |
|---|---|
| $x_0$ | $\begin{pmatrix} 0.6 & 0.5 & 0.8 & 1 \end{pmatrix}$ |
| $\hat{x}_0$ | $\begin{pmatrix} 0 & 0.8 & 0.2 & 0.2 \end{pmatrix}$ |
| $K_{HGO}$ | $\begin{pmatrix} 2 & 1.5 & 1.5 & 0.0625 \end{pmatrix}^T$ |
| $K_{LHGO}$ | $\left( \begin{pmatrix} k_{11} \\ k_{12} \end{pmatrix} \begin{pmatrix} k_{21} \\ k_{22} \end{pmatrix} \begin{pmatrix} k_{31} \\ k_{32} \end{pmatrix} \right)^T = \left( \begin{pmatrix} 0.45 \\ 0.25 \end{pmatrix} \begin{pmatrix} 0.6 \\ 0.1 \end{pmatrix} \begin{pmatrix} 0.5 \\ 0.025 \end{pmatrix} \right)^T$ |
| $K_{LPLHGO}$ | $\left( \begin{pmatrix} \alpha_1 & \alpha_2 & \alpha_3 & \alpha_4 \\ \beta_1 & \beta_2 & \beta_3 \end{pmatrix} \right)^T = \left( \begin{pmatrix} 1.5 & 1.5 & 1.5 & 1.5 \\ 0.1 & 0.01 & 0.002 \end{pmatrix} \right)^T$ |
| $K_{n_f}$ | $0.5 I_4$ |
| $\theta_{HGO}$ | 4.5 |
| $\theta_{LHGO}$ | 4.5 |
| $\theta_{LPLHGO}$ | 8 |
| $\epsilon$ | 0.5 |

Table 4.6: Initial conditions and gains for the system and observers

in Table 4.6. The performance comparison is led through nominal case, singularity avoidance case and the last case to study the effect of the noise and give insight about robustness to noise for each observer.

#### 4.6.3.1 Case A: Nominal Case

For the first case we chose the initial condition of $x_{10} = 0.21$ i.e. fairly near to the system. Even though the high gain parameter is chosen quite small, the peaking effect is quite significant in the case of HGO (Fig. 4.23(a)) and is a reduced a little bit for LHGO (Fig. 4.23(c)). However, in the case of LPLHGO (Fig. 4.23(e)), the peaking effect is rather small despite choosing a high gain value greater than for HGO and LHGO. The convergence time for HGO and LPLHGO is almost the same, while for LHGO, the convergence is bit slower.

#### 4.6.3.2 Case B: Singularity avoidance case

Handling with the singularity avoidance is analyzed for each observer, taking a singular initial condition for $\hat{x}_0$. The fictitious outputs are activated during the initial time period but quickly returned to zero for HGO (Fig. 4.24(c)) and LPLHGO (Fig. 4.25(c)). However, for LHGO, the fictitious outputs are triggered twice i.e. during $t[0-1]s$ and then again during $t[2-3]s$ as can be seen in Figure 4.26(c). An increase in peaking effect can be seen for the three observers that accounts for the activation of fictitious outputs and in turn the $\tau$ states. The increase in peaking

for HGO (Fig. 4.24(a)) and LHGO (Fig. 4.25(a)) is large compared to LPLHGO (Fig. 4.26(a)) owing to the effectiveness of the saturations inside the cascade structure of the observer.

#### 4.6.3.3 Case C: Output noise

Finally, we add some measurement noise in the system whereas the cutoff frequency is chosen as $1000Hz$ in this case in addition to observability defects to see the overall performance of the three observers. Since the gains and high gain parameter are chosen small for the simulations, the effect of measurement noise on the system dynamics is also quite insignificant, still the presence of the noise can be seen in the zoomed out figures of the observed states. Overall, the three observers have been proven to be quite successful in avoiding the singularity and robust in the presence of high frequency noise in the system as can be seen in Figures 4.27,4.28 and 4.29.

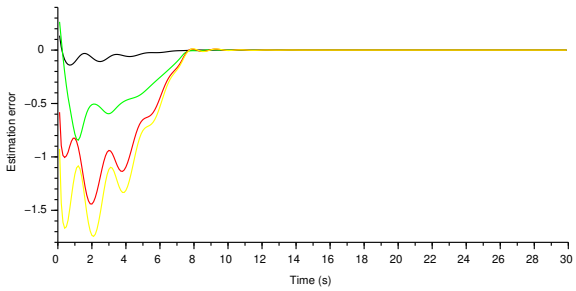


(a) HGO estimation error

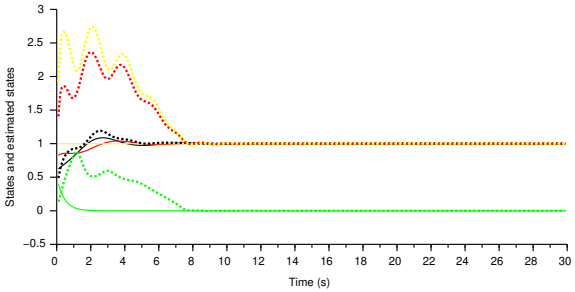


(b) HGO states and estimated states

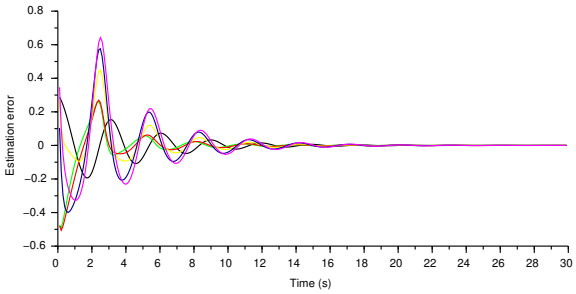


(c) LHGO estimation error

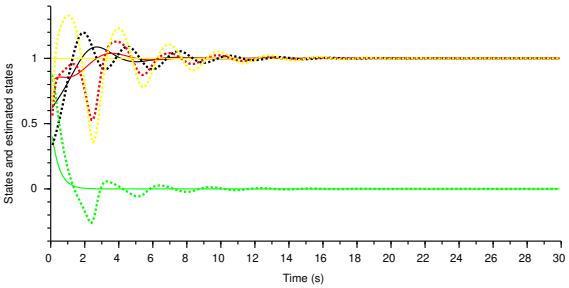


(d) LHGO states and estimated states

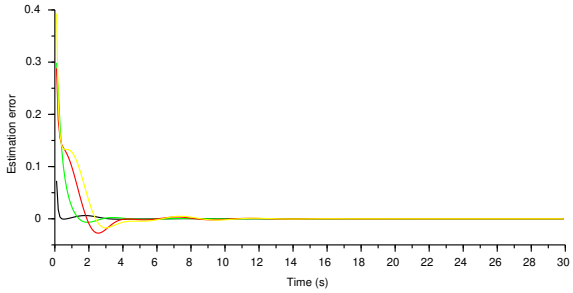


(e) LPLHGO estimation error

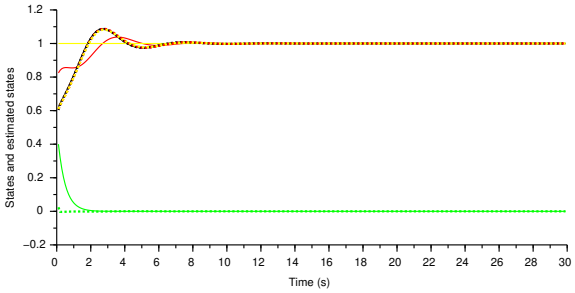


(f) LPLHGO states and estimated states

Figure 4.23: Hybrid Model: Case A from (a) to (f): simulation for nominal case. Figures (a) and (e) depicts the estimation error $\tilde{x}_1, \tilde{x}_2, \tilde{x}_3$ and $\tilde{x}_4$ by black, green, red and yellow lines for HGO and LPLHGO respectively and by black, green, red, yellow, blue and purple lines for LHGO in Figure (c). Figures (b), (d) and (e) represents the states and estimated states, such that states are in solid while the estimated states $\hat{x}$ are in dotted black, green, red and yellow lines respectively for HGO, LHGO and LPLHGO.

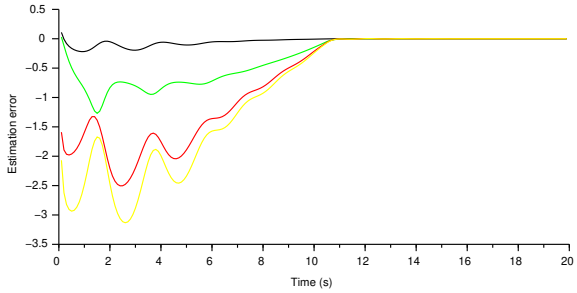


(a) HGO estimation error

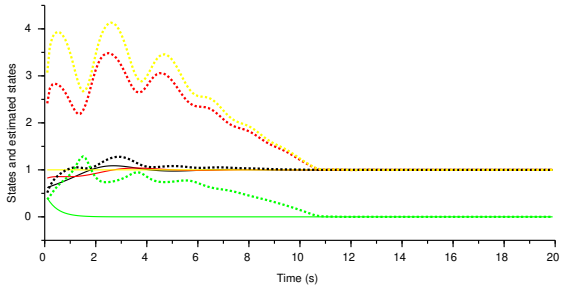


(b) HGO states and estimated states

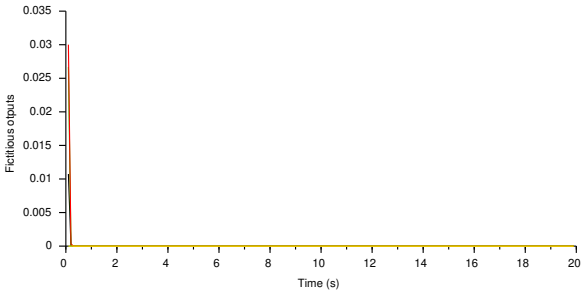


(c) HGO fictitious outputs $y_f$

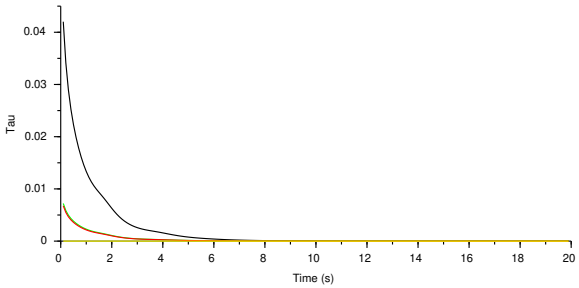


(d) HGO $\tau$ states

Figure 4.24: Hybrid Model: Case B: HGO with observability defects avoidance. Figure (a) depicts the estimation error $\tilde{x} = x - \hat{x}$ in black, green, red and yellow respectively, figure (b) represents the states in solid and the estimated states in dotted black, green, red and yellow lines respectively. figures (c) and (d) shows the activated fictitious outputs $y_f$ and $\tau$ in black, green, red and yellow lines respectively.

## 4.7 Conclusion and Perspectives

The goal of this chapter is to study the wake flow dynamics and to estimate it in order to minimize the energy consumption. A brief literature review along with the modeling of wake flow dynamics is provided. A first contribution comprises in studying four different models for the dynamics of wake flow based on ROM i.e., the minimal model, the Spod model, multi-output wake flow dynamics and the hybrid model. For each model, observability analysis is given where it has been shown that all the models suffer from the observability defects. Three different observers namely the high gain observer, the limited high gain observer and finally low peaking limited high gain observer have been designed for each model. However, since the models suffer from observability defects, we provide a method that can help to bypass those singularities using fictitious outputs to modify the system around singularity and further augmentation to a diffeomorphism. Finally the three observers for each model is presented in original coordinates where they are capable of

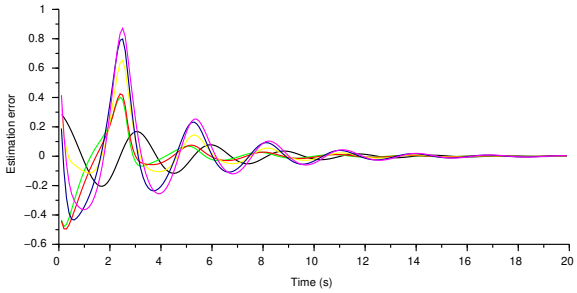


(a) LHGO estimation error

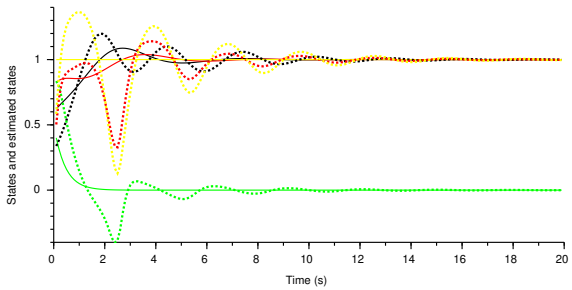


(b) LHGO states and estimated states

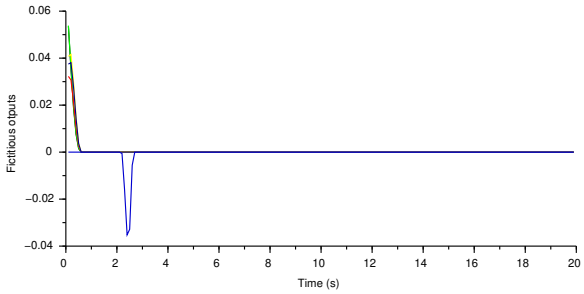


(c) LHGO fictitious outputs $y_f$

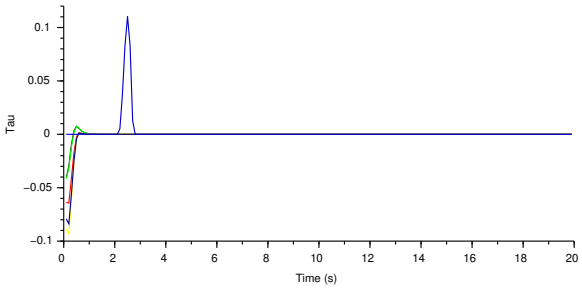


(d) LHGO $\tau$ states

Figure 4.25: Hybrid Model: Case B: LHGO with observability defects avoidance. Figure (a) depicts the estimation error $\tilde{x} = x - \hat{x}$ in black, green, red, yellow, blue and purple lines respectively, figure (b) represents the states in solid and the estimated states in dotted black, green, red and yellow lines respectively. Figures (c) and (d) shows the activated fictitious outputs $y_f$ and $\tau$ in black, green, red, yellow, blue and dark blue lines respectively.

avoiding those observability defects.

In the last section of all models, simulation results are provided accompanied by a brief discussion for three different scenarios. A detail study is provided for a performance comparison for the three observers with care about peaking and robustness to noise. In the case of minimal systems, experimental results have also been provided along with the comments on test bench where it proves that even a simplistic model is able to capture the wake flow dynamics in a very good manner atleast at a given Reynolds number.

The on-going works are on one hand, the experimental validation of the observer in real conditions where the experimental setup is being fully equipped by sensors and actuators to get a better knowledge of physical phenomenon and, on the other hand, the design of feedback laws based on the estimated state to control the flow in order to reduce the drag force. Both perspectives are of great interest for applications in fluid mechanics.

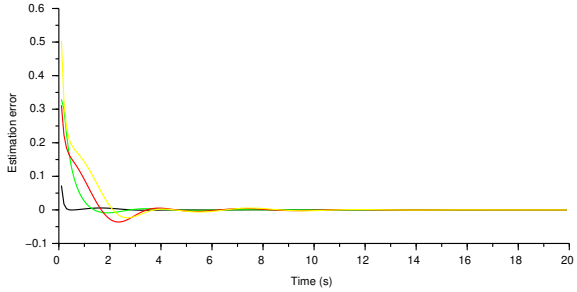


(a) LPLHGO estimation error

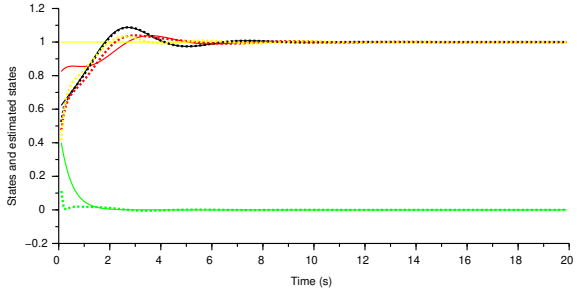


(b) LPLHGO states and estimated states

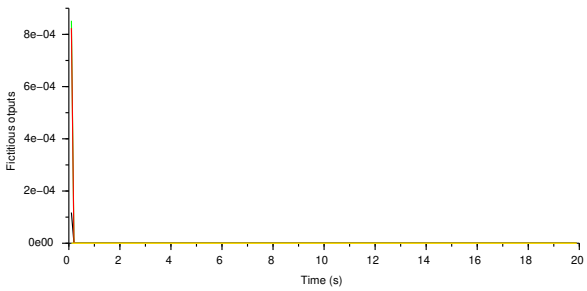


(c) LPLHGO fictitious outputs $y_f$

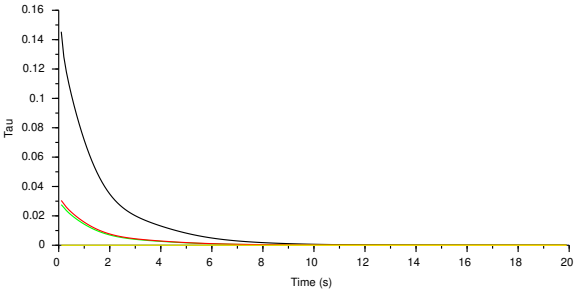


(d) LPLHGO $\tau$ states

Figure 4.26: Hybrid Model: Case B: LPLHGO with observability defects avoidance. Figure (a) depicts the estimation error $\tilde{x} = x - \hat{x}$ in black, green, red and yellow respectively, figure (b) represents the states in solid and the estimated states in dotted black, green, red and yellow lines respectively. figures (c) and (d) shows the activated fictitious outputs $y_f$ and $\tau$ in black, green, red and yellow lines respectively.

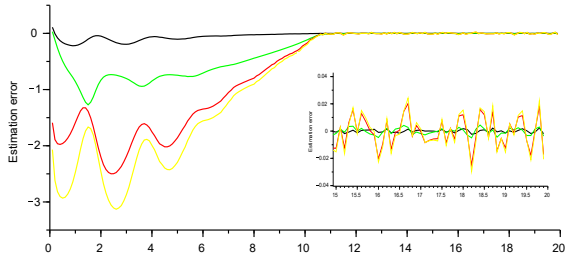


(a) HGO estimation error

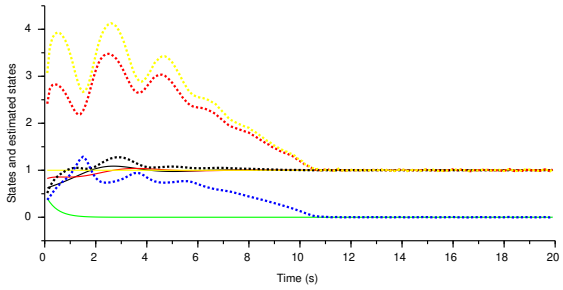


(b) HGO states and estimated states

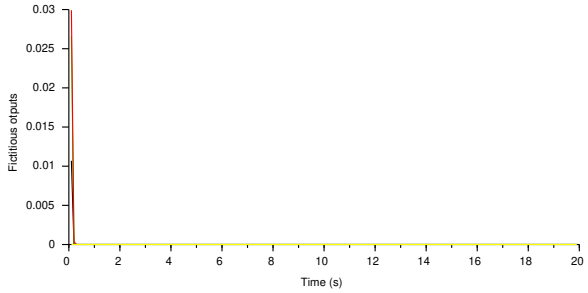


(c) HGO fictitious outputs $y_f$

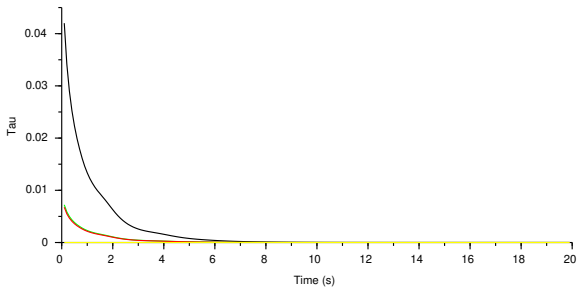


(d) HGO $\tau$ states

Figure 4.27: Hybrid Model: Case C: HGO with observability defects avoidance and additional output noise. Figure (a) depicts the estimation error $\tilde{x} = x - \hat{x}$ in black, green, red and yellow respectively, figure (b) represents the states in solid and the estimated states in dotted black, green, red and yellow lines respectively. figures (c) and (d) shows the activated fictitious outputs $y_f$ and $\tau$ in black, green, red and yellow lines respectively.

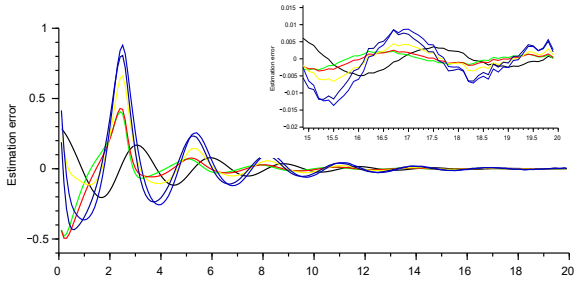


(a) LHGO estimation error

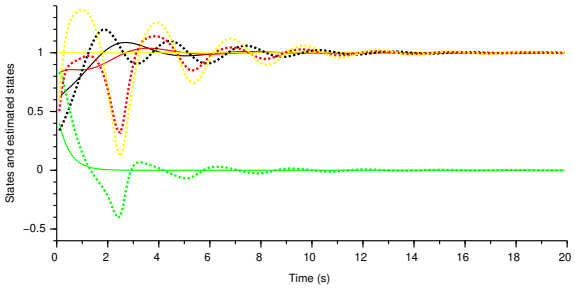


(b) LHGO states and estimated states

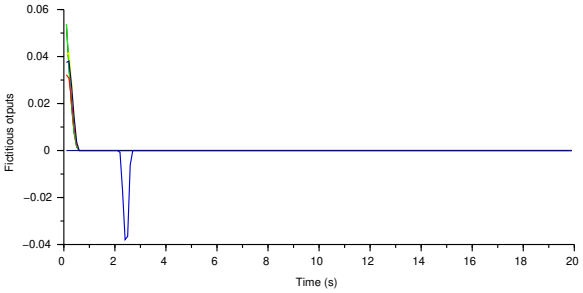


(c) LHGO fictitious outputs $y_f$

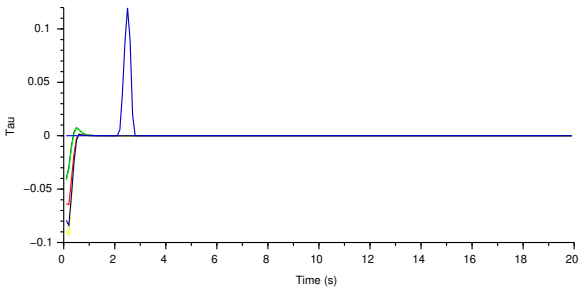


(d) LHGO $\tau$ states

Figure 4.28: Hybrid Model: Case C: LHGO with observability defects avoidance and additional output noise. Figure (a) depicts the estimation error $\tilde{x} = x - \hat{x}$ in black, green, red, yellow, blue and purple lines respectively, figure (b) represents the states in solid and the estimated states in dotted black, green, red and yellow lines respectively. Figures (c) and (d) shows the activated fictitious outputs $y_f$ and $\tau$ in black, green, red, yellow, blue and dark blue lines respectively.

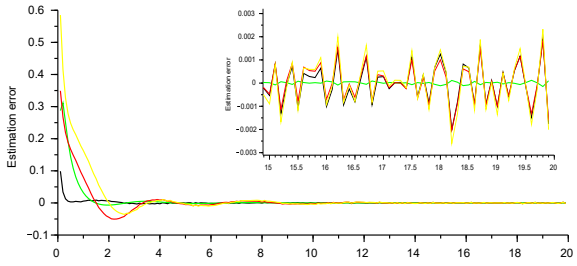


(a) LPLHGO estimation error

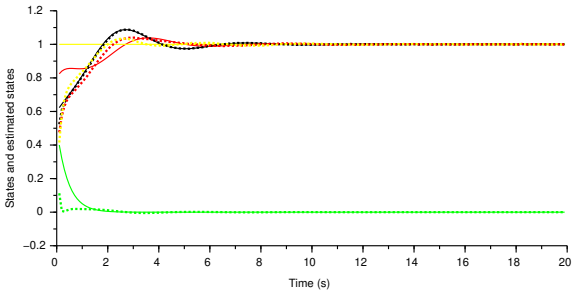


(b) LPLHGO states and estimated states

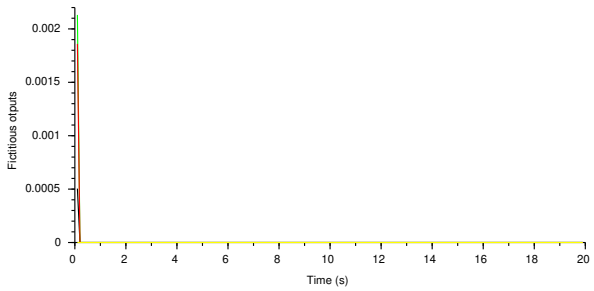


(c) LPLHGO fictitious outputs $y_f$

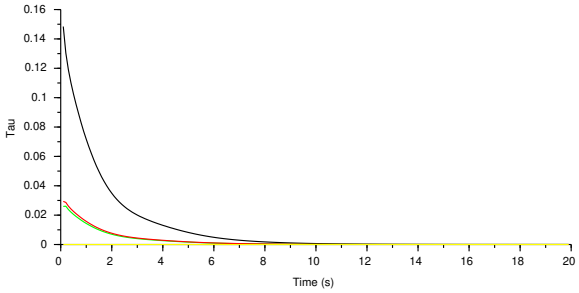


(d) LPLHGO $\tau$ states

Figure 4.29: Hybrid Model: Case C: LPLHGO with observability defects avoidance and additional output noise. Figure (a) depicts the estimation error $\tilde{x} = x - \hat{x}$ in black, green, red and yellow respectively, figure (b) represents the states in solid and the estimated states in dotted black, green, red and yellow lines respectively. figures (c) and (d) shows the activated fictitious outputs $y_f$ and $\tau$ in black, green, red and yellow lines respectively.

# General Conclusion

## Contributions

In this thesis, we addressed the design of nonlinear observers for nonlinear systems in phase variable form affected by oscillating disturbances whose dynamics are either linear or not. Such systems exhibit observability singularities that may prevent from using the standard mappings to normal forms. Hence, a first contribution was to provide a methodology to tackle the observability defects.

The method used in our work is based on Bernard et al. [2018] and employed some fictitious knowledge by adding some fictitious states to modify the system in a neighborhood of the singularities so as to remove them. This procedure thus caused the cardinality of the targeted normal form to be greater than the cardinality of the original system. Besides, a special attention was paid to systems whose observability analysis requires differentiating the output more than $(n-1)$ times so the mapping to normal form is no more a diffeomorphism yet only an injective immersion outside the observability singularities set. In order to estimate the state in the original coordinates whilst avoiding the mapping inversion, a method for extending the immersion into a global diffeomorphism was then proposed through coordinates augmentation and Jacobian completion.

Nonlinear systems augmented by the disturbance modeling result in an increased dimension that amplifies the major drawbacks of the high gain observer, such as the peaking phenomenon, the sensitivity to measurement noise, and the innovation term overdomination due to the high gain parameter power increase. Recently proposed enhancements of the high gain paradigm Astolfi and Marconi [2015]; Astolfi et al. [2016] consequently have been considered to develop their singularity-free enhancements.

The proposed methodology was further applied to nonlinear oscillators and nonlinear systems perturbed by periodic disturbances through two different applications, both related to fluid me-

chanics. Chapter 3 is devoted to the application of the proposed methodology to a therapeutic magnetic microrobot swimming in the blood vessels. Despite often considered as known or even constant in the literature, the periodic blood velocity is both hardly accessible to measurement and nonlinearly impacts severely the microrobot dynamics; the estimation of its unknown amplitude and pulse are decisive for both stabilization and diagnosis purposes. An application to wake flow dynamics was then considered in Chapter 4: for bluff bodies, the flow separation induces vortex shedding structures pumping energy, thus causing both an increase and oscillations in the drag force responsible for energy overconsumption and vibrations. Extended Hopf oscillators have proved to be able to capture the rise and evolution of these structures, but the measurement of the system state in real conditions proved difficult. Besides such systems are affected by observability singularities precisely at the control objective. Observers have been developed to address the estimation of the wake flow state, even around the singularity. Experiments and simulation results illustrated the effectiveness of the proposed observers and were encouraging for diagnosis purposes and advanced control laws in the future.

## Perspectives

A methodology to remove the observability defects for a certain class of nonlinear system has been provided in this thesis. The approach proposed in this work makes use of fictitious access to unobservable states, thus providing some fake knowledge while the system becomes unobservable. These results can be extended to singularity-free observation of nonlinear systems affected by any periodic signal, considered as a Fourier series decomposition, and by multi-frequencies signals, with the goal of rebuilding the disturbance. For example, biological, medical, mechanical systems as well as cryptography can benefit from such an approach. However, contrary to the single harmonic disturbance considered in the Chapter 2, in such a case the singularity avoidance requires using fictitious outputs and Jacobian completion depending on states whose observability is jeopardized by observability singularities, so the resulting global diffeomorphim objective is relaxed to a local result. In such a case, alternative solutions such as local observers Menini et al. [2017]; Astolfi and Possieri [2019] can be considered.

The present work focused on observation but Lyapunov stabilizing output feedbacks synthesis is the next step. The proposed methodology allows for rebuilding the state anywhere, but the system is modified around the singularity, so the estimate is not reliable. In some cases, where the singularity is far away from the control objective as for instance in the microrobotic application of Chapter 3, this is not really an issue since the singularity is even not admissible for the system, meaning that the physical system always remains far from the singularity. However it is far more challenging when the control objective is to stabilize the system at a point where the system is

no more observable and a possible approach would be to guarantee practical stability using a priori known bounds on the estimation at singularity.

# Bibliography


Abbott, J. J., Peyer, K. E., Lagomarsino, M. C., Zhang, L., Dong, L., Kaliakatsos, I. K., and Nelson, B. J. (2009). How should microrobots swim? *The international journal of Robotics Research*, 28(11-12):1434–1447.

Ahmed, J., Fruchard, M., Courtial, E., and Touré, Y. (2020). Low-power high gain observers for wake flow rebuild. In *2020 59th IEEE Conference on Decision and Control (CDC)*, pages 5428–5434. IEEE.

Ahrens, J. H. and Khalil, H. K. (2009). High-gain observers in the presence of measurement noise: A switched-gain approach. *Automatica*, 45(4):936–943.

Alamir, M. (1999). Optimization based non-linear observers revisited. *International Journal of Control*, 72(13):1204–1217.

Alamir, M. (2007). Nonlinear observers and applications, volume 363 of lncis, chapter nonlinear moving horizon observers: Theory and real-time implementation. *Springer*, 3:40.

Alvarez-Ramirez, J. and Femat, R. (1999). Robust pi stabilization of a class of chemical reactors. *Systems & Control Letters*, 38(4-5):219–225.

Andrieu, V. (2014). Convergence speed of nonlinear luenberger observers. *SIAM Journal on Control and Optimization*, 52(5):2831–2856.

Andrieu, V., Eytard, J.-B., and Praly, L. (2014). Dynamic extension without inversion for observers. In *53rd IEEE Conference on Decision and Control*, pages 878–883. IEEE.

Andrieu, V. and Praly, L. (2004). Remarks on the existence of a kazantzis-kravaris/luenberger observer. In *2004 43rd IEEE Conference on Decision and Control (CDC)(IEEE Cat. No. 04CH37601)*, volume 4, pages 3874–3879. IEEE.

Andrieu, V. and Praly, L. (2006). On the existence of a kazantzis–kravaris/luenberger observer. *SIAM Journal on Control and Optimization*, 45(2):432–456.

Andrieu, V., Praly, L., and Astolfi, A. (2009). High gain observers with updated gain and homogeneous correction terms. *Automatica*, 45(2):422–428.

Arcese, L., Fruchard, M., and Ferreira, A. (2011). Endovascular magnetically guided robots: navigation modeling and optimization. *IEEE Transactions on Biomedical Engineering*, 59(4):977–987.

Arcese, L., Fruchard, M., and Ferreira, A. (2013). Adaptive controller and observer for a magnetic microrobot. *IEEE Transactions on Robotics*, 29(4):1060–1067.

Astolfi, D., Bernard, P., Postoyan, R., and Marconi, L. (2021). Constrained state estimation for nonlinear systems: a redesign approach based on convexity. *IEEE Transactions on Automatic Control*, 67(2):824–839.

Astolfi, D., Isidori, A., and Marconi, L. (2017). Output regulation via low-power construction. In *Feedback stabilization of controlled dynamical systems*, pages 143–165. Springer.

Astolfi, D. and Marconi, L. (2015). A high-gain nonlinear observer with limited gain power. *IEEE Transactions on Automatic Control*, 60(11):3059–3064.

Astolfi, D., Marconi, L., Praly, L., and Teel, A. R. (2018). Low-power peaking-free high-gain observers. *Automatica*, 98:169–179.

Astolfi, D., Marconi, L., and Teel, A. (2016). Low-power peaking-free high-gain observers for nonlinear systems. In *2016 European Control Conference (ECC)*, pages 1424–1429. IEEE.

Astolfi, D. and Possieri, C. (2019). Design of local observers for autonomous nonlinear systems not in observability canonical form. *Automatica*, 103:443–449.

Astolfi, D. and Praly, L. (2013). Output feedback stabilization for siso nonlinear systems with an observer in the original coordinates. In *52nd IEEE Conference on Decision and Control*, pages 5927–5932. IEEE.

Back, J. and Seo, J. H. (2006). An algorithm for system immersion into nonlinear observer form: Siso case. *Automatica*, 42(2):321–328.

Ball, A. A. and Khalil, H. K. (2009). High-gain-observer tracking performance in the presence of measurement noise. In *2009 American Control Conference*, pages 4626–4627. IEEE.

Baras, J., Bensoussan, A., and James, M. (1988). Dynamic observers as asymptotic limits of recursive filters: Special cases. *SIAM Journal on Applied Mathematics*, 48(5):1147–1158.

Baude, M., Dussud, F.-X., Ecoiffier, M., Moreau, S., Bottin, A., Duvernoy, J., and Vailles, C. (2017). Key figures on climate france, europe and worldwide. edition 2018.

Berkooz, G., Holmes, P., and Lumley, J. L. (1993). The proper orthogonal decomposition in the analysis of turbulent flows. *Annual review of fluid mechanics*, 25(1):539–575.

Bernard, P. (2019). *Observer design for nonlinear systems*, volume 479. Springer.

Bernard, P., Andrieu, V., and Praly, L. (2018). Expressing an observer in preferred coordinates by transforming an injective immersion into a surjective diffeomorphism. *SIAM Journal on Control and Optimization*, 56(3):2327–2352.

Bernard, P., Praly, L., and Andrieu, V. (2015). Tools for observers based on coordinate augmentation. In *2015 54th IEEE Conference on Decision and Control (CDC)*, pages 6324–6329. IEEE.

Besançon, G. (2003). High-gain observation with disturbance attenuation and application to robust fault detection. *Automatica*, 39(6):1095–1102.

Besançon, G. (2007). *Nonlinear observers and applications*, volume 363. Springer.

Besancon, G. and Ticlea, A. (2006). Immersion-based observer design for nonlinear systems. In *Proceedings of the 45th IEEE Conference on Decision and Control*, pages 4615–4620. IEEE.

Bestle, D. and Zeitz, M. (1983). Canonical form observer design for non-linear time-variable systems. *International Journal of control*, 38(2):419–431.

Bittanti, S. and Moiraghi, L. (1994). Active control of vibrations in helicopters via pole assignment techniques. *IEEE Transactions on Control Systems Technology*, 2(4):343–351.

Bodson, M. (2005). Rejection of periodic disturbances of unknown and time-varying frequency. *International Journal of Adaptive Control and Signal Processing*, 19(2-3):67–88.

Boizot, N., Busvelle, E., and Gauthier, J.-P. (2010). An adaptive high-gain observer for nonlinear systems. *Automatica*, 46(9):1483–1488.

Bonnabel, S. and Slotine, J.-J. (2014). A contraction theory-based analysis of the stability of the deterministic extended kalman filter. *IEEE Transactions on Automatic Control*, 60(2):565–569.

Bornard, G. and Hammouri, H. (1991). A high gain observer for a class of uniformly observable systems. In *[1991] Proceedings of the 30th IEEE Conference on Decision and Control*, pages 1494–1496. IEEE.

Bossane, D., Rakotopara, D., and Gauthier, J. (1989). Local and global immersion into linear systems up to output injection. In *Proceedings of the 28th IEEE Conference on Decision and Control,*, pages 2000–2004. IEEE.

Bouhadjra, D., Zemouche, A., Alessandri, A., and Bagnerini, P. (2020). High-gain nonlinear observer using system state augmentation. In *2020 59th IEEE Conference on Decision and Control (CDC)*, pages 4182–4187. IEEE.

Boutat, D., Zheng, G., and Hammouri, H. (2010). A nonlinear canonical form for reduced order observer design. *IFAC Proceedings Volumes*, 43(14):409–414.

Brunton, S. L., Proctor, J. L., and Kutz, J. N. (2016). Discovering governing equations from data by sparse identification of nonlinear dynamical systems. *Proceedings of the national academy of sciences*, 113(15):3932–3937.

Busawon, K., Farza, M., and Hammouri, H. (1998). Observer design for a special class of nonlinear systems. *International Journal of Control*, 71(3):405–418.

Byrnes, C. I., Celani, F., and Isidori, A. (2005). Omega-limit sets of a class of nonlinear systems that are semiglobally practically stabilized. *International Journal of Robust and Nonlinear Control: IFAC-Affiliated Journal*, 15(7):315–333.

Ciccarella, G., Dalla Mora, M., and Germani, A. (1993). A luenberger-like observer for nonlinear systems. *International Journal of Control*, 57(3):537–556.

Clément, F. and Françoise, J.-P. (2007). Mathematical modeling of the gnrh pulse and surge generator. *SIAM Journal on Applied Dynamical Systems*, 6(2):441–456.

Cooper, K. (1993). Bluff-body aerodynamics as applied to vehicles. *Journal of Wind Engineering and Industrial Aerodynamics*, 49(1-3):1–21.

Dario, P., Carrozza, M. C., Stefanini, C., and D'Attanasio, S. (1998). A mobile microrobot actuated by a new electromagnetic wobble micromotor. *IEEE/ASME transactions on mechatronics*, 3(1):9–16.

Deane, A., Kevrekidis, I., Karniadakis, G. E., and Orszag, S. (1991). Low-dimensional models for complex geometry flows: application to grooved channels and circular cylinders. *Physics of Fluids A: Fluid Dynamics*, 3(10):2337–2354.

Decuzzi, P., Lee, S., Bhushan, B., and Ferrari, M. (2005). A theoretical model for the margination of particles within blood vessels. *Annals of biomedical engineering*, 33(2):179–190.

Dekker, R., Bloemhof, J., and Mallidis, I. (2012). Operations research for green logistics–an overview of aspects, issues, contributions and challenges. *European journal of operational research*, 219(3):671–679.

Deza, F., Busvelle, E., Gauthier, J., and Rakotopara, D. (1992). High gain estimation for nonlinear systems. *Systems & control letters*, 18(4):295–299.

Dreyfus, R., Baudry, J., Roper, M. L., Fermigier, M., Stone, H. A., and Bibette, J. (2005). Microscopic artificial swimmers. *Nature*, 437(7060):862–865.

Eckmann, B. (2006). *Mathematical survey lectures 1943-2004*. Springer.

Ergeneman, O., Abbott, J. J., Dogangil, G., and Nelson, B. J. (2008). Functionalizing intraocular microrobots with surface coatings. In *2008 2nd IEEE RAS & EMBS International Conference on Biomedical Robotics and Biomechatronics*, pages 232–237. IEEE.

Esfandiari, F. and Khalil, H. K. (1992). Output feedback stabilization of fully linearizable systems. *International Journal of control*, 56(5):1007–1037.

Evans, A. A. and Lauga, E. (2010). Propulsion by passive filaments and active flagella near boundaries. *Physical Review E*, 82(4):041915.

Farhangfar, A. and Shor, R. (2020). State observer design for a class of lipschitz nonlinear system with uncertainties. *IFAC-PapersOnLine*, 53(1):283–288.

Farza, M., M'Saad, M., Triki, M., and Maatoug, T. (2011). High gain observer for a class of non-triangular systems. *Systems & Control Letters*, 60(1):27–35.

FitzHugh, R. (1961). Impulses and physiological states in theoretical models of nerve membrane. *Biophysical journal*, 1(6):445–466.

Fliess, M. and Kupka, I. (1983). A finiteness criterion for nonlinear input–output differential systems. *SIAM Journal on Control and Optimization*, 21(5):721–728.

Fruchard, M., Arcese, L., and Courtial, E. (2013). Estimation of the blood velocity for nanorobotics. *IEEE Transactions on Robotics*, 30(1):93–102.

Fussmann, G. F., Ellner, S. P., Shertzer, K. W., and Hairston Jr, N. G. (2000). Crossing the hopf bifurcation in a live predator-prey system. *Science*, 290(5495):1358–1360.

G. Bornard, F. C.-C. and Gilles, G. (1995). Observability and observers in nonlinear systems. *Nonlinear Systems - T.1, Modeling and Estimation*, pages 173–216.

Gangloff, J., Ginhoux, R., de Mathelin, M., Soler, L., and Marescaux, J. (2006). Model predictive control for compensation of cyclic organ motions in teleoperated laparoscopic surgery. *IEEE Transactions on Control Systems Technology*, 14(2):235–246.

Gatehouse, P. D., Keegan, J., Crowe, L. A., Masood, S., Mohiaddin, R. H., Kreitner, K.-F., and Firmin, D. N. (2005). Applications of phase-contrast flow and velocity imaging in cardiovascular mri. *European radiology*, 15(10):2172–2184.

Gauthier, J. and Bornard, G. (1980). Observability for any u (t) of a class of nonlinear systems. In *1980 19th IEEE Conference on Decision and Control including the Symposium on Adaptive Processes*, pages 910–915. IEEE.

Gauthier, J. and Kupka, I. (1996). Observability for systems with more outputs than inputs and asymptotic observers. *Mathematische Zeitschrift*, 223(1):47–78.

Gauthier, J. P., Hammouri, H., and Othman, S. (1992). A simple observer for nonlinear systems applications to bioreactors. *IEEE Transactions on automatic control*, 37(6):875–880.

Gauthier, J.-P. and Kupka, I. (2001). *Deterministic observation theory and applications*. Cambridge university press.

Gauthier, J.-P. and Kupka, I. A. (1994). Observability and observers for nonlinear systems. *SIAM journal on control and optimization*, 32(4):975–994.

Gelb, A. et al. (1974). *Applied optimal estimation*. MIT press.

Gilardi, G. and Sharf, I. (2002). Literature survey of contact dynamics modelling. *Mechanism and machine theory*, 37(10):1213–1239.

Gillies, G., Ritter, R., Broaddus, W., Grady, M., Howard III, M., and McNeil, R. (1994). Magnetic manipulation instrumentation for medical physics research. *Review of Scientific Instruments*, 65(3):533–562.

Glumineau, A., Moog, C. H., and Plestan, F. (1996). New algebraic-geometric conditions for the linearization by input-output injection. *IEEE Transactions on Automatic Control*, 41(4):598–603.

Gonzalez-Trejo, J., Ramirez, J. A., and Fernandez, G. (1999). Robust control with uncertainty estimation for feedback linearizable systems: application to control of distillation columns. *Journal of Process Control*, 9(3):221–231.

Guay, M. (2002). Observer linearization by output-dependent time-scale transformations. *IEEE Transactions on Automatic Control*, 47(10):1730–1735.

Hammouri, H., Ahmed, F. S., and Othman, S. (2018). Observer design based on immersion technics and canonical form. *Systems & Control Letters*, 114:19–26.

Hammouri, H., Bornard, G., and Busawon, K. (2010). High gain observer for structured multi-output nonlinear systems. *IEEE Transactions on automatic control*, 55(4):987–992.

Hammouri, H. and Farza, M. (2003). Nonlinear observers for locally uniformly observable systems. *ESAIM: Control, optimisation and calculus of Variations*, 9:353–370.

Hammouri, H., Targui, B., and Armanet, F. (2002). High gain observer based on a triangular structure. *International Journal of Robust and Nonlinear Control: IFAC-Affiliated Journal*, 12(6):497–518.

Handbook, A., Andra, W., and Nowak, H. (2007). Magnetism in medicine.

Hermann, R. and Krener, A. (1977). Nonlinear controllability and observability. *IEEE Transactions on automatic control*, 22(5):728–740.

Hethcote, H. W., Yi, L., and Zhujun, J. (1999). Hopf bifurcation in models for pertussis epidemiology. *Mathematical and Computer Modelling*, 30(11-12):29–45.

Holloway Jr, G. A. and Watkins, D. W. (1977). Laser doppler measurement of cutaneous blood flow. *Journal of Investigative Dermatology*, 69(3):306–309.

Hou, M. (2005). Amplitude and frequency estimator of a sinusoid. *IEEE Transactions on Automatic Control*, 50(6):855–858.

Hou, M. and Pugh, A. (1999). Observer with linear error dynamics for nonlinear multi-output systems. *Systems & Control Letters*, 37(1):1–9.

Hsu, L., Ortega, R., and Damm, G. (1999). A globally convergent frequency estimator. *IEEE Transactions on Automatic Control*, 44(4):698–713.

Hucho, W.-H. et al. (1998). Aerodynamics of road vehicle: From fluid mechanics to vehicle engineering. *SAE International, Warrendale, PA*, 177.

Iaccarino, G., Ooi, A., Durbin, P., and Behnia, M. (2003). Reynolds averaged simulation of unsteady separated flow. *International Journal of Heat and Fluid Flow*, 24(2):147–156.

Iimura, K., Watanabe, S., Suzuki, M., Hirota, M., and Higashitani, K. (2009). Simulation of entrainment of agglomerates from plate surfaces by shear flows. *Chemical Engineering Science*, 64(7):1455–1461.

Ishiyama, K., Sendoh, M., Yamazaki, A., and Arai, K. (2001). Swimming micro-machine driven by magnetic torque. *Sensors and Actuators A: Physical*, 91(1-2):141–144.

Isidori, A. (1997). A remark on the problem of semiglobal nonlinear output regulation. *IEEE transactions on Automatic Control*, 42(12):1734–1738.

Isidori, A. (2000). A tool for semi-global stabilization of uncertain non-minimum-phase nonlinear systems via output feedback. *IEEE transactions on automatic control*, 45(10):1817–1827.

Jiang, Z.-P., Hill, D. J., and Guo, Y. (1998). Stabilization and tracking via output feedback for the nonlinear benchmark system. *Automatica*, 34(7):907–915.

Jouan, P. (2003). Immersion of nonlinear systems into linear systems modulo output injection. *SIAM Journal on Control and Optimization*, 41(6):1756–1778.

Jouan, P. and Gauthier, J.-P. (1996). Finite singularities of nonlinear systems. output stabilization, observability, and observers. *Journal of Dynamical and Control systems*, 2(2):255–288.

Kalman, R. E. (1960). A new approach to linear filtering and prediction problems.

Kalman, R. E. and Bucy, R. S. (1961). New results in linear filtering and prediction theory.

Karagueuzian, H. S., Stepanyan, H., and Mandel, W. J. (2013). Bifurcation theory and cardiac arrhythmias. *American journal of cardiovascular disease*, 3(1):1.

Kazantzis, N. and Kravaris, C. (1998). Nonlinear observer design using lyapunov's auxiliary theorem. *Systems & Control Letters*, 34(5):241–247.

Kehlenbeck, R. and Felice, R. D. (1999). Empirical relationships for the terminal settling velocity of spheres in cylindrical columns. *Chemical Engineering & Technology: Industrial Chemistry-Plant Equipment-Process Engineering-Biotechnology*, 22(4):303–308.

Khalil, H. K. (2017). *High-gain observers in nonlinear feedback control*. SIAM.

Khalil, H. K. and Priess, S. (2016). Analysis of the use of low-pass filters with high-gain observers. *IFAC-PapersOnLine*, 49(18):488–492.

Kim, C. S., Kiris, C., Kwak, D., and David, T. (2006). Numerical simulation of local blood flow in the carotid and cerebral arteries under altered gravity.

Kosa, G., Shoham, M., and Zaaroor, M. (2007). Propulsion method for swimming microrobots. *IEEE Transactions on Robotics*, 23(1):137–150.

Kravaris, C., Sotiropoulos, V., Georgiou, C., Kazantzis, N., Xiao, M., and Krener, A. J. (2007). Nonlinear observer design for state and disturbance estimation. *Systems & Control Letters*, 56(11-12):730–735.

Kreisselmeier, G. and Engel, R. (2003). Nonlinear observers for autonomous lipschitz continuous systems. *IEEE Transactions on Automatic Control*, 48(3):451–464.

Krener, A. J. and Isidori, A. (1983). Linearization by output injection and nonlinear observers. *Systems & Control Letters*, 3(1):47–52.

Krener, A. J. and Respondek, W. (1985). Nonlinear observers with linearizable error dynamics. *SIAM Journal on Control and Optimization*, 23(2):197–216.

Krener, A. J. and Xiao, M. (2002). Nonlinear observer design in the siegel domain. *SIAM Journal on Control and Optimization*, 41(3):932–953.

Kristo, B., Liao, J. C., Neves, H. P., Churchill, B. M., Montemagno, C. D., and Schulam, P. G. (2003). Microelectromechanical systems in urology. *Urology*, 61(5):883–887.

Kurtulus, D., Scarano, F., and David, L. (2007). Unsteady aerodynamic forces estimation on a square cylinder by tr-piv. *Experiments in fluids*, 42(2):185–196.

Lagomarsino, M. C., Capuani, F., and Lowe, C. P. (2003). A simulation study of the dynamics of a driven filament in an aristotelian fluid. *Journal of theoretical biology*, 224(2):215–224.

Lehmann, O., Tadmor, G., Gonzalez, J., Noack, B., Morzynski, M., and Stankiewicz, W. (2007). Shift modes and transient dynamics in low order, design oriented galerkin models. In *45th AIAA Aerospace Sciences Meeting and Exhibit*, page 111.

Levine, J. and Marino, R. (1986). Nonlinear system immersion, observers and finite-dimensional filters. *Systems & Control Letters*, 7(2):133–142.

Lin, Z. and Saberi, A. (1997). Low-and-high gain design technique for linear systems subject to input saturation—a direct method. *International Journal of Robust and Nonlinear Control: IFAC-Affiliated Journal*, 7(12):1071–1101.

Loiseau, J.-C. and Brunton, S. L. (2018). Constrained sparse galerkin regression. *Journal of Fluid Mechanics*, 838:42–67.

Luchtenburg, D. M., Günther, B., Noack, B. R., King, R., and Tadmor, G. (2009). A generalized mean-field model of the natural and high-frequency actuated flow around a high-lift configuration. *Journal of Fluid Mechanics*, 623:283–316.

Luenberger, D. (1966). Observers for multivariable systems. *IEEE Transactions on Automatic Control*, 11(2):190–197.

Luenberger, D. (1967). Canonical forms for linear multivariable systems. *IEEE Transactions on Automatic Control*, 12(3):290–293.

Luenberger, D. (1971). An introduction to observers. *IEEE Transactions on Automatic Control*, 16(6):596–602.

Luenberger, D. G. (1964). Observing the state of a linear system. *IEEE transactions on military electronics*, 8(2):74–80.

Lynch, A. F. and Bortoff, S. A. (2001). Nonlinear observers with approximately linear error dynamics: The multivariable case. *IEEE Transactions on Automatic Control*, 46(6):927–932.

Ma, X., Karamanos, G.-S., and Karniadakis, G. (2000). Dynamics and low-dimensionality of a turbulent near wake. *Journal of fluid mechanics*, 410:29–65.

Maggiore, M. and Passino, K. M. (2003). A separation principle for a class of non-uco systems. *IEEE Transactions on Automatic Control*, 48(7):1122–1133.

Maggiore, M. and Passino, K. M. (2005). Output feedback tracking: A separation principle approach. *IEEE Transactions on Automatic Control*, 50(1):111–117.

Mantič-Lugo, V., Arratia, C., and Gallaire, F. (2014). Self-consistent mean flow description of the nonlinear saturation of the vortex shedding in the cylinder wake. *Physical review letters*, 113(8):084501.

Marconi, L., Praly, L., and Isidori, A. (2007). Output stabilization via nonlinear luenberger observers. *SIAM Journal on Control and Optimization*, 45(6):2277–2298.

Marino, R. and Tomei, P. (2002). Global estimation of n unknown frequencies. *IEEE Transactions on Automatic Control*, 47(8):1324–1328.

Martel, S. and Mohammadi, M. (2010). Using a swarm of self-propelled natural microrobots in the form of flagellated bacteria to perform complex micro-assembly tasks. In *2010 IEEE international conference on robotics and automation*, pages 500–505. IEEE.

Mathieu, J.-B., Beaudoin, G., and Martel, S. (2006). Method of propulsion of a ferromagnetic core in the cardiovascular system through magnetic gradients generated by an mri system. *IEEE Transactions on Biomedical Engineering*, 53(2):292–299.

Matsuyama, T. and Yamamoto, H. (1998). The electrostatic force between a charged dielectric particle and a conducting plane [translated]. *KONA Powder and Particle Journal*, 16:223–228.

Medvedev, G. S. and Cisternas, J. E. (2004). Multimodal regimes in a compartmental model of the dopamine neuron. *Physica D: Nonlinear Phenomena*, 194(3-4):333–356.

Meeker, D. C., Maslen, E. H., Ritter, R. C., and Creighton, F. M. (1996). Optimal realization of arbitrary forces in a magnetic stereotaxis system. *IEEE transactions on magnetics*, 32(2):320–328.

Meliga, P., Cadot, O., and Serre, E. (2016). Experimental and theoretical sensitivity analysis of turbulent flow past a square cylinder. *Flow, turbulence and combustion*, 97(4):987–1015.

Menini, L., Possieri, C., and Tornambe, A. (2017). A "practical" observer for nonlinear systems. In *2017 IEEE 56th Annual Conference on Decision and Control (CDC)*, pages 3015–3020. IEEE.

Michalska, H. and Mayne, D. Q. (1995). Moving horizon observers and observer-based control. *IEEE Transactions on Automatic Control*, 40(6):995–1006.

Miloro, P., Sinibaldi, E., Menciassi, A., and Dario, P. (2012). Removing vascular obstructions: a challenge, yet an opportunity for interventional microdevices. *Biomedical microdevices*, 14(3):511–532.

Mita, T. (1977). On zeros and responses of linear regulators and linear observers. *IEEE Transactions on Automatic Control*, 22(3):423–428.

Moehlis, J. (2002). Canards in a surface oxidation reaction. *Journal of Nonlinear Science*, 12(4).

Morfin, E., Astolfi, D., and Andrieu, V. (2020). Adaptive low-power high-gain observers for lower-triangular systems with input-dependent lipschitz constant. *IFAC-PapersOnLine*, 53(2):4904–4909.

Narendra, K. S. and Annaswamy, A. M. (2012). *Stable adaptive systems*. Courier Corporation.

Nelson, B. J., Kaliakatsos, I. K., and Abbott, J. J. (2010). Microrobots for minimally invasive medicine. *Annual review of biomedical engineering*, 12:55–85.

Nguyen, A. and Schulze, H. J. (2003). *Colloidal science of flotation*. CRC Press.

Noack, B. R., Afanasiev, K., MORZYŃSKI, M., Tadmor, G., and Thiele, F. (2003). A hierarchy of low-dimensional models for the transient and post-transient cylinder wake. *Journal of Fluid Mechanics*, 497:335–363.

Obregon-Pulido, G., Castillo-Toledo, B., and Loukianov, A. (2002). A globally convergent estimator for n-frequencies. *IEEE Transactions on Automatic Control*, 47(5):857–863.

Östh, J., Noack, B. R., Krajnović, S., Barros, D., and Borée, J. (2014). On the need for a nonlinear subscale turbulence term in pod models as exemplified for a high-reynolds-number flow over an ahmed body. *Journal of Fluid Mechanics*, 747:518–544.

Oueder, M., Farza, M., Abdennour, R. B., and M'Saad, M. (2012). A high gain observer with updated gain for a class of mimo non-triangular systems. *Systems & Control Letters*, 61(2):298–308.

Palmer, A. (2007). The development of an integrated routing and carbon dioxide emissions model for goods vehicles.

Panteley, E., Loria, A., and El Ati, A. (2015). Analysis and control of andronov-hopf oscillators with applications to neuronal populations. In *2015 54th IEEE Conference on Decision and Control (CDC)*, pages 596–601. IEEE.

Passaggia, P.-Y. and Ehrenstein, U. (2018). Optimal control of a separated boundary-layer flow over a bump. *Journal of Fluid Mechanics*, 840:238–265.

Phelps, A. R. (1991). On constructing nonlinear observers. *SIAM Journal on Control and Optimization*, 29(3):516–534.

Polotskii, V. (1978). Maximal errors of an asymptotic state identifier. *Automation and Remote Control*, 39(8):1116–1121.

Ponzini, R., Vergara, C., Rizzo, G., Veneziani, A., Roghi, A., Vanzulli, A., Parodi, O., and Redaelli, A. (2010). Womersley number-based estimates of blood flow rate in doppler analysis: in vivo validation by means of phase-contrast mri. *IEEE Transactions on biomedical engineering*, 57(7):1807–1815.

Praly, L. (2003). Asymptotic stabilization via output feedback for lower triangular systems with output dependent incremental rate. *IEEE Transactions on Automatic Control*, 48(6):1103–1108.

Praly, L., Isidori, A., and Marconi, L. (2006). A new observer for an unknown harmonic oscillator. In *17th international symposium on mathematical theory of networks and systems*, pages 24–28.

Praly, L. and Jiang, Z.-P. (2004). Linear output feedback with dynamic high gain for nonlinear systems. *Systems & Control Letters*, 53(2):107–116.

Prieur, C., Tarbouriech, S., and Zaccarian, L. (2012). Hybrid high-gain observers without peaking for planar nonlinear systems. In *2012 IEEE 51st IEEE conference on decision and control (CDC)*, pages 6175–6180. IEEE.

Purdy, P. D., Fujimoto, T., Replogle, R. E., Giles, B. P., Fujimoto, H., and Miller, S. L. (2005). Percutaneous intraspinal navigation for access to the subarachnoid space: use of another natural conduit for neurosurgical procedures. *Neurosurgical Focus*, 19(1):1–5.

Quate, E. G., Wika, K. G., Lawson, M. A., Gillies, G. T., Ritter, R., Grady, M., and Howard, M. (1991). Goniometric motion controller for the superconducting coil in a magnetic stereotaxis system. *IEEE Transactions on Biomedical Engineering*, 38(9):899–905.

Ramos, L. d. C., Di Meglio, F., Morgenthaler, V., da Silva, L. F. F., and Bernard, P. (2020). Numerical design of luenberger observers for nonlinear systems. In *2020 59th IEEE Conference on Decision and Control (CDC)*, pages 5435–5442. IEEE.

Respondek, W., Pogromsky, A., and Nijmeijer, H. (2004). Time scaling for observer design with linearizable error dynamics. *Automatica*, 40(2):277–285.

Rowley, C. W. and Dawson, S. T. (2017). Model reduction for flow analysis and control. *Annu. Rev. Fluid Mech*, 49(1):387–417.

Rowley, C. W., Mezić, I., Bagheri, S., Schlatter, P., and Henningson, D. S. (2009). Spectral analysis of nonlinear flows. *Journal of fluid mechanics*, 641:115–127.

Roy, S., Ferrara, L. A., Fleischman, A. J., and Benzel, E. C. (2006). Mems and neurosurgery. In *BioMEMS and biomedical nanotechnology*, pages 95–123. Springer.

Sadelli, L., Fruchard, M., and Ferreira, A. (2015). Estimation de la pulsation cardiaque et la vitesse du sang. *6èmes Journées Doctorales/Journées Nationales MACS Bourges (France)*.

Sadelli, L., Fruchard, M., and Ferreira, A. (2016). 2d observer-based control of a vascular microrobot. *IEEE Transactions on Automatic Control*, 62(5):2194–2206.

Sanfelice, R. G. and Praly, L. (2011). On the performance of high-gain observers with gain adaptation under measurement noise. *Automatica*, 47(10):2165–2176.

Schaffner, J. and Zeitz, M. (1999). Decentral nonlinear observer design using a block-triangular form. *International Journal of Systems Science*, 30(10):1131–1142.

Schmid, P. J. (2010). Dynamic mode decomposition of numerical and experimental data. *Journal of fluid mechanics*, 656:5–28.

Seo, K., Chung, S.-J., and Slotine, J.-J. E. (2010). Cpg-based control of a turtle-like underwater vehicle. *Autonomous Robots*, 28(3):247–269.

Sharma, A., Morrison, J., McKeon, B., Limebeer, D., Koberg, W., and Sherwin, S. (2011). Relaminarisation of re$\tau$= 100 channel flow with globally stabilising linear feedback control. *Physics of Fluids*, 23(12):125105.

Shen, J. (1991). Hopf bifurcation of the unsteady regularized driven cavity flow. *Journal of Computational Physics*, 95(1):228–245.

Shim, H., Son, Y. I., and Seo, J. H. (2001). Semi-global observer for multi-output nonlinear systems. *Systems & Control Letters*, 42(3):233–244.

Shim, H. and Teel, A. R. (2003). Asymptotic controllability and observability imply semiglobal practical asymptotic stabilizability by sampled-data output feedback. *Automatica*, 39(3):441–454.

Shoshitaishvili, A. (1992). On control branching systems with degenerate linearization. In *IFAC Symposium on Nonlinear Control Systems*, pages 495–500.

Sipp, D., Marquet, O., Meliga, P., and Barbagallo, A. (2010). Dynamics and control of global instabilities in open-flows: a linearized approach. *Applied Mechanics Reviews*, 63(3).

Sipp, D. and Schmid, P. J. (2016). Linear closed-loop control of fluid instabilities and noise-induced perturbations: a review of approaches and tools. *Applied Mechanics Reviews*, 68(2).

Sovran, G. (2012). *Aerodynamic drag mechanisms of bluff bodies and road vehicles*. Springer Science & Business Media.

Stuart, J. T. (1958). On the non-linear mechanics of hydrodynamic stability. *Journal of Fluid Mechanics*, 4(1):1–21.

Teel, A. and Praly, L. (1994). Global stabilizability and observability imply semi-global stabilizability by output feedback. *Systems & Control Letters*, 22(5):313–325.

Teel, A. and Praly, L. (1995). Tools for semiglobal stabilization by partial state and output feedback. *SIAM Journal on Control and Optimization*, 33(5):1443–1488.

Thacker, A., Aubrun, S., Leroy, A., and Devinant, P. (2013). Experimental characterization of flow unsteadiness in the centerline plane of an ahmed body rear slant. *Experiments in fluids*, 54(3):1–16.

Than, T. D., Alici, G., Zhou, H., and Li, W. (2012). A review of localization systems for robotic endoscopic capsules. *IEEE transactions on biomedical engineering*, 59(9):2387–2399.

Tornambè, A. (1992). Output feedback stabilization of a class of non-minimum phase nonlinear systems. *Systems & Control Letters*, 19(3):193–204.

Trias, F., Gorobets, A., and Oliva, A. (2015). Turbulent flow around a square cylinder at reynolds number 22,000: A dns study. *Computers & Fluids*, 123:87–98.

Ullah, H., Malik, F. M., Saeed, A., Akbar, Z. A., and Hussain, S. (2019). Sampled-data control of pan-tilt platform using discrete-time high gain observer. In *IOP Conference Series: Materials Science and Engineering*, volume 707, page 012005. IOP Publishing.

Ullrich, F., Bergeles, C., Pokki, J., Ergeneman, O., Erni, S., Chatzipirpiridis, G., Pané, S., Framme, C., and Nelson, B. J. (2013). Mobility experiments with microrobots for minimally invasive intraocular surgery. *Investigative ophthalmology & visual science*, 54(4):2853–2863.

Vartholomeos, P. and Mavroidis, C. (2012). In silico studies of magnetic microparticle aggregations in fluid environments for mri-guided drug delivery. *IEEE transactions on biomedical engineering*, 59(11):3028–3038.

Vasiljevic, L. K. and Khalil, H. K. (2006). Differentiation with high-gain observers the presence of measurement noise. In *Proceedings of the 45th IEEE Conference on Decision and Control*, pages 4717–4722. IEEE.

Viel, F., Busvelle, E., and Gauthier, J.-P. (1995). Stability of polymerization reactors using i/o linearization and a high-gain observer. *Automatica*, 31(7):971–984.

Volpe, R., Devinant, P., and Kourta, A. (2015). Experimental characterization of the unsteady natural wake of the full-scale square back ahmed body: flow bi-stability and spectral analysis. *Experiments in Fluids*, 56(5):1–22.

Wang, L., Astolfi, D., Marconi, L., and Su, H. (2017). High-gain observers with limited gain power for systems with observability canonical form. *Automatica*, 75:16–23.

Wazewski, T. (1935). Sur les matrices dont les éléments sont des fonctions continues. *Compositio Mathematica*, 2:63–68.

Womersley, J. R. (1955). Method for the calculation of velocity, rate of flow and viscous drag in arteries when the pressure gradient is known. *The Journal of physiology*, 127(3):553.

Wynn, A., Pearson, D., Ganapathisubramani, B., and Goulart, P. J. (2013). Optimal mode decomposition for unsteady flows. *Journal of Fluid Mechanics*, 733:473–503.

Xia, X. (2002). Global frequency estimation using adaptive identifiers. *IEEE Transactions on Automatic Control*, 47(7):1188–1193.

Xia, X.-H. and Gao, W.-B. (1989). Nonlinear observer design by observer error linearization. *SIAM Journal on Control and Optimization*, 27(1):199–216.

Ye, X. (2000). Semiglobal output feedback control of uncertain nonlinear systems with unknown high frequency gain sign. *IEEE Transactions on Automatic Control*, 45(12):2402–2405.

Yi, B., Ortega, R., and Zhang, W. (2018). On state observers for nonlinear systems: A new design and a unifying framework. *IEEE Transactions on Automatic Control*, 64(3):1193–1200.

Yong, R., Yu-Shan, N., and Chac-Feng, L. (2008). Multi-bifurcation effect of blood flow by lattice boltzmann method. *Chinese Physics Letters*, 25(11):4038.

Zeitz, M. (1984). Observability canonical (phase-variable) form for non-linear time-variable systems. *International journal of systems science*, 15(9):949–958.

Zeitz, M. (1987). The extended luenberger observer for nonlinear systems. *Systems & Control Letters*, 9(2):149–156.

Zemouche, A., Zhang, F., Mazenc, F., and Rajamani, R. (2018). High-gain nonlinear observer with lower tuning parameter. *IEEE Transactions on Automatic Control*, 64(8):3194–3209.

Zhang, L., Abbott, J. J., Dong, L., Kratochvil, B. E., Bell, D., and Nelson, B. J. (2009). Artificial bacterial flagella: Fabrication and magnetic control. *Applied Physics Letters*, 94(6):064107.

Zheng, G., Boutat, D., and Barbot, J.-P. (2007). Single output-dependent observability normal form. *SIAM Journal on Control and Optimization*, 46(6):2242–2255.

Ziarani, A. K. and Karimi-Ghartemani, M. (2005). On the equivalence of three independently developed phase-locked loops. *IEEE transactions on automatic control*, 50(12):2021–2027.

Zimmer, G. (1994). State observation by on-line minimization. *International Journal of Control*, 60(4):595–606.

Javeria Ahmed

# Prise en compte des singularités d'observabilité dans la synthèse d'observateurs non linéaires

Résumé :
Dans ce travail de thèse, nous nous intéressons à la synthèse d'observateurs pour une classe particulière de systèmes non linéaires, à savoir les systèmes triangulaires affectés par des perturbations périodiques, modélisées par exemple par des oscillateurs harmoniques ou non linéaires. Ces systèmes rencontrent des pertes d'observabilité en certains points appelés défauts ou singularités d'observabilité. Ces pertes d'observabilité peuvent advenir dans ou hors de la région où évolue le système; cependant, la synthèse d'observateurs non linéaires requiert génériquement une transformation vers une forme normale, dont l'inversion est problématique en cas de singularité. La méthodologie adoptée dans ce travail repose sur l'ajout d'états fictifs au vecteur d'état de l'observateur pour gérer ces singularités d'observabilité en modifiant le système dans leur voisinage. Nous avons ensuite proposé une modification de récents observateurs non linéaires de type grand gain, sans peaking, avec une sensibilité réduite aux bruits de mesure et une réduction des gains en dépit de l'augmentation de la dimension de l'observateur. Afin d'appliquer cet observateur sur le système original, nous avons garanti que la transformation du système original en un système sous forme normale, était un difféomorphisme global, prévenant ainsi les défauts d'observabilité. La méthodologie proposée est ensuite appliquée aux oscillateurs non linéaires et aux systèmes non linéaires perturbés périodiquement à travers deux applications différentes, liées à la mécanique des fluides. La première application traite de l'observation et contrôle d'un microrobot thérapeutique naviguant dans le système sanguin et soumis à la force de traînée causée par la vitesse du sang, considérée comme inconnue. La seconde application traite de l'évolution des structures principales dans l'écoulement à l'arrière d'un corps non profilé, responsables d'une part importante de la surconsommation des véhicules, et de la reconstruction de leur état. Les résultats expérimentaux et de simulation illustrent l'efficacité des observateurs proposés et sont encourageants pour envisager des lois de commandes avancées dans ces deux domaines applicatifs.
Mots clés : observateurs non linéaires, oscillateurs non linéaires, défauts d'observabilité, microrobotique, dynamique des lâchers tourbillonnaires dans le sillage

# Nonlinear observers handling observability singularities

Abstract :
The main subject of the thesis is to synthesize observers for a class of nonlinear systems, namely systems in phase variable form affected by oscillating disturbances, modeled e.g. by harmonic or nonlinear oscillators. This class of system suffers from a loss of observability on some sets, refered to as observability defects or observability singularities. These defects may arise either inside or outside the region of interest. Since mappings to normal forms are often required to synthesize nonlinear observers, such singularities have to be addressed. This work proposes a methodology to handle such singularities by adding some fictitious states to the observer state vector, thus modifying the system around singularities to avoid them. Providing a way to tackle those observability defects further leads to the second objective of the thesis i.e. propose observers synthesis for nonlinear oscillators in the presence of those observability defects. The proposed observers rely on recent enhancements of high gain observers removing the peaking phenomenon, and reducing sensitivity to noise as well as the high gain parameter impact.The proposed methodology is further applied to nonlinear oscillators and nonlinear systems perturbed by periodic disturbances through two different applications related to fluid mechanics. The first application considers the navigation of a magnetic therapeutic microrobot in blood vessels for targeted drug delivery, where the unknown blood velocity affects the microrobot's dynamics. The second application concerns the wake flow dynamics at the rear of a bluff body to investigate the dynamics of the main structures in flow which are responsible for the drag force and in turn for vibrations and energy overconsumption. The experimental and simulation results illustrate the effectiveness of the proposed observers and are encouraging for advanced control law and diagnosis purposes in the future.
Keywords : nonlinear observers, nonlinear oscillators, observability defects, microrobotics, wake flow dynamics

Université d'ORLÉANS

**Laboratoire PRISME, IUT de Bourges**
**63, avenue de Lattre de Tassigny**
**18020 Bourges**